UNIVERSITY OF ADELAIDE

DEPARTMENT OF ELECTRICAL ENGINEERING

ELECTROMAGNETIC TRAFFIC SENSING
AND
SURVEILLANCE

by

Kamran ESHRAGHIAN, B.Tech., M.Eng.Sc.

A thesis submitted to the Faculty of Engineering of the
University of Adelaide for the degree of Doctor of Philosophy.

December 1980.

CONTENTS

SUMMARY

The research program entails theoretical studies supported by experimental work on the non-contact identification of road vehicles for traffic control, monitoring and surveillance purposes. After an overview in which the more prominent approaches in traffic control and surveillance systems are reviewed, two approaches based on the requirements of modern traffic control strategies are selected for detailed investigation.

The first technique is directed towards traffic control systems where broad classification of road vehicles in preference to the individual vehicle identification is the prime consideration. In this study, attention is focussed on the feasibility of grouping vehicles into makes and models without the need for additional on-board equipment. The main aim in this portion of the work was to conduct an examination of data on electromagnetic vehicle-sensor signatures previously obtained by the author, with a view to establishing the feasibility of achieving the required grouping by signature analysis, and with the objective of defining appropriate directions for future research in this area.

When more varied and detailed information associated with individual vehicles within the traffic flow is to be extracted an alternative approach is required. Non-contact identification or interrogation of road vehicles involves the detection of some form of radiated or reflected energy from the vehicle. The selected vehicle requiring identification is equipped with a transponder which may be either a passive or an active unit capable of sending out a coded signal.

The second section of this study, which constitutes the major part of the research program is devoted in exploring such technologies. As a

first step the performance of several vehicle identification systems
have been reviewed to provide a basis for understanding the choice of
the particular methods which were selected for detailed investigation.
Analysis of two alternative technologies i.e. the surface acoustic wave
(SAW) labelling system and the two-port passive subharmonic transponder
which may be considered as possible alternatives in the realization of
non-contact vehicle identification is then presented.

The remainder of the work entails a detailed exploration of the
behaviour and characteristics of a new class of passive subharmonic
transponder employing near-field coupling, designed for such applications.
The transponder which has been developed uses single magnetic antenna
for simultaneous extraction of power from the transmitting source at one
frequency and its subsequent reradiation, with substantially no resultant
energy loss, at another frequency. The process by which the reradiated
energy is provided is one of direct synthesis within the antenna by using
switching circuits rather than conversion involving d.c. paths. The
advantages of this approach are not only that high efficiency is achieved
but also the constraints relating to the communication bandwidth required
by the signal and the qualify factor of the circuit are broken. For these
reasons, considerable improvement in power transfer between the trans-
mitter and transponder is achieved.

The thesis also contains the development of principles which are
useful in understanding the mechanics of energy exchange process between
two antennas operating within near field environment, and hence allow
local optimizations to be performed.

PREFACE

This thesis contains no material which has been accepted for the award of any other degree or diploma in any University, and to the best of the author's knowledge and belief contains no material previously published or written by another person, except where due reference is made in the text of the thesis.

K. Eshraghian.

25th December, 1980.

ACKNOWLEDGEMENT

PUBLICATIONS

with R. E. Bogner, "Vehicle Traffic Monitoring", IREE Proc., Vol. 40, No. 2, pp 25-37, March 1979.

with R. E. Bogner, "Remote Classification of Road Vehicles", IREE International Convention Proc., pp 273-276, Aug. 1979.

with P. H. Cole, and A. K. Roy, "Theory and Operation of a Passive Subharmonic Transponder", IREE International Convention Proc., pp 51-54, Aug. 1979.

with P. H. Cole and A. K. Roy, "Measurement and Characteristics of Environmental Noise Affecting Low Frequency Transponder Operations", IREE International Convention Proc., pp 456-459, Aug. 1979.

with F. S. Sin, "Multiprocessor Based Vehicle Sensor", Conference on Microprocessor Systems Proc., Vol. 8/11, pp 1-5, 1980.

with P. H. Cole and A. K. Roy, "Efficient Object Identification System" Patent Spec. PD4594 (Aust., U.S.A., Canada, Japan, G.B., France, Germany, Holland, Italy), 1979.

CHAPTER 1

AUTOMATIC TRAFFIC CONTROL

1.1 Introduction

Until recent years the road traffic problems were handled in a straightforward manner by construction of larger and faster roads. However, the present rate of growth and the need for energy conservation, has made it necessary to review many of the basic concepts associated with traffic movement in order to maximise the efficiency and safety of existing roads and to improve the traffic flow.

Consequently in the last decade there has been a significant increase in the activities associated with traffic control, monitoring and surveillance. Numerous research reports have emerged, as the result of these investigations on the feasibility and implementation of various intelligent traffic control, monitoring and surveillance systems[1 - 19].

The objective of these studies has been not only to evaluate the behaviour of the systems according to some performance criteria (such as travel time, travel delay, number of stops, pollution, noise, accident rate, handling of excessive traffic load, priority and energy conservation) but also to provide justification in terms

1.

of reliability, maintenance, economical and the ease with which the systems can be implemented. The successful operation and effectiveness of such systems are generally dependent on the availability and the accuracy of traffic data such as vehicle count and speed, traffic density and volume, vehicle identification, and the determination of the location of a selected vehicle.

Subsequently, the present research has been directed towards theoretical studies supported by experimental work associated with non-contact identification of road vehicles for traffic control, monitoring and surveillance. Two approaches based on the traffic control strategy and requirements have been persued in this program.

The first technique is directed towards traffic control systems where classification of vehicles is of prime consideration in preference to the individual identities. The classification process entails categorizing vehicles in a particular group such as sedans, vans, trucks, buses, etc. In general, the degree of refinement is dependent on the traffic control strategy. Thus, in this study attention is focussed on the feasibility of such refinement where vehicles in a given class are subgrouped in terms of their make and models without the need for additional on-board equipment. The main aim in this portion of the work was to conduct an examination of limited already available data[20] on electromagnetic vehicle-sensor signatures with a view to establishing the feasibility of achieving the required grouping by signature analysis, and with the objective of defining appropriate directions for future research in this area.

When more varied and detailed information associated with

individual vehicles within the traffic flow is to be extracted, an alternative approach is required.   Non-contact identification of road vehicles involve the detection of some form of radiated or reflected energy from the vehicle. The selected vehicle requiring identification is generally equipped with a transponder which may be either a passive or an active unit capable of sending out a coded signal.

The second section of the study which constitutes the major part of this research program, explores the behaviour and characteristics of a new class of passive transponders employing near-field coupling. The transponder which has been developed uses a single magnetic antenna for simultaneous extraction of power from the transmitting source at one frequency and its subsequent reradiation at another frequency with substantially no resultant energy loss. The process by which the reradiated energy is provided is one of direct synthesis within the antenna by using switching circuits rather than conversions involving d.c. paths.

The advantages of this approach are not only that high efficiency is achieved but also the constraints relating the communication bandwidth required by the signal and the quality factor of the circuit are broken. For these reasons, considerable improvement in power transfer between the transmitter and transponder is achieved.

In order to have an appreciation of the present research program, it is considered desirable to provide an over-view of the more prominent approaches in traffic control, monitoring and surveillance systems, and give a brief summary of the technologies available.

1.2 Traffic Control Structures

There are two basic approaches associated with traffic control systems: "fixed-time" and "traffic actuated". The fixed-time systems are primarily used for downtown urban-area streets, where the daily traffic patterns are well known. Their operation is based on traffic control plans derived statistically for different parts of the day for a given site. Such systems are gradually being replaced by the traffic-activated controls, the operation of which depends on traffic variables obtained from vehicle sensors[21-25].

Consequently many researchers have directed their activities towards the development of intelligent traffic dependent control systems, and have followed two directions. The first looks for car-borne equipment in the form of an information system whereby traffic and safety information is conveyed to the motorist by radio communications and by variable signal panels in the vehicle. The complexities and problems with such systems are well known and various proposals are still being evaluated by various researchers.

The second approach is traffic responsive control and monitoring systems where traffic controllers dynamically control and co-ordinate the complex switching tasks of visual displays according to the traffic flow demand. The visual displays can take the form of the conventional traffic lights or a series of signal gantries span the roadway at regular distances. Generally, the gantries display the recommended speeds and warning messages to motorists in each lane. These displays are automatically controlled as queues of vehicles form and then disappear[26-28].

Additional intelligence can be also built into such systems so

that service and emergency vehicles approaching the signal controlled junctions or sections, obtain priority by modifying the flow control patterns of traffic signals.

The fundamental component of such structures is the microprocessor based traffic controllers grouped into several zones as shown in Figure 1.1. Each zone is subsequently controlled by a regional minicomputer linked to a central processor. These hierarchial levels are further, individually linked to the adjacent level by means of a serial communication network. This network of distributed intelligence enable independent control of traffic by the local controller most of the time but with the ability of the master systems to act in a supervisory role.

There are two distinct levels of control:

(i) Macrocontrol; where a multiple choice of synchronisation schemes based on vehicle sensor information are made possible. On the basis of received data, the processor decides on the strategy which best fits that traffic data.

(ii) Microcontrol; in which detailed measurements of traffic inputs at strategic locations are used by the processor to modify the traffic signal cycle of a single intersection or alternatively a group of intersections.

The overall tactical decision by the master processor is generally governed by one or more of the traffic variables such as count, speed, vehicle-spacing, volume and density. Consequently a considerable amount of effort has been expanded by numerous research-

FIGURE 1.1. INTELLIGENT COMPUTER BASED TRAFFIC CONTROL SYSTEM.

Zone 1

Zone 2

Zone 3

Zone 4

M1

M2

M3

M4

M5
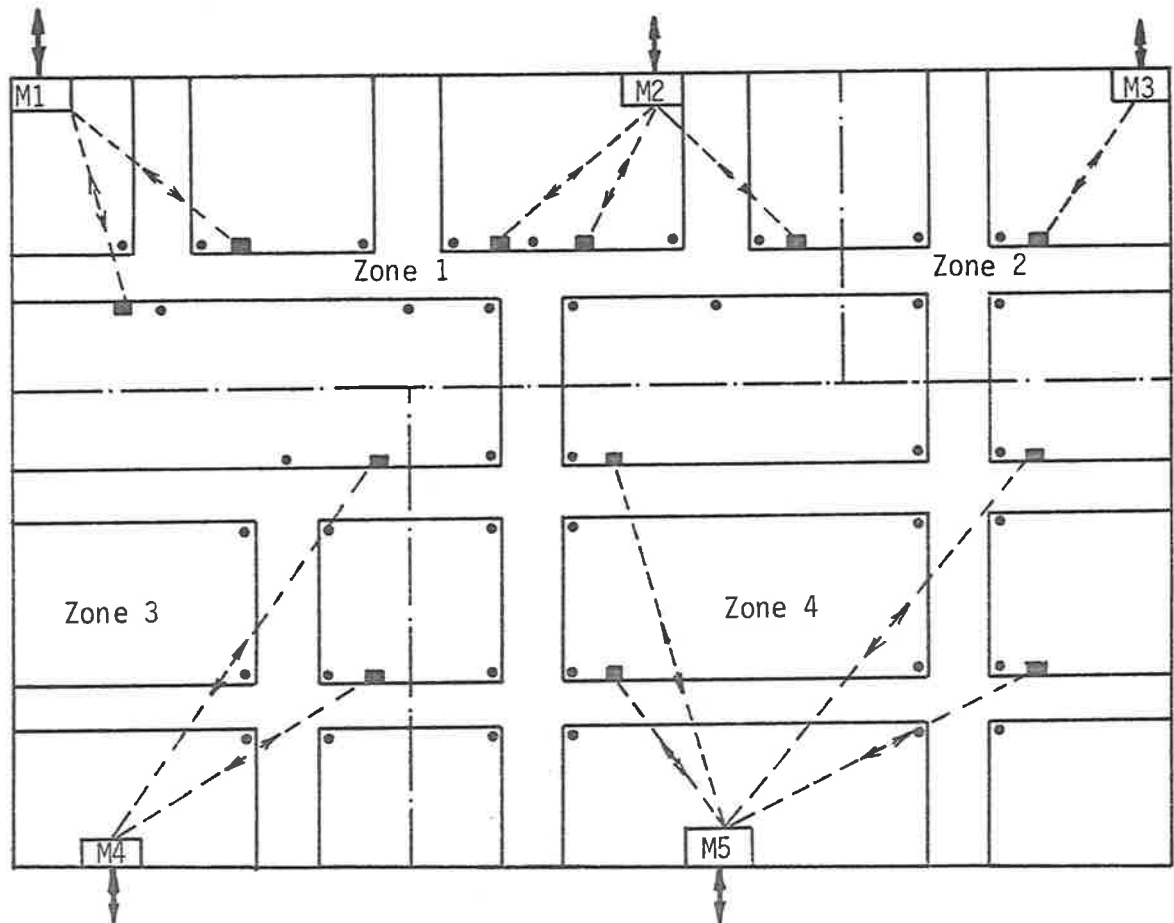
• Traffic Signals.

▪ Local Controller.

☐ Master Controller.

⟷ Communication link between Master Controller and Central Supervising System.

⟷ Communication link between local Controller and Master.

ers in characterising the traffic flow in terms of the above variables. Although substantial progress has been made in estimation methods, an analytical formulation still remains a non-trivial and complex problem.

1.3 Traffic Models

The traffic on a freeway is generally characterised in terms of macroscopic or microscopic models[29-30]. If the objective is to describe average behaviour of traffic on the freeway segment, several kilometers in length for several hours, one is concerned with gross features of traffic such as volume (vehicles per hour per lane), mean speed (kilometers per hour) and average travel time. Models developed with this objective in mind need only provide an accurate representation of these parameters and are generally termed macroscopic models.

Lighhill and Whitham[31] developed a model based on continuum variables associated with fluid mechanics flow and proposed the identity,

$$Q = D.S \qquad\qquad (1.1)$$

where Q is the traffic volume, D describes the traffic density and S defines the mean speed.

Theoretical studies and empirical evaluation have indicated that for normal flow, traffic volume decreases with increasing speeds[32]. At a point of maximum volume, flow becomes unstable and eventually turns into a forced flow. Thus simultaneous decrease

7.

of volume and speed results. A typical speed-volume curve is illustrated in Figure 1.2.

An important factor which emerges from this simple model is that a relatively small increase in traffic demand on an already heavily loaded freeway can have a very detrimental effect on the operating conditions for all the traffic on the facility. Speeds and volumes are reduced, densities and travel times are increased, and the freeway immediately looses much of its efficiency.

Although methods for accurate measurements of traffic variables over the entire length of the freeway are still relatively limited, several authors have formulated various schemes on the data obtained from vehicle detectors placed at regular intervals on the freeway.

Gazis and Knapp[33] developed a modelling scheme for estimating the number of vehicles on a section of freeway from speed and flow measurements at the entrance and exit points of a section. From the estimate of the travel time a rough measure of density was obtained. Mikhalkin[34] developed an alternative approach where the occupancy (the percentage of time the sensor is activated by the vehicle during a given period) was utilised in place of the section density. Nahi and Trivedie[35] applied modern estimation theory and presented an improved modelling technique which provided simultaneous estimation of traffic variables such as section density and section speed based on various averages over the freeway section.

The main objectives associated with these techniques are to predict traffic conditions and indicate congestion. However, there are situations particularly in incident detection, identification

8.
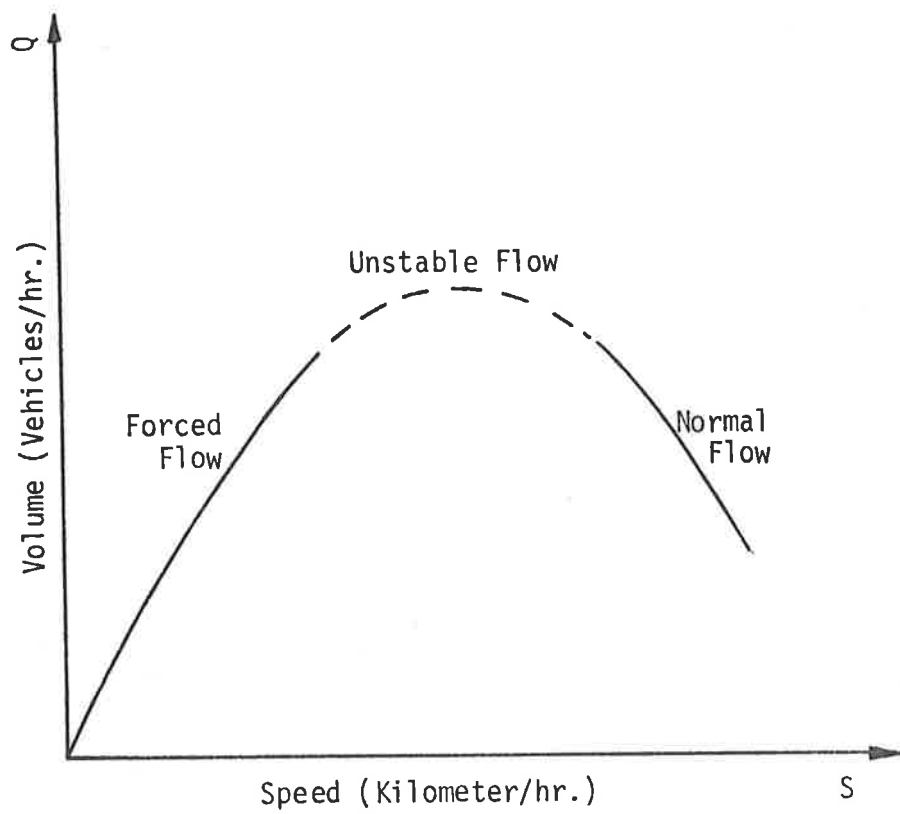
FIGURE 1.2. TYPICAL SPEED- VOLUME CHARACTERISTICS.

and priority allocation schemes, in which detailed representation of traffic flow down to the level where individual vehicles are concerned, is required. These models are known as microscopic models and are extremely useful tools in studying problems concerned with and developing control strategies for relatively short lengths of freeway and relatively short periods of time.

1.4 Automatic Vehicle Monitoring

The consequence of the above need has caused the designers of urban communication systems to be actively involved with the development of services and systems which can continuously monitor the location, and status of vehicles operating in an urban environment[36].

The potential of such systems is the promise of an economical and automated method of monitoring transit operations so that timely system-wide information is available for fleet management, speeding-up or slowing-down particular lanes, automatic entry to selected locations, and priority allocations at signal controlled sites for service and emergency vehicles.

The automatic vehicle location systems use one of the several currently available technologies to estimate a vehicle's position. The approaches which have received considerable attention may be divided into three broad categories: dead-reckoning, radio frequency positioning and proximity systems[37-45].

10.

1.4.1   Dead-Reckoning[39]

In this method a vehicle is located by determining its distance and direction of travel from a fixed point. A radio link is subsequently used to relay this information to a central control station. The distance and azimuth measurements are made by using precision odometer and a compass type instrument respectively. An approach to the implementation of such a structure is shown in Figure 1.3.

1.4.2   Radio Frequency Ranging[40-41]

The approach entails the determination of the difference in distance between a vehicle and two or more fixed pairs of sites. This information is subsequently used to obtain the location based on known geometrical relationships.

Two techniques have received significant attention. The first being the pulse trilateration where in response to a synchronising pulse from the control centre, the vehicle transmits a reply pulse which is received by three receivers. The difference in the time of arrival is subsequently used to obtain the location. In the second approach, using synchronised radio signals, an on-board receiver measures the difference in distance between station pairs and transmits this information to the control centre computer for determination of the geographic location.

A typical approach using circular trilateration is shown in Figure 1.4.
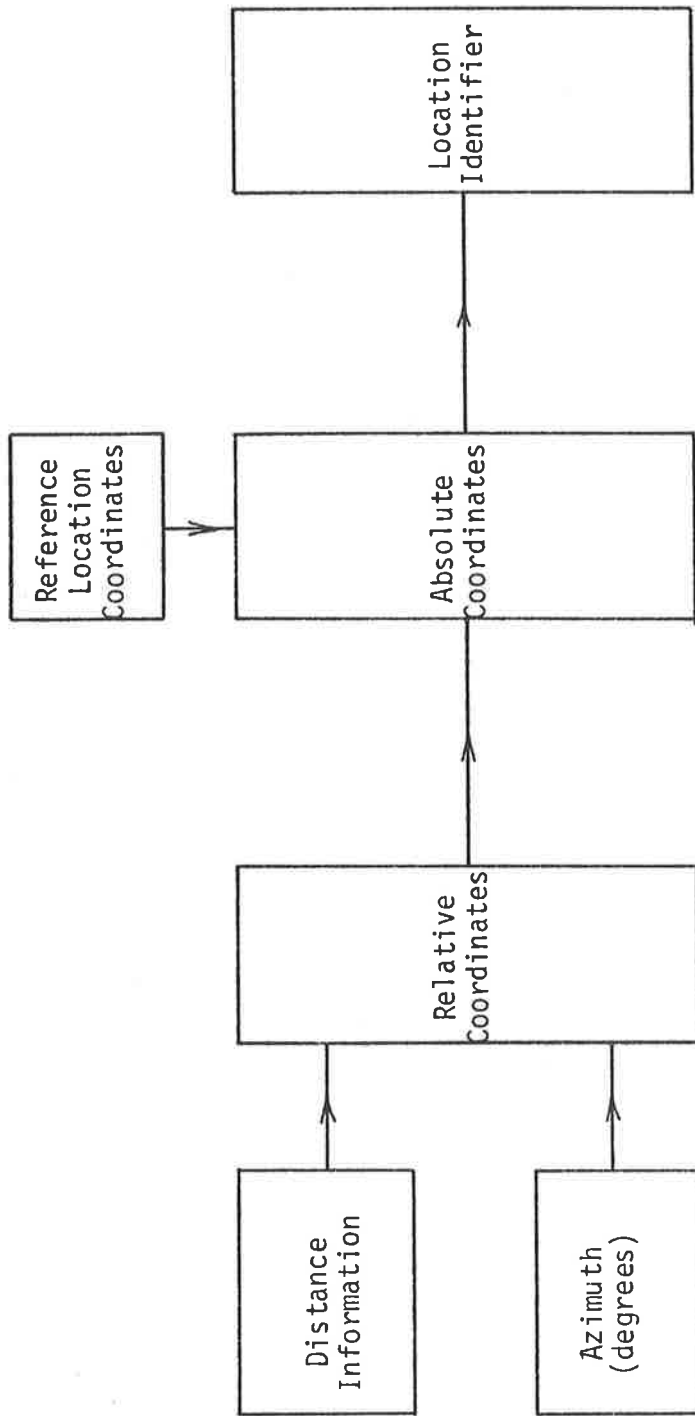
FIGURE 1.3. SYSTEM REALISATION FOR DEAD-RECKONING TECHNIQUE.
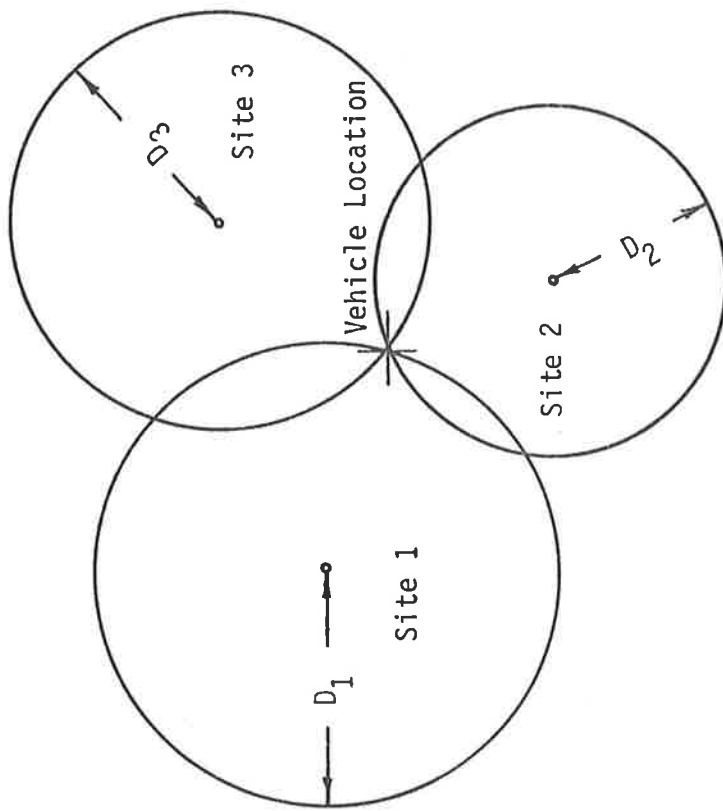
FIGURE 1.4. RADIO LOCATION USING CIRCULAR TRILATERATION.

The environment has a singificant influence in the overall system performance.

1.4.3 Proximity Systems[42-45]

The concept of proximity systems is that of determining the positional relationship between a vehicle and fixed "signposts" placed at selected strategic locations. A number of different technologies such as magnetic sensors, optical and ultrasonic radiators, as well as conventional radio transmitter and receivers have been proposed.

The basic principle associated with such an approach is illustrated in Figure 1.5 where either the magnetic or electromagnetic fields may be used as the coupling mechanism between the signposts and the vehicle.

One of the major advantages of such a system is its ability to service many users without the need for changes to the site equipment. However the accuracy of the system is directly related to the number and characteristics of the signposts.

1.4.4 Comparison of Technologies

The implementation of automatic vehicle monitoring systems is dependent on the economics of installation, the accuracy of the system, the number of vehicles to be serviced and the size of the zone.

Transmitted Signal carrying location information (101111)

Base Station

Pick-up loop 5' × 4.5" × 1" located 5" above ground in the under-carriage.

Vertically mounted uniquely positioned magnets (101111)

(a)

Retransmitted signal carrying location information

Microwave Transmitter

Base Station

(b)
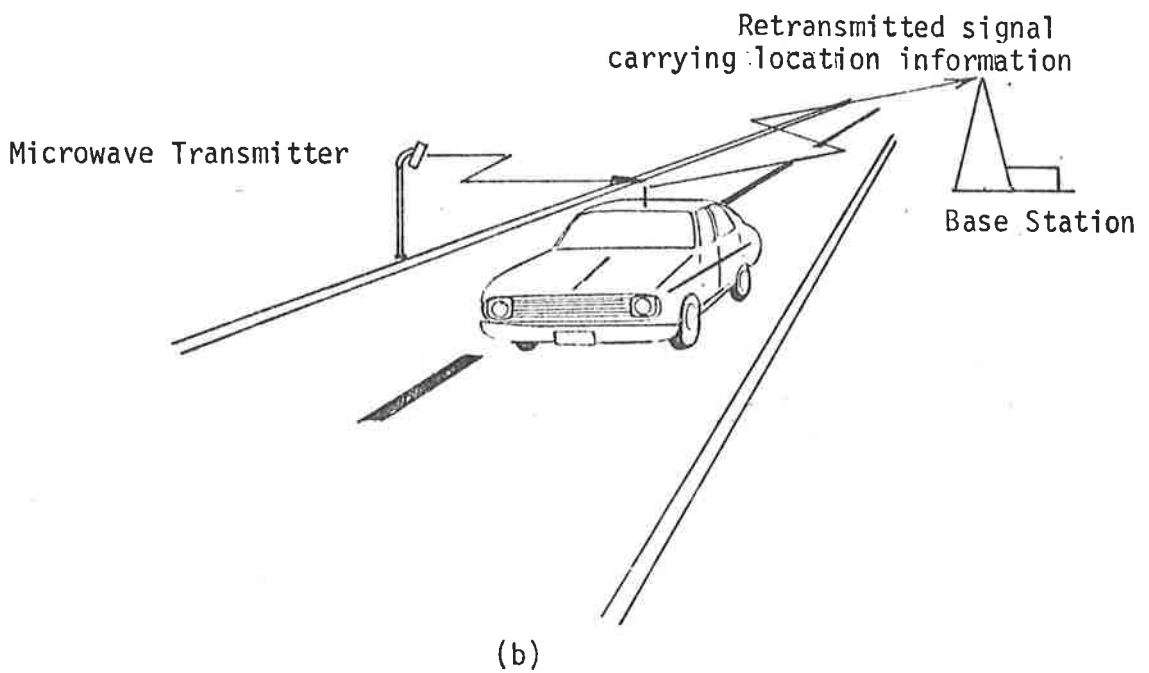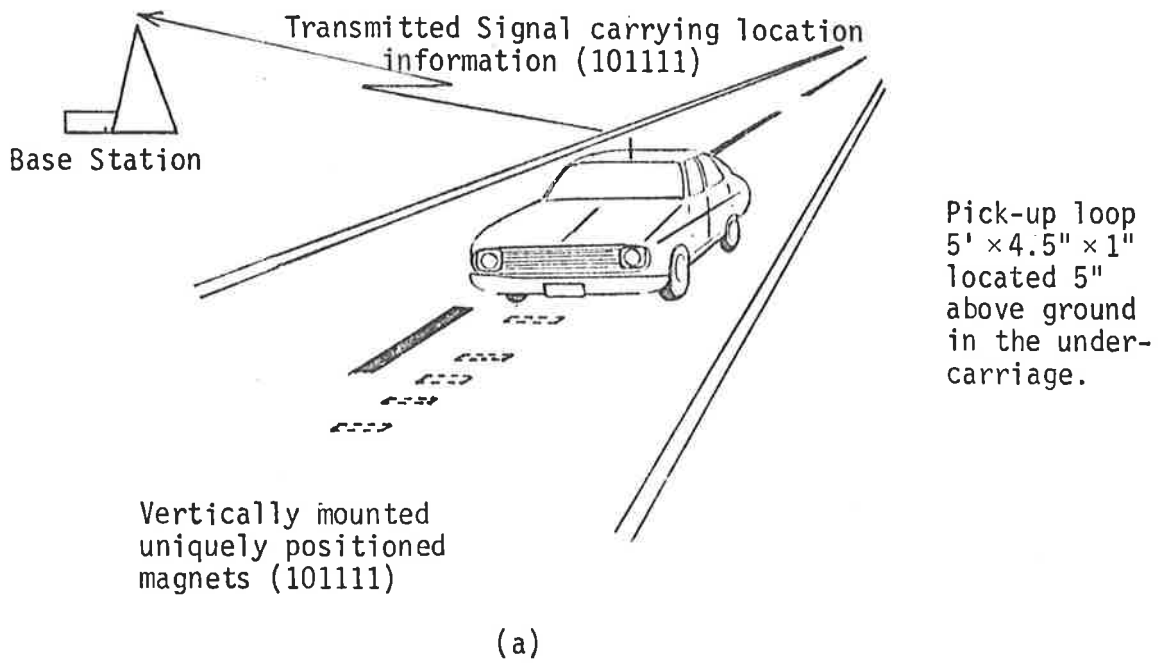
FIGURE 1.5. LOCATION SYSTEMS USING SIGNPOSTS

(a) Magnetic.

(b) Electromagnetic.

15.

A detailed comparative analysis associated with several of the technologies have been carried out by Skomal[46] and Wilson[47]. The scope of these investigations is summarised in Table 1.1 in which the performance of the three approaches defined above are described in terms of the relative acceptance criteria:

good (G); satisfactory (S); marginal (M); unsatisfactory (U).

Although this type of assessment depends on the user's judgement, the technique provides a basis for the assignment of a figure of merit which may be used as a guide for comparison of various systems.

1.5 Conclusions

Although a number of pilot systems incorporating one or more of these technologies have been implemented for traffic control, monitoring and surveillance, there are still significant problems remaining to be solved.

One such question is the desired characteristics and practical implementation of the link between the vehicle and the control system. The link can generally be realized by either vehicle sensors or information bearing transponders.

The simplicity of the proximity technique shows the most promise since the failure of a component in the system such as a

TABLE 1.1   COMPARISON OF THREE TECHNOLOGIES SUITABLE FOR AUTOMATIC

VEHICLE MONITORING

	Reliability	Accuracy	Area Coverage	On-board Relative Unit Cost	Relative † System Cost	Fail-Safe Characteristics	Environment	Compatibility of Service to Different Users
Dead Reckoning	M	S	S	5.0	2.0	S	M	U
R.F. Ranging	S	G	G	5.0	1.0	S	S	U
Proximity	G	S*	S*	1.0	1.0	G	G	G

* depends on the number of signposts

† 1000 vehicles per 400 sq. miles

17.

signpost does not influence the overall operation. In addition the system has a "non-exclusive" characteristic and can be utilised simultaneously by many users without the need to modify or expand the site equipment. However, one major drawback for large area coverage is the complexity and economy of the signposts. Mangetic arrays are undesirable due to their physical size and layout. The "active" signposts require on-site power and hence drastically influence the cost structure and the reliability of the system.

Thus the complexity of the signpost and the need for reliable and economically feasible systems provided the necessary motivation for the investigations into the area of electromagnetic traffic sensing and surveillance at both the micro and macro levels with particular attention towards the development of systems for classification and identification of road vehicles.

CHAPTER 2

REMOTE CLASSIFICATION OF ROAD VEHICLES

2.1 Introduction

The classification process entails categorising different vehicles into a particular group such as sedans, vans, trucks, buses etc. The degree of refinement, in general, is dependent on the traffic control strategy.

Although reports on traffic control and surveillance systems are numerous, only a very limited research has been carried out in relation to vehicle classification.

Thilo and Drebinger[48] used the vehicle length and the undercarriage height as the criteria for vehicle classification. The vehicle length was measured using two inductive loops as shown in Figure 2.1, while the undercarriage height was estimated from the maximum value of the change in the inductance. In this manner they were able to provide a very rough indication of the class to which a vehicle belongs.

Ziolkowski and Tsao[49] proposed a similar scheme using a single electric dipole antenna. The antenna was placed under the road surface and positioned in the lane in the direction of motion of the
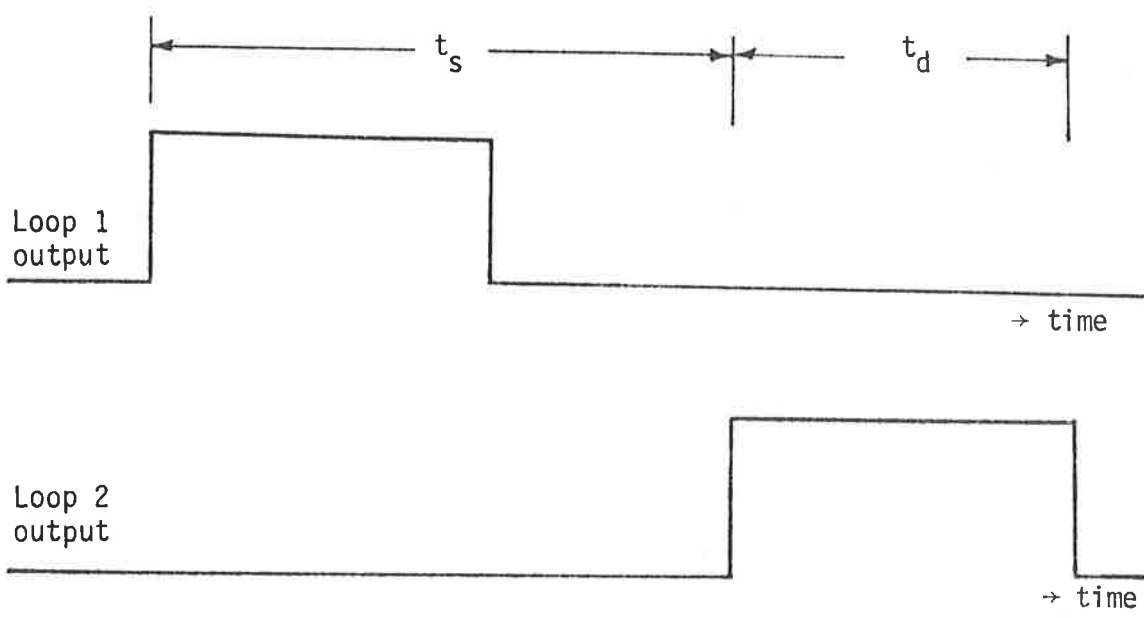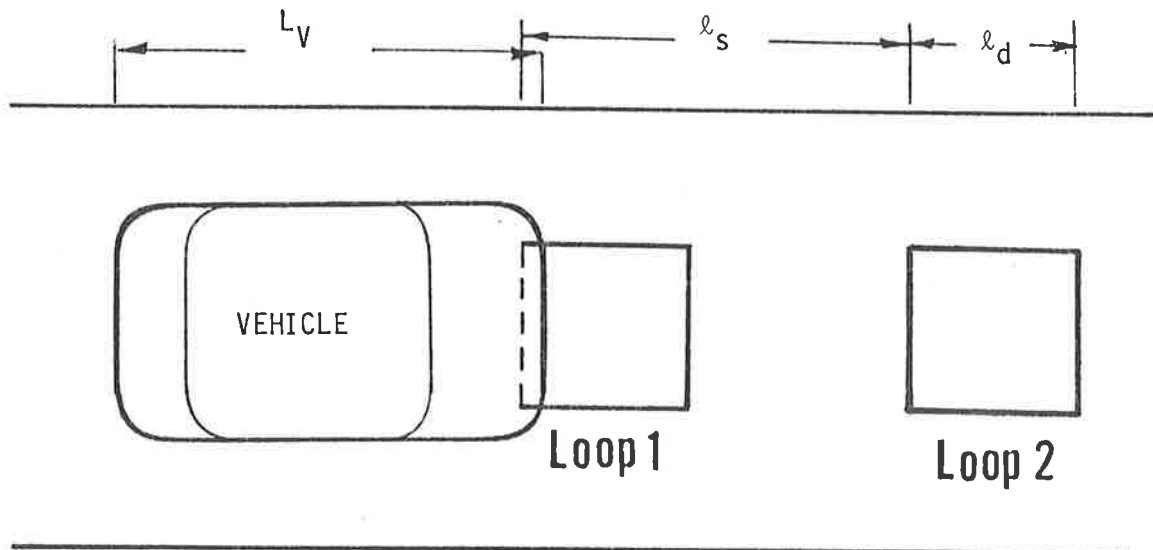
$$\text{Speed} = \frac{L_v}{t_s}$$

$$L_v = \ell_s \left(\frac{t_d}{t_s}\right)$$

FIGURE 2.1. DOUBLE LOOP CONFIGURATION FOR DETERMINATION OF

VEHICLE LENGTH L_v.

vehicle as illustrated in Figure 2.2. Motion of a vehicle over the antenna resulted in a change in the input impedance as shown in Figure 2.3. From the knowledge of the length of the antenna and times t_R, t_S and t_f, the vehicle length was subsequently estimated. The average undercarriage height was also approximated using the magnitude of the change in the input impedance.

The critical factor associated with the above classification methods is the need for an accurate measure of vehicle's speed for length estimation. Further, the geometry associated with the above techniques impose severe restrictions in their use for discriminating between closely following vehicles, since it is possible for two vehicles to cover the same loop or antenna.

Due to the complex nature of the undercarriage, the impedance change deviates from the clean plateau as shown by Figure 2.3 and therefore the undercarriage height and vehicle length estimates become highly unreliable. In addition, examination of the distribution of vehicle classes in terms of vehicle length associated with a given section of a highway[48] as illustrated in Figure 2.4, indicate that there exists a noticeable overlap of lengths of vehicles belonging to different classes. Thus vehicle length does not contribute significantly in the classification process.

The inductive loop has a further drawback with vehicles which cover only part of the loop. Transverse displacement of the vehicle from the centre position results in a smaller change in the inductance and subsequently results in inaccurate height estimation.

Previous studies in relation to suitability of various vehicle sensors for speed measurements, by the aughor as part of a M.Eng.Sc. research program[20] provided the initial motivation to explore
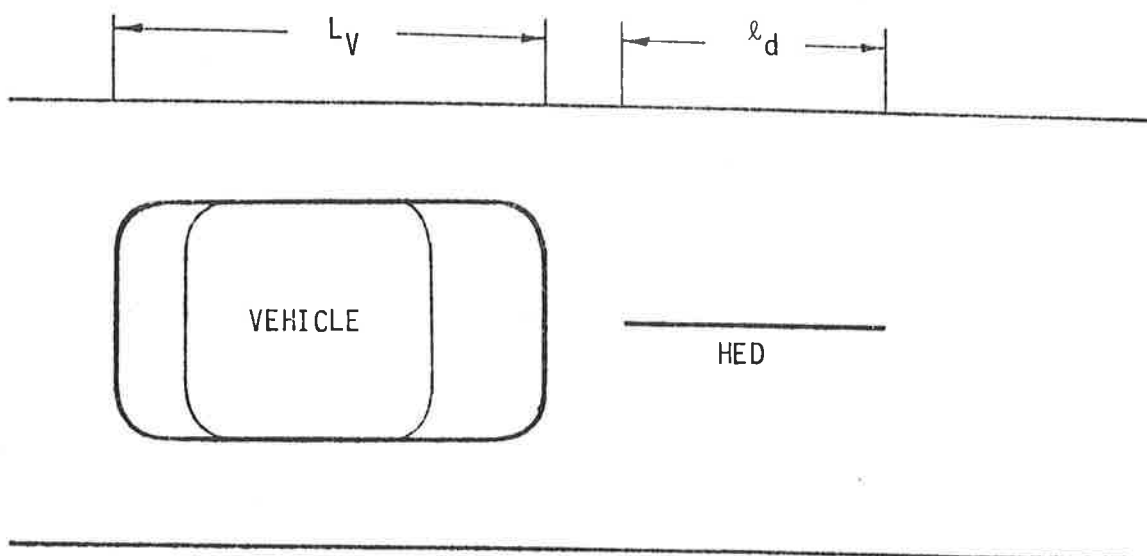
FIGURE 2.2. DETERMINATION OF VEHICLE LENGTH USING A HORIZONTAL ELECTRIC DIPOLE ANTENNA (HED).
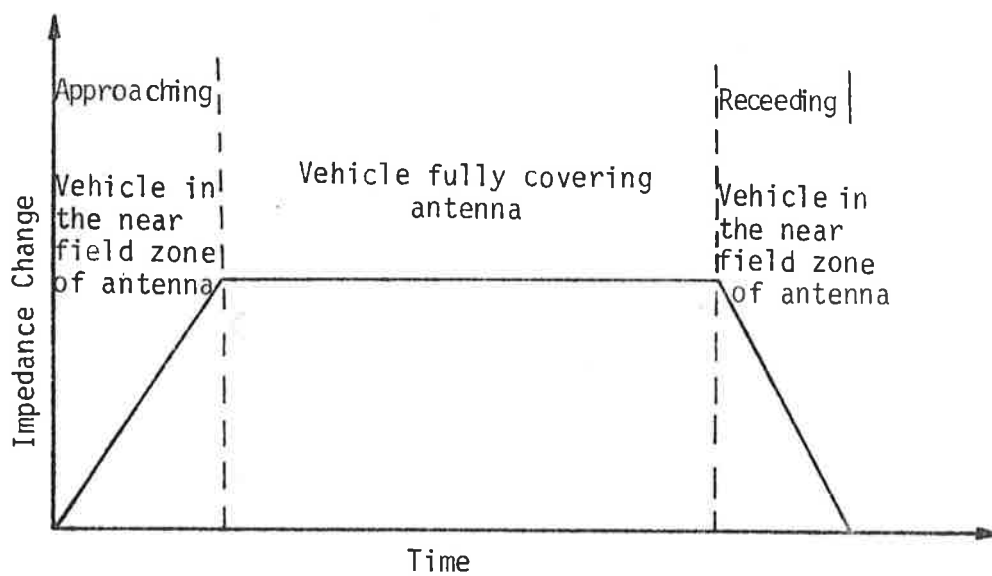
FIGURE 2.3. IMPEDANCE CHANGE FOR HED ANTENNA AS A FUNCTION OF TIME.
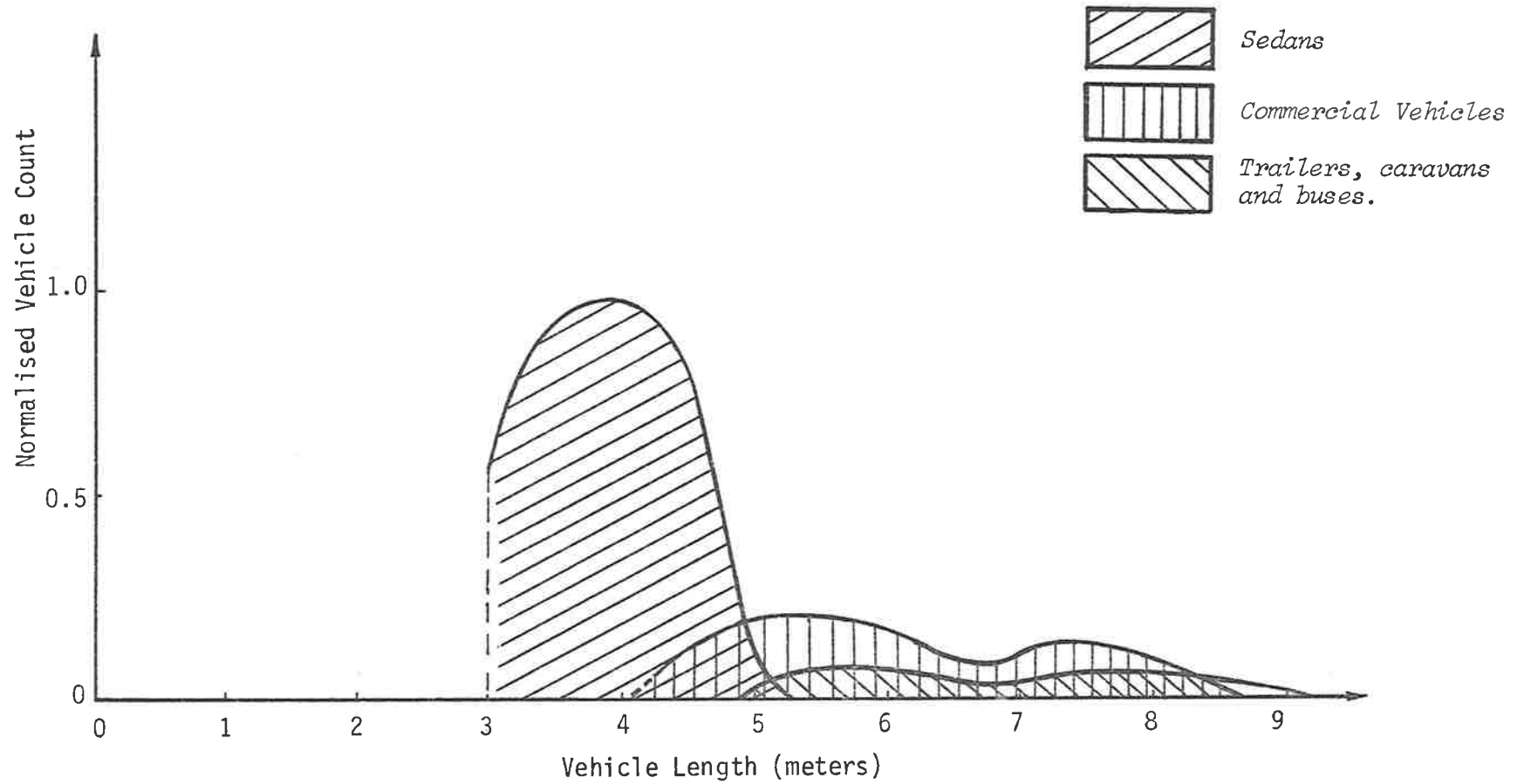
FIGURE 2.4. TYPICAL CURVES ILLUSTRATING NORMALISED VEHICLE COUNT AS A FUNCTION OF VEHICLE LENGTH FOR A PARTICULAR SECTION OF A HIGHWAY.

23.

further the characteristics and behaviour of a two coupled-coils sensor shown in Figure 2.5, for the classification process. The sensor consists of two coils with a common axis located horizontally in the road surface. The axis being orthogonal to the direction of travel of the vehicle.

This choice was based on the simplicity of the structure, the ability of the sensor to discriminate between closely moving traffic and the availability of a limited data. In addition, due to the low frequency operational characteristic of the sensor, i.e. 100 KHz, interface problems such as reflection and attenuation which one may encounter in the alternative microwave structures are non-existant.

Thus, in this portion of the study attention is focussed in exploring the possibilities that may exist in the already available data to provide the desired refinement where vehicles in a given class are further subgrouped in terms of their make and models without the need for additional speed and length information.

For convenience a brief summary of the sensor is provided in the following section.

2.2 Vehicle Sensor

The operating principle of the sensor is based on the fact that one coil (transmitter T_χ) is energised by a low frequency time-varying current and a conducting body placed in the resultant magnetic field has eddy currents induced in it. The magnetic field created by these currents is in opposition to the applied field and results in a change in the induced voltage in the second coil (receiver R_χ).

Copper Coil   Ferrite Rod
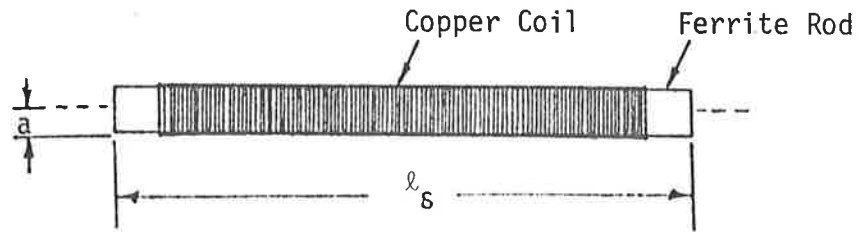
Ferrite type	:	4302 020 35401 (Philips Elcoma)
μ_r	:	330
No. of turns	:	420 turns ployester wire 206-170
Coil radius a	:	4.32mm
Wire radius r	:	0.2mm

Housing

R_X T_X

ℓ_d

(a)

100 KHz
Sinusoidal
Oscillator

R_X T_X

Lead-in Cable

Receiver and
Processing
Unit

(b)

Flow

Vehicle   Sensor

(c)
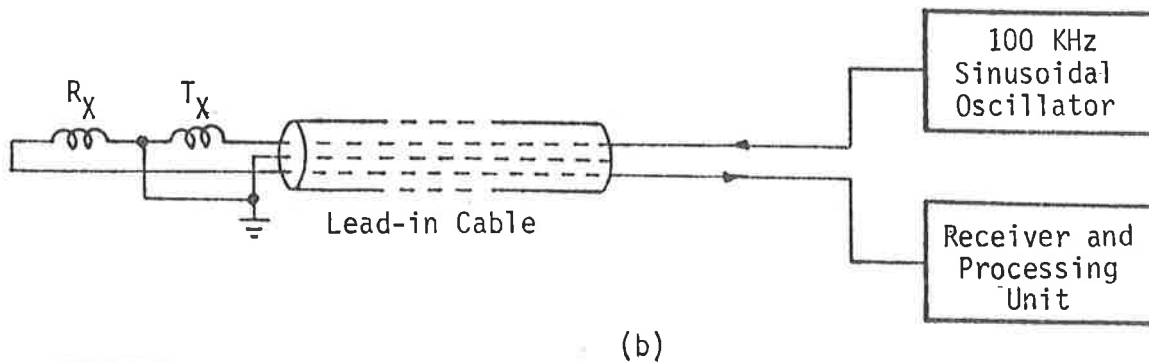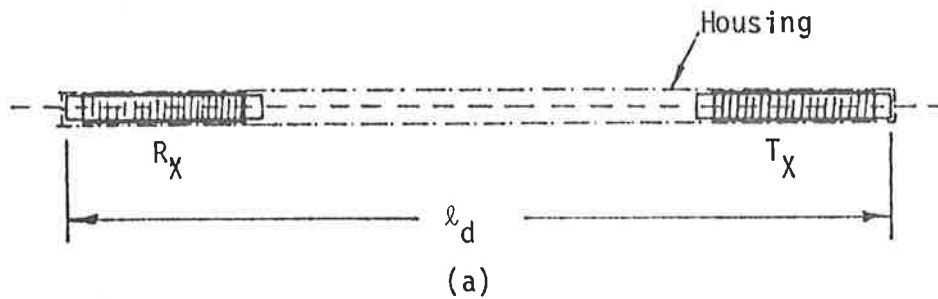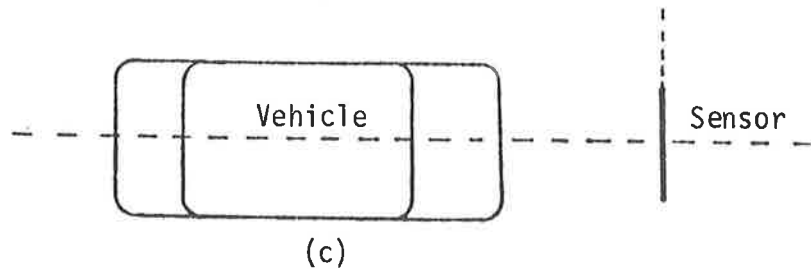
FIGURE 2.5.   VEHICLE SENSOR USING COUPLED COILS STRUCTURE.

    (a)   Sensor Structure.
    (b)   Operating System.
    (c)   Sensor Position Under the Road Surface.

To describe the signal generating source in terms of the irregularities associated with the undercarriage* is impractical due to the very complex structure of that undercarriage. However the method of images may be used to provide an insight into the relationship between the undercarriage height h, coil separation x, and the change in the induced voltage V_p' in the receiver coil R_X. With reference to co-ordinate system of Figure 2.6 and from Appendix A, the change in voltage is

$$V_p' = K_i \left[\frac{x^2 - 2h^2}{\left(4h^2 + x^2\right)^{5/2}} \right] \qquad (2.1)$$

where

$$K_i = \frac{1}{2} \left[N^2 \omega I \pi a^4 \mu_e \right] \qquad (2.2)$$

and   N = number of turns

           I = peak current in the coil

           a = radius of the coil

           μ_e = effective permeability.

The effective permeability μ_e used in Equation (2.1) takes into consideration the demagnetisation effect when ferrite material is used in the coils and its value is obtained emperically for a given structure.

* *By undercarriage it is meant the whole of the vehicle's under-section including the wheels.*
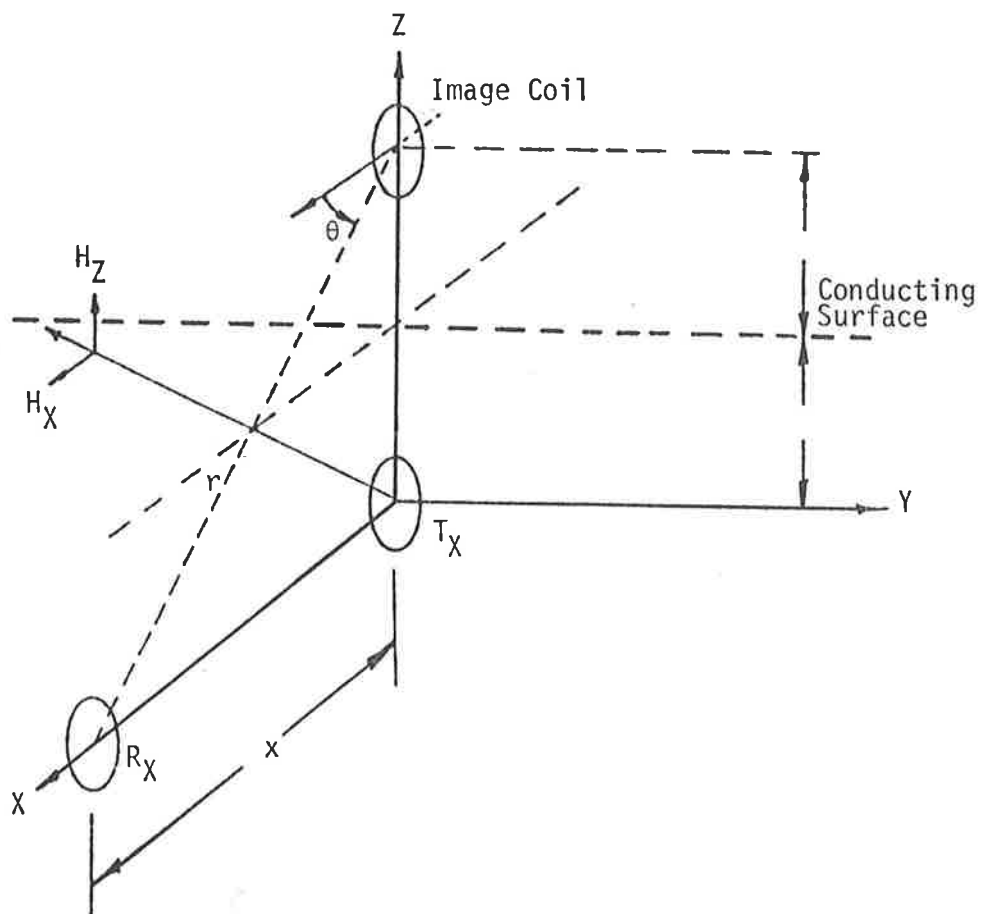
FIGURE 2.6. GEOMETRY OF THE COORDINATE SYSTEM.

If the coils are tuned, then Equation (2.6) is modified by
the quality factors Q_t and Q_r associated with the transmitter (T_X)
and receiver (R_X) coils respectively. Thus the modified voltage V_p
becomes

$$V_p = Q_t \, Q_r \, V_p^{'} \qquad\qquad (2.3)$$

The model defined by Equation (2.3) is based on the assumption
that the introduced conducting body is a perfect electrical conduc-
tor and is a flat plane. In practice we find that the first assump-
tion is justified since the materials associated with the under-
carriage are aluminium or steel, and have large conductivities com-
pared with space or air, so that the conductivities might reasonably
be considered infinite. The second assumption introduces severe
restrictions in the use of the model when irregularities associated
with the undercarriage of a vehicle are considered.

Although the model defined by Equations (2.1) - (2.3) fails to
describe the behaviour of the change in induced voltage as a vehicle
passes over the sensor, the simplicity of the expression provides an
insight into the relationships between the undercarriage height and
the induced voltage.

In order to enhance the magnitude of the image voltage as a
function of the irregularities in the undercarriage, the following
modifications to the operating characteristics of the sensor were
made.

The transmitter coil T_X was tuned to resonance by a voltage
dependent tuning capacitor. The structure of this configuration is

shown in Figure 2.7(a). The phase of the voltage in the transmitter tuned circuit is compared with that of a reference oscillator. A change in the coil inductance due to the presence of a conducting body causes a shift in the resonant frequency which subsequently results in the generation of an error voltage feedback to a tunable capacitor. The tuning capacitor subsequently adjusts its value such that the amplitude of the voltage across the transmitter coil remains at its peak.

The receiver coil R_X however, is tuned to just off resonance. An approaching vehicle causes the inductance of the receiver to vary and depending on the irregularities of the undercarriage i.e. distance between the undercarriage and the receiver coil, the resultant induced voltage in the receiver coil also varies. This principle is illustrated in Figure 2.7(b) where the separation between the undercarriage and the receiver coil is reduced, point A on the resonance moves towards point B corresponding to $h = h_{opt}$. This results in an increase in the magnitude of the image voltage. However as the separation is reduced further one arrives at the new point C with the subsequent reduction in the magnitude of the image voltage. This approach has the desirable feature which enhances the variations in the induced voltage in the receiver coil due to the undercarriage irregularities.

Due to the complexity of the undercarriage the description of the signal generating source in terms of the undercarriage geometry as a vehicle moves over the sensor, is a nontrivial task and precludes the use of mathematical analysis. However, the resultant effect can be obtained experimentally in terms of a time varying voltage known as the "signature".

29.
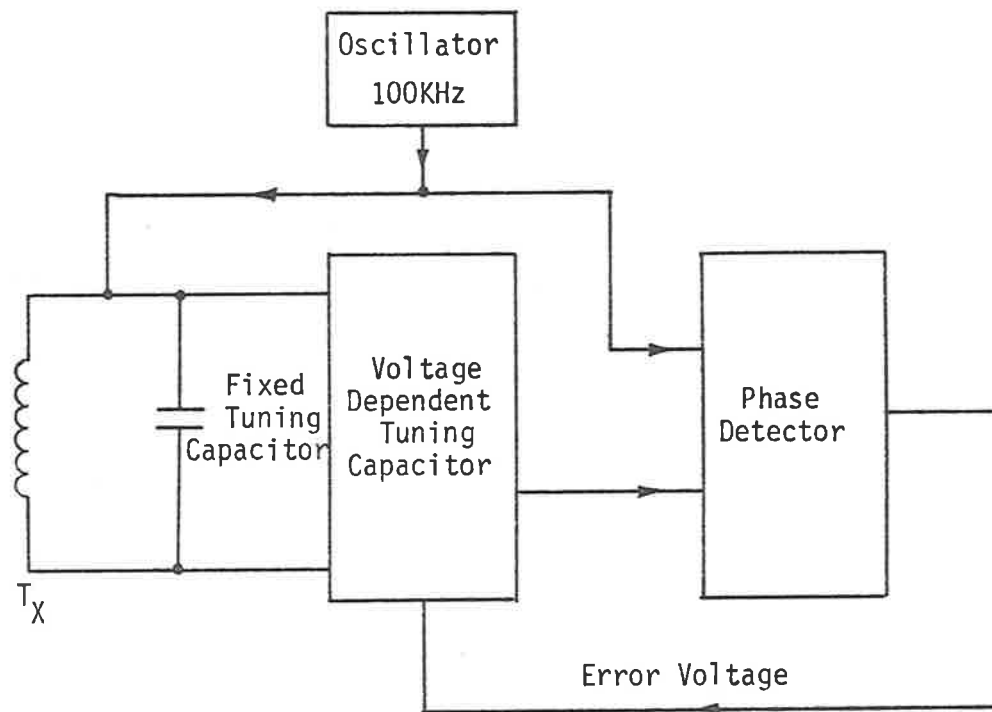
FIGURE 2.7 (a). SELF TUNING TRANSMITTER COIL STRUCTURE.
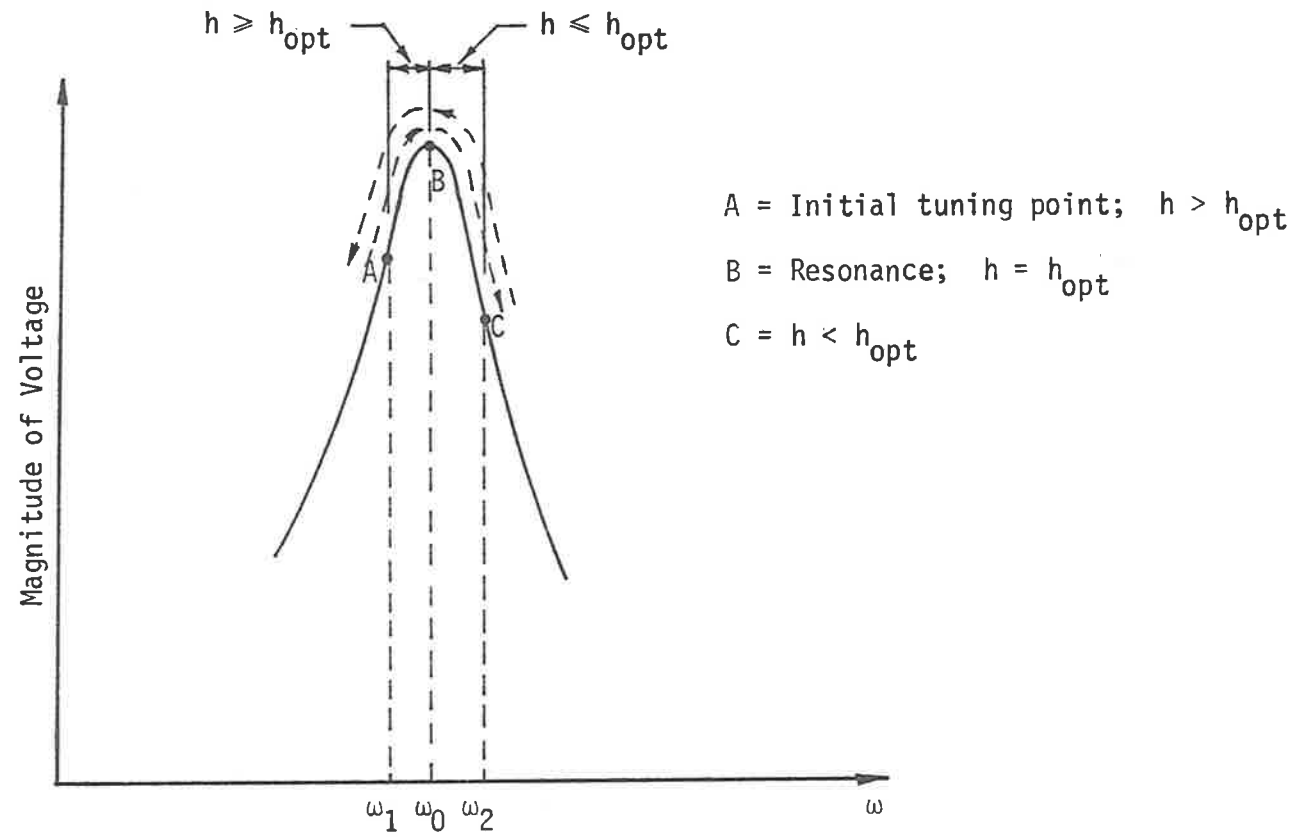
FIGURE 2.7 (b).   VARIATION OF THE VOLTAGE AS A FUNCTION OF

SEPARATION h IN RELATION TO OPTIMUM SEPARATION h_{opt}.

2.3 Signature Recording

Using the microprocessor based data acquisition system shown in Figure 2.8 the signatures of several vehicles were recorded by driving the vehicles at constant speed over the coupled coil sensor situated on a road surface at a controlled experimental site. The experimental set up showing the position of the sensor in relation to the vehicle is also illustrated in Figure 2.9.

The frequency components associated with the signatures are proportional to the speed and generally varies between 0.2 Hz at 5 Km/h to 150 Hz for vehicles travelling at 120 Km/h. In order to eliminate the influence of speed the signatures were time normalized i.e. either time-compressed or time-stretched such that they could be accommodated within a unity reference frame. Such an approach appeared promising since it provided the possibility for the development of a general principle for the classifications of vehicles where the influence of speed and vehicle length could be eliminated.

Augmentation of the limited already available data[20] by additional signatures enabled the creation of two data files. The first file contained time-normalized signatures of thirteen sedans and a Bedford truck. In this segment of data recording the vehicles were positioned centrally with respect to the sensor, as illustrated in Figure 2.10. The signatures corresponding to this file are shown in Figure 2.11(a) - (n).

Since the major perturbation of the signature is caused by lateral displacement of vehicles from the centre location, the second file held signatures of many trial runs associated with each

32.
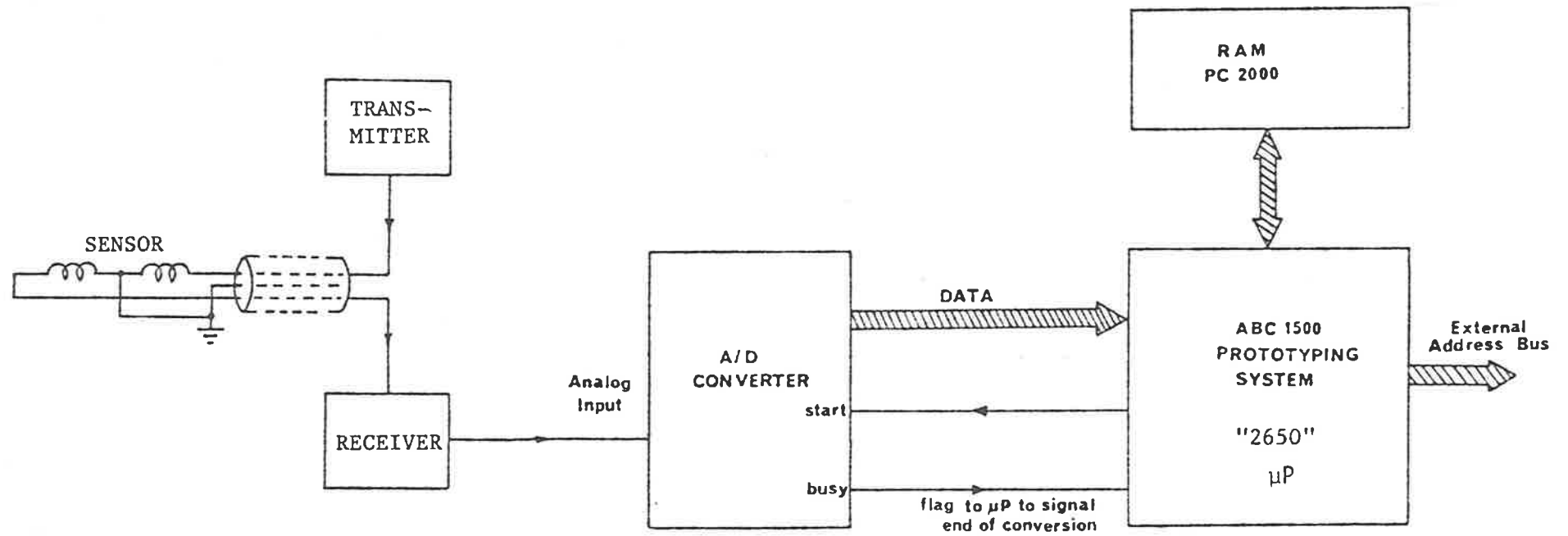
FIGURE 2.8.   MICROCOMPUTER BASED DATA ACQUISITION SYSTEM.

FIGURE 2.9.   EXPERIMENTAL SET UP SHOWING POSITION OF SENSOR RELATIVE TO THE VEHICLE.

Sensor

(a)

Sensor

d_c = displacement

(b)

Sensor

(c)
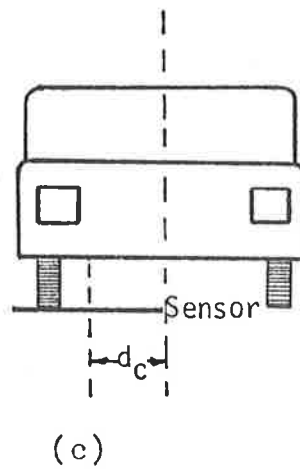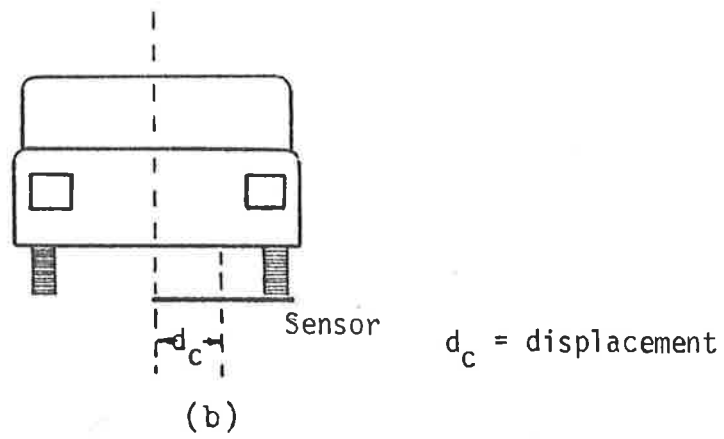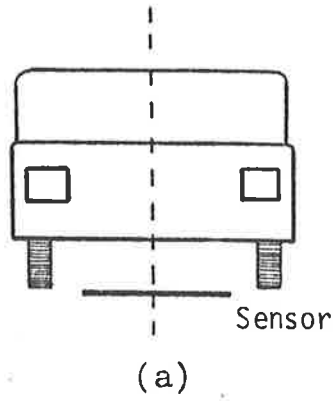
FIGURE 2.10. LATERAL DISPLACEMENT OF VEHICLE IN RELATION TO
THE SENSOR.

(a)   Centre Position.
(b)   Left Displacement
(c)   Right Displacement

FIGURE 2.11. SIGNATURES, DIFFERENTIATED SIGNAL AND BINARY REPRESENTATION OF THE ZERO CROSSING OF DIFFERENTIATED SIGNALS.

(a) 1972 Ford Futura.   (b) 1976 Chrysler Centura.   (c) 1974 Volvo.   (d) 1976 Datsun 180B.
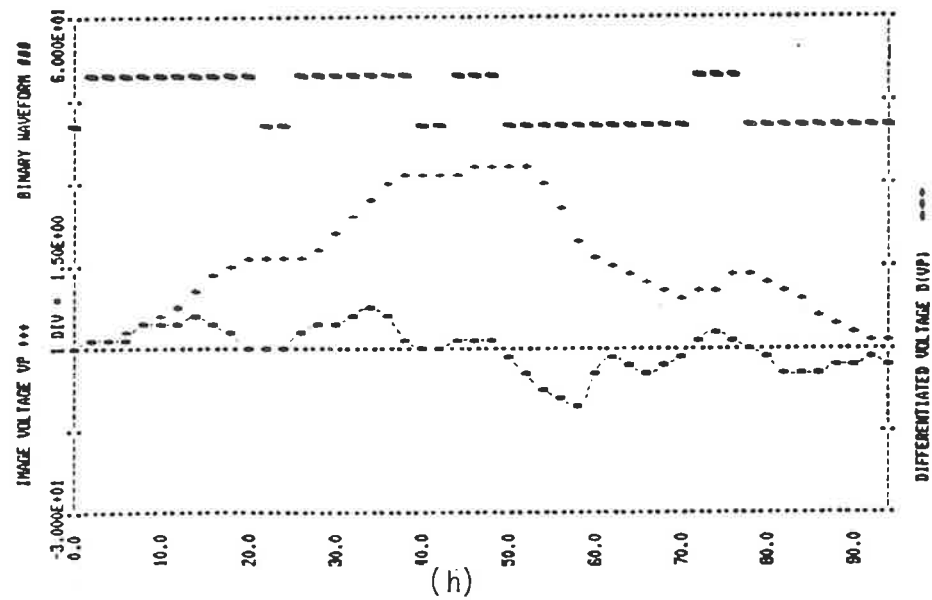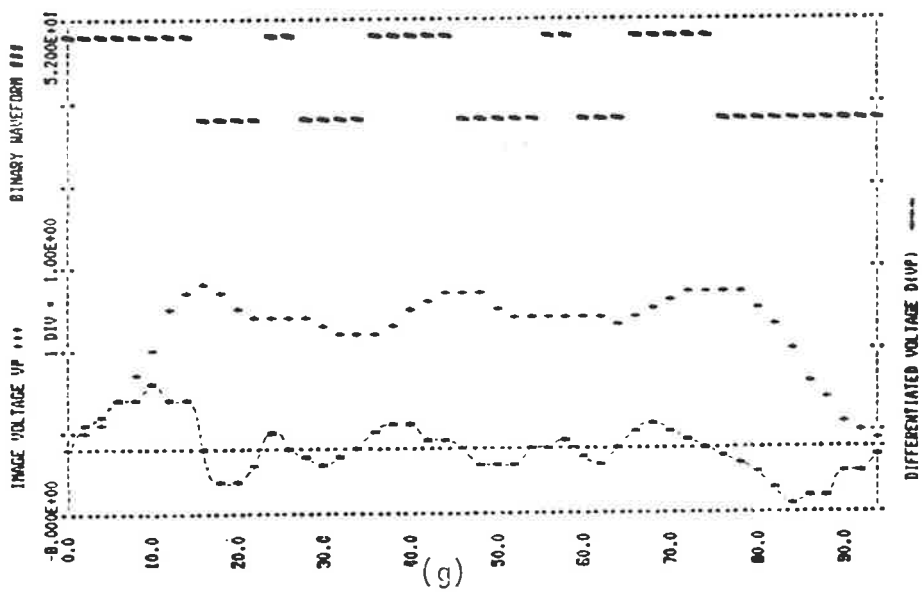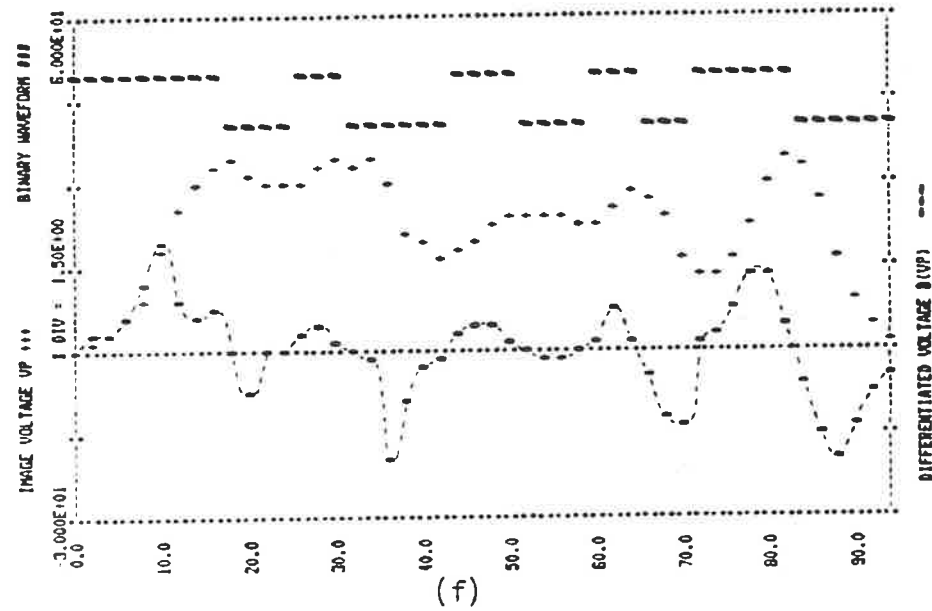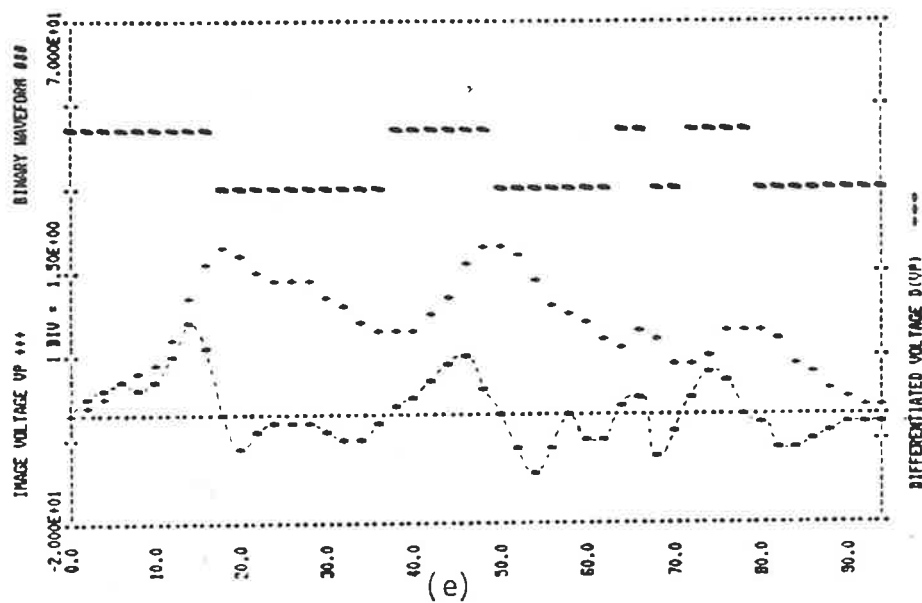
36.

FIGURE 2.11. SIGNATURES, DIFFERENTIATED SIGNAL AND BINARY REPRESENTATION OF THE ZERO CROSSING OF DIFFERENTIATED SIGNALS.

(e) 1966 Hillman.   (f) 1976 Valiant Wagon.   (g) Mazda 929.   (h) 1976 VW Passat.
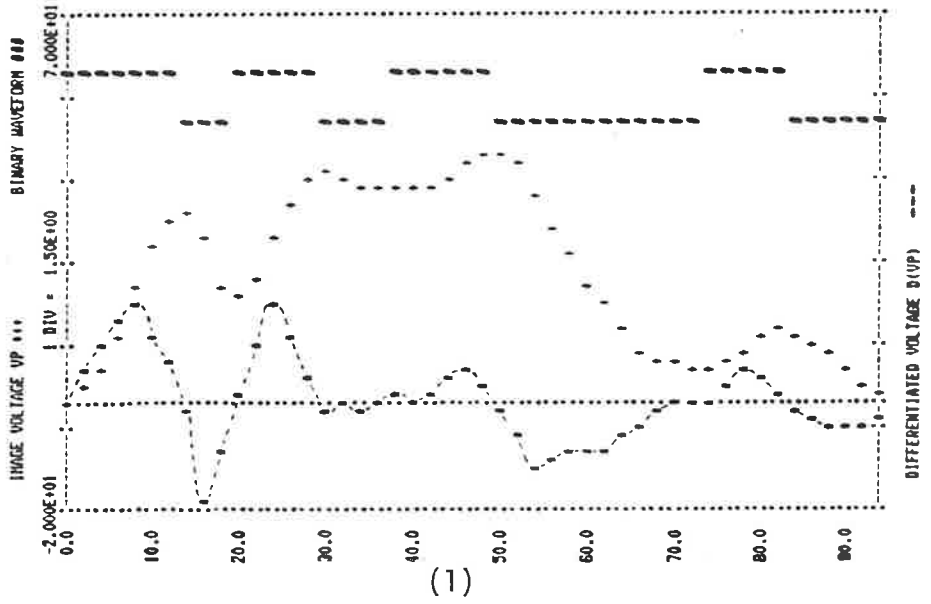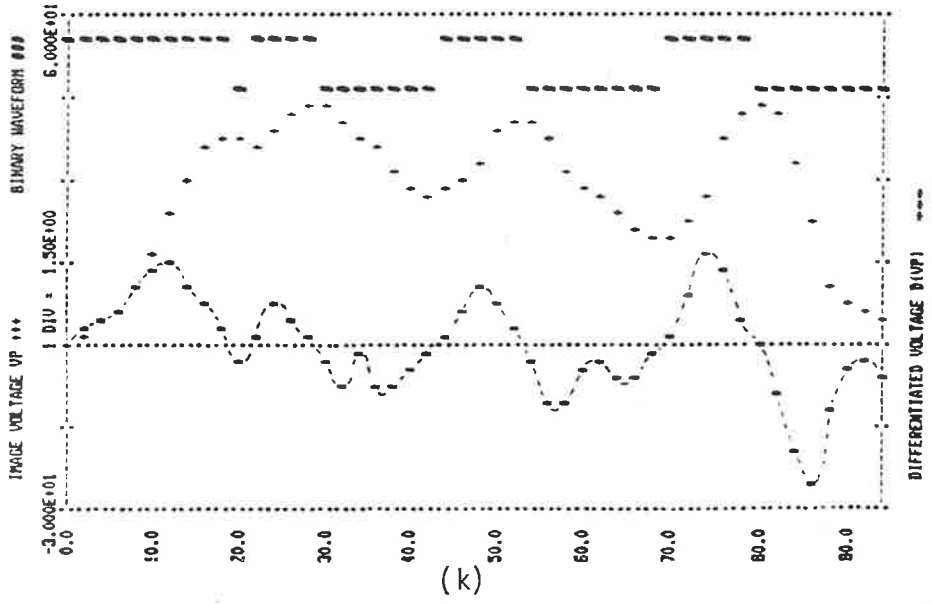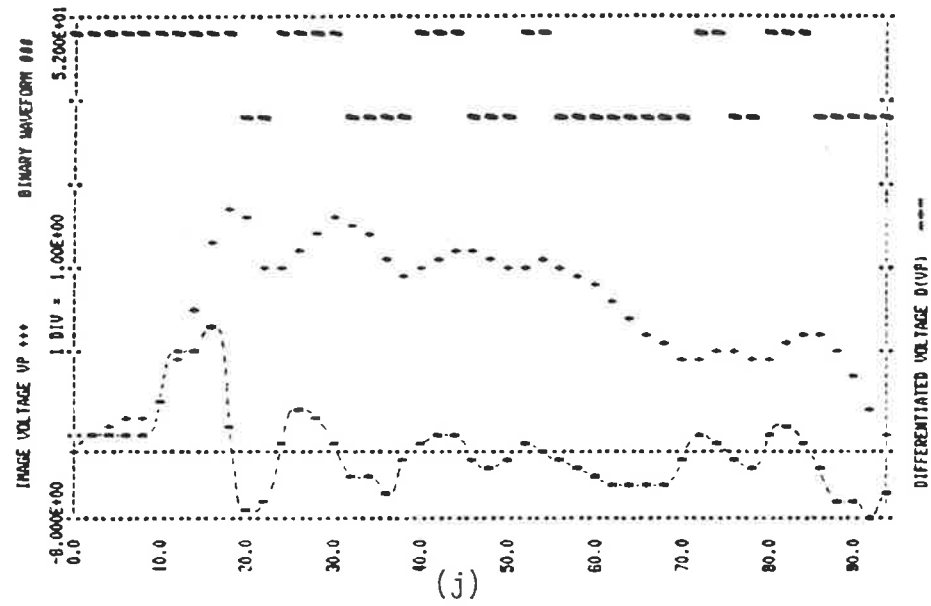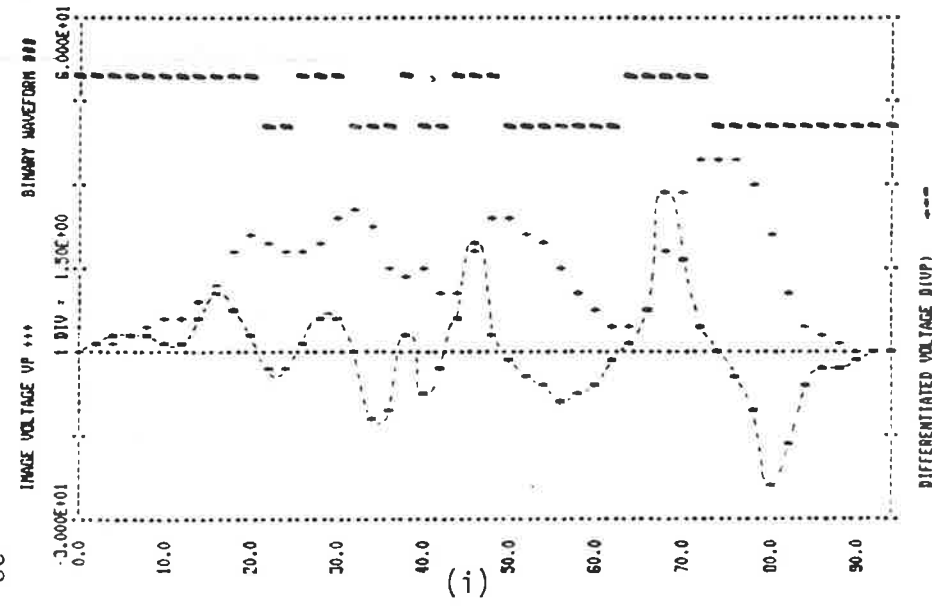
FIGURE 2.11.   SIGNATURES, DIFFERENTIATED SIGNAL AND BINARY REPRESENTATION OF THE ZERO CROSSING OF DIFFERENTIATED SIGNALS.

(i) Holden Kingswood.   (j) 1976 Cortina.   (k) 1976 Lancer.   (l) Fiat 124.
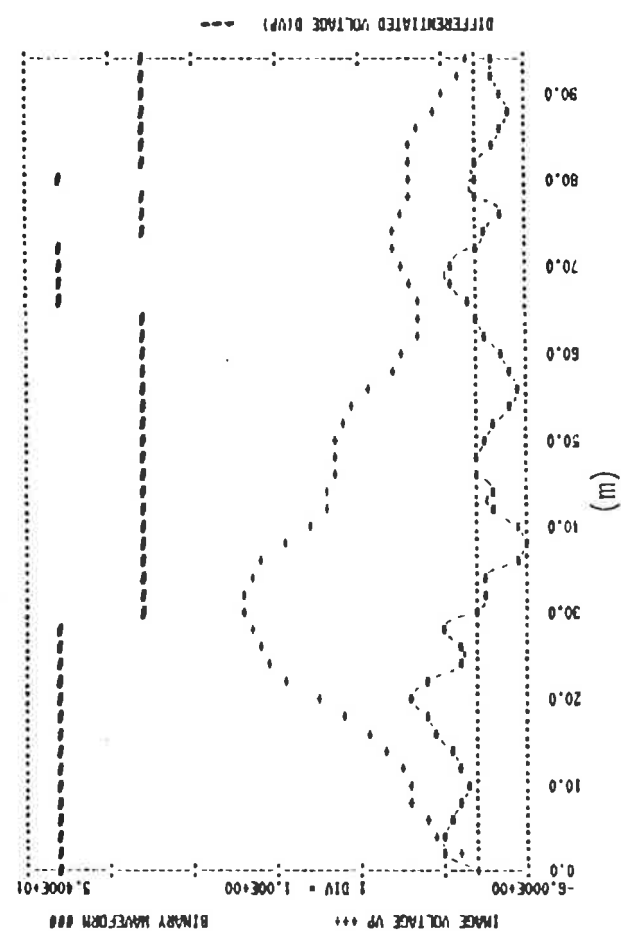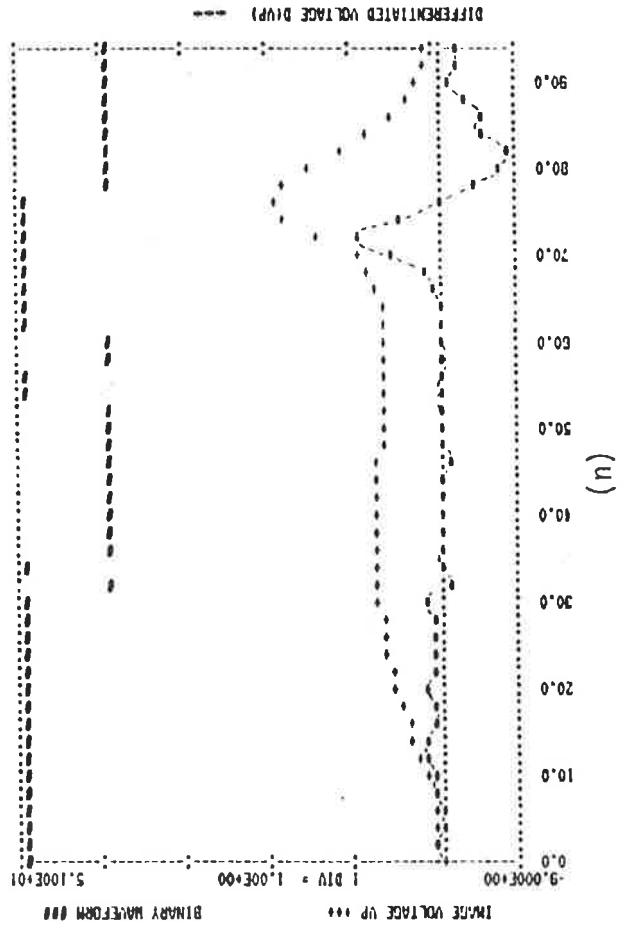
FIGURE 2.11. SIGNATURE, DIFFERENTIATED SIGNAL AND BINARY REPRESENTATION OF THE ZERO CROSSING OF DIFFERENTIATED SIGNALS.

(m) Escort.   (n) Ford Truck.

39.

of three vehicle makes and models appearing in the first file but displaced within ±25 cm limits[*] from centre position. The content of this file is illustrated by Figure B.1 (Appendix B).

2.4 Signature Analysis

Signature analysis and the subsequent vehicle classification can be approached in terms of the established field of "pattern recognition and verification"[50 - 57]. The problem of classification can be described in terms of labelling a group of objects on the basis of certain common behaviour and subjective requirements. The objects classified into the same class usually have some common properties based on a set of selected measurements extracted from input.

The measurements referred to as the "feature vector" can be arranged in the form of a multi-dimensional feature vector, $^i\tilde{X}$, written as

$$^i\tilde{X} = \left(^ix_1, \; ^ix_2, \; \ldots \; ^ix_n\right)^T ; \quad i = 1, 2, \ldots m \qquad (2.4)$$

where ^ix_j represents the jth feature measurement associated with class v_i, T is the transpose of the feature vector $^i\tilde{X}$ and n is the dimensionality.

---

* *The choice of ±25cm variation from centre position was based on the observation that vehicles travelling in guided sections tend to travel within the above limits.*

40.

If there are m different vehicle makes and models* denoted by vector $\tilde{V}$ written as

$$\tilde{V} = \left(v_1, \ v_2, \ \ldots \ v_m \right) \tag{2.5}$$

then the feature space can be considered as consisting of m regions, each of which encloses the feature points of a class. The classification problem can then be approached in terms of finding separating surfaces in n dimensions which will partition the feature space into m mutually exclusive regions.

Intuitively, it is expected that signatures of similar vehicles would produce feature vectors that are near to each other, whereas dissimilar vehicles which appear substantially different would produce feature vectors that are far apart. This assumption leads to the expectation that similar appearing signatures will produce groups of vectors that are close together in the feature space.

The determination of the separating surface can then be made through the use of "training" features or proto-types** whose correct classification is known.

---

*   Vehicle makes and models and vehicle class are one and the
     same thing in this text and often are used interchangeably.

**   "Training" features or proto-types refere to stored reference
     vectors.

41.

Thus in a typical process the characteristics of the signature
are first interpreted according to "features" which are known to
have some significance. The decision process is then performed by
comparing the presence or absence of such features.

A hierarchy of processing levels is shown in Figure 2.12, where
with input data present the data analysis is described in terms of
"feature selection" and "decision" formulation. Different methods
can subsequently be adopted to find out whether a pattern point
produced by the passage of a vehicle can be assumed to belong to a
given vehicle or not.

2.5 Feature Vector Characterisation

The selection of features is generally considered as the most
important part of studies associated with many of the pattern
recognition concepts[58] [62] and is closely related to the perfor-
mance of the classification systems. In order to extract convenient
features from the signature two broad methods have been considered:

(i)   frequency domain, where the frequency components of the
        signature are considered as the elements of the feature
        vector;

(ii)   time-dependent, in which the components of the feature vector
        are derived from the time function.

42.

Vehicle Sensor

R_X T_X

Lead-in Cable

INPUT DATA PROCESSOR

FEATURE EXTRACTOR

x_1
x_2
x_3
x_N

CLASSIFIER

Output
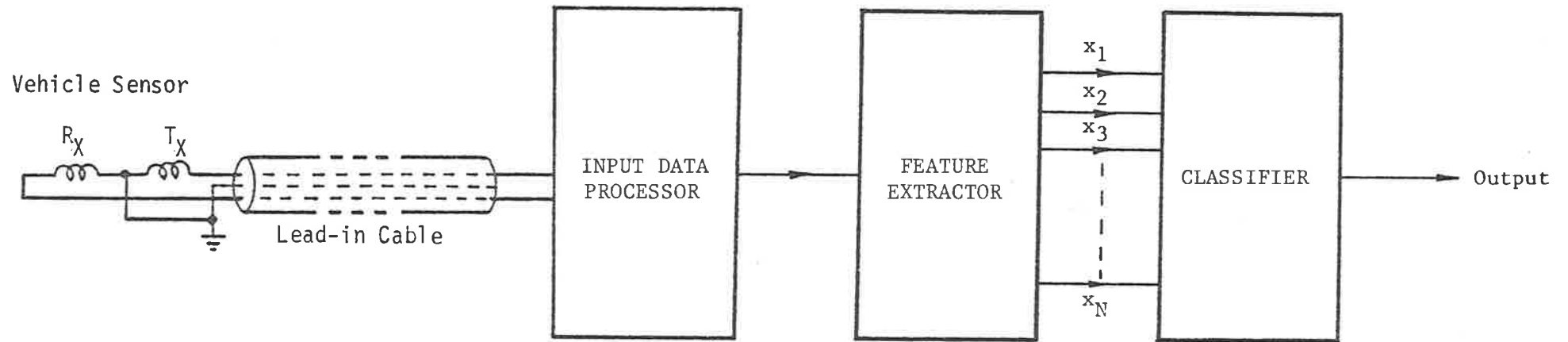
$$\tilde{X} = (x_1, \ x_2, \ \ldots \ x_n)^T$$

FIGURE 2.12.   A TYPICAL APPROACH TO THE CLASSIFIER DESIGN.

Since the main objective in this section is to provide guide-
lines for the future work and to establish qualitative estimates
to the kind of results one can expect, several possibilities
associated with each of the two approaches are explored.

2.5.1 Frequency Domain Analysis

The components of the feature vector characterising a
vehicle in the frequency domain can be described in terms
of the coefficients of the Fourier spectrum given by,

$$g(\omega t) = {}^{i}A_{0} + \sum_{k=1}^{\infty} {}^{i}A_{n} \cos k\omega t + \sum_{k=1}^{\infty} {}^{i}B_{n} \sin k\omega t; \quad i = 1, 2, \ldots, m. \quad (2.6)$$

The components of the feature vector are subsequently
written in terms of the amplitude coefficients ${}^{i}C_{n}^{\prime}$ defined
as

$$
{}^{i}C_{n}^{\prime} = \sqrt{{}^{i}A_{n}^{2} + {}^{i}B_{n}^{2}} \; ; \quad n = 1, 2, \ldots \quad (2.7)
$$
$$
; \quad i = 1, 2, \ldots m
$$

It is possible to normalize the amplitude terms as
defined by Equation (2.7) with respect to the fundamental
components ${}^{i}C_{1}^{\prime}$. The modified relation is

$$^iC_n = \frac{^iC_n'}{^iC_1'} \; ; \quad \begin{array}{l} i = 1, 2, \ldots , m \\ \\ n = 1, 2, \ldots , \end{array} \qquad (2.8)$$

The feature vector in terms of Equation (2.8) can be expressed as

$$^i_c\tilde{X} = \left(1, \; ^iC_2, \; ^iC_3, \; \ldots , \; ^iC_n\right)^T \qquad (2.9)$$

where the fundamental component is now considered as redundant. The feature vector for centrally positioned vehicles is identified by inclusion of an "asterisk" i.e. $^i_{*c}\tilde{X}$.

The spectral analysis was performed by using 1024 sample data points windowed by a Gaussian window to limit the influence of the higher order frequency components, and Fourier transformed giving the frequency components. Graphical representation of the normalized Fourier spectrums for the first data file corresponding to Figures 2.11(a) - 2.11(n) are shown in Figure 2.13. Details of the Fourier components for the two files as described in Section 2.3, are also tabulated in Tables B.1 - B.2 (Appendix B).

In order to describe the variation of the signatures as a function of the random displacement, the signatures in the second file corresponding to the several trial runs by

45.
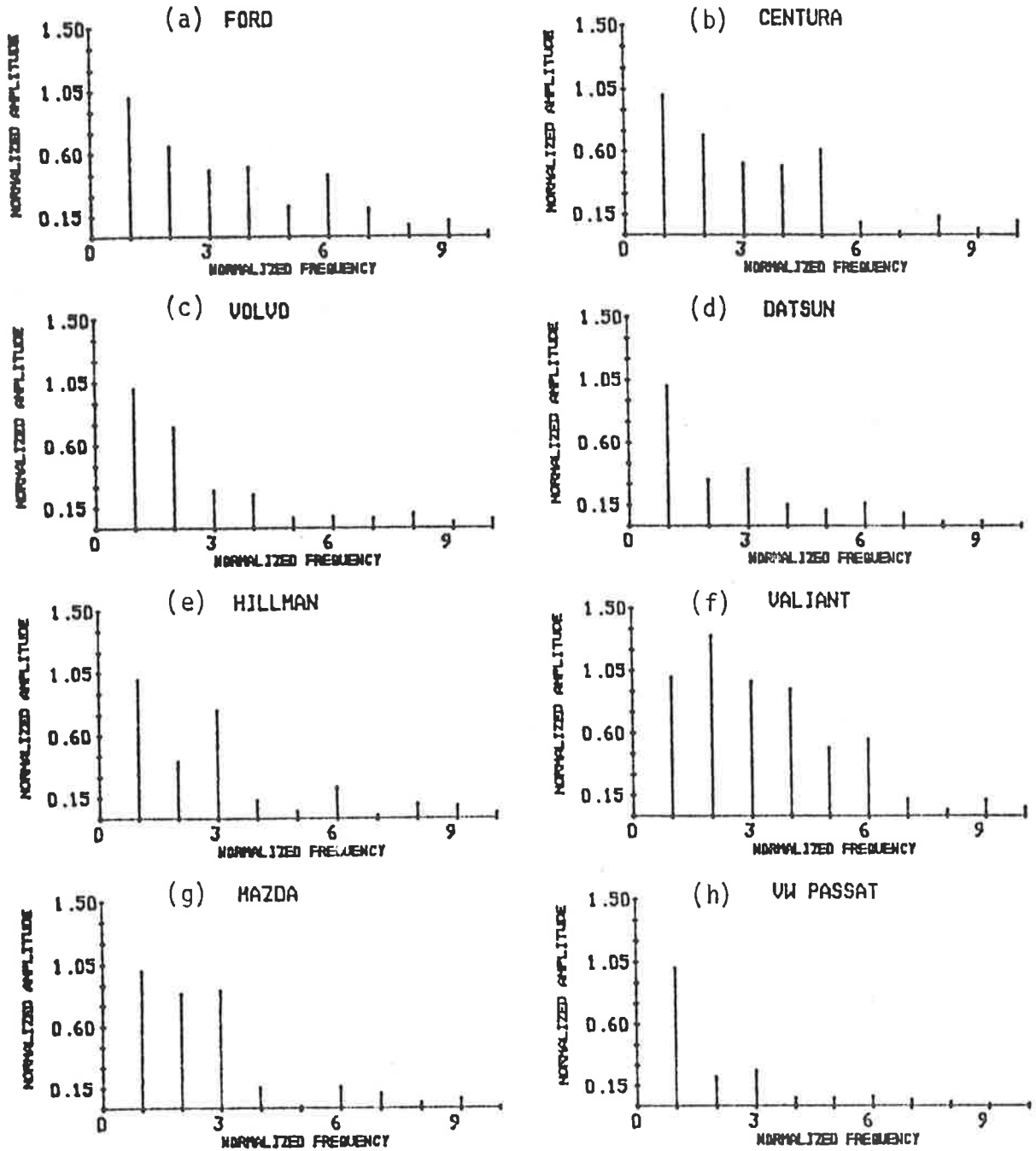
FIGURE 2.13 (a) - (h). NORMALISED AMPLITUDES OF FEATURE VECTOR $_c^i\tilde{X}$

AS A FUNCTION OF NORMALISED FREQUENCY.

46.
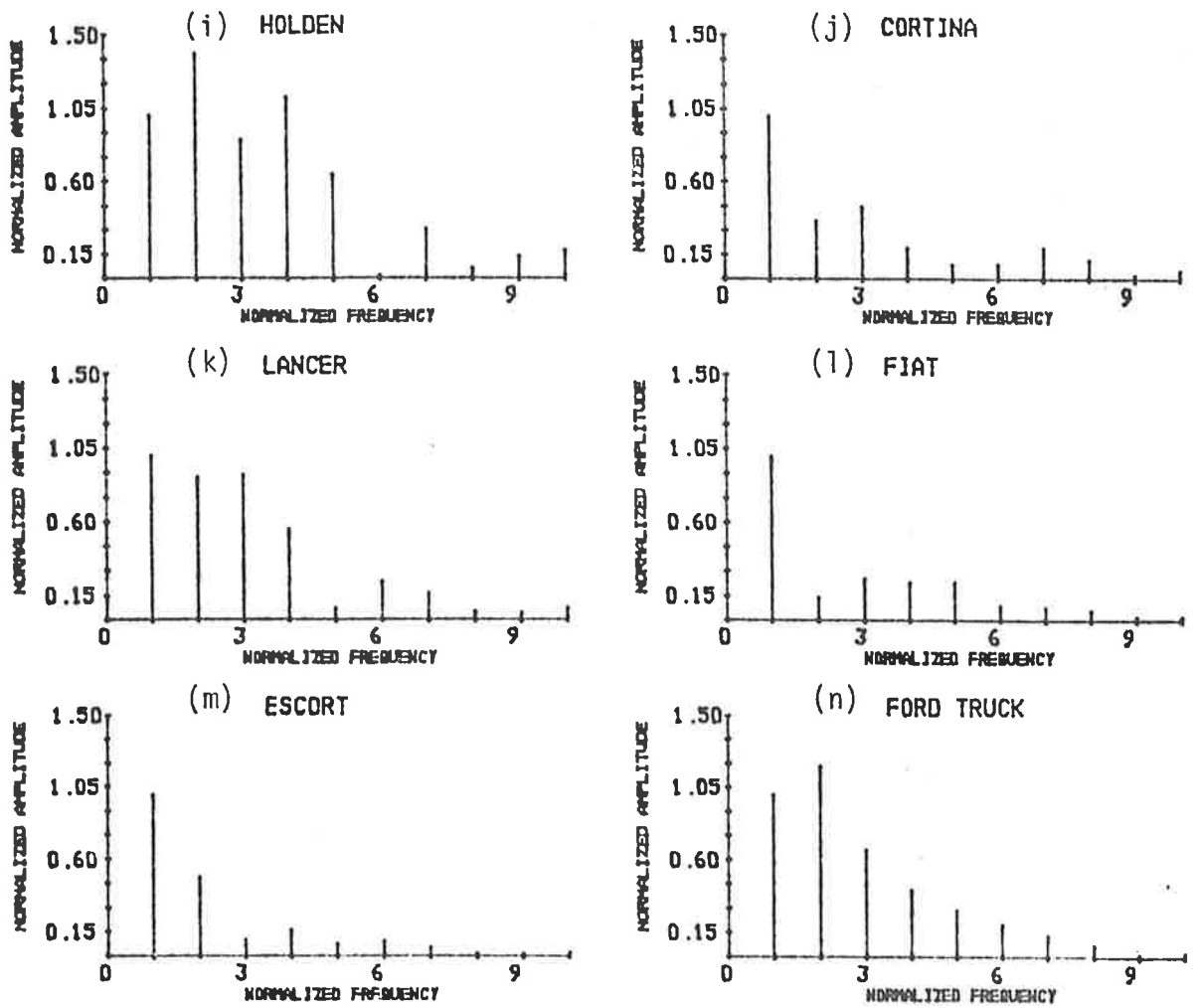
FIGURE 2.13 (i) - (n). NORMALISED AMPLITUDES OF FEATURE VECTOR $_c^i\tilde{X}$

AS A FUNCTION OF NORMALISED FREQUENCY.

47.

three vehicles of different makes and models were analysed to produce the sample means ${}^{i}\hat{C}_{n}$ and variances σ_{c}^{2}, expressed as

$$ {}^{i}\hat{C}_{n} = \frac{1}{N} \sum_{j=1}^{N} {}^{i}C_{nj} \qquad (2.10) $$

and

$$ \sigma_{c}^{2} = \frac{1}{N} \sum_{d=1}^{N} \left({}^{i}C_{nj} - {}^{i}\hat{C}_{nj} \right)^{2}; \quad i = 1, 2, \ldots, m. \qquad (2.11) $$

The results of these analyses are tabulated in Tables 2.1 - 2.2. Several properties may be inferred from the tables. Firstly, since the variances are roughly the same, then the cluster domains can be expected to be approximately similar and somewhat spherical in nature. The measurements corresponding to small variances are more reliable and perhaps can be considered as being more significant for the classification process.

Secondly, when it is known or can be assumed that the probability density function $p({}^{i}\tilde{x}/v_{i})$ are normal, then such an assumption provides a means for analytical traceability. Normally distributed samples tend to cluster about the mean, with a dispersion proportional to the standard deviation σ. 95% of the samples drawn from a normal popula-

TABLE 2.1. THE MEAN VALUES OF THE NORMALIZED FOURIER COEFFICIENT $^{i}c_n$ FOR THREE VEHICLES WITH ±25cm DISPLACEMENT LIMITS

$\tilde{V}$ \ MEAN	$\hat{c}_1$	$\hat{c}_2$	$\hat{c}_3$	$\hat{c}_4$	$\hat{c}_5$	$\hat{c}_6$	$\hat{c}_7$	$\hat{c}_8$	$\hat{c}_9$	$\hat{c}_{10}$
Ford	1.0	0.65	0.50	0.51	0.21	0.43	0.19	0.0	0.11	0.0
Centura	1.0	0.82	0.55	0.48	0.64	0.11	0.0	0.14	0.0	0.09
Datsun	1.0	0.33	0.40	0.14	0.11	0.17	0.09	0.0	0.0	0.0

49.

TABLE 2.2. THE VARIANCES OF THE NORMALIZED FOURIER COEFFICIENT $^{i}c_n$ FOR THREE VEHICLES WITH ±25cm DISPLACEMENT LIMITS

$\tilde{V}$ \ Variance	σ_1	σ_2	σ_3	σ_4	σ_5	σ_6	σ_7	σ_8	σ_9	σ_{10}
Ford	0.0	0.06	0.04	0.05	0.09	0.05	0.09	0.05	0.05	0.04
Centura	0.0	0.14	0.10	0.03	0.08	0.08	0.03	0.02	0.02	0.02
Datsun	0.0	0.02	0.04	0.02	0.03	0.02	0.03	0.02	0.02	0.02

tion will fall within the 2σ centred about the mean. Due to limited data no firm conclusions can be made in regards to the statistical description of the feature vector ${}^{i}\tilde{X}_{c}$ based on the results of Tables 2.1 - 2.2. However the analysis has provided an insight into the kind of variations one could expect if the lateral displacement is controlled within some specified limits.

In order to explore the possibility of utilising the data in the first file in the absence of suitable statistical descriptions, it appeared sensible for the analysis to be extended to observe the difference that exists between the mean value of Fourier component ${}^{i}\hat{C}_{n}$ and the component ${}^{i}\overset{*}{C}_{n}$ obtained when a vehicle is located centrally with respect to the sensor. Such representation for the second file is described in terms of the percentage error E_{c}, given by

$$E_{c} = \left| \frac{{}^{i}\hat{C}_{n} - {}^{i}\overset{*}{C}_{n}}{{}^{i}\hat{C}_{n}} \right| \times 100\% \qquad (2.12)$$

and is tabulated in Table 2.3. The results indicate that if the Fourier components ${}^{i}\overset{*}{C}_{n}$ are used instead of the mean values ${}^{i}\hat{C}_{n}$, a worst case error in the order of 15% can be expected when the lateral displacement is controlled within the ± 25 cm deviation.

Although no classification scheme could be based on exactly single runs, the results obtained is suggestive of

50.

TABLE 2.3. COMPARISON BETWEEN MEAN VALUES OF NORMALIZED FOURIER COEFFICIENTS AND THOSE DERIVED WITH VEHICLES LOCATED CENTRALLY - EXPRESSED AS PERCENTAGE ERROR

$\tilde{V}$ \ E_c	Fourier Coefficients									
	1	2	3	4	5	6	7	8	9	10
Ford	0	0.3	4.9	1.7	5.1	1.5	0.6	9.5	4.4	13
Centura	0	12.8	4.8	3.0	3.8	16.4	0	6.3	0	17.4
Datsun	0	2.0	1.0	9.7	4.9	2.3	2.1	0	0	0

$$E_c = \left| \frac{\hat{C}_n - \overset{*}{C}_n}{\hat{C}_n} \right| \times 100\%$$

$$\hat{C}_n = \frac{1}{N} \sum_{j=1}^{N} C_{nj}$$

the fact that single runs results with no displacement, are representative of the multiple run results when lateral displacement is controlled. This is highly desirable, since the feature vector can now be described from a single run by a vehicle positioned centrally with respect to the sensor. On the basis of this observation further analysis of the first file as shown in Figures 2.11(a) - (n) appeared warranted. Therefore the fourteen signatures in the first file are used as a representative of fourteen different classes of vehicles.

An alternative description of the feature vector as defined by Equation (2.13) provides the possibility of increasing the influence of the higher order frequency components. This is achieved by differentiating the Fourier series giving

$$\dot{g}(\omega_0 t) = - \sum_{k=1}^{\infty} k \, {}^i\!A_n \sin k \, \omega_0 t + \Sigma \, k \, {}^i\!B_n \cos k \, \omega_0 t; \quad i = 1,2,\ldots,m. \quad (2.13)$$

From Equation (2.13) we note that the components of the feature vector are modified by the order of the harmonics. The magnitude of the feature vector components normalised with respect to the fundamental component ${}^i\!C_1$ can be expressed as

$$^i\!d_n = k \; ^i\!C_n; \quad i = 1, 2, \ldots, m \quad (2.14)$$
$$k = 1, 2, \ldots, n$$

52.

The feature vector based on this description is

$$\begin{array}{c} i\\ d \end{array}\tilde{X}_n = \left[1, \ {}^{i}d_2, \ {}^{i}d_3, \ \ldots, \ {}^{i}d_n\right] \quad i = 1, 2, \ldots, m. \qquad (2.15)$$

The result of this analysis corresponding to the second files for the three vehicles are shown in Table B.3 (Appendix B).

Changes in the amplitudes of components of $\begin{array}{c} i\\ c \end{array}\tilde{X}_n$ due to the displacement of the vehicle from the centre position may be represented by an error term Δc. Incorporation of Δc in Equation (2.14) results in

$$\begin{array}{ll} {}^{i}d_n = k\left({}^{i}C_n \pm \Delta c\right) ; & i = 1, 2, \ldots, m.\\ & n = 1, 2, \ldots. \end{array} \qquad (2.16)$$

$$= k \ {}^{i}C_n \pm k \ \Delta c$$

Although the contribution by the higher order harmonics are magnified as the result of the differentiation process, the corresponding variation in the amplitude terms as the consequence of the vehicle displacement, is also amplified. The resultant effect leads into substantial errors when higher order harmonics are implemented.

The suspicion was in fact confirmed by the detailed analysis of the data in the second file. Thus, this approach is considered unsuitable for further investigations.

2.5.2   Time-Dependent Analysis

The time-dependent analysis method is based on the principle of zero crossing measurements. A zero crossing can be said to occur between instants k and (k - 1) if

$$\text{sign}\big(x(k)\big) \neq \text{sign}\big(x(k - 1)\big) \qquad (2.17)$$

where

$x(kt) =$ discrete-time real signal

$t =$ period

Such an approach is motivated by the observation that if the signal is a sinusoid of frequency ω, then the average number of zero crossing is 2ω crossings per second. Whereas this is true for a sinusoid, the interpretation of zero crossing measurements is rather trivial and its use is very limited when directly applied to vehicle signatures. However by differentiating the signature it is possible to detect relative locations of peaks and troughs in the original waveform by observing the zero crossings of the differentiated signal.

Thus, in this approach the feature vector $_b^i\tilde{X}$ is described by

$$_b^i\tilde{X} = \left({}^i b_1, \; {}^i b_2, \; \ldots, \; {}^i b_n \right)^T \; ; \; i = 1, 2, \; \ldots, m \qquad (2.18)$$

54.

where the components of the feature vector $_b^i\tilde{X}$ are obtained by dividing the binary waveform derived from the binary representation of the zero crossings of the differentiated signature, into N equally spaced segments. The dimension of the feature vector in this case is equal to the number of segments N chosen. This approach is shown in Figure 2.14. Tabulation of the results corresponding to signatures in the two files are also presented in Table B.4 and Table B.5 (Appendix B). Several values of N were considered. It was found that the minimum value that can be utilized without noticeable variation in $_b^i\tilde{X}$ was in the order of 90. Therefore N was chosen as 96, which permitted the vehicle signature to be represented by twelve 8-bit words. This structure is compatible with 8-bit microprocessors for subsequent data manipulation.

In this representation where the components of the binary vector $_b^i\tilde{X}$ can take the two possible values of '1' or '0' the definition of the 'mean' becomes ambiguous. However on the basis of the alternative description in terms of the correlation between two binary vectors, an initial exploratory data analysis was carried out. The results based on the data in Table B.5 indicated that the elements of the feature vector corresponding to several runs of the same vehicle were highly correlated. Therefore this method also warranted further investigation.

A variation of the above approach provided an alternative method for describing the components of the feature vector in terms of the ratio of the length associated with the binary waveform written as

$$_u^i\tilde{X} = \left(^iu_1, \ ^iu_2, \ \ldots, \ ^iu_k \right)^T; \quad i = 1, 2, \ldots, m. \quad (2.19)$$

where
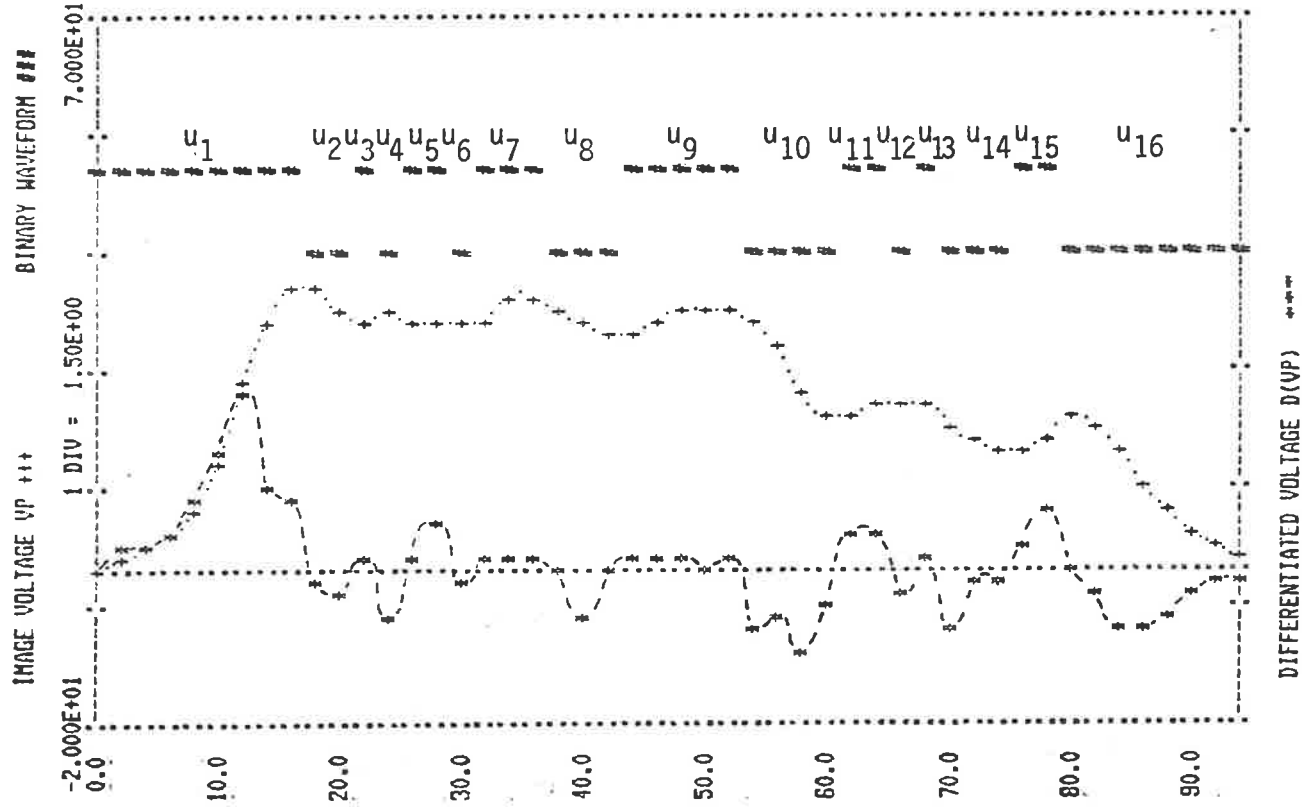
FIGURE 2.14. TYPICAL WAVEFORMS FOR DETERMINATION OF UNDERCARRIAGE VECTOR $i\tilde{u}X$ AND $i\tilde{b}X$.

56.

$$^i u_k = \frac{q^i_k}{t_p} ; \quad i = 1, 2, \ldots, m. \tag{2.20}$$

$$k = 1, 2, \ldots .$$

and

$^i q_k$ = duration of the interval corresponding to the kth section of the binary representation of the zero crossings of the differentiated signal associated with i^{th} class;

t_p = total duration of the signal.

Typical waveforms which describes Equation (2.20) are illustrated by Figure 2.14. The elements of the feature vector $^i_u \tilde{X}$ corresponding to first file are also tabulated in Table B.6 (Appendix B).

The emphasis placed on the ratio of lengths of the elements of the feature vector corresponds to an scaling process and ensures that $^i_u \tilde{X}$ is independent of the vehicle's speed. Therefore some savings in the computational time during pre-processing of data can be expected.

Although this procedure showed an early promise, two remarks are pertinent at this stage. Firstly, from Table B.6 (Appendix B), it is evident that the dimensions of the feature vector $^i_u \tilde{X}$ associated with each class of vehicle are not necessarily the same. This implies that conventional techniques as used in pattern matching to be described in the next section, can not be applied directly.

Secondly, a detailed analysis of the second file indicated that vehicles of the same make and model when displaced from centre position may have different dimensions. Therefore, unless the lateral displacement of the vehicles are tightly controlled large errors can be expected in the classification process. Thus this method was precluded from further analysis.

2.6 Classification Process

An important class of linear classifiers uses the distances between the input feature vector $\tilde{Y}$ and a set of reference vector points in the feature space as the classification criterion[63][64]. The proposal to use distance functions as classification tools follows from the fact that the most obvious way of establishing a measure of similarity between vectors is by determining their proximity.

If there are m possible classes of vehicles designated by v_1, v_2, ..., v_m, then $\tilde{Y}$ is assigned to class v_i if $^iD < {}^jD$ for all $j \neq i$. This can be written in a more convenient form:

$$\tilde{Y} \in v_i; \quad \text{if } {}^iD < {}^jD \text{ for all } i \neq j. \tag{2.21}$$

Thus the classification looks for the smallest distance D between the unknown vector $\tilde{Y}$ and the stored vector $^i\tilde{X}$.

58.

In a classification trial the information stored in a reference file is compared with information extracted from the signature of an unknown vehicle. This comparison may be defined in terms of Euclidean distance D_E given by the unknown vector $\tilde{Y}$ and stored reference vector $\tilde{X}$ associated with class i. This is expressed as

$$^iD_E\left(^i\tilde{X},\tilde{Y}\right) = \sqrt{\left(^i\tilde{X} - \tilde{Y}\right)^T \left(^i\tilde{X} - \tilde{Y}\right)}$$

$$= \sqrt{\sum_{i=1}^{n} \left(x_i - y_i\right)^2} \qquad (2.22)$$

For binary vectors corresponding to $^i_b\tilde{X}$ an alternative approach may be implemented. The proximity of an unknown vector $\tilde{Y}$ to the stored feature vector $^i\tilde{X}$ can be expressed in terms of the correlation $R(^iX,Y)$, written as

$$R(^iX,Y) = \frac{1}{n} \sum_{j=1}^{n} {}^ix_j\, y_j\,;\ i = 1,\, 2,\, \ldots,\, m. \qquad (2.23)$$

The equivalent definition of correlation for binary vectors in terms of 'one' and 'minus one' representation is then

$$R(^iX,Y) = \frac{A - D}{A + D} \qquad (2.24)$$

where

A = number of term-by-term agreements of $^i\tilde{X}$ with $\tilde{Y}$.

D = number of term-by-term disagreements of $^i\tilde{X}$ with $\tilde{Y}$.

By subtracting the true correlation from 1 we obtain the proximity measure ^iD_r expressed as

$$D_r = 1 - R \, (^iX, \, Y) \, . \tag{2.25}$$

The above process has the technically desirable feature of requiring only a binary representation of the zero crossings of the differentiated waveforms and is therefore conveniently compatible with pattern matching by polarity correlation using serial access to stored data.

As a first approach in exploring the potential of the proximity measure for vehicle classification, based on Equation (2.22), the feature vectors $^i_{\hat{c}}\tilde{X}$ corresponding to the mean values of the Fourier components in the second file, and the components obtained for no lateral displacement, were used to construct proximity measure tables as illustrated by Tables 2.4 - 2.5. The magnitude of entries denoted by $_{\hat{c}}D_E$ and $_{\overset{*}{c}}D_E$ indicates the relative measure of similarity between two vectors.

The difference between the corresponding proximity measures in the two tables are described by the error E_d, given by

$$E_d = \left| \frac{_{\hat{c}}D_E - _{\overset{*}{c}}D_E}{_{\hat{c}}D_E} \right| \times 100\% \tag{2.26}$$

indicate that this difference is less than 10% when $^i_{\overset{*}{c}}\tilde{X}$ is chosen instead of $^i_{\hat{c}}\tilde{X}$.

60.

TABLE 2.4. PROXIMITY MEASURES IN TERMS OF EUCLIDEAN DISTANCE D_E WITH $^i\hat{C}_n$ AS THE COMPONENTS OF THE STORED REFERENCE VECTOR $^i_c\tilde{X}$

$_c^{\wedge}D_E$ $\tilde{V}$	Ford							
	0	a	b	c	d	e	f	g
Ford	0.04	0.08	0.09	0.10	0.05	0.05	0.05	0.11
Centura	0.59	0.61	0.61	0.64	0.60	0.60	0.58	0.53
Datsun	0.59	0.62	0.61	0.58	0.63	0.58	0.57	0.60

$_c^{\wedge}D_E$ $\tilde{V}$	Centura							
	0	a	b	c	d	e	f	g
Ford	0.57	0.59	0.89	0.62	0.52	0.70	0.58	0.51
Centura	0.12	0.09	0.53	0.09	0.15	0.15	0.10	0.19
Datsun	0.76	0.81	1.27	0.82	0.70	0.90	0.77	0.68

$_c^{\wedge}D_E$ $\tilde{V}$	Datsun							
	0	a	b	c	d			
Ford	0.59	0.60	0.61	0.59	0.58			
Centura	0.82	0.83	0.85	0.83	0.81			
Datsun	0.02	0.15	0.05	0.04	0.05			

Notes: Number of trials associated with each vehicle.

(i)   Ford   —   8 trials
(ii) Centura —   8 trials
(iii) Datsun   —   5 trials

TABLE 2.5. PROXIMITY MEASURES IN TERMS OF EUCLIDEAN DISTANCE D_E WITH $^i C_n^*$ AS THE COMPONENTS OF THE STORED REFERENCE VECTOR $^j_c \tilde{X}$

$^*_c D_E$ / $\tilde{V}$	Ford							
	0	a	b	c	d	e	f	g
Ford	0	0.11	0.12	0.12	0.05	0.04	0.03	0.09
Centura	0.57	0.59	0.59	0.61	0.58	0.58	0.56	0.51
Datsun	0.58	0.61	0.61	0.57	0.63	0.57	0.57	0.59

$^*_c D_E$ / $\tilde{V}$	Centura							
	0	a	b	c	d	e	f	g
Ford	0.57	0.58	0.89	0.62	0.51	0.69	0.58	0.51
Centura	0	0.12	0.64	0.08	0.16	0.22	0.04	0.10
Datsun	0.75	0.80	1.21	0.81	0.70	0.90	0.77	0.67

$^*_c D_E$ / $\tilde{V}$	Datsun							
	0	a	b	c	d			
Ford	0.58	0.60	0.61	0.59	0.58			
Centura	0.75	0.76	0.78	0.76	0.74			
Datsun	0	0.05	0.06	0.04	0.06			

Notes: *Number of trials associated with each vehicle:*

(i)   Ford   – 8 trials
(ii)   Centura – 8 trials
(iii) Datsun – 5 trials

The corresponding analysis associated with the binary vector $_b^i\tilde{X}$ uses Equation (2.25) to construct the proximity measure table in which the data from several runs are correlated with that of centrally positioned vehicles. This is illustrated in Table 2.6 in which the table entries are denoted by D_r. From the table we note that the magnitude of D_r is subject to approximately 15% variation from different trials.

Based on the above analysis it is now possible to extend the approach to the data for centrally positioned vehicles with some degree of assurance.

Since the proximity of two signals is a relative measure of similarity, it is necessary to establish some rules upon which to evaluate the performance.

2.6.1   Performance Evaluation

The performance of the proximity measures as expressed by Equation (2.22) and Equation (2.23) may be modelled in terms of the error rates ε_a, ε_r and threshold level β. These parameters are defined as

$$\varepsilon_a = \frac{\text{number of false acceptance}}{\text{total number}} \qquad (2.27)$$

$$\varepsilon_r = \frac{\text{number of false rejection}}{\text{total number}} \qquad (2.28)$$

and

$$\beta = K \hat{D} (k, m) \qquad (2.29)$$

63.

TABLE 2.6. PROXIMITY MEASURE D_r WHEN FEATURE VECTOR ${}_b^i\tilde{x}$ IS USED AS THE STORED SIGNATURE.

D_r	Number of Trials						
	a	b	c	d	e	f	g
Ford	0.12	0.12	0.25	0.01	0.06	0.02	0.17
Centura	0.19	0.17	0.04	0.23	0.27	0.02	0.08
Datsun	0.08	0.06	0.15	0.29	-	-	-

where K is used as a scaling factor having an adjustable range between 0 - 1 and

$$\hat{D}(k,m) = \frac{1}{mk} \sum_{i=1}^{m} \sum_{j=1}^{k} D_{ji} \qquad (2.30)$$

k and m are further defined as

k = total number of signatures per class,

m = total number of vehicle classes.

In general the value of β can be adjusted in accordance to some performance criteria, such as minimizing the probabilities of error when making the following decisions:

$$D \leqslant \beta \left\{ \begin{array}{l} \text{the unknown vehicle is the same as} \\ \text{the stored reference signature.} \end{array} \right. \qquad (2.31)$$

$$D > \beta \left\{ \begin{array}{l} \text{the unknown vehicle is different} \\ \text{from stored reference signature} \end{array} \right. \qquad (2.32)$$

The overall classification process may then be assessed by the performance factor P expressed by

$$P = S_1 \varepsilon_a + S_2 \varepsilon_r \qquad (2.33)$$

where

S_1 = cost for false acceptance.

S_2 = cost for false rejection.

S_1 and S_2 are functions of the traffic control strategy and may be obtained empirically.

As an approximate approach in assessing the potential of this research, the data in the first file corresponding to centrally located vehicles were used to create both a reference signature table as well as to represent the unknown input signatures.

Based on the definition of the proximity measures given by Equation (2.22) and Equation (2.25), two 14 × 14 proximity tables corresponding to $_c^i\tilde{X}$ and $_b^i\tilde{X}$ were constructed. The results of this analysis which have been normalized with respect to the mean value of the proximity measure in accordance with Equation (2.30) are shown in Figures 2.15 - 2.16 in a "grey" scale format. The details of their representation are also presented in Tables B.7 - B.8 (Appendix B).

Although the proximity tables are insufficient by themselves for arriving at firm conclusions, they have provided a further insight in verifying that vehicles of different makes and models can indeed be differentiated from one another through the kind of modelling described in Section 2.5.

D_E

	Ford	Centura	Datsun	Volvo	Hillman	Valiant	Mazda	VW	Holden	Cortina	Lancer	Fiat	Escort	Ford Truck
Ford														
Centura														
Datsun														
Volvo														
Hillman														
Valiant														
Mazda														
VW														
Holden														
Cortina														
Lancer														
Fiat														
Escort														
Ford Truck														

Legend:

$0 \leqslant D_E < 0.5$

$0.5 \leqslant D_E < 1.0$

$1.0 \leqslant D_E$
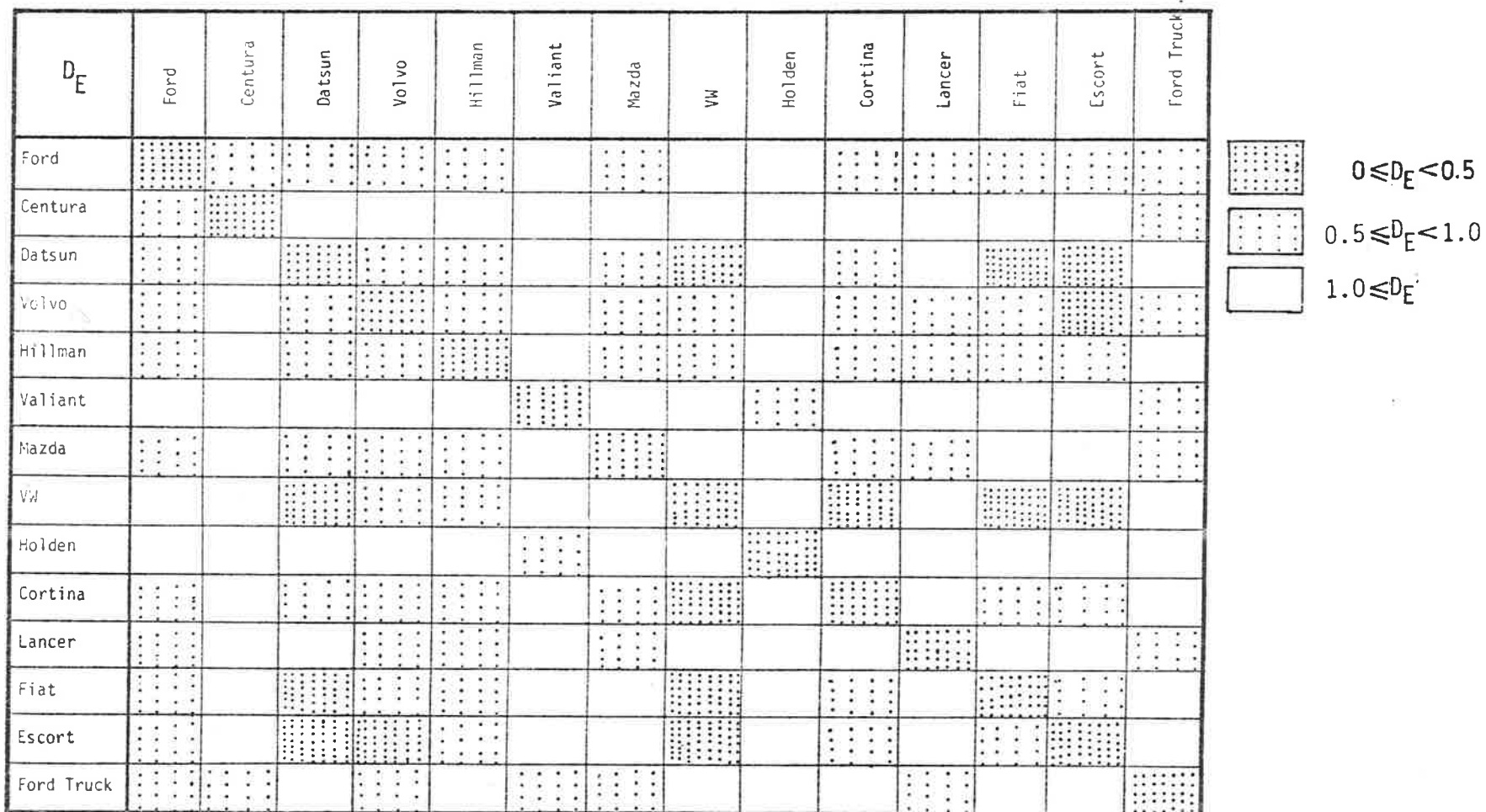
FIGURE 2.15.   DISTANCE MEASURE D_E USING COMPONENTS OF FEATURE VECTOR $^i_c \tilde{x}$.

D_r	Ford	Centura	Datsun	Volvo	Hillman	Valiant	Mazda	VW	Holden	Cortina	Lancer	Fiat	Escort	Ford Truck
Ford														
Centura														
Datsun														
Volvo														
Hillman														
Valiant														
Mazda														
VW														
Holden														
Cortina														
Lancer														
Fiat														
Escort														
Ford Truck														

Legend:
- $0 \leqslant D_r < 0.5$
- $0.5 \leqslant D_r < 1.0$
- $1.0 \leqslant D_r$
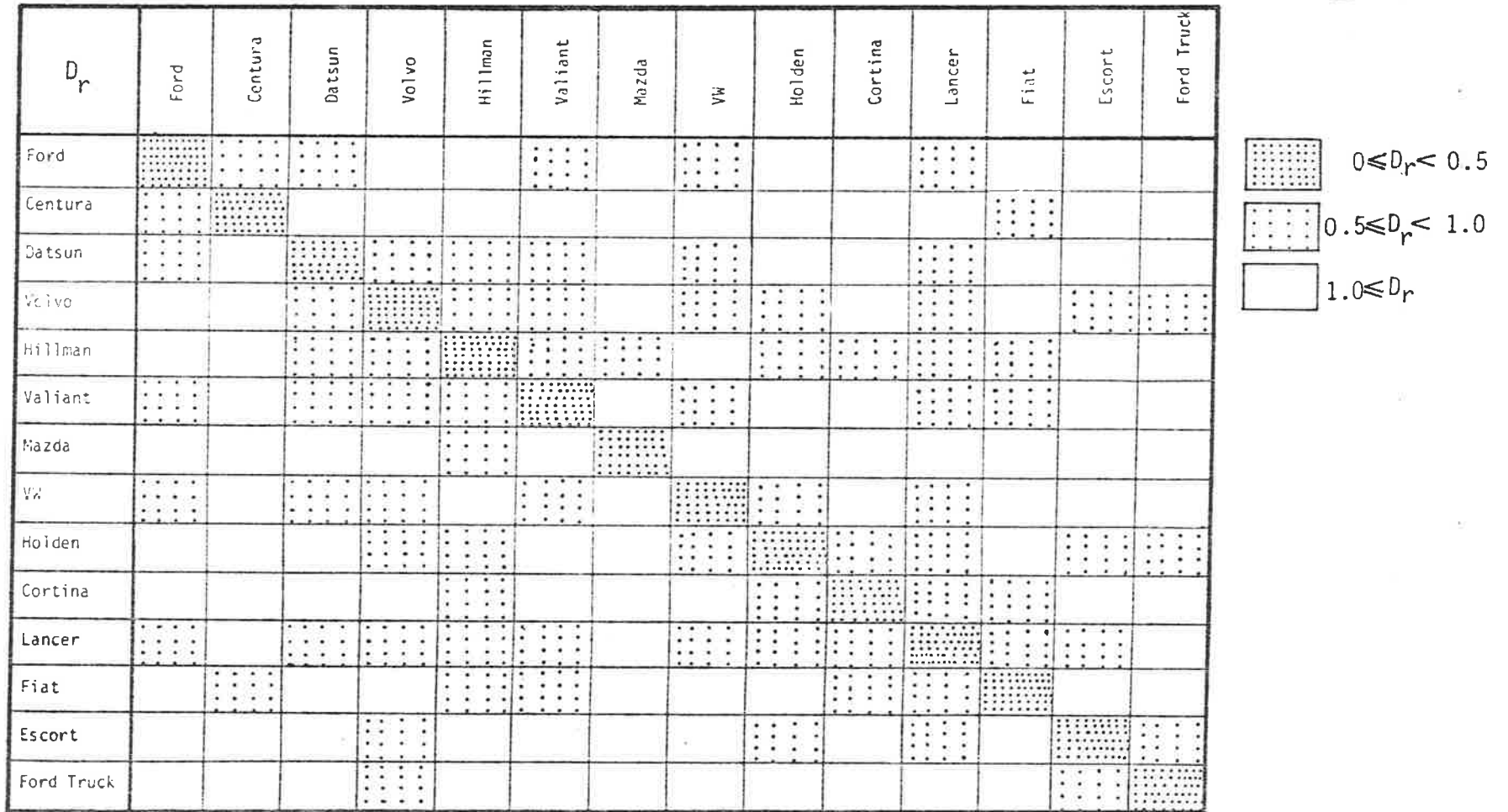
FIGURE 2.16.   PROXIMITY MEASURE D_r WITH COMPONENTS OF FEATURE VECTOR $_b^i \tilde{X}$.

There are two remarks pertinent in regards to the structure of the proximity tables. Firstly, since the same data is used for both the stored vector $\tilde{X}$ and the unknown $\tilde{Y}$, the diagonal elements of the resultant proximity tables are zero. Therefore false rejection rate ε_r cannot be derived directly. The second point is that the table entries are symmetrical about the diagonal elements and therefore only one-half of the table provides useful information.

The false acceptance rate ε_a was calculated for the two approached based on the definition of Equation (2.27) and Equation (2.29). This is shown in Figure 2.17(a). However the evaluation of the false rejection rate ε_r could only be obtained through the limited results of the second file which were augmented by the data in the first. Although this approach was limited in nature and perhaps not fully justifiable, it provided an approximate means to test the two models and gave an insight to the kind of results that one might expect. The results of this analysis is shown in Figure 2.17(b).

These curves illustrate the relations between the two error rates and the threshold level β. If the threshold value is too low, many vehicles will be falsely rejected because of the variability of their signature due to lateral displacement. On the other hand if the threshold is too high, vehicles with some similarity in their signature will be falsely classified. Thus the value of the threshold β is a trade-off between the security of the system, i.e. low false-acceptance rate, and low false-rejection rate.
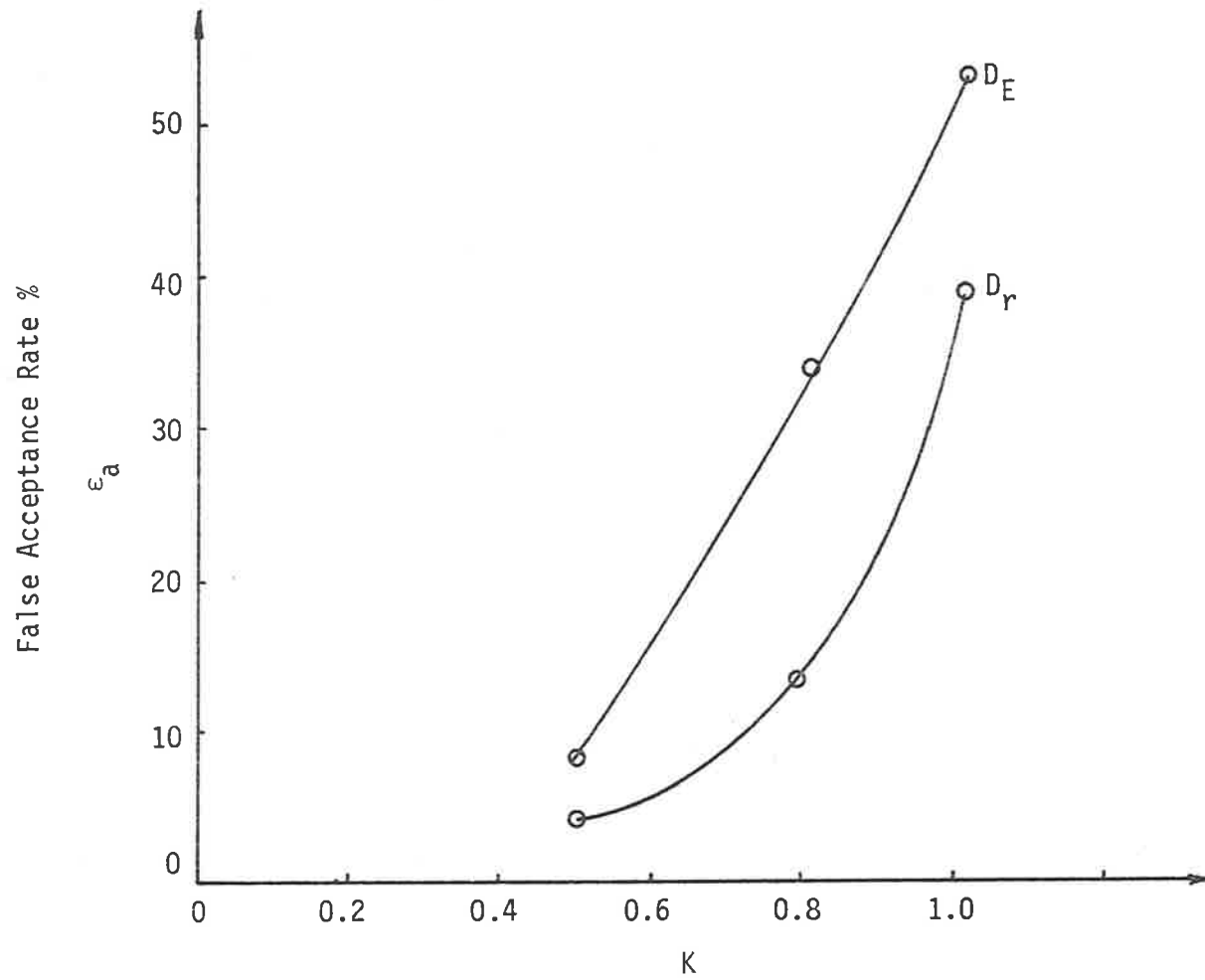
FIGURE 2.17 (a).   FALSE ACCEPTANCE RATE ε_a AS A FUNCTION OF SCALLING FACTOR K.
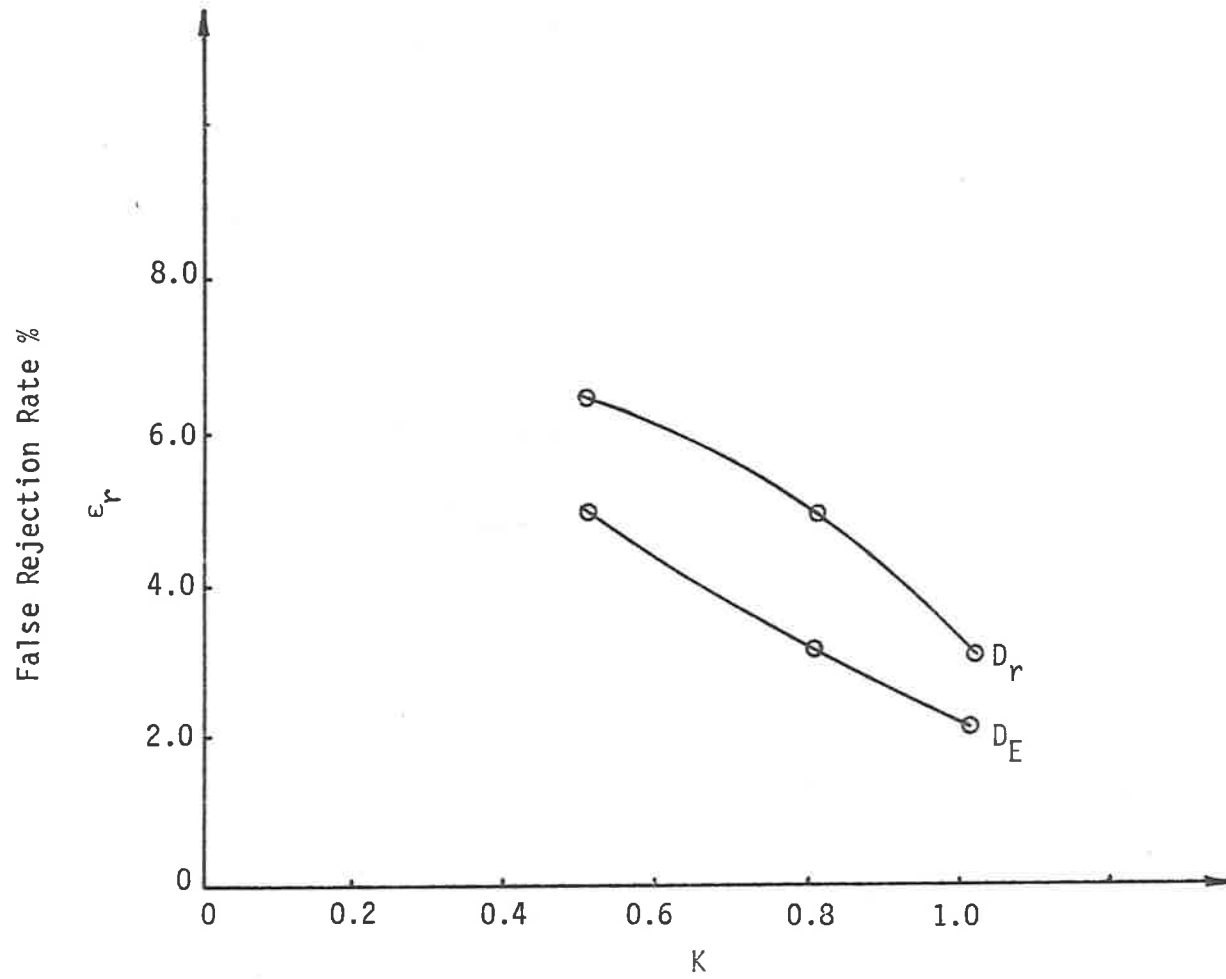
FIGURE 2.17 (b).   FALSE REJECTION RATE ϵ_r AS A FUNCTION OF SCALLING FACTOR K.

The overall performance as expressed by Equation (2.33) for two different arbitary cost factors are illustrated in Figure 2.18.

From these limited evaluations it appears that better performance can be expected from a classification method using feature vector $_b^i\tilde{X}$ in preference to feature vector $_c^i\tilde{X}$ derived from the Fourier spectrum. Since extraction of the components of $_b^i\tilde{X}$ are carried out in time domain significant savings in computation time as well as hardware can also be expected.

2.7 Classifier Hardware

In order to assess the suitability of the classification method for real time applications some preliminary investigation into the structure of the classifier was also conducted. The main requirements of the classifier are its ability to perform many thousands of comparison in "almost" real-time and further the system must be flexible enough such that changes in the stored data resulting from introduction of new models can be implemented readily.

Since results of computation are required to be available within approximately two seconds [65], uniprocessing is inappropriate. The approach which is taken to increase the processing speed is through parallelism. Studies of various multiprocessing

72.
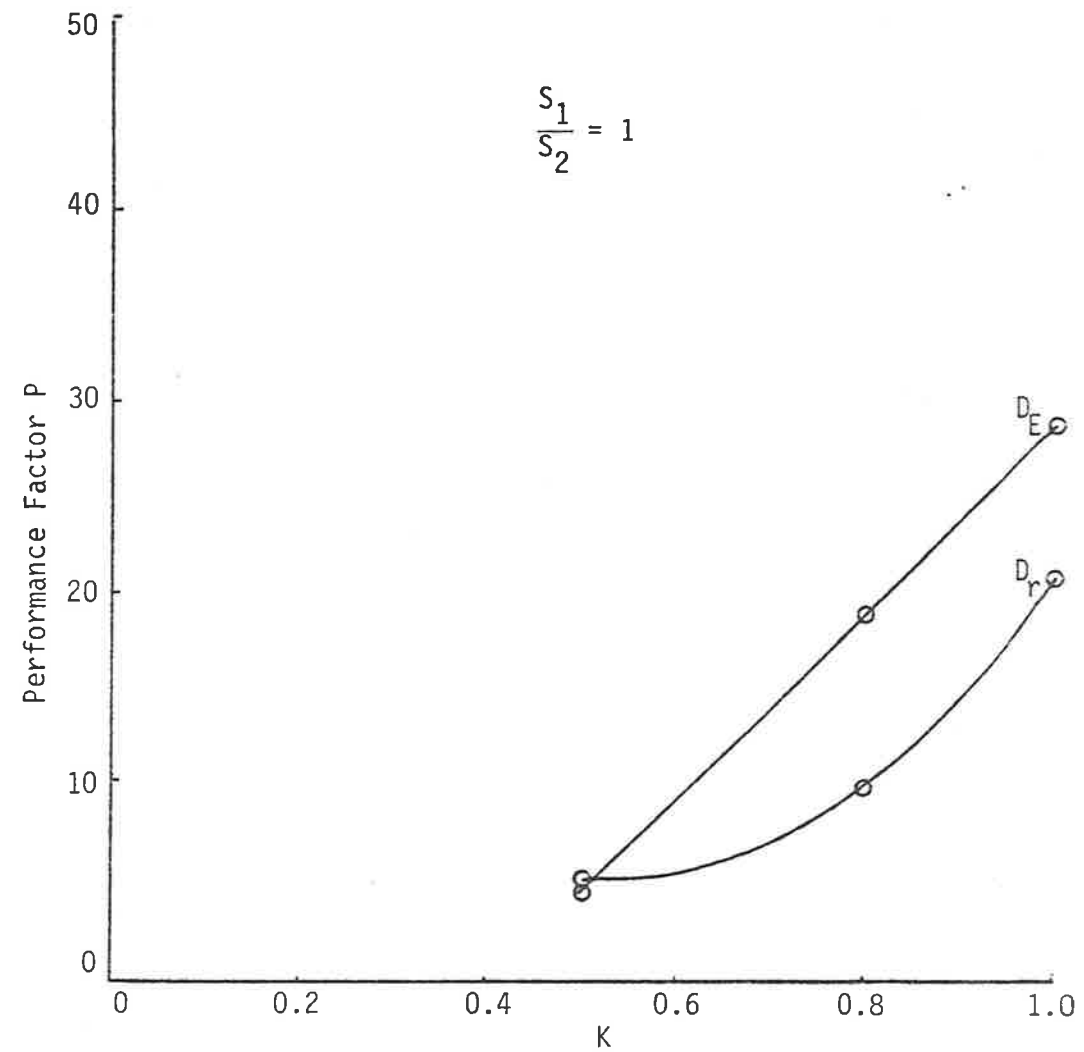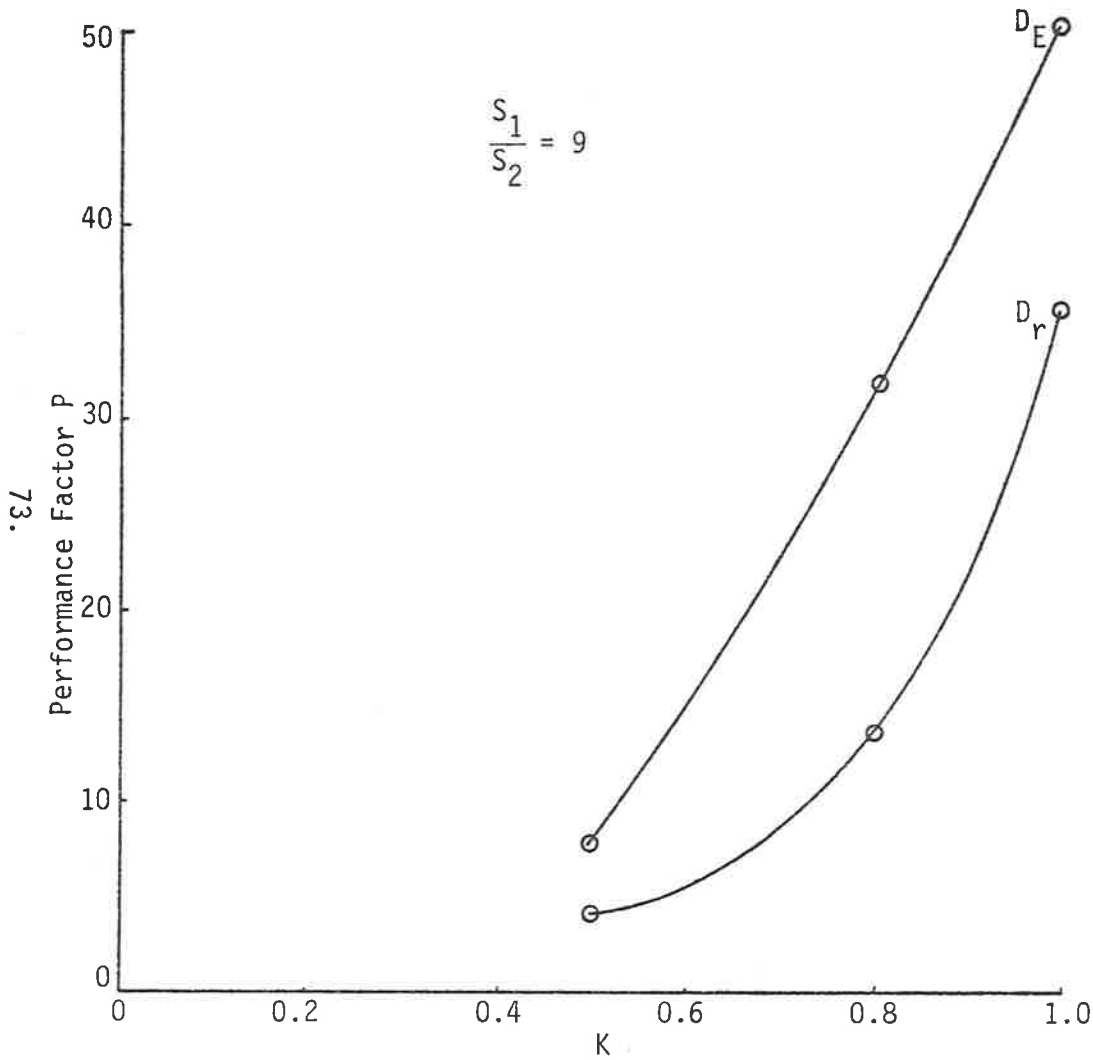
FIGURE 2.18. OVERALL PERFORMANCE ESTIMATION OF THE CLASSIFIER AS A FUNCTION OF THE SCALLING FACTOR K FOR TWO ARBITRARY COST FACTOR RATIOS.

73.

structures[118 - 120] indicated that the Single-Instruction-Multiple-Data stream (SIMD) appeared as a suitable contender for this application and therefore a system based on the above configuration using Intel 8085 microprocessors was developed[116]. Block diagram of the system illustrating the main components of the system incorporating 8 microprocessors is shown in Figures 2.19 - 2.20. This structure was constructed by Mr. F.S. Sin.

The binary feature vector $_b^i\tilde{X}$ which characterise the various vehicle classes are arranged cyclically into blocks of twelve 8-bit words and are stored in 1K EPROMS called local signature table (LS). Two additional 8-bit words are also augmented to each class and serve as a tag to identify the class of vehicles represented by that vector. Each processor in the classifier has only access to a local signature table.

The classification process is divided into two sequential tasks: the primary and the secondary "nearest match" algorithms[116]. The primary match computes the minimum value of the proximity measure D_r in each local signature table. At the end of the primary match, each processor yields a "best" correlated result. Consequently a secondary match is required between all the processors to determine the global minimum. Thus interprocessor communication must be encouraged during this phase to ensure some degree of parellism. This is achieved by organising the processors 1, 3, 6 and 8 shown in Figure 2.20 to read the accumulator data outputed by the processors 2, 4, 5 and 7 respectively. This latter set, are subsequently HALTed. Processor 1 and 8 repeat the sequence by reading the accumulator data of 3 and 6. The operation continues until all comparisons are completed and the global minimum for $D_{r_{min}}$ is found. The tag corresponding to the minimum value is used for

CS: Common Storage for common instructions.

LS: Local Storage; signature table, uncommon instructions.
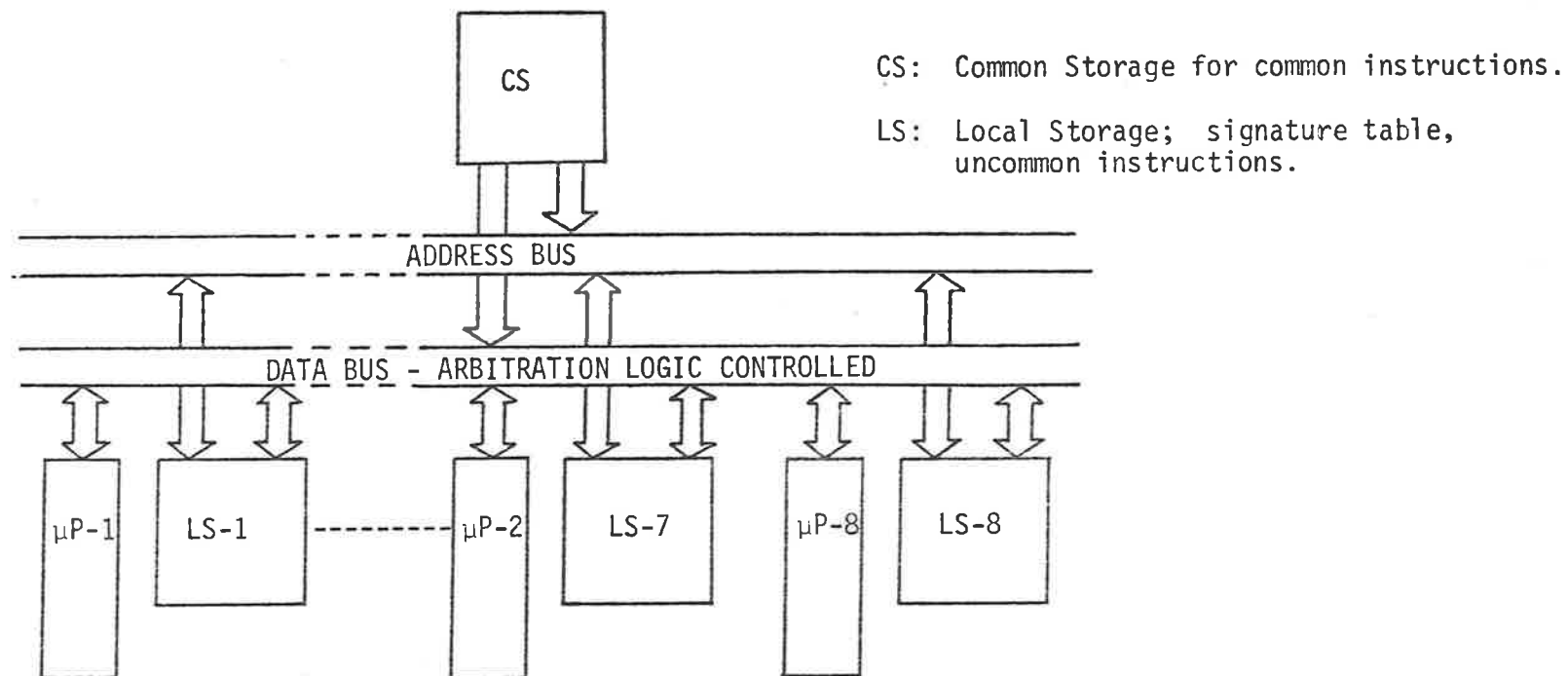
FIGURE 2.19 (a). BLOCK DIAGRAM ILLUSTRATING THE ARCHITECTURE OF THE CLASSIFIER.
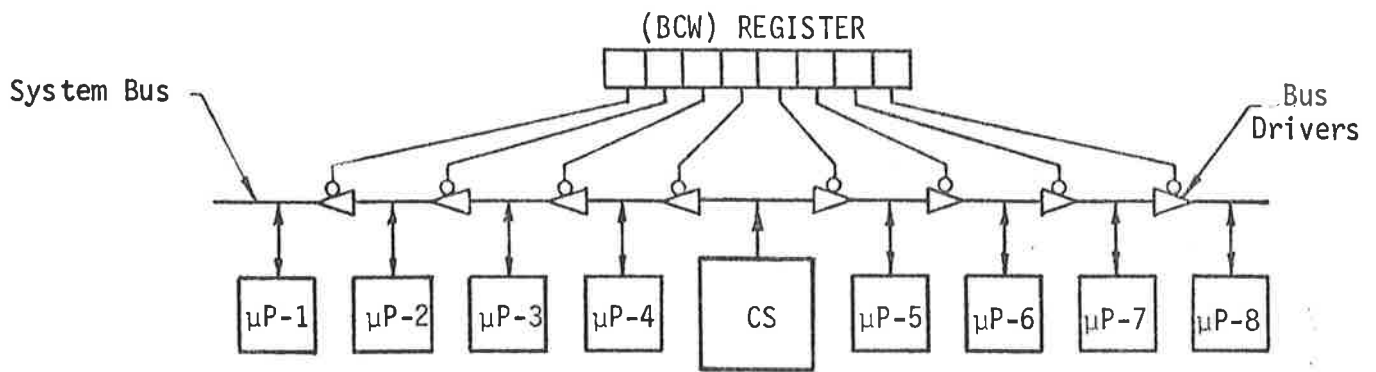
(a)
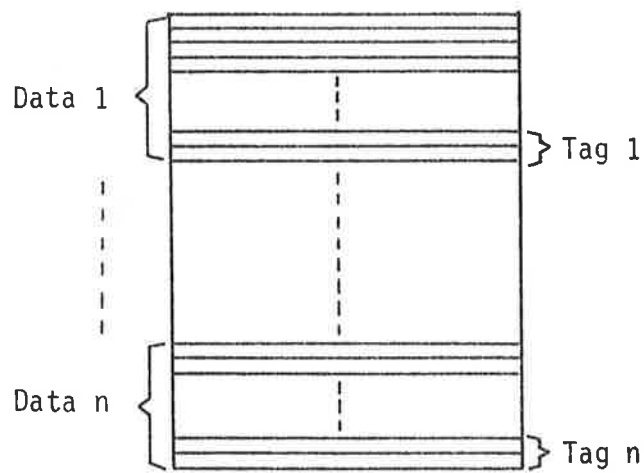
(b)

FIGURE 2.20. STRUCTURE FOR SECONDARY MATCH.

(a) Parallel Configuration.

(b) Local Signature Table.

Notes: *The state of bus drivers are controlled by an 8-bit*

control word register (BCW).

the subsequent identification.

Although the local storage (LS)'s share common addresses the
data located at each common address may be different. This requires
isolation of the appropriate processors from the system bus during
the period when data is being transferred between the processor,
the local store, and the accumulator. Therefore in this manner
the problems of competition for the bus is eliminated.

Since the processors share instruction streams generated from
a common memory and are subsequently executed on a common programme
counter the problem associated with synchronization is also avoided.

The time associated with secondary match for large number
of data is small and therefore improvements that are achieved by
parallel processing is approximately proportional to the number
of parallel processors used. For 1000 comparisons using eight
8085 microprocessors the required time required is in the order
of 400mSec[116]. Comparisons between a uniprocessor and SIMD
structure in terms of required the computational times is illus-
trated by Table 2.7.

TABLE 2.7. COMPARISON BETWEEN UNI-PROCESSOR AND SIMD STRUCTURE

Operation	Number of States	
	Uni-Processor (8085)	SIMD (8085)
Compute D_r	3800	3900
Determine $D_{r_{min}}$	20	64
Primary Match	3820×100	$3964 \times \dfrac{1000}{N}$
Secondary Match		$84 \log_2 N$
Total Time (Sec)	2.0	2.0/N

Notes: *(i)* N = *total number of processors.*

          (ii)   *Clock period = 350nS.*

2.8 Conclusion

This study has presented evidence that it is possible to extract suitable features from a two-coils sensor in order to classify vehicles in terms of their makes and models without the need for speed or length information.

The criterion of feature selection based on Fourier components and the alternative binary representation of the zero crossings of the differentiated signal has shown promising results and therefore has provided the basis for the kind of future research that may proceed in this area using a broader class of vehicles.

Based on the observations and analysis of the limited data the following remarks seem justifiable:

(i)   If displacement of a vehicle from centre position in relation to the vehicle sensor is controlled, then only a small perturbation in the amplitude characteristics of the signature of the same vehicle can be expected.

(ii) Vehicles of the same makes and models when subjected to the same displacement in relation to the sensor have similar signatures.

(iii) There appears to be more differences between different vehicles than between different runs of the same vehicles.

(iv)   Time normalization has not influenced the differences

that exist between different classes of vehicles.

Thus the need for length information has been

eliminated.

Since the modelling was based on a limited amount of available
data the application of the principle to a broader class of vehicles
await confirmation by other investigators. However it is hoped that
this work will stimulate further research in this area in particular
when the constraints associated with displacement are relaxed. This
may entail statistical consideration in order to arrive at a classi-
fication rule which is optimal, in the sense that, on an average
basis, its use yields the lowest probability of committing classifi-
cation errors.

CHAPTER 3

VEHICLE IDENTIFICATION SYSTEMS

3.1 Introduction

Many agencies in the transportation field both governmental and private, have indicated their need for cost effective systems that will automatically identify and establish the location of a selected vehicle. The severe conditions encountered in the various traffic situations makes the choice of technology an important task. Therefore this chapter is concerned with a comparative study of several technologies which have the potential of being used for vehicle identification and surveillance.

Generally the systems can be configured in accordance with two operational requirements. The first entails a vehicle-mounted coded label or "transponder". As the vehicle comes within the range of an interrogation, the code is read and the identity of the selected vehicle is obtained by the interrogation. The interrogation can subsequently add its own location information and transmit the augmented code to a central processor. In the second technique the transponder can be installed under the road surface or alternatively along the highway as a series of "signposts". The signpost imparts

its location information to vehicles that pass the signpost. These vehicles are subsequently interrogatdd via a two-way mobile radio for transfer of location information.

Transponders can be broadly classified according to whether they are active or passive devices[*], suitable for interrogation either from near to or far from the interrogation apparatus. free or otherwise of registration and orientation constraints between themselves and the interrogation apparatus, and according to the capacity of their almost invariably digital coding.

The requirements of passive operation and interrogation over electromagnetic propagation path are normally sufficient to ensure that the reply signal is very weak in relation to that performing the interrogation. The requirement of registration and orientation freedom is normally sufficient to ensure that the interrogation signal produces strong fields not only in the vicinity of the transponder but also in the region of the receiver antenna. The separation of the reply signal from the strongly coupled interrogation signal is therefore of vital importance. The necessary separation can be performed basically in the time or frequency domains. A precise knowledge of the reply signal frequency or other signal statistics is desirable as this knowledge is necessary to the attainment of low receiver noise bandwidth.

---

[*] *Passive is referred to devices where no internal energy source such as a battery is required.*

During the last decade a number of technologies including optical, sonic, radioactive, magnetic, microwave and inductive have been developed and tested[66 - 69]. Subsequent to these studies the following criteria have been formulated to decide the choice of technology:

(a) The transponder should be maintenance-free and operate without the need for an external power source, i.e. a "passive transponder".

(b) The information transfer between the transponder and the interrogator should not be impaired due to environment such as rain, snow, oil, etc.

(c) The transponder should be read within an accurately defined reading zone.

(d) The transponders and interrogators should have convenient physical dimensions as well as being able to be produced at low costs.

(e) It is highly desirable for the transponder to be field programmable.

(f) Operating characteristics should be such that it does not interfere with other users of the spectrum.

(g) Due to the congestion of the electromagnetic spectrum, either a narrow-band device should be used or alternatively the congested portions of the spectrum should be avoided.

It was concluded on the basis of the available information that optical and sonic could not operate reliably in the contaminated environment. The hazards associated with radioactive systems made the approach unsuitable. The magnetic also could not be considered due to installation difficulties. Therefore it was decided to explore further the remaining two technologies, namely the microwave and low frequency inductive system in more detail.

3.2 Microwave Systems[70 - 75]

Microwave identification systems generally incorporate one of several approaches. In one approach, as shown in Figure 3.1, the transponder extracts power from the interrogator at one frequency and subsequently reradiates power at a second frequency harmonically related to the first. Several variations based on this principle have subsequently been developed.

In an alternative technique a passive label having a number of dipoles arranged in accordance with a code is illuminated by a source radiating microwave energy. As the vehicle moves across the microwave beam each dipole produces a frequency modulated pulse or chirp signal as illustrated in Figure 3.2. Successive dipoles produce time displaced frequency modulated signals. The sum of these signals is detected and subsequently resolved into a serial code corresponding to the dipole pattern.

At frequencies below 1GHz, the Doppler shift caused by a slow

84.
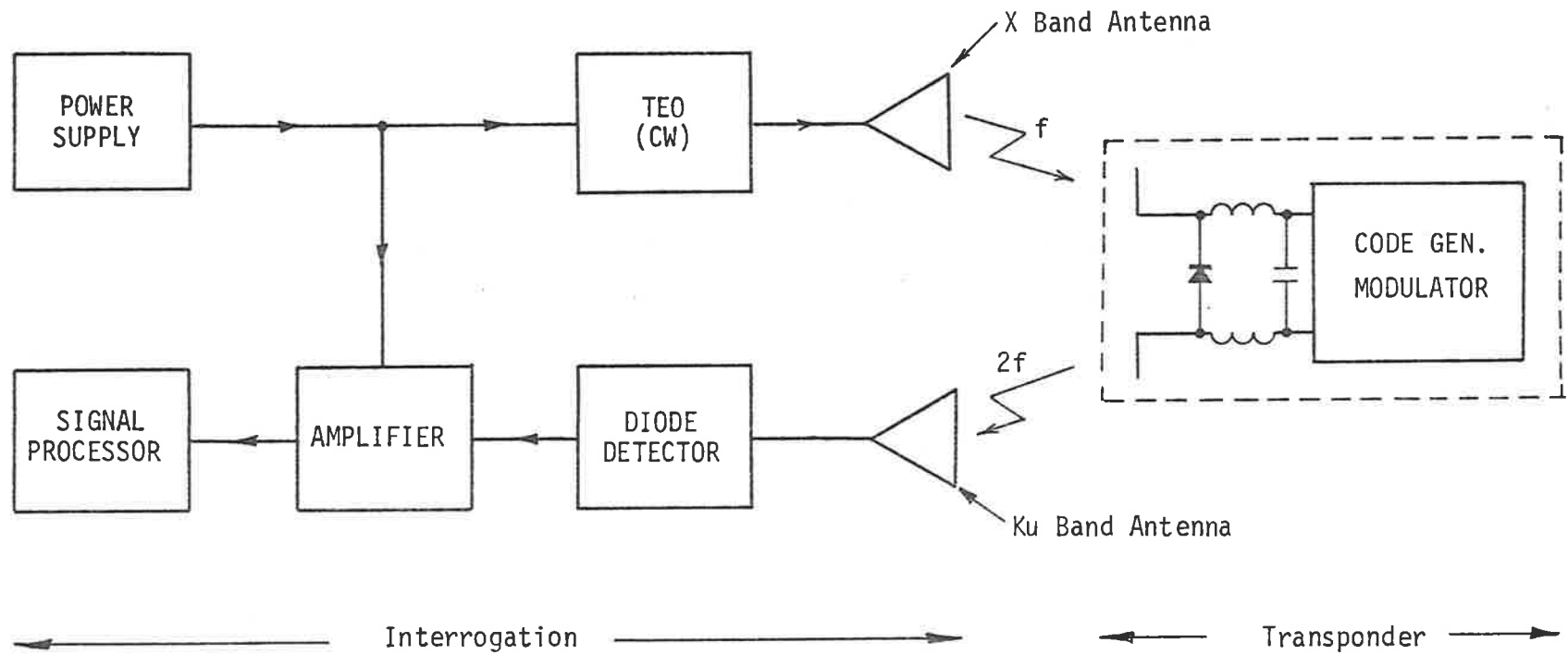
FIGURE 3.1. MICROWAVE IDENTIFICATION SYSTEM USING HARMONICALLY RELATED REPLY SIGNAL.

Microwave Antenna

Label with Dipoles

s = dipole spacing
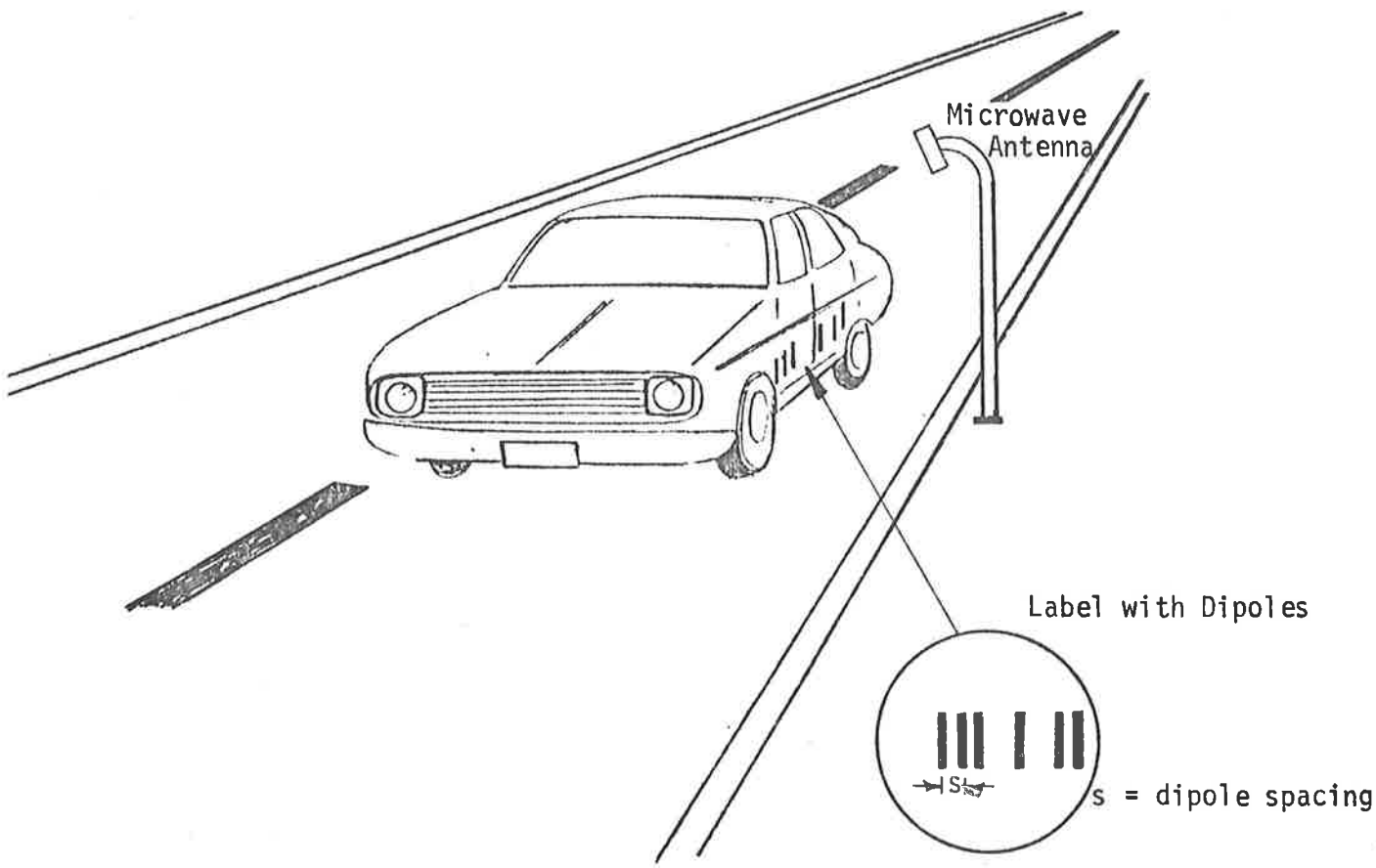
FIGURE 3.2. MICROWAVE IDENTIFICATION SYSTEM USING UNIQUELY SPACED DIPOLES ON THE VEHICLE AS LABEL.

moving vehicle is small, making detection rather difficult. In addition the label length becomes rather long, i.e. with 25 digit label with half wavelength spacing the length is 3.6 meters, which limits the application to a small class of systems.

At higher frequencies than 1GHz, unwanted reflections caused by the surface of vehicles become comparable with respect to the signals caused by dipoles and therefore detection of the legitimate signal becomes difficult.

A more recent development utilizing ceramic resonators has been described by Sakuragi et al[76]. The basic principle aassociated with this class of transponder is shown in Figure 3.3, where several ceramic resonators having different resonance frequencies are operated in parallel.

A sweep-frequency signal f_s, generated by a sweep frequency generator, modulate the microwave carrier f_o and produces the interrogation signal $f_o \pm f_s$. The received signal at the transponder is demodulated by the diode circuitry and subsequently provides the sweep frequency f_s to the ceramic resonators. Each resonator starts to resonate at each of the individual frequencies. The identification code consists of a particular combination of these resonators.

The resultant signal from the transponder is received and the frequency components associated with each of the ceramic resonators are determined.

There are several problems associated with this structure. The major one being the need for complex signal processing as the number

Sweep Frequency Signal Generator
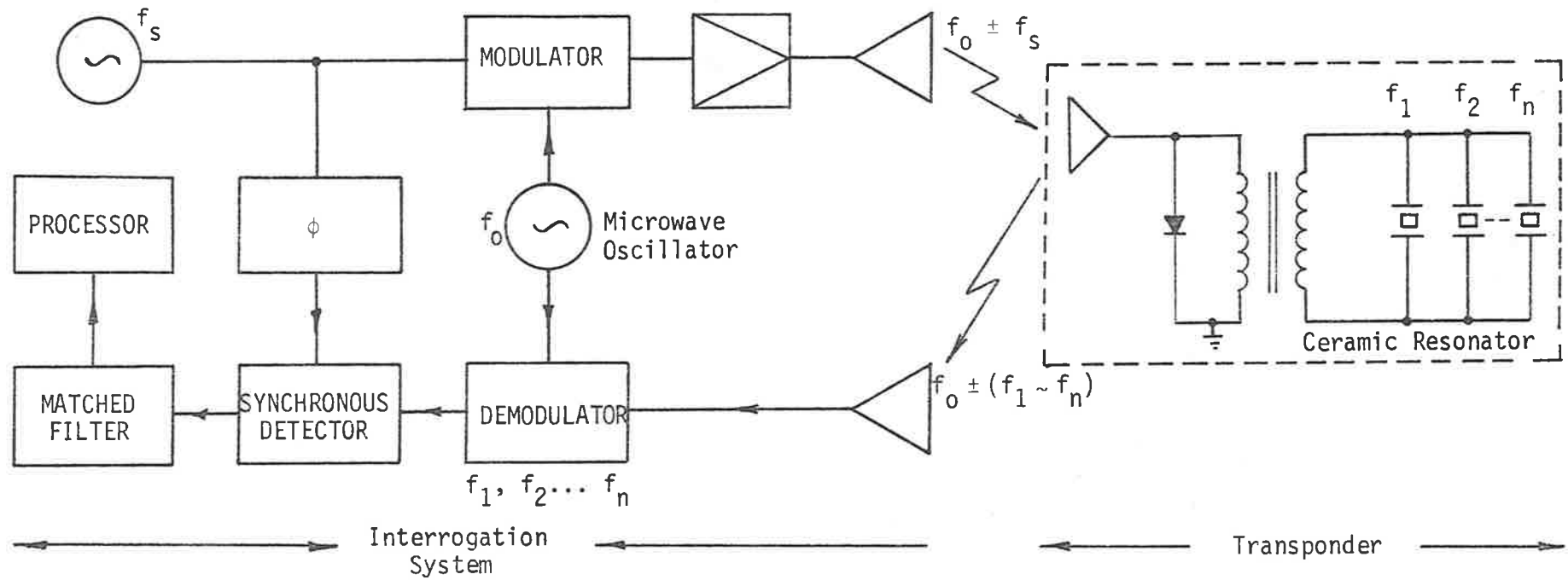
FIGURE 3.3.   INDENTIFICATION SYSTEM USING CERAMIC RESONATORS.

of bits in the code are increased. In addition the transponder
cannot readily be adapted for usage in systems where the transponder
is required to be field programmable.

Another development which has emerged as a strong con-
tender for many of the passive labelling applications is based on
surface acoustic wave (SAW) technology[77 - 82]. However no reports
appear to have been published on its suitability for vehicle iden-
tification and surveillance systems. Therefore it is considered
desirable to record some preliminary analysis of the feasibility of
applying the SAW labelling technology to the task of vehicle iden-
tification in traffic monitoring operations.

3.3   Surface Acoustic Wave Labelling

The surface acoustic wave (SAW) device may be realised by
deposition on a suitable piezoelectric substrate a group of metal
strips or "fingers". The device is then electrically coupled to a
planar antenna as shown in Figure 3.4[77 - 84].

The SAW device is basically an acoustic delay line excited by
electro-acoustic transducers which in turn act as receivers at dis-
crete points on the delay line and hence provide the coded informa-
tion as a sequence of discrete echoes, each corresponding to the
presence of each individual transducers on the delay line[81]. When
the transponder is interrogated by a short rf pulse (20ns), at a
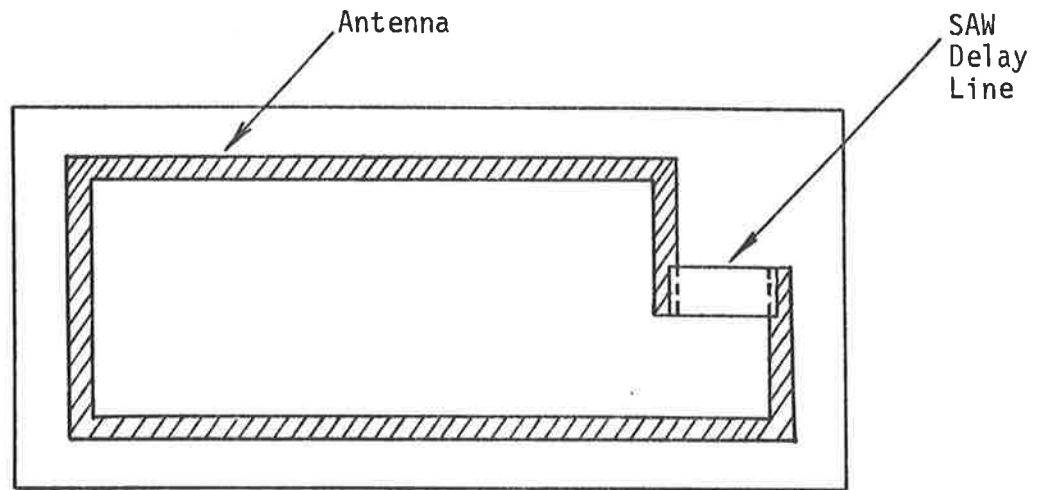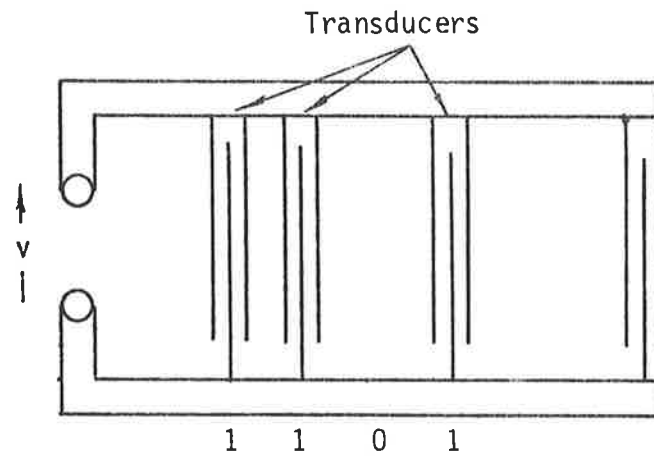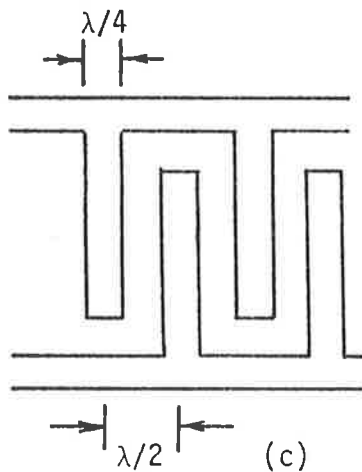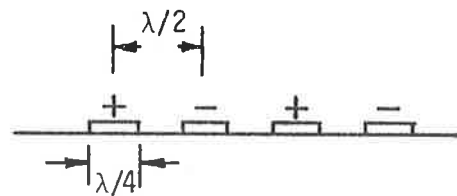
FIGURE 3.4. SURFACE ACOUSTIC WAVE TECHNOLOGY.

(a) ASW one-port label.
(b) ASW pattern.
(c) Finger spacing.
(d) Metalisation.

convenient frequency, i.e. 200MHz, a train of reply pulses are returned from each group of fingers. Figure 3.5 shows a typical delay line response corresponding to the SAW pattern of Figure 3.4(b).

The operating principle of a typical system is then that of separation of the transmitted and reply signals and of achievement of code generation by storing the interrogation energy in a one-port acoustic surface delay line for a time sufficient to allow the retransmission of a reply signal at a time after all of the transients and spurious responses associated with the illumination of the scanned area by a high power transmitted signal have died away[83].

In common with all passive labelling systems, especially those which interrogate labels at a distance, the reply signal reaching the receiver is quite weak and special signal processing techniques are needed for its recovery in the face of thermal noise and other interfering signals. These techniques include the achievement of a low receiver noise level through the establishment of a narrow intermediate frequency amplifier bandwidth sufficient only to contain the spectrum of the received signal.

The signal processing operations are approximately those of an ideal correlation detector, in that each bit of the reply signal is multiplied by an appropriately shaped and timed local oscillator signal with the low frequency product signal being detected and integrated for the interrogation period. In a simple correlation detector one would expect to set the local oscillator carrier frequency to be exactly equal to the transmitter carrier frequency, and to amplify the mixer output at d.c. However, for reasons related to the non-ideal performance components performing gating operations

91.

RF ENERGY BURST

REPLY SIGNAL

1   1   0   1

TIME

CODE
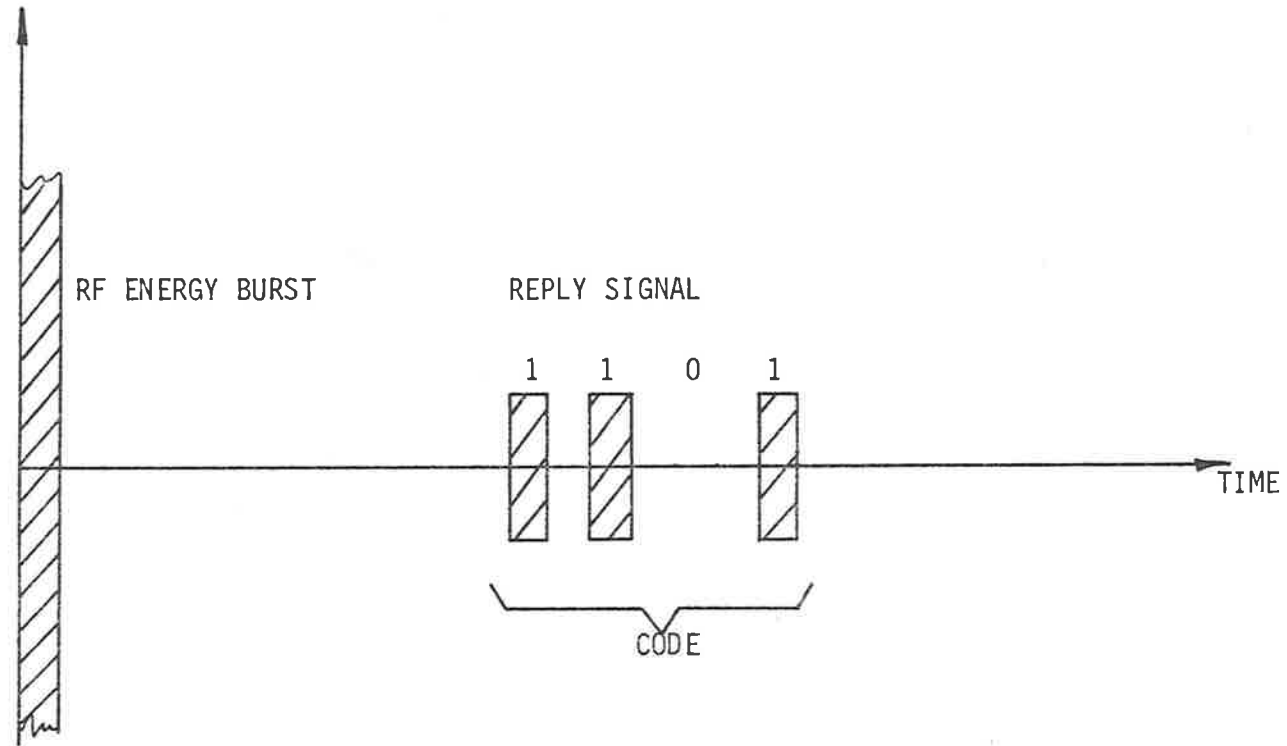
FIGURE 3.5.   THE RELATIONSHIP BETWEEN THE INTERROGATION RF ENERGY AND THE TIME DISPLACED REPLY SIGNAL.

within the receiver instead, the local oscillator carrier frequency is slightly offset from the transmitter oscillator carrier frequency and the mixer product is subsequently amplified in a narrow band intermediate frequency amplifier before it is detected and integrated. The bandwidth of this intermediate frequency amplifier could vary from several hundred to only a few Hertz depending upon the needs of the application[81].

It should be realised that the interrogation operation does not consist of the issuing of a single transmitter pulse. Transmitter pulses are in fact continuously reissued with the time between them only sufficient to allow for the reception of the reply code. In practice the time between interrogation pulses is of the order of $1\mu s$, and the results of an interrogation are the average of the replies from many thousands of such pulses.

If one views the results of all these signal processing operations in the frequency domain, we see that the transmitted signal consists of a line spectrum with lines spaced by an amount equal to the pulse repetition frequency (of the order of 1MHz) with most of the energy contained within a band of width equal to the inverse of the pulse length (several tens of MHz), and centred at the transmitter carrier frequency (several hundred MHz to 1GHz). The effect of the receiver signal processing is to surround each one of these transmitted signal sidebands by a narrow (several Hz to several hundred Hz) receiver passband, the contributions from which are coherently summed at the mixer. Each of these partial receiver passbands has a bandwidth equal to that of the intermediate frequency amplifier. The receiver passband is illustrated in Figure 3.6.

93.
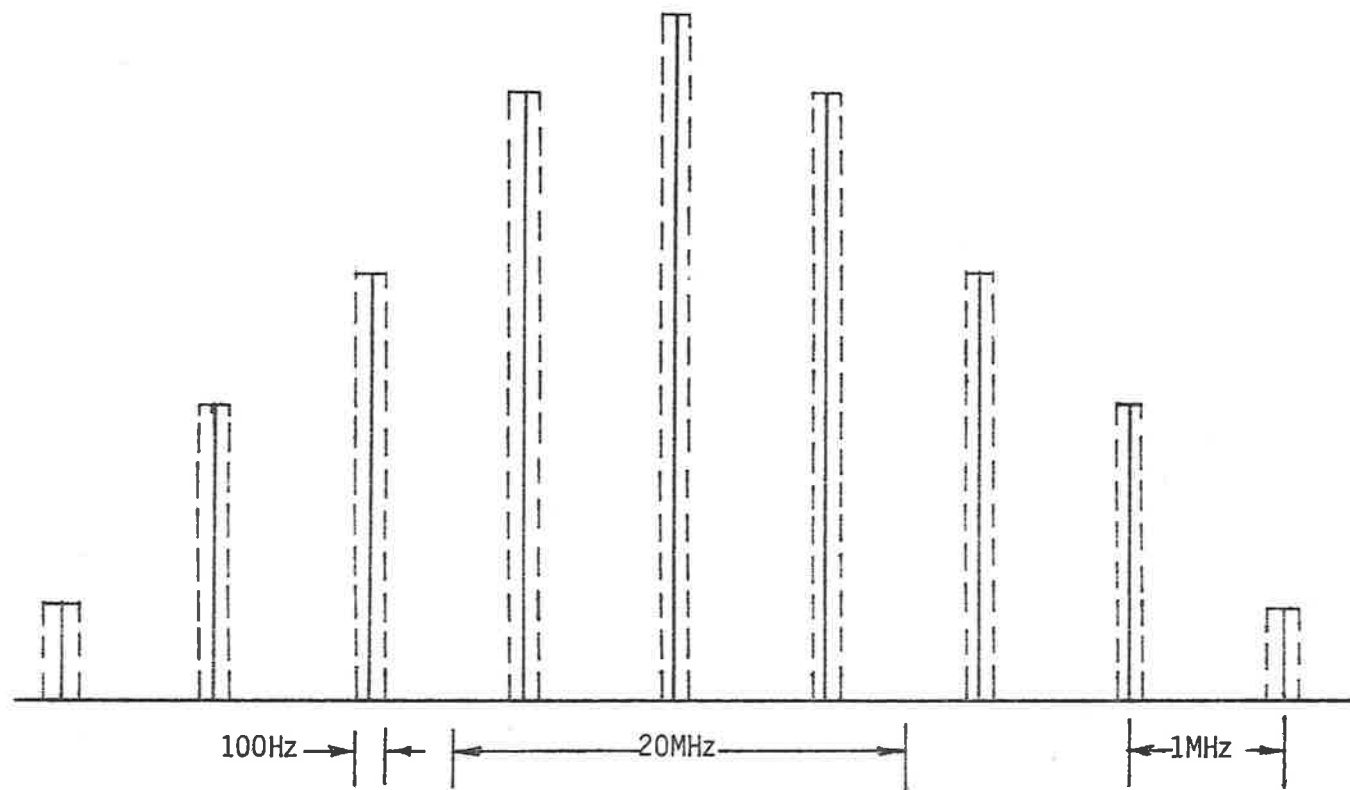
FIGURE 3.6.   RECEIVER BAND PASS COMB FILTER.

The achievement of system sensitivity rests in significant measure on the use of only sufficient if bandwidth to assure the capturing of the reply signal. Since the carrier frequency and modulation parameters of the transmitted signal can be precisely controlled, the principled determinant of uncertainty in the reply signal is Doppler shift due to the label motion. In vehicle identification operations where label velocities can be relatively high, this matter is of importance and will be given more detailed consideration in Section 3.3.4.

3.3.1 Factors influencing the design

The principle problems encountered in designing acoustic surface wave passive labelling systems are those of achieving sufficient system sensitivity, i.e. the reply signal at the receiver which is sufficiently large in relation to both thermal noise and other sources of interfering signal, while at the same time employing sufficiently low transmitted power to avoid creating interference to other uses of the electro-magnetic spectrum or biological hazards to persons who may come within the scanned area. The discussion below considers a number of factors which have to be taken into account in the achievement of these aims.

At the beginning of the design exercise one must have of course in mind the number of bits to be provided in the reply code. The system sensitivity however is not strongly influenced by this parameter. If it is realised that very

many tens of dB separate the transmitter and reply signal levels, and that for a given peak transmitted power level the reply signal-to-noise ratio will deteriorate by only 3dB for a doubling of the code length, it will be seen that this factor becomes critical only for systems that are barely operable.

System design is probably most strongly influenced in all of its aspects by the frequency band chosen for operation. Because the transmitted signal bandwidth extends over several tens of MHz, and radiated powers are substantial, and because in the vehicle monitoring application no opportunity for containment of the interrogation energy is available, it is probably necessary to employ a frequency band reserved for industrial uses in which significant stray levels of radiation are allowed.

Whatever frequency band is chosen, the level of manmade interference picked up by a roadway antenna in this frequency band is crucial to operation. Such interference could be generated by vehicles themselves or by other users of the spectrum.

Another set of factors influencing system design are the cost and available size of delay line substrates. There is a direct relation between the number of bits required in the reply code and the substrate length and an inverse relation between the substrate length and the bandwidth of the transmitted pulse. In some applications in which large numbers of throw-away labels are required, substrate lengths

96.

must be kept short (of the order of 5mm) in the interests of economy, and transmitted pulse bandwidths of several tens of MHz result. In the vehicle monitoring application, tags of significantly greater cost than can be contemplated in throw-away applications can be used, and transmitter bandwidths can be substantially reduced. In the absence of precise details of available spectrum bandwidths and costs of very long substrates, the system to be described below has not sought to exploit this possibility. It is however one which could merit further examination.

Another factor strongly influencing system performance is that of electromagnetic propagation loss between the interrogation apparatus and the responding label. In the determination of this loss we must consider the size of antenna, the separation between interrogation apparatus and label in relation to the freespace wavelength, and any additional electromagnetic attenuation which may be provided by the roadway surface beneath which one of the antennae may be buried. Generally speaking one may expect that all of these losses would increase at the higher operating frequencies. However against this one might set the fact that resonant antennae of convenient size are achieved more easily at high frequencies than low ones.

Cole[83] provided a detailed analysis for both 50MHz and 200MHz systems in which the field was confined within a tunnel. Therefore it was decided to extend these analyses in order to explore the kind of results one could expect if the system is operated in the non-shielded environment in

97.

the medical diathermy band centred at 915MHz.

3.3.2 Selection of system parameters

In order to proceed with the evaluation of the likely performance of the system operating at 915MHz, a particular set of operating parameters are required. As a start it is assumed that the number of bits required in the reply code is 32. Allowing for a number of level setting and parity check bits in the full reply code it will be assumed that the number of transducers in the coding set on the delay line is 38.

Furthermore, it is considered that tags are mounted underneath vehicles and are interrogated from a dipole antenna placed beneath the roadway surface.

At the time when this analysis was performed, for a system operating in the medical diathermy band centred at 915MHz[86] an operating bandwidth of 40MHz was available. However, moves have now been made to reduce this bandwidth to 16MHz.

An interrogation pulse length of 33ns and a separation of 50ns between bits of the reply code are next chosen. The pulse length is slightly longer than the minimum of 25ns which can be employed with the above bandwidth. The consequence is an acceptable lengthening of the delay line combined with a slight increase of system sensitivity resulting from the fact that more of the sidebands of the transmitter

pulse lie within the passband of the transmitter output filter. The ratio of 1.5 between the separation of bits in the reply code and transmitted pulse length is one which has been found to permit the achievement of low crosstalk between bits of the reply code, provided appropriate equal-isation of other system passband factors is incorporated into the delay line pattern period[83].

For quartz as substrate the surface velocity is 3.16km/sec so that with f = 915MHz and a tag having 38 transducers a delay line propagation length of 12.2mm is required.

The bandwidth of 40MHz is sufficient to permit the use of acoustic surface delay line substrates of moderate length as calculated above. The centre frequency of 915MHz is also sufficiently high to enable a resonant antenna of dimensions, $\lambda/4$ = 82mm, to be used in the tag.

The separation in time between successive transmitter pulses is arranged to be slightly greater than the total time occupied by the reply code. The latter time is, using the normal transducer pattern, just twice the number of bits in the reply code times the spacing between bits. For the above bit spacing and number of bits in the reply code, the total reply time is then 3.8µs, making a suitable allowance for reclosure of the receiver time gates before the occurrence of the next transmitter pulse. Thus, a time interval between transmitter pulses of 4.25µs is appropriate. A parameter which will be required in later calculations of system sensitivity is the duty cycle, i.e. the ratio of pulse length

to pulse separation of the transmitter pulse. In the
currently outlined design this parameter comes to
7.75×10^{-3} (-21dB).

3.3.3 Delay line insertion loss

The delay line insertion loss can be defined as the
ratio of the power delivered back to the label antenna from
the delay line during one bit of the reply code to the power
incident from the label antenna to the delay line during the
occurrence of the transmitted pulse. For a one-port delay
line employing only a single pair of parallel connected
transducers, it is theoretically possible[83] for this
parameter to be reduced to 6dB through the employment of an
appropriate number of fingers and a pulse length long in
relation to the propagation time across one transducer. The
6dB loss here results from the bidirectionality property of
the interdigital transducers which requires that each trans-
ducer radiates half its power in the wanted direction. This
minimum insertion loss may be procured only over a maximum
bandwidth determined by the number of fingers required to
establish the match between the antenna impedance and the
transducer input impedance[81]. On strong coupling materials
such as lithium niobate ($LiNoO_3$) fractional bandwidths of 25%
are possible, while for low coupling materials like quartz
this bandwidth has been reduced to 5%.

For the more complex situation of a one port delay line
returning a many bit reply code, the delay line insertion loss

depends on many factors. These include substrate electro-
mechanical coupling coefficient, the number of fingers in
the transducers, number of bits in the reply code, and the
degree of matching between the delay line input impedance
and the antenna impedance. When the number of bits in the
reply code becomes large and when the transducers are closely
spaced to achieve economy of substrate length and a good
duty cycle for the transmitted pulse, adjustments to the
transducer pattern are made both to control the second order
responses of the delay line and to equalise for the other
aspects of the shape of the radio frequency passband. In
this situation the analysis of the delay line performance
becomes a complex matter.

The most recent designs for one port delay lines made
at the University of Adelaide have required 20 transducers
in the coding set, have operated at a fractional bandwidth
of 20%, and on the low coupling material of single crystal
quartz. Using a slightly different (but appropriate for the
case) definition of insertion loss, for these delay lines a
figure of 32dB was predicted[83].

In the present instance delay lines with a number of 38
transducers in the coding set, to be operated at a fractional
bandwidth of 3.3% on a material whose electromechanical
coupling coefficient may be chosen without significant regard
to cost, is required. In these circumstances it will be
assumed that delay lines with an insertion loss of 30dB may
be fabricated with correct attention to suppression of second
order responses and control of cross-talk between bits in the

reply code.

3.3.4 Doppler shift considerations

The principle determinant of the intermediate frequency
amplifier bandwidth is the need to cater for Doppler shift
in the reply signal frequency arising from motion of the tag
in relation to the interrogating antenna. The variance of
Doppler shift with speed of the vehicle and its position in
relation to the interrogating antenna needs to be analysed
so that the time for which the reply frequency will fall
within the receiver bandwidth may be determined. This time
is roughly speaking proportional to that bandwidth. Another
relation, in this case an inverse one, between interrogation
time and receiver bandwidth may be obtained by noting that
if the receiver bandwidth is greater than the inverse of
the interrogation time it has been made unnecessarily broad,
while if the receiver bandwidth is less than the inverse of
the time for which the reply signal will lie within it the
receiver will not have time to respond to the reply. From
these two relationships will be derived an optimum receiver
bandwidth and accompanying interrogation time.

The geometrical arrangement between the interrogation
and tag antennae A and B respectively is illustrated in
Figure 3.7. Both antennae are considered as horizontally
polarised dipoles, which may be oriented parallel or perpen-
dicular to the direction of motion of the vehicle. The tag
antenna is mounted a vertical height h above the interroga-

A = Horizontal Dipole Antenna.

B = Transponder.

(a)

(b)
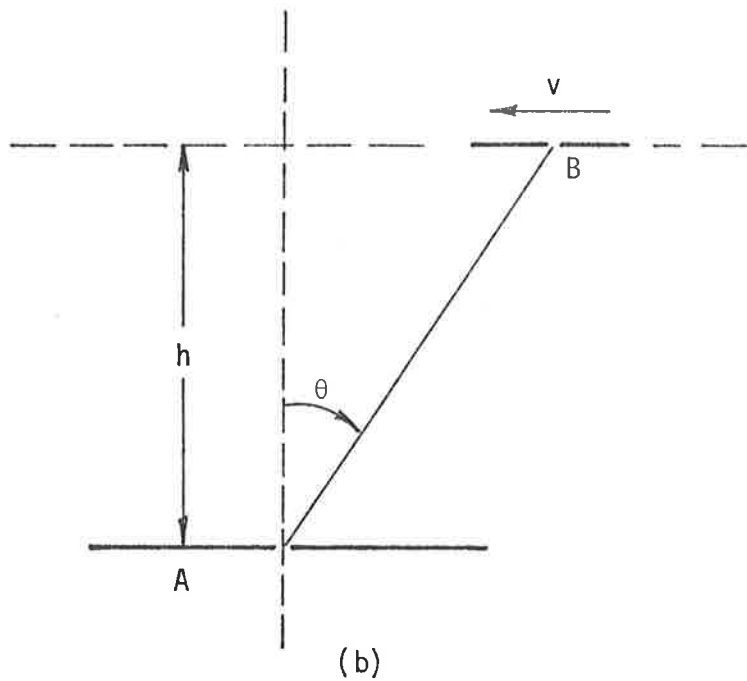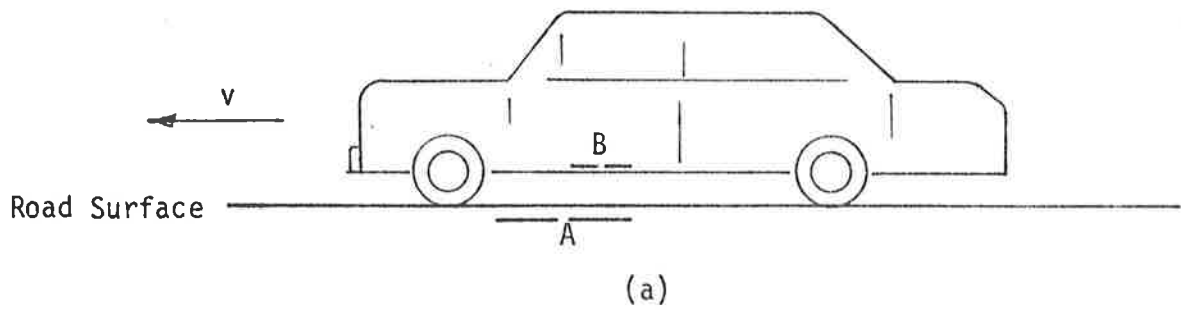
FIGURE 3.7.   BASIC GEOMETRY ASSOCIATED WITH VEHICLE MOUNTED TRANSPONDER
AND BURIED ANTENNA.

(a)   Relative position.
(b)   Geometry.

·tion antenna which would be some distance below the roadway surface, along which the vehicle is assumed to proceed with the velocity v. The carrier frequency of the transmitted pulse is f Hz, the 3dB bandwidth of the if channel is B Hertz, and T is the total time for which the reply signal frequency lies within the receiver 3dB passband. The angle $\Delta\theta$ is that at which the reply signal first falls within the received 3dB passband. At this angle the Doppler shift frequency is denoted by Δf.

The fractional frequency shift Δf of the tag antenna that crosses the beam is

$$\frac{\Delta f}{f} = \frac{\text{relative velocity}}{\text{velocity of electromagnetic propagation}} \qquad (3.1)$$

This relation describes the Doppler shift and for small values of the angle θ it can be written as

$$\frac{\Delta f}{f} = \frac{2v\theta}{c} \qquad (3.2)$$

where c is the velocity of electromagnetic propagation.

Using the geometrical relationships in Figure 3.7

$$\Delta\theta = \frac{vT}{2h} \qquad (3.3)$$

104.

where T is the time in which Δf is less than the bandwidth B of the relative system.

Combining Equation (3.2) and Equation (3.3) results in

$$\frac{\Delta f}{f} = \frac{v^2 T}{ch} .$$ (3.4)

If Δf is defined as

$$\Delta f = \frac{B}{2}$$ (3.5)

and

$$BT = 1$$ (3.6)

then

$$B = \sqrt{2f \, v^2/ch} .$$ (3.7)

For a vehicle velocity of 36m/second, a centre frequency of 915MHz and a tag antenna mounting height of 750mm, the optimum receiver bandwidth based on Equation (3.7) is

$$B = 103Hz.$$ (3.8)

105.

The time this is within the bandwidth B is given by 1/B.

The analysis has therefore indicated a 3dB receiver bandwidth of about 100Hz and a total interrogation time of 10mS are appropriate. A check of the distance travelled by the vehicle in this time justifies the assumption made that the angle $\Delta\theta$ is reasonably small.

3.3.5 System noise level

The signal processing operations in the receiver system as shown in Figure 3.8 result in a signal-to-noise ratio on the if channel given by[83].

$$(S/N)_2 = \frac{PWSR_1^2 R_2}{kT_0^2 B_2 F_1} . \tag{3.9}$$

In this equation P and S are the peak power level and duty cycle of the transmitted pulse. R_1 and R_2 are the one-way electromagnetic propagation path power transfer ratio and delay line echo return power ratio respectively. The product kT_0 is room temperature noise per unit bandwidth, while B_2 is the noise bandwidth of the if channel. F_1 is the noise factor of the receiver preamplifier, and W is a factor of the order of unity which accounts for various small losses to the interrogation energy arising from the limited passbands of the radio frequency portions of the systems.

106.
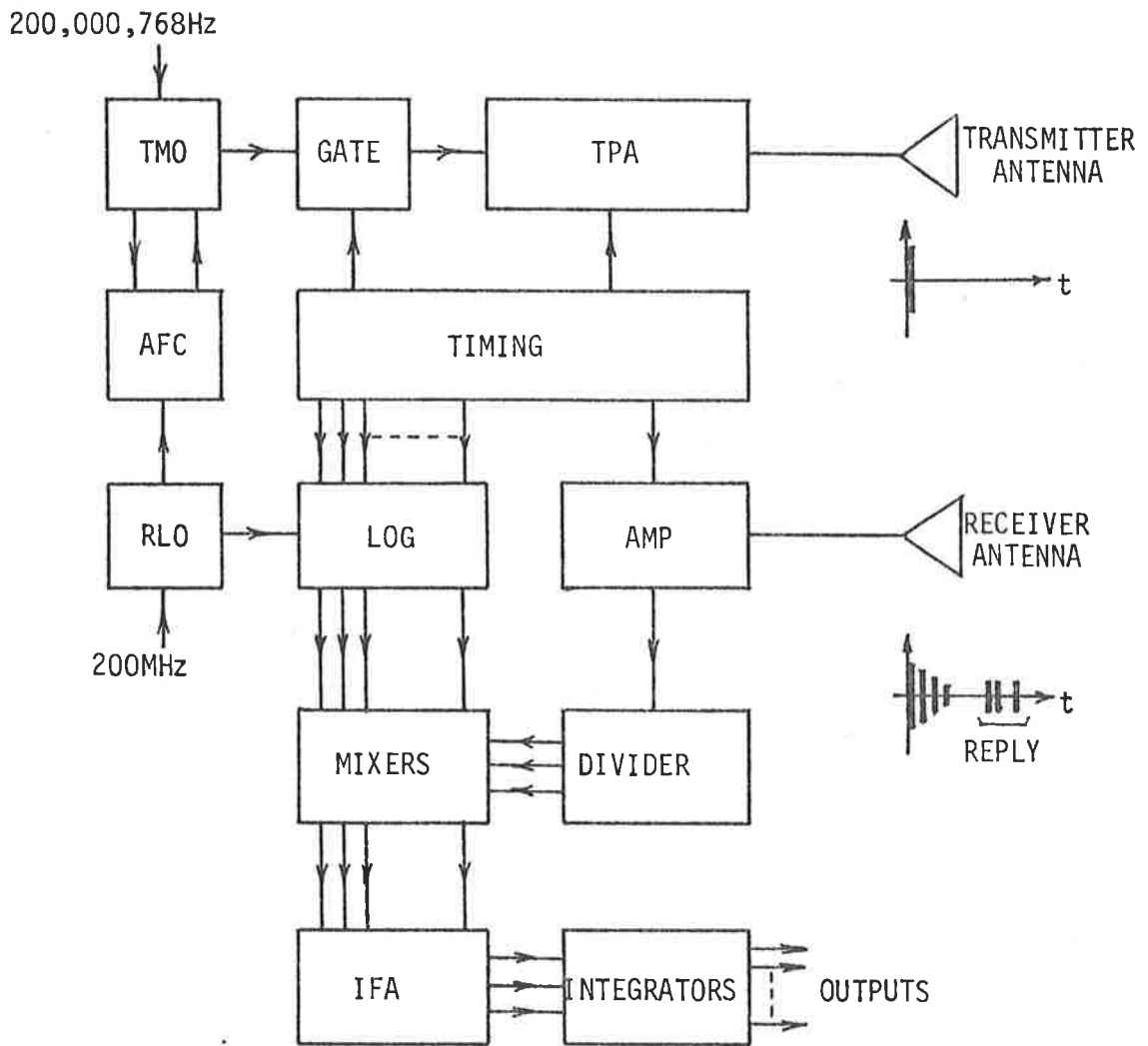
FIGURE 3.8. INTERROGATION SIGNAL PROCESSING FOR SAW SYSTEM.

In the above equation if it can be recognised that the product $PSR_1^2R_2$ as the mean power neglecting effects of limited rf passbands present in each bit of the reply code which reaches the reciever, then the receiver noise level N_r is

$$N_r = kT_0 2B_2 F_1/W.$$ (3.10)

Suitable values for insertion in the above expression are $kT_0 = -204.4dBW/Hz$, $B_2 = 22dBHz$, $F_1 = 5dB$, and $W = -2dB$, the last value being an estimate based on experience with other designs[83]. Evaluating this expression then gives a system noise level of

$$kT_0 2B_2 F/W = -174.4dBW.$$ (3.11)

This noise level may be compared with a mean transmitted power level of PD = -11dBW, leaving a difference of 163.4dB. If the estimated delay line loss of 30dB is subtracted a difference of 133.4dB remains to be allocated to electromagnetic propagation loss and signal-to-noise ratio.

3.3.6 Electromagnetic propagation loss

In this section estimates of the electromagnetic propagation loss between the interrogation and tag antenna in representative situations will be made. Both of these antennae will be assumed to be half wave dipoles employing horizontal polarisation. The interrogation antenna will be assumed to be placed beneath the roadway surface, on which a layer of salt/sand/ice may be present. The tag antenna will be assumed to be in free space, although a more careful calculation should probably take into account the effect of a conducting backing plane which is likely to be present.

The calculation will first ignore the effect of the roadway material and its covering, and proceed to evaluate the electromagnetic propagation loss in its absence. Under these conditions the one way power transfer ratio is[87]

$$\frac{P_r}{P_t} = g_t \; g_r \; \left(\frac{\lambda}{4\pi R}\right)^2 \tag{3.12}$$

where g_t and g_r are the gains of the interrogation and tag antennae, λ is the free space wave length and R is the range. For $g_t = g_r = 1.64$ (dipole gain), $\lambda = 328$mm, R = 750mm we have a propagation power ratio of

$$\frac{P_r}{P_t} = -24.9\text{dB} \tag{3.13}$$

109.

To proceed with an evaluation of the additional losses caused by the roadway material and its covering, as a first estimate of this effect, it will be considered that the roadway material and its covering to be a single layer of a uniform material, of a thickness to be specified later. An additional contribution to the propagation loss above that described in Equation (3.12) can arise from each of two effects:

(a) the dissipative nature of the medium; and

(b) the reflection at the interface between the medium and free space.

The effects of plane wave propagation in the medium may be described by a complex propagation constant

$$\lambda = \alpha + j\beta \tag{3.14}$$

of which the components may be expressed in terms of material parameters by the equations

$$\alpha = \frac{\omega}{c} \left(\frac{\left(1 + k^2\right)^{\frac{1}{2}} - 1}{2} \right)^{\frac{1}{2}} \tag{3.15}$$

$$\beta = \frac{\omega}{c} \left(\frac{\left(1 + k^2\right)^{\frac{1}{2}} + 1}{2} \right)^{\frac{1}{2}} \tag{3.16}$$

where $k = \sigma/\omega\varepsilon$ is the ratio between conduction current and displacement current in the material, and $c = 1/\sqrt{\omega\varepsilon}$ is the velocity of electromagnetic propagation in a material of the same permeability and permittivity and zero conductivity [88].

Here we are interested to observe the behaviour of α and k as a function of frequency for practically encountered values of σ and relative dielectric permittivity ε_r.

The values of conductivity and relative permittivity for some relevant materials are shown in Table 3.1.

Assuming that the roadway material and its covering may be characterised by a relative permittivity of 10 and values of σ in the range 0.01 to 1.0 s/m, values of k and α have been plotted as a function of frequency in Figures (3.9) and (3.10).

The effect of reflections at the interface between the medium and free space are described by an amplitude reflection factor Γ which for a horizontally polarised wave making an angle of incidence ϕ_i has for lossless materials the form [89]

$$\Gamma = \frac{\cos\phi_i - \left(p - \sin^2\phi_i\right)^{\frac{1}{2}}}{\cos\phi_i + \left(p - \sin^2\phi_i\right)^{\frac{1}{2}}} \qquad (3.17)$$

111.

TABLE 3.1. VALUES OF CONDUCTIVITY AND RELATIVE
PERMITTIVITY FOR SOME RELEVANT MATERIALS

Material	σ s/m	ε_r
Dry Earth	10^{-5}	5
Wet Earth	10^{-2}	10
Sea Water	4.0	78
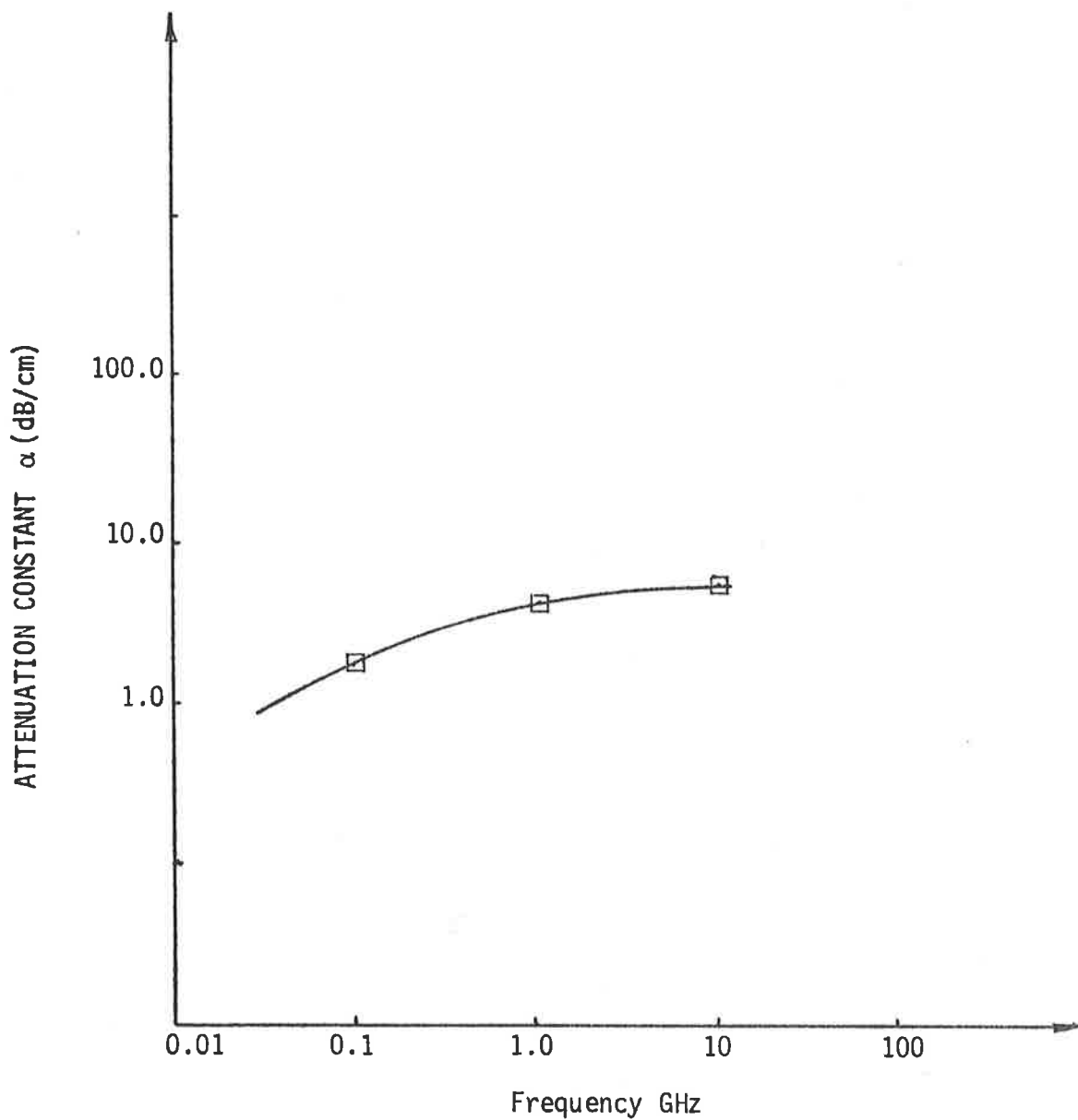
FIGURE 3.9.   PLOT OF ATTENUATION CONSTANT α AS A FUNCTION OF

FREQUENCY WITH σ = 1mho/m AND ε_r = 10.
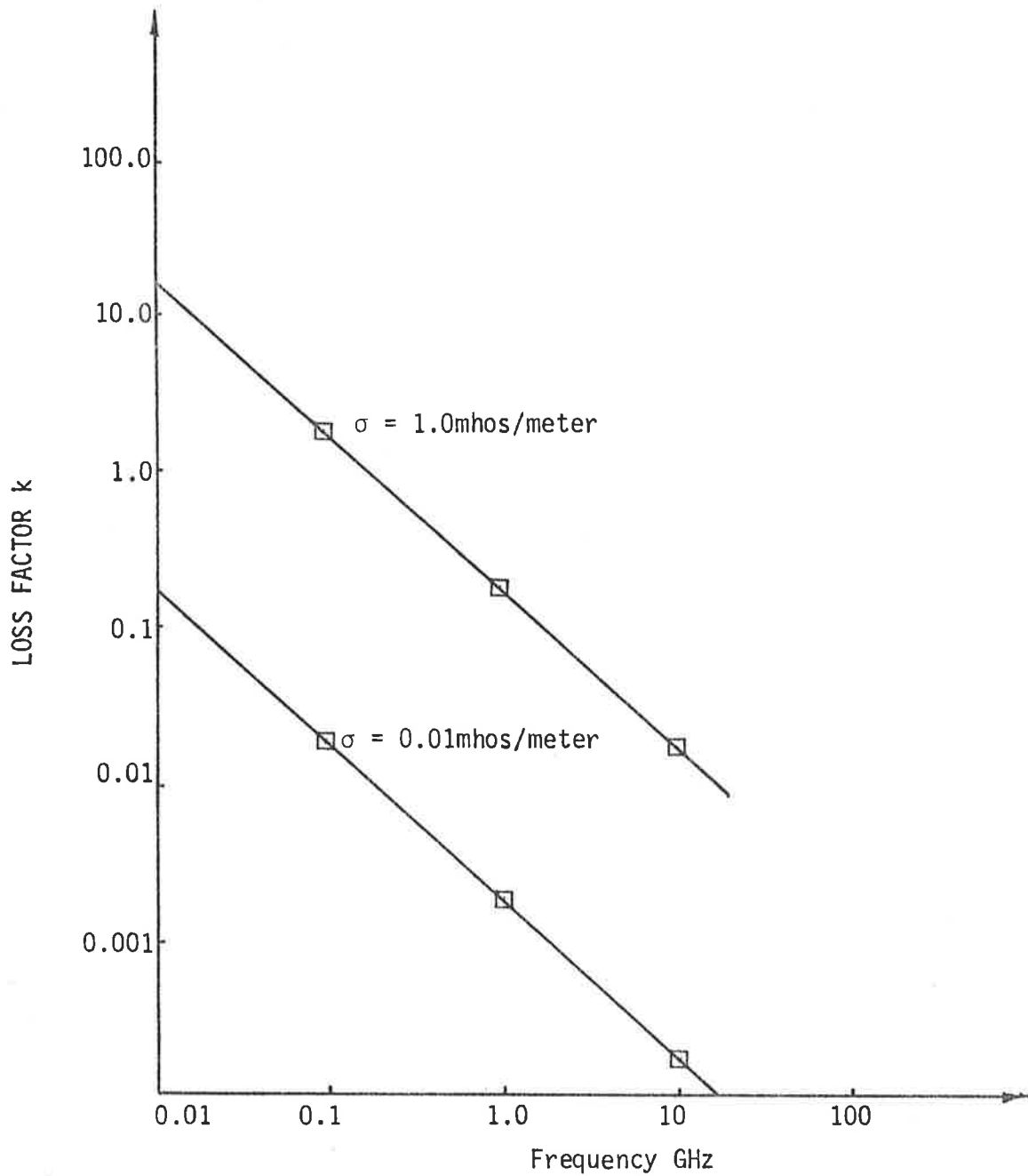
FIGURE 3.10. PLOT OF LOSS FACTOR k AS A FUNCTION OF FREQUENCY FOR

TWO VALUES OF CONDUCTIVITY σ WITH ε_r = 10.

114.

where p is the ratio of the dielectric constants of the two materials. This reflection is plotted in Figure (3.11) as a function of p for normal incidence.

From this brief analysis we may conclude that the attenuation of a signal generated within a media depends on the frequency and the conductivity of that media. For a 1GHz signal generated within a salt-slush layer this is in the order 4dB/cm.

By considering a combination of transmitting-receiving antennae situated in a 5cm deep salt-slush layer, the overall attenuation due to the conductive layer is in the order of 40dB.

The interface also introduces further 6dB loss, due to the reflection of the power at the boundary.

The overall conclusion of this section is that the two-way electromagnetic propagation loss in the system can vary from about 56dB in good weather to 96dB in poor weather conditions.

In order to provide an assessment of the overall performance of this technology, the next section explores the characteristics of noise which arise from several sources.
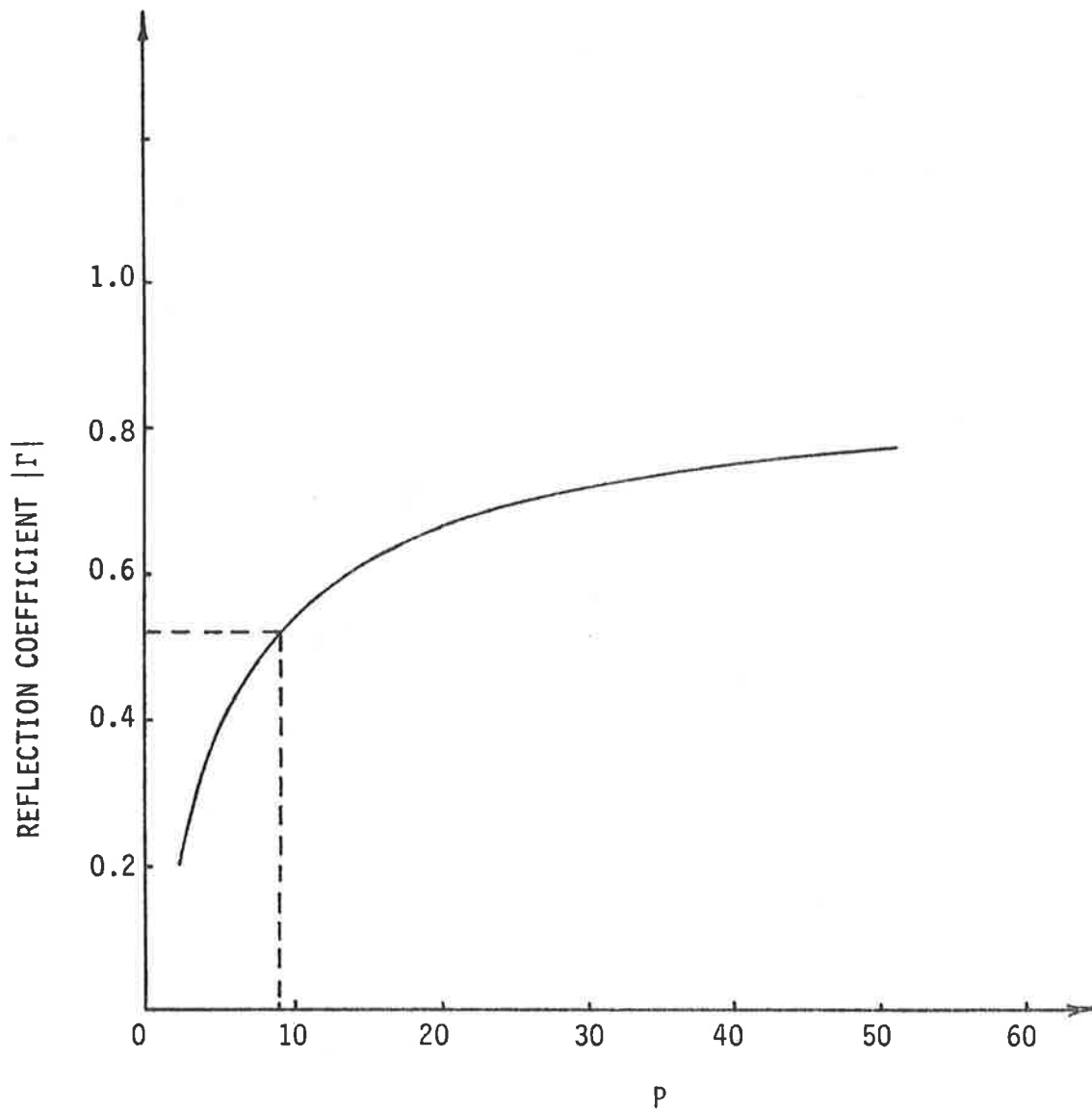
FIGURE 3.11. PLOT OF REFLECTION COEFFICIENT $|\Gamma|$ AS A FUNCTION OF p WITH $\phi_i = 0$.

3.3.7   Spurious reply signals

The interfering signals which can mask the reply from the label being interrogated and produce erroneous output code readings can arise from several possible sources. These sources include broadband noise generated by the vehicle being interrogatdd or others nearby, signals from other uses of the frequency band, and radar echoes of the interrogation pulse from distant objects. Therefore in this section estimates of the level of noise produced by nearby vehicles and of the strength of radar echoes from a number of representative objects are made. The noise data used in this analysis has been derived from roadside measurements and in the absence of other noise information, has dubiously been applied to antennas placed under the vehicle.

Digital signals are affected differently by different types of noise. Thermal noise has little effect on digital signals provided its magnitude does not approach that of the signal. On the other hand, impulsive noise which has high peak-to-rms level often causes errors.   There are two major sources of impulsive noise which affect digital communication systems:

(a) atmospheric noise; and

(b) man-made noise, including industrial and ignition noise.

It has been shown[90 - 91] that atmospheric noise is negligible in the higher part of VHF band and the lower part of UHF band and virtually non-existent beyond that. Moreover, industrial noise and power line noise are not sig-

117.

nificant at these frequencies.

However in the ignition process the discharge current lasts for only a few nanoseconds for a sprak gap of one millimeter. Thus a very broad frequency spectrum is created which is distributed throughout the VHF and lower part of the UHF band. Noise from a single stationary vehicle is more or less periodic in nature. However, the noise from one or more passing vehicles or from several stationary vehicles is aperiodic[91]. Normally the radiation is modified by the body of the vehicle and polarization can be of all kinds. In a real life situation, ignition noise would consist of the combined effects of several vehicles. The noise pulses often occur in groups with irregular spacing. These groups may have duration ranging between tens of microseconds to a few milliseconds. The various parameters of interest in noise measurements are:

(i) peak amplitude distribution;

(ii) time distribution;

(iii) duration of noise pulses at different amplitude levels.

There are a number of measurement techniques to derive the above information:

(i) quasi-peak method;

(ii) amplitude probability distribution (APD) method[92]; and

118.

(iii) noise amplitude distribution (NAD) method[91].

Roy[93] used these results to derive a set of curves for both APD and NAD methods.

APD measurement test results are shown in Figures 3.12(a) and 3.12(b)[94] and NAD test results in Figure 3.13[91]. The latter show that for dense traffic situations about 10^3 pulses per second of appreciable amplitude occur.

To assess the significance of such pulses the characteristics shown in Figure 3.12 is examined. The figure shows that at 915MHz all except 0.1% of noise pulses have an amplitude less than +65dB relative to $1\mu V$ m^{-1} MHz^{-1}. Since the total interrogation time is 10ms, about 10 noise pulses can be expected to occur within it, of which only one can be expected to reach the indicated amplitude.

The reference field strength of $1\mu V$ m^{-1} MHz^{-1} corresponds to a power density in a uniform plane wave of E^2/η = -145.8dBW m^{-2} MHz^{-2}. Taking into account a receiver bandwidth of 100Hz and a noise pulse frequency of 1000 per second we find the reference power density is -215.8dBW/m^2, and the noise level 65dB above this is -150.8dB/W/m^2. At 915MHz a half wave dipole antenna has an effective area of[87]

$$A_e = \frac{g\lambda^2}{4\pi} \qquad (3.18)$$

119.
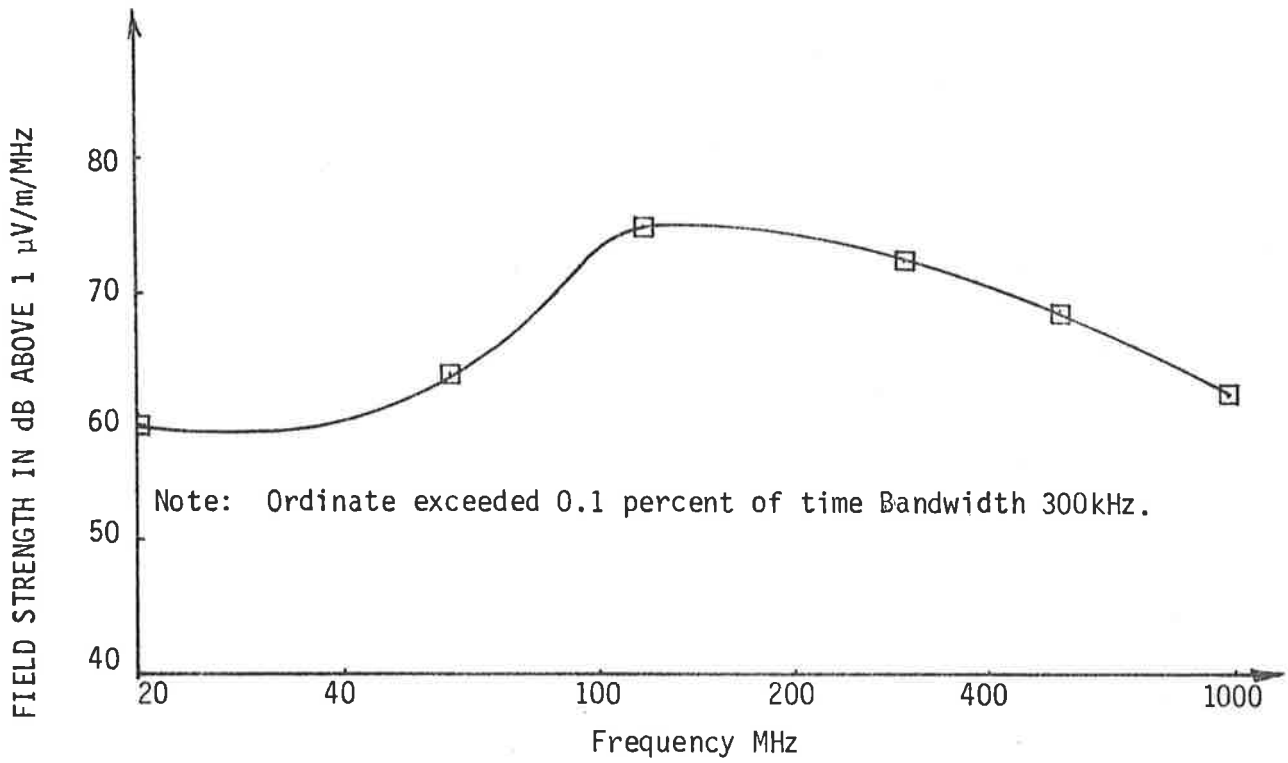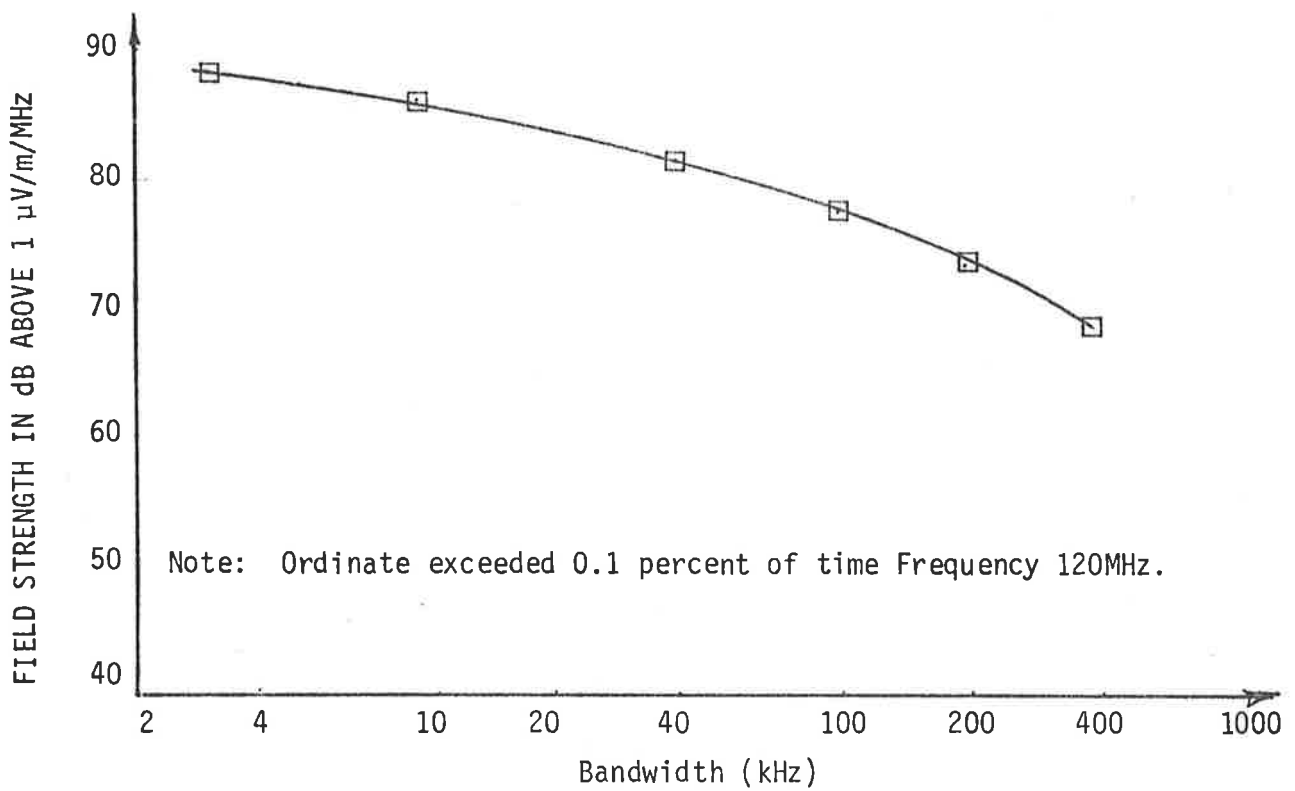
FIGURE 3.12. FIELD STRENGTH VARIATION WITH

(a) Frequency.
(b) Bandwidth.

120.
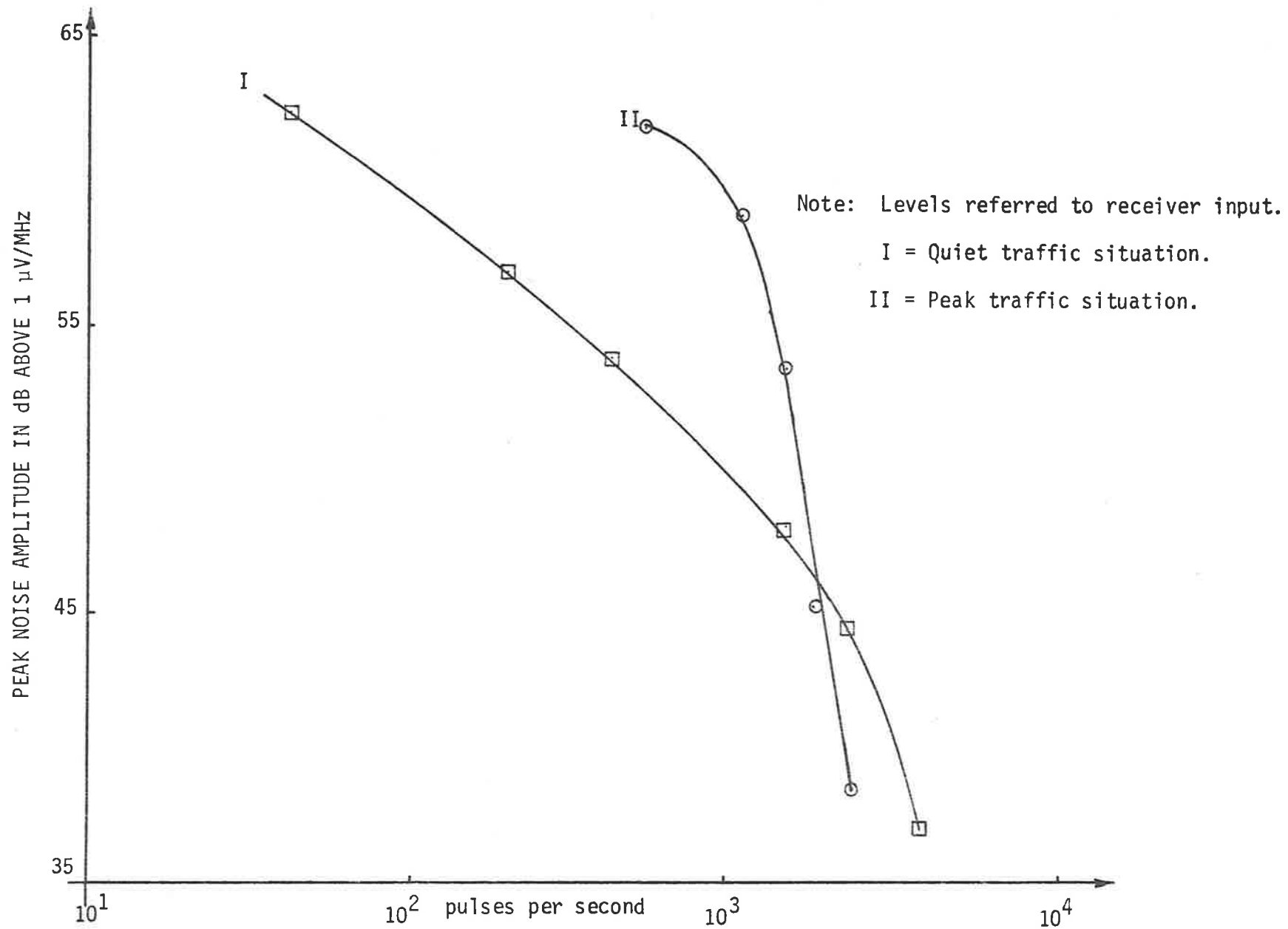
FIGURE 3.13. NOISE AMPLITUDE DISTRIBUTION DUE TO MOTOR VEHICLE TRAFFIC.

Note: Levels referred to receiver input.

I = Quiet traffic situation.

II = Peak traffic situation.

and on substitution of appropriate values in Equation 3.18 the value of 1.42×10^2 m^2 is obtained. So the noise level below which most pulses fall is -169.3 dBW.

This noise power should be compared with a planned peak transmitted power level of +10dBW. The result shows that the total electromagnetic propagation and delay line return loss must exceed 190dB before the ignition noise becomes dominant.

A further factor which needs consideration is the evaluation of the strength of a different form of interference, that of radar echo from a number of representative objects. The first such object consists of a simple dipole resonant at the interrogation band centre frequency, such as is formed by any approximately 165mm length of wire or rod. The second type of object considered consists of a flat conducting plate of area 1m^2 positioned so that it faces towards the interrogation antenna.

In both cases the position of the reflecting object will be chosen so that the arrival of the echo coincides with the occurrence of the first bit of the reply code. In this case the two-way propagation time between the interrogation antenna and the reflecting object is 1.95µs, and the object is therefore sited approximately 300m from the interrogation apparatus.

For the simple half wave dipole object the ratio of the reflected power P_r arriving back at the interrogation point

to the original power P_t is given by

$$P_r/P_t = \left[g_t \; g_r \; (\lambda/4\pi R)^2 \right]^2 \tag{3.19}$$

where g_t is the gain of the interrogation antenna

       g_r is the gain of the reflecting object

       λ is the freespace wave length

       R is the range of the reflecting object.

For half wave dipole antennae with a gain of 1.64 operating at 915MHz at a distance of 300m we find a reflected power ratio of -154.3dB. For the flat plate reflecting object whose dimensions are large compared with a wave length[89] the radar cross section gives the reflected power ratio

$$P_r/P_t = \left[g_t \; A_p/4\pi R^2 \right]^2 \tag{3.20}$$

where A_p is the area of the reflecting plate. For a half wave dipole interrogation antenna, and a $1m^2$ reflecting plate at a range of 300m the reflected power ratio is -116.8dB.

When the flat plate is not oriented directly towards the interrogation source the reflected power is reduced in amplitude. Some idea of the beam width of the reflection pattern may be obtained by approximating the object as a circular plate for which, when the diameter is large in relation to a

123.

wave length, the antenna pattern has a beam width between zeros of

$$\Delta = 2.44\lambda/d \hspace{3cm} (3.21)$$

where d is the diameter of the circle.   For a circle of area $1m^2$ we find a beam width of approximately 50°. Although the accuracy of the claculation is somewhat in question as a result of the moderate size of the object in relation to a wave length, the results do indicate that for the object chosen the scattering would be well distributed in space.

3.3.8   System evaluation

The estimates of parameters for a typical system are shown in Table 3.2. The results show the kind of signal-to-noise ratio one could expect for systems operated in the 915MHz frequency band. The analysis indicate that the system would appear to be just workable under unfavourable weather conditions, and eminently workable under good weather.

However the main draw-back arises in that the tags are not readily field programmable and some problems can be envisaged with the delay line when long codes are required. Furthermore, because the reply signals from this type of transponder are weak, complex signal processing is necessary to extract the reply signal from noise.

TABLE 3.2. SUMMARY OF SYSTEM PARAMETERS FOR 915 MHz SURFACE ACOUSTIC WAVE LABEL

Delay line return loss	30dB
Free space part of propagation loss	50dB
Under road part of propagation loss	46dB
Free space reflection loss $1m^2$ plate	117dB
Ignition peak noise level	179dB
Mean transmitter power	11dBW
Total reply loss for unity S/N Peak ratio	163dB
Resultant signal-to-noise ratio	37dB

Notes:

(a) *Peak transmitted power is 10 watts.*

(b) *Average transmitted power is 90mW.*

(c) *For free space reflection assoaiated with $1m^2$ plate the reflection is 37dB below reply from tag.*

(d) *The table as applied is not valid due to usage of the roadside noise. However the results could be applied to the situations in which the antenna is placed on the side of the vehicle.*

3.4   The Two Port Passive Subharmonic Transponder

The passive subharmonic transponder (PST) is an example of a device which makes use of very low frequency communications substantially by magnetic field and achieves the required separation in the frequency domain, by providing a reply code which is a modulated subharmonic of the continuous wave interrogation signal. The subharmonic nature of the reply signal provides a precise knowledge of the reply signal frequency in cases where narrow band detection is used to maximise signal-to-noise ratio[95].

The PST is an electronic label, which when interrogated by a cw signal at a frequency f_t, sends a coded reply in a lower frequency band via a carrier which is harmonically related to the interrogation frequency. Operational characteristics of this device have been reported elsewhere[69] [96]. In general the circuit design questions are reasonably straightforward. The most important issues governing their practical application are concerned with strength of the electromagnetic coupling links, and the levels of environmental noise. Therefore attention is focussed principally on these latter issues.   An equivalent circuit which shows the essential characteristics of the electromagnetic coupling links is illustrated for a two-port system in Figure 3.14. From the diagram it can be noted that the transponder receives power and a reference frequency ω_t from the transmitter system over the coupling link established between the transmitter antenna L_1 and the receptor antenna L_2, and returns a biphase (PSK) coded reply signal ω_r to the receiver system over the coupling link established between the transponder antenna L_3 and receiver antenna L_4.
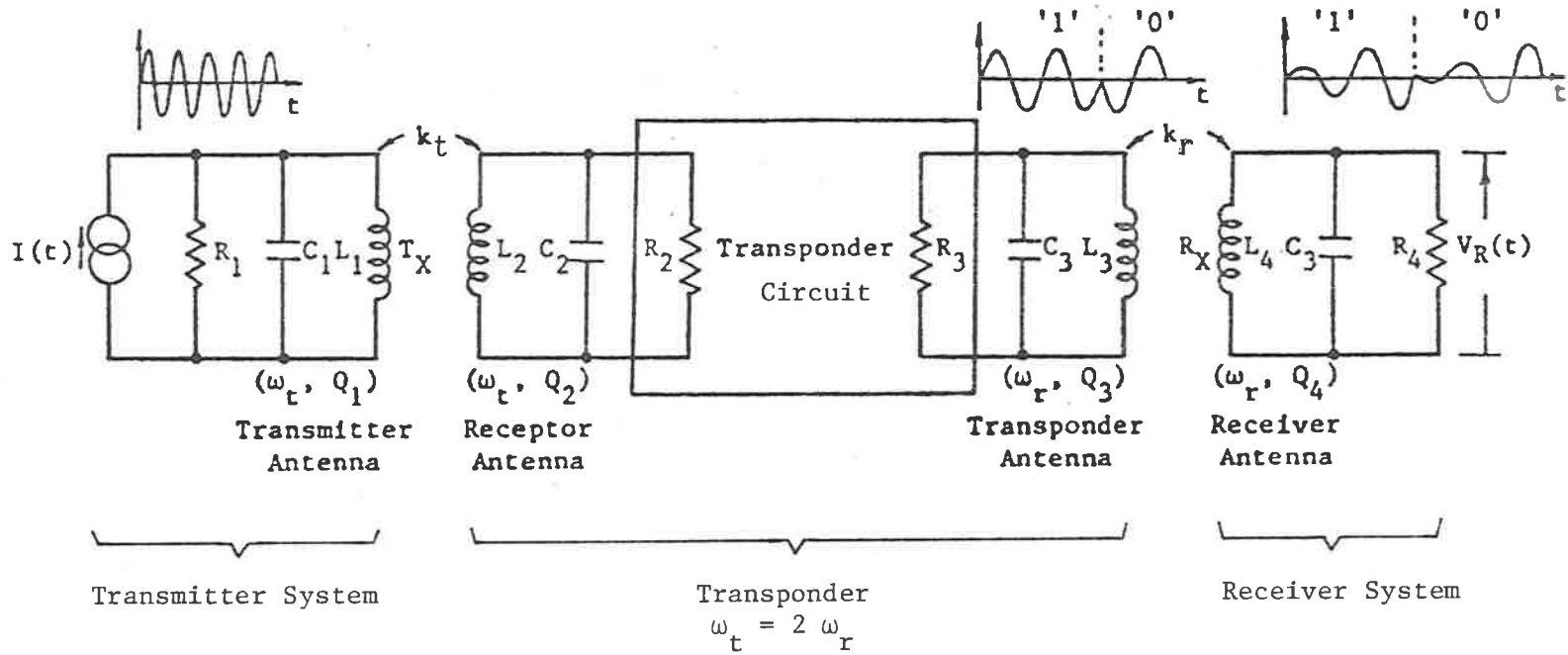
FIGURE 3.14. BLOCK DIAGRAM - TWO PORT PST SYSTEM.

3.4.1 Power transfer consideration

Because these devices are normally operated at low radio frequencies over short interrogation distances the coupling between the antennas is basically provided by their near fields. It is interesting to note that in the near field situation the coupling is provided not be radiated far fields which require real power to be provided by the transponder, but is instead provided by the reactive energy storage fields established by the transponder in the space surrounding itself. When the electromagnetic power loss between the transmitter and the label of a PST system is large, the real power coupled to the label is to an excellent approximation proportional to the reactive power density of the energy storage field created by the transmitter at location of the receptor antenna. The power transfer ratio P_2/P_1 can be shown to be given by:

$$P_2/P_1 = k_t^2 \, Q_1 \, Q_2 \qquad (3.22)$$

where P_1 is power input to the transmitter antenna having a quality factor Q_1, and P_2 is the power transferred to the receptor coil with quality factor Q_2, and k_t is the coefficient of coupling between transmitter and receptor antennas.

Similarly the power transfer ratio P_4/P_3 in the link from the transponder antenna to the receiver antenna can be calculated by using the relation:

$$P_4/P_3 = k_r^2 \, Q_3 \, Q_4 \qquad (3.23)$$

where P_3 is power dissipated in transponder antenna having a quality factor Q_3, and P_4 is the power received by the

receiver antenna with quality factor Q_4 and k_r is the co-efficient of coupling between transponder and receiver antennas.

The overall power transfer can now be expressed as:

$$P_4/P_1 = \eta_c \, k_t^2 \, k_r^2 \, Q_1 \, Q_2 \, Q_3 \, Q_4. \qquad (3.24)$$

η_c is the conversion efficiency factor and is included in Equation 3.24 to take into consideration the losses associated in powering the control circuitry within the transponder. In practice control circuits require only a small portion of the power received by the label.

3.4.2 Calculation of coefficient of coupling

In order to obtain results that are simple in structure for calculation of the power transfer, it is assumed that all antenna* structures of interest have simple shapes and behave in much the same way. Therefore the calculations are based on the shape which is most convenient mathematically, viz. a circle. Such an approach can also be extended approximately to a square antenna where the dimensions for the transmitter and receptor antennas are

---

* *The near field antenna operates at frequencies sufficiently low such that for the distances involved, the principle coupling is by the near fields. Strictly speaking, it is not a radiator and, therefore, is not an antenna in the usual sense.*

129.

$$D = d \sqrt{\frac{\pi}{4}} \qquad\qquad (3.25)$$

and

$$C = c \sqrt{\frac{\pi}{4}} \qquad\qquad (3.26)$$

where D and C are the length of the sides of the trans-
mitter and receptor antennas having the same area as a
corresponding circular antenna with diameters d and c res-
pectively.

By considering the geometry shown in Figure 3.15, the
magnetic field H at a distance h along the axis from the
centre of a circular coil of diameter d and carrying a
current I is given by (Appendix D),

$$H = \frac{I}{d \left[1 + \left(\frac{2h}{d} \right)^2 \right]^{3/2}} \qquad\qquad (3.27)$$

If the diameter d of the transmitting antenna is much
larger than the diameter c of the receptor antenna, then
the field intensity can be considered constant over the
area covered by the receptor.

Using Equation (3.27) in conjunction with the induc-
tances L1 and L2 corresponding to the transmitter and

130.
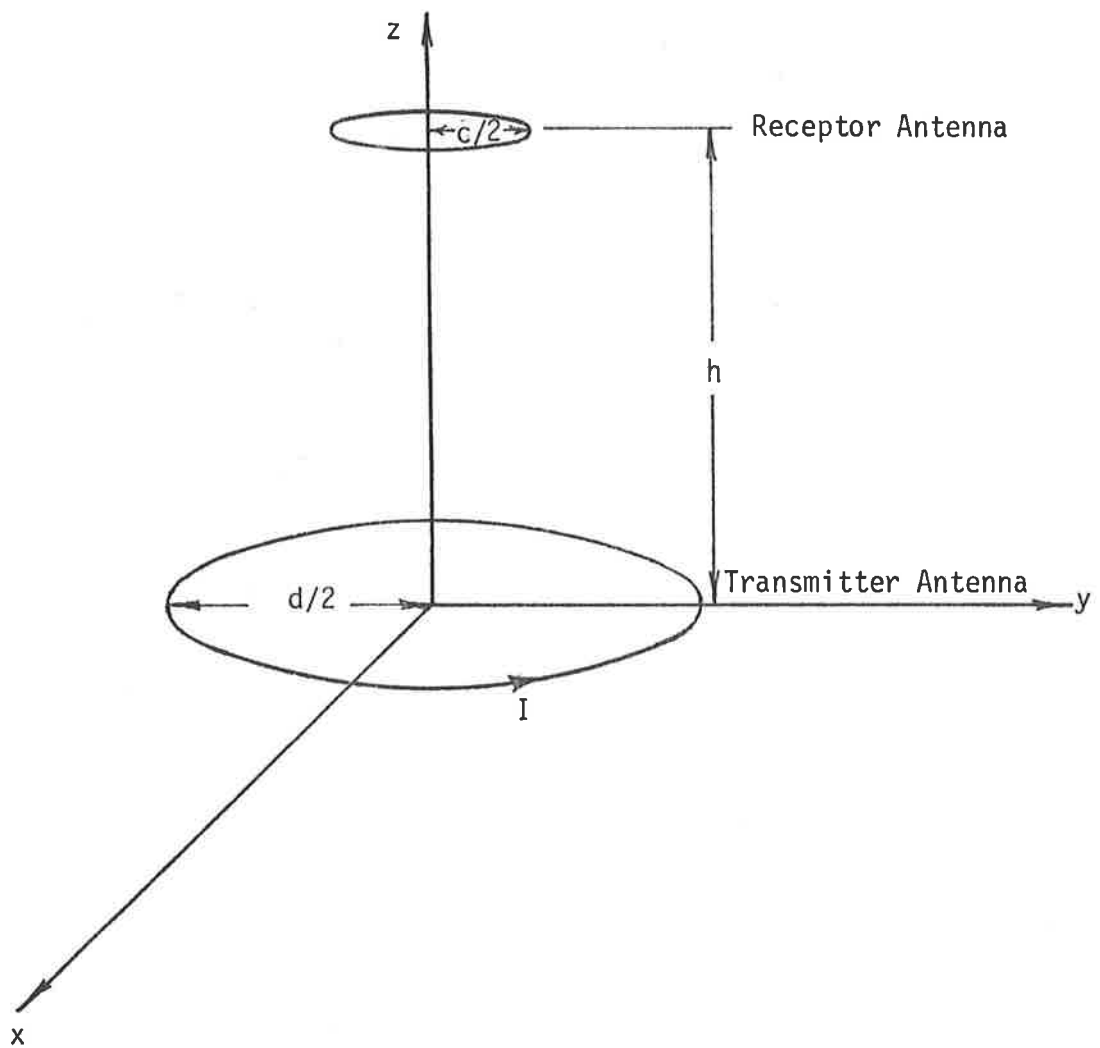
FIGURE 3.15.   RELATIONSHIP BETWEEN TRANSMITTER AND TRANSPONDER ANTENNAS.

receptor antennas respectively, the coefficient of coupling can be expressed as

$$k = \frac{\alpha_t^{3/2} \beta_t}{\left(1 + \phi^2\right)^{3/2}} \tag{3.28}$$

where

$$\phi = \sqrt{\pi} \, (h/D) \tag{3.29}$$

$$\alpha_t = \frac{C}{D} \tag{3.30}$$

$$\beta_t = \frac{\pi}{2} \left\{ \left[\log_e \frac{4d}{r_1} - 2 \right] \left[\log_e \frac{4c}{r_2} - 2 \right] \right\}^{-\frac{1}{2}} \tag{3.31}$$

and r_1 and r_2 are wire radii corresponding to the transmitter and receptor antennas. Figure 3.16 shows the plot of k as a function of ϕ for several values of α_t.

If the transmitter and receptor antennas are square with sides D and C respectively, the relation for the coefficient of coupling remains the same. However the value of β_t becomes

$$\beta_t = \frac{\pi^{3/2}}{4} \left\{ \left[\log_e \frac{4D}{r} + \frac{r}{D} - 2.16 \right] \left[\log_e \frac{4C}{r} + \frac{r}{C} - 2.16 \right] \right\}^{-\frac{1}{2}} \tag{3.32}$$

132.
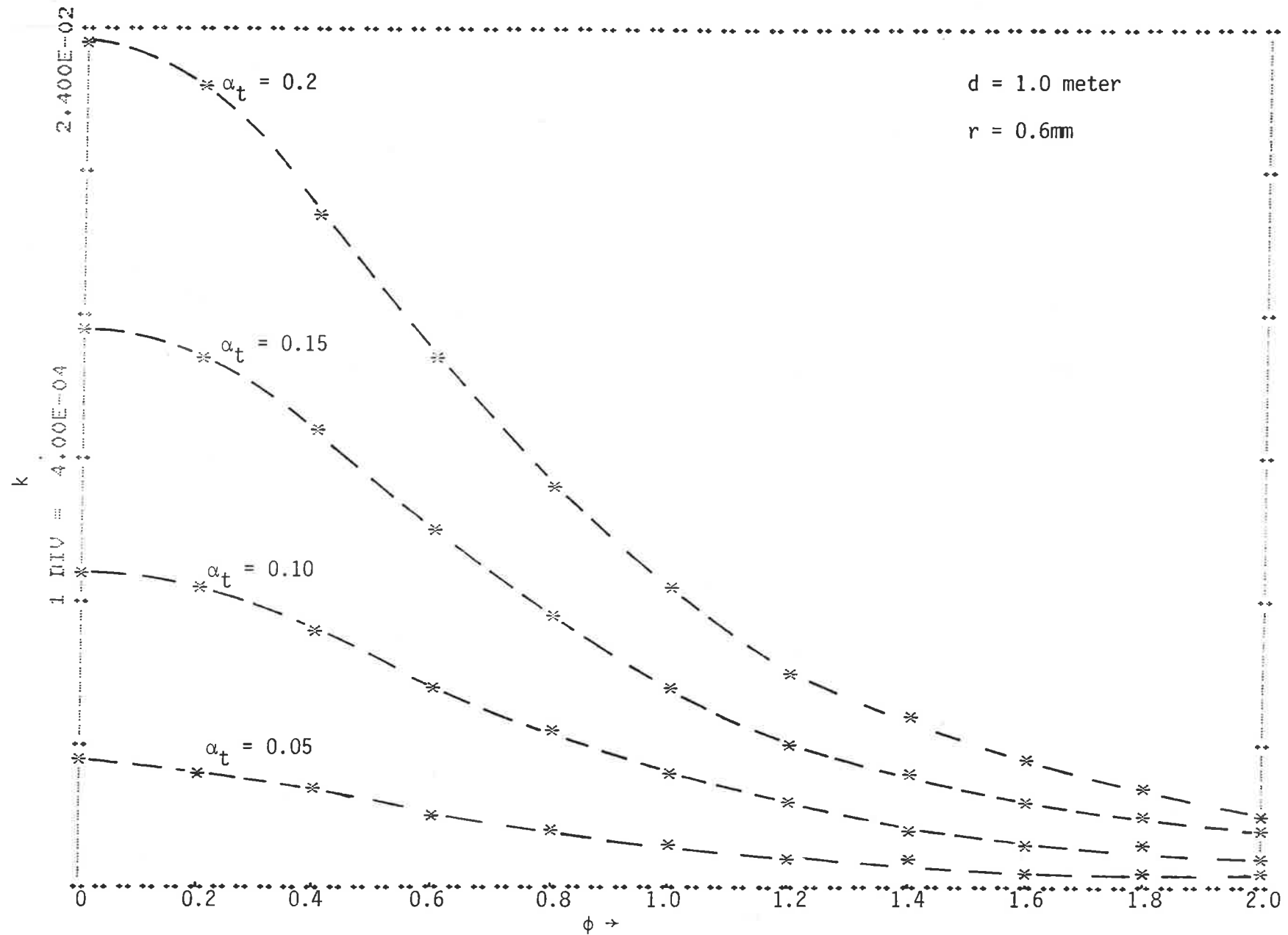
FIGURE 3.16.   PLOT OF COEFFICIENT OF COUPLING k AS A FUNCTION OF φ FOR SEVERAL VALUES OF α_t USING CIRCULAR ANTENNAS.

133.

The structure of the relation given by Equation (3.28) is of interest. The first term $\alpha_t \, \beta_t$ gives the value of the coefficient of coupling at the centre of the antenna, i.e. $h = 0$. The second term indicates the extent to which the coefficient of coupling is changed as the separation h between the transmitter and receptor antennas is varied. The curves of Figure 3.16 illustrate the high sensitivity of the electromagnetic propagation loss to transponder position.

3.4.3. Power transfer evaluation

In seeking to maximize the received power, the quality factors Q_1 and Q_2 of the transmitter and receptor coils can be made as high as conveniently practicable, the relevant constraints being the intrinsic losses in inductor of convenient size and the undesirability of employing excessively high Q factors in coils which are subject to detuning by changing environments. The quality factors Q_3 and Q_4 of the transponder and receiver antennas are limited by the same factors as well as by constraints provided by the reply signal bandwidth.

In practice it is not difficult to achieve control circuits of fairly low power so that the majority of the power received by the receptor coil is available for exciting the transponder.

Consideration of power matching in its general sense between the transponder circuit and its input and output ports is made complicated by several factors. Apart from the fact that at low power levels the nonlinear behaviour

134.

of the circuit makes general theorems from linear circuit theory inapplicable, we have the important characteristic that coupling between near-field antennas occurs basically through their stored energies rather than any dissipated or radiated power. The question of optimum impedance level is therefore one of maximizing these stored energies rather than matching of power between a source and a radiation impedance.

In the development of power transfer ratio expressions as shown by Equation (3.22) and Equation (3.23) the power dissipated in resistor R_1 shown in Figure 3.14 is considered to be the sum of the powers dissipated in the receptor antenna and transferred to the electronic transponder circuit, while the power dissipated in R_2 is that necessarily involved in establishing the desired stored energy in the transponder antenna.

In the PST system, the method by which phase modulation of the reply signal is achieved places a limit (dependent on the retransmitting antenna quality factor) on the information rate achievable in the reply signal. The bandwidth of the retransmitting coil tuned circuit establishes the rate at which signals of one phase will be attenuated and signals of another will be built-up, when a change in the reply code takes place. Such limitation is a significant one as the electromagnetic coupling between the transponder and the receiver also depends on the transponder antenna quality factor with the result that a narrow tuned circuit is normally desired.

135.

In the design of a practical system a wide choice of
system parameters are possible. To have an appreciation
of the level of power transferred across the electromagnetic
link of the following system parameters are used in the analysis.   ✗
The receptor coil is assumed to have a loaded quality factor
of Q_2 = 50 with its internal losses and the power delivered
to the circuit contributing equally to the damping. To pro-
vide the required reply channel bandwidth the transponder
coil is loaded to provide a quality factor of Q_3 = 8. In
both cases planar coils having a diameter of 0.113m are
used. The coils are also overlapped for zero coupling
between them.

The transponder positions considered are on the axis
of the transmitter receiver coil at distances which range
from zero through 1 metre. The transmitter and receiver
antennas are provided by a single turn planar coil of dia-
meter 1.13 metre, operated in a duplex mode, with respec-
tive quality factor Q_1 = 8 at the transmitter frequency and
Q_4 = 8 at the receiver frequency.

The predicted losses in the two electro-magnetic coup-
ling links using Equation (3.28) are shown as a function of
transponder position in Figure 3.17. The larger loss in
the receiver coupling link arises simply from the limitation
imposed by the requirement of providing adequate communica-
tion bandwidth for the reply signal.

The curves of Figure 3.17 illustrate the high sensitivity
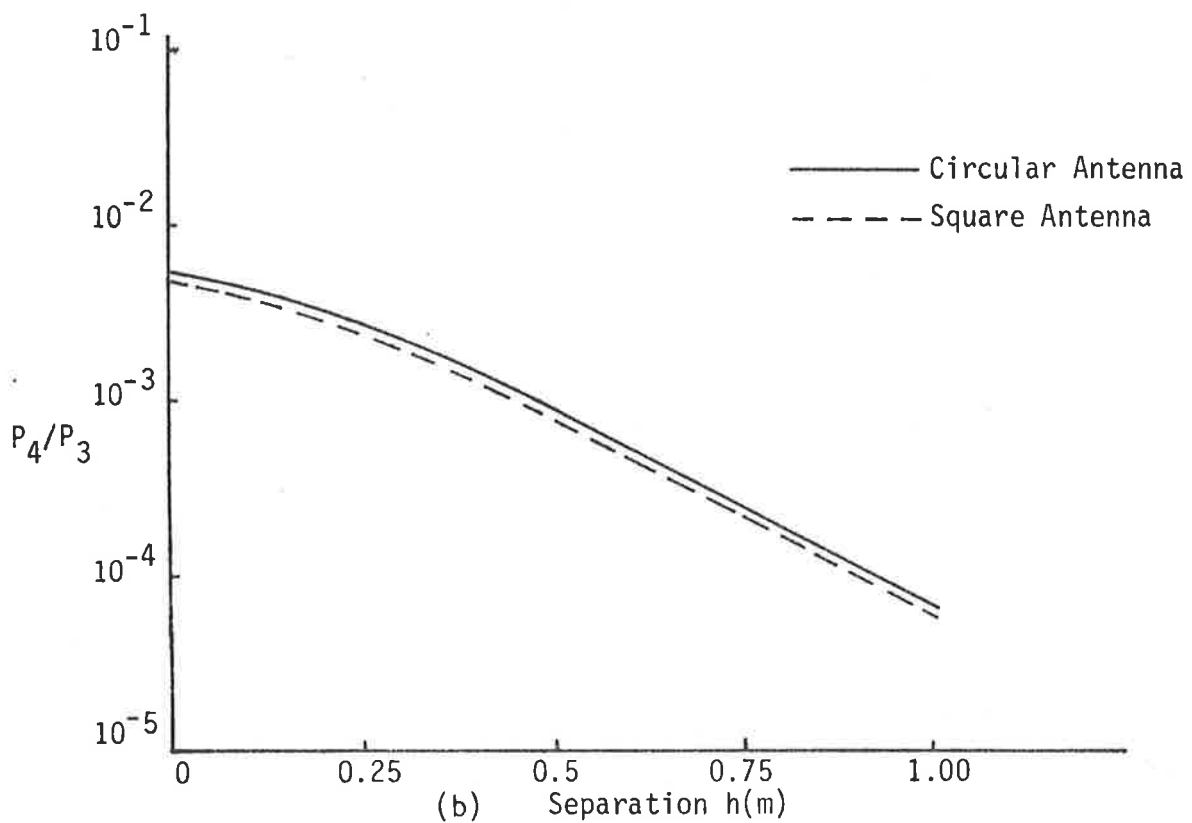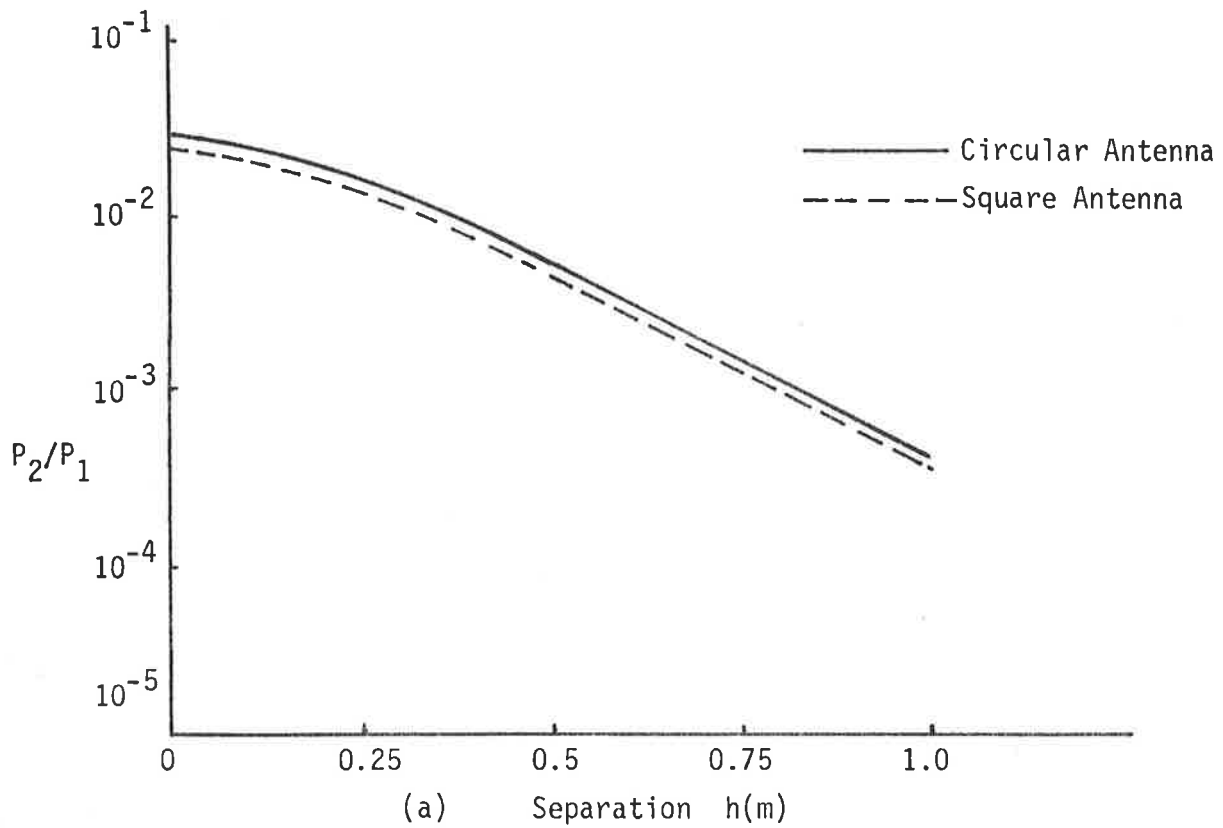
FIGURE 3.17. PLOT OF ELECTROMAGNETIC COUPLING LINK LOSSES AS A FUNCTION OF SEPARATION h FOR CIRCULAR AND SQUARE PLANAR COILS.

(a)   Transmitter - Receptor Path.

(b)   Transponder - Receiver Path.

of the coupling loss to transponder position in operational
situations. A consequence of this sensitivity, as well as
the relatively low loss in the transmitter as opposed to
the receiver coupling link, is that the transponder itself
is normally designed, through the inclusion of internal
limiting circuits, to operate without damage over a substan-
tial range of excitation field strengths.

3.4.4   Signal-to-noise characterizations

For such technology experiments have shown that a con-
servative estimate of the achievable ratio P_3/P_2 of the
power delivered to the transponder coil to that received
by the receptor coil is 30%,   this ratio being mainly
determined by the equal power division between the receptor
losses and power available for circuit operation and reply
signal generation. With such a conversion efficiency and
the electromagnetic propagation losses calculated in the
previous section, the power delivered to the receiver system
can be shown to be -59.9 dBW at the sensing distance of 750mm.

Successful operation of the transponder with this level
of excitation and at this distance depends upon the achieve-
ment of satisfactory signal-to-noise ratio at the receiver.
In practical systems it is found that environmental noise
dominates noise generated in well designed receivers.
Studies of environemntal noise in several indoor situations
[91 - 93] containing a variety of operating electronic in-
strumentation indicated that noise is impulsive in character

with impulse repetition ratio related to power line fre-quencies. The worst case peak noise amplitude with the receiver antenna as described was -88.6 dBw.

From the above results, for a transmitted power of 10 watts, a curve of signal-to-peak impulse noise level (S/N_{peak}) as a function of separation h is plotted in Figure 3.18. These results show that if the acceptable error rate for individual reply code is at 1 in 10^{-8}, for PSK, then a signal-to-noise ratio of 18.5 dB provides satisfactory performance up to the range of 1 metre in the environments tested, without the need for complex reply signal processing.

Larger impulsive noise levels have been observed in more hostile environments, such as beneath an operating motor vehicle. The practical options available to improve reply signal integrity are an increase in transponder antenna size, a decrease in the range of operation, and the use of error correcting codes which exploit the high ratio of peak to rms noise levels, or in some cases the coherent integra-tion of replies over many message lengths.

Summary of a two-port PST system and its overall perfor-mance at a sensing distance of 750mm is illustrated in Table 3.3. Althouth these results are illustrated for circular coils, similar results can also be obtained for the square coils. Using the definition of equivalent area, the dimension of receptor (transponder) coil becomes $0.1m^2$. For these dimensions at a sensing distance of 750mm the $S/N_{peak} = 27.5dB$. For zero coupling it is necessary to overlap the transponder and receptor coils. Experiments have shown the amount of overlap is in the order of 20% of length.
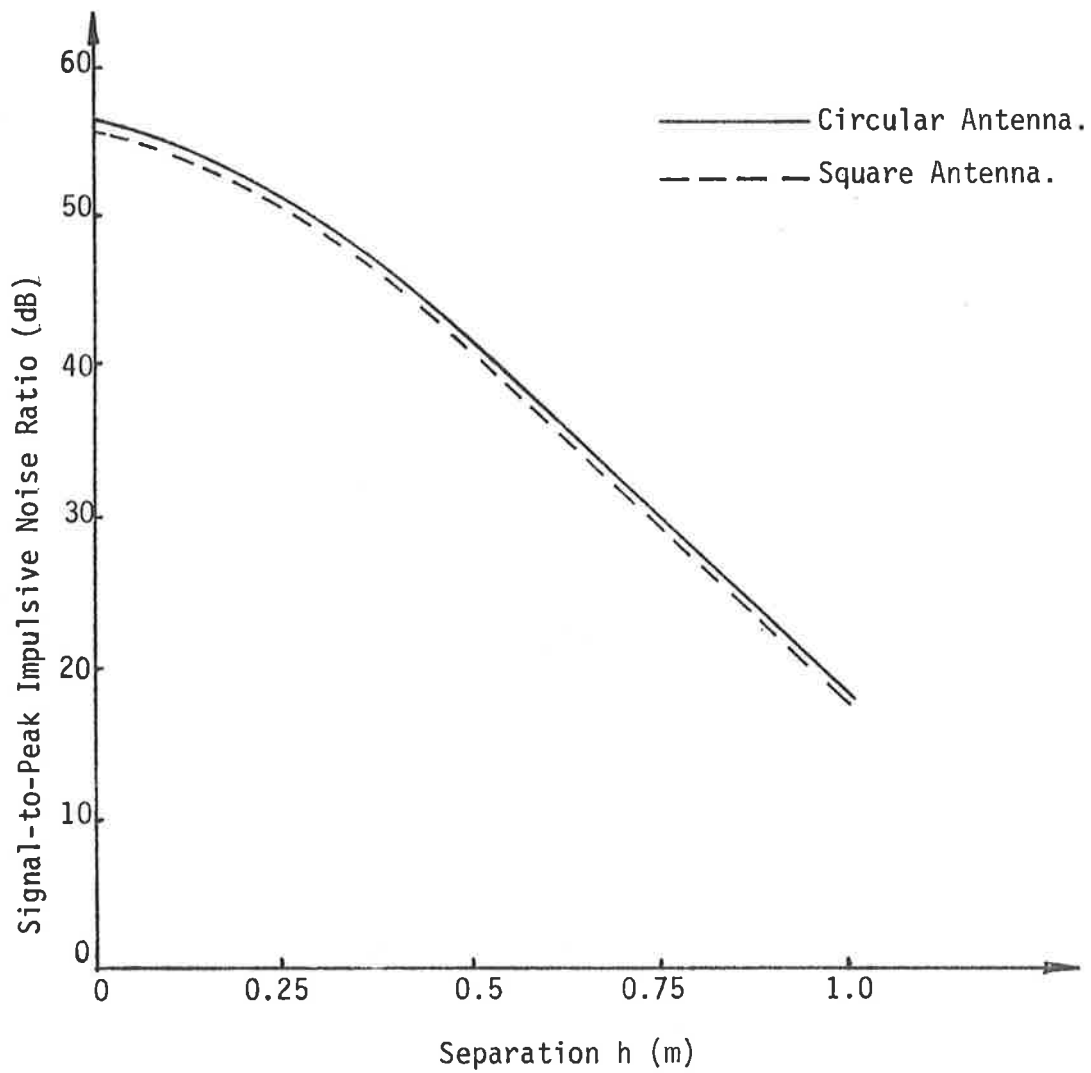
FIGURE 3.18. PLOT OF SIGNAL TO PEAK IMPULSIVE NOISE AS A FUNCTION OF SEPARATION h (METERS).

140.

TABLE 3.3. SUMMARY OF SYSTEM PARAMETERS FOR A TWO PORT PST

Antenna Dimensions:	
Transmitter antenna diameter	1.13m
Receiver antenna diameter	1.13m
Receptor antenna diameter	0.11m
Transponder antenna diameter	0.11m
Quality Factors:	
Q_1	8
Q_2	50
Q_3	8
Q_4	8
Conversion Efficiency η	30%
Sensing Distance	0.75m
Electromagnetic coupling link losses	
P_2/P_1:	1.45×10^{-3}
P_4/P_3:	2.33×10^{-4}
Interrogation Frequency	100KHz
Reply Frequency	50KHz
Modulation Technique	BPSK
Number of cycles per bit	8
Number of bits in message	64
Total loss from transmitter to the demodulator	-59.9dBW
Peak impulsive noise power	-88.6dBW
Transmitted power	10 watts
Signal-to-peak noise power at demodulation input	28.7dB

Notes: (i) *It is assumed that the propagation loss in both the transmitter and receiver paths are identical.*

(ii) *Noise power was derived from noise recordings taken at several sites.*

(iii) *The value of quality factor assigned to Q_1 is based on practical consideration due to burial of the transmitter antenna beneath the road surface.*

3.4.5 System considerations

Technologies suitable for the realization of a PST label are CMOS, I^2L or the mW bipolar logic. In practice it is not difficult to achieve a power level consumed by the control circuits of only a minor fraction of the energy passing through and converted by the transponder (i.e. 50μW at 100KHz), so the questions of greatest interest are concerned with:

(i)   the achievement of sufficient power transfer across both electromagnetic propagation links to enable a healthy reply signal level at the demodulation input to be obtained in the face of substantial levels of electromagnetic interference that may be encountered in many practical traffic situations;

(ii)   the selection of optimum antenna geometrics and orientations;

(iii)   the influence of mass of metal such as that of a motor vehicle on the power transfer.

(iv)   the selection of reply signal encoding parameters which are optimum in relation to the generally known characteristics of interfering signals; and

(v)   the selection of transponder antenna impedance levels so that sufficient voltage to operate the transponder circuits results.

These questions will be dealt with in the chapter to follow.

3.5 Comparisons and Conclusions

An important consideration concerning a microwave system is that is has to live with the existing controversy over the hazard of human exposure to microwave radiation and the difficulties of licensing for high frequency operation. The inability of the tags being field programmed also detracts from their suitability for vehicle monitoring and surveillance. In addition, interface problems associated with buried antennas could be a significant factor in some applications. Generally the reading zone is not well defined and therefore problems can be expected in multi-lane systems.

The alternative low frequency induction system has several advantages. First, the reading zone is well defined and therefore it is suitable for multi-lane operation. Second, it is also free of the objections associated with microwave technology since it makes use of very low frequency communications substantially by magnetic field and operates at frequencies at which licensing requirements are absent or relaxed. Finally, preliminary analysis has indicated that satisfactory performance can be achieved for practically encountered situations and therefore the technology can be considered as a suitable contender for vehicle identification and location determination systems.

On the basis of the above findings, the remaining portion of this research has subsequently been directed towards detailed evaluation and analysis of low frequency induction systems with the objective of deriving principles on which an optimum system can be developed.

143.

CHAPTER 4

A NEW CLASS OF PASSIVE TRANSPONDERS

4.1 Introduction

An inherent problem associated with two-port PST systems lies in their need for two uncoupled antennas requiring additional space on the transponder, which in practical applications is normally desired to be small. Furthermore, for the kind of circuits used for coupling, the bandwidth which must be provided is determined by the information rate required in the reply signal while for near-field antennas the strength of the electromagnetic coupling between the transponder and the interrogation is proportional to the quality factor.

The well known inverse relationship between quality factor and bandwidth therefore provides unwelcome constraints on the performance of the overall system. These systems have the further dis-advantage that the energy available for generating the reply signal has been attenuated by the losses involved in conversion of the interrogation signal energy first to dc and the conversion of this energy to the frequency of the reply signal.

144.

All of these limitations are removed in the one-port PST structure to be described. A model of the system showing the transponder in relation to the transmission paths is shown in Figure 4.1.

If a constant-parameter linear system being excited by a sine wave at frequency ω_t, the steady state output will also contain a sine wave of frequency ω_t. However, the amplitude and phase of the output wave may have been altered. If the excitation source contains two frequencies ω_1 and ω_2 the output will contain these two frequencies. In general the output will contain the frequencies present in the input.

In a non linear system the situation is rather different. A single input frequency may produce a response having harmonics or subharmonics of the input frequency present in the output. This concept is being exploited in the development of the one-port subharmonic transponder.

4.2 Basic Structure of One-Port PST

The new concept recognises that power transfer in the electromagnetic propagation paths at two frequencies are independent. As a consequence there must be a fundamental component of current in the transponder antenna in order to extract power from the applied field at the fundamental frequency ω_t created by the interro-
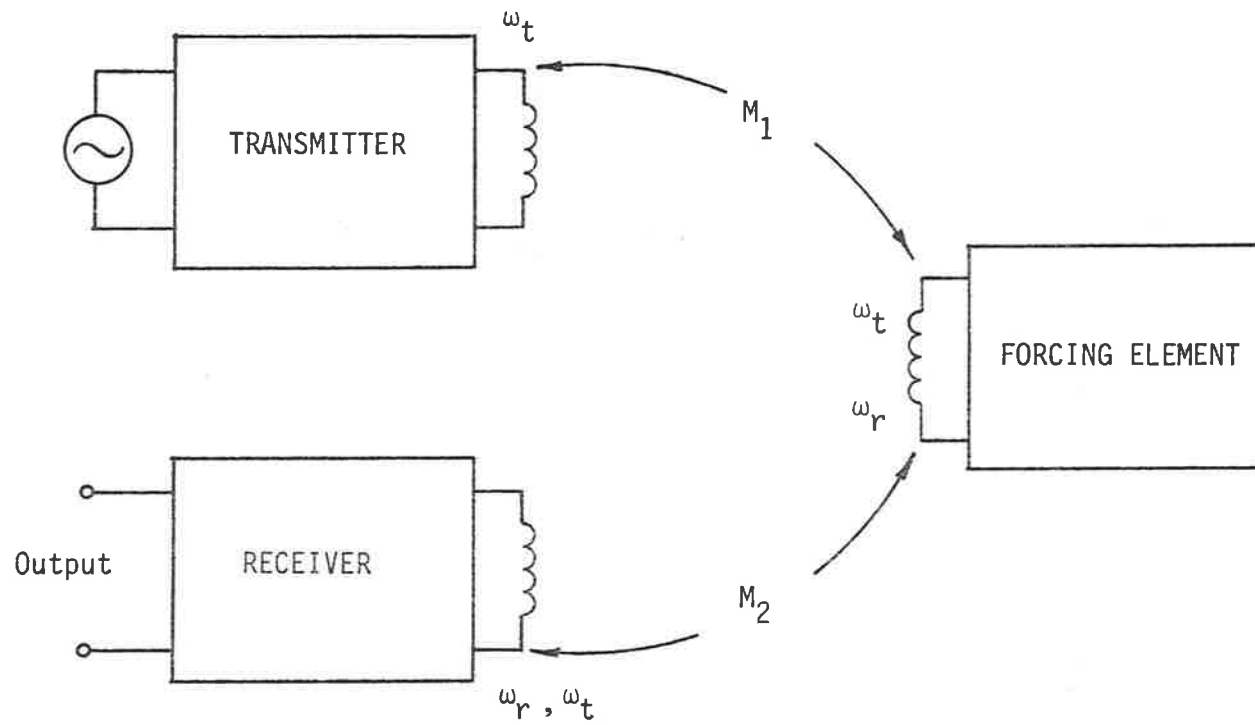
FIGURE 4.1.   CONCEPTUAL MODEL OF THE IDENTIFICATION SYSTEM.

gation signal, and there must also be a second frequency component of current in the transponder coupling element in order to transmit the reply signal.

It is further recognised that efficient power transfer between near-field coupling elements proceeds when these coupling elements are reactive storage elements resonated with high quality factor by reactive energy storage elements of the complementary type as illustrated in Figure 4.2.

The one-port transponder consists of a single coupling element Z which is used for simultaneous extraction of power from the transmitting source at one frequency and its subsequent reradiation at another harmonically related frequency.

The coupling between the transmitter and transponder may be achieved by either magnetic field or the alternative electric field.

However practical consideration such as shielding problems, small mutual capacitance that can be expected between the interrogation antenna and the transponder for moderate size conductors and relatively high impedance at low frequencies, have directed this work towards inductive coupling only.

In its general form the one-port PST as illustrated by Figure 4.3. consists of a single inductor* energised by a transmitter and

---

* *In this chapter the term inductor and antenna are one and the same thing when applied to coupling elements between the transmitter and transponder.*

147.
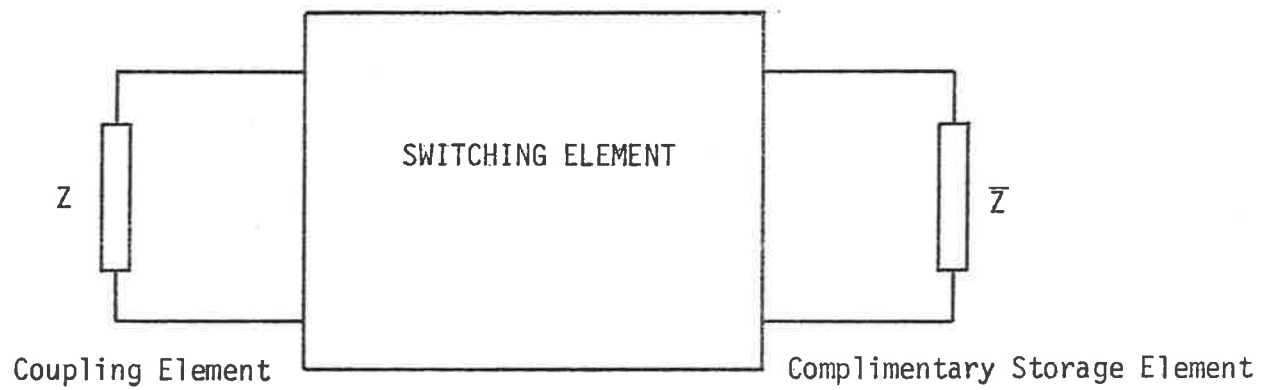
FIGURE 4.2.   STRUCTURE FOR EFFICIENT POWER TRANSFER.

coupled to a receiver by mutual inductances M1 and M2. The transmitter and receiver operate at frequencies ω_t and ω_r respectively. The inductor is resonated, in general sense, by capacitor array C1, C2, ..., CN, which are connected to the inductor L2 by a low loss switching network. The network is operated by a control circuit so that energy is exchanged bwtween the inductor and the capacitor array in a cyclic fashion whose fundamental period is some multiple of the transmitter frequency period $2\pi/\omega_t$ so that the current in the inductor consists of a series of harmonically related frequencies among which ω_t and ω_r are of importance.

The two frequencies are related by

$$\omega_r = \frac{\omega_t}{s + 1} \; ; \quad s = 1, 2, 3, \ldots. \tag{4.1}$$

where s is the order of subharmonic frequency required to be generated.

These two frequencies are responsible for the transfer of energy from the transmitter to the general resonant system and transfer of a reply code from the transponder to the receiver.

The control circuit shown in Figure 4.3 must perform several important functions. One is that it must provide signals which implement in a cyclic fashion a suitable set of interconnections for the energy exchange process. The switching is however constrained to interact with the energy exchange process in such a way as to provide for preservation, as far as possible, of stored energy

149.
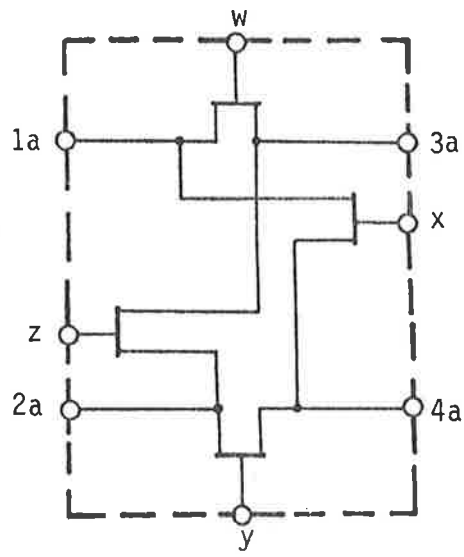
(a)
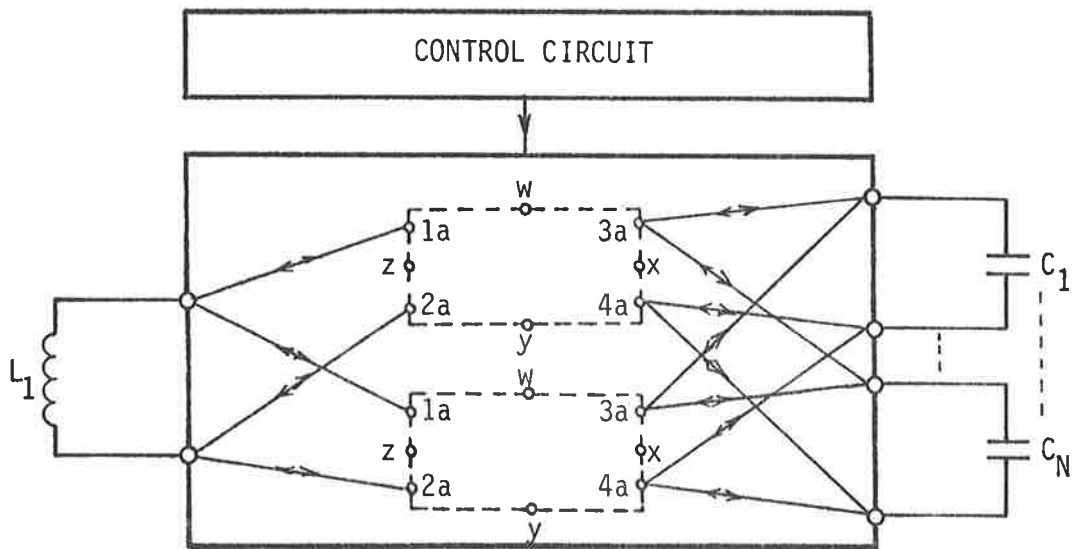
(b)

FIGURE 4.3. GENERAL STRUCTURE FOR ONE-PORT PASSIVE TRANSPONDER.

(a) *Switching Block.*

(b) *Basic Structure.*

150.

within the purely reactive elements.

This objective is achieved by arranging the switching times so that capacitors are only short circuited at the time at which they have reached zero voltage, and inductors are only open circuited at the time at which they have reached zero current.

A further consideration is that the polarity of the capacitors must be such that the direction of energy flow between the transmitter and the transponder is not disturbed due to the switching.

Since the main objective is the generation of frequencies which are subharmonically related to the interrogation frequency, for convenience the following definitions are used to assist with the description of the synthesis method to follow:

(i)   a logic '1' is used to describe the half period corresponding to the interrogation frequency ω_t during which oscillation is permitted to build up in the resonant structure;

(ii) a logic '0' is used to denote the half period of the interrogation frequency during which oscillation is suspended;

(iii) a positive sign corresponds to the positive portion of the amplitude of oscillation;

(iv) a negative sign indicates the negative portion of the amplitude of oscillation.

The above definitions are represented diagramatically in Figure 4.4. Therefore combination of the above symbols and their cyclic representation result in generation of various harmonically related waveforms.

4.2.1 Subharmonic frequency synthesis

The main consideration in this section is directed towards the generation of the first subharmonic frequency ω_r. This is achieved by generating a sequence of four symbols (in accordance with the definition provided by Figure 4.4) and the resultant combination is repeated cyclically. Clearly there are 81 possibilities which can be used to synthesize the desired frequency ω_r. However some combinations are redundant due to the displacement in time of an amount equal to the lowest frequency of the entire process, and some others are not permitted due to the requirement of continual power flow at the interrogation frequency ω_t as stipulated in the previous section.

A further restriction imposed on the control structure is that only a single switching element is permitted to be incorporated within the resonant circuit. This restriction is a useful one since not only it simplifies realisation of   control circuitry, but also the losses incurred in the tuned circuit as the result of the introduction of the switching element can be kept to a minimum. The consequence of this restriction is that structures which require reversal of the polarity of the capacitor are auto-
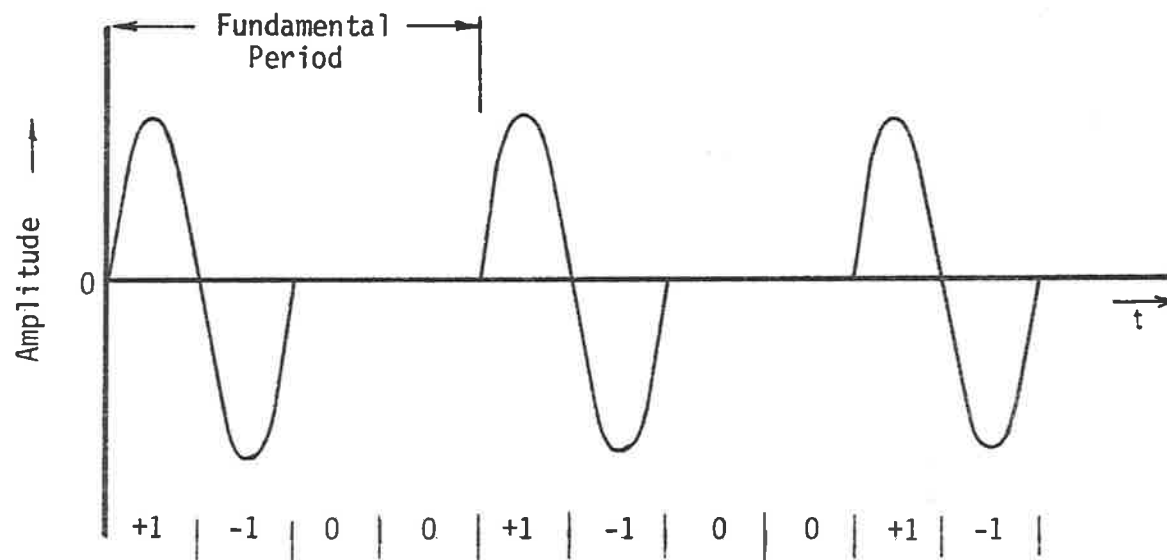
FIGURE 4.4.   WAVEFORM DESCRIPTION USING SYMBOLS '+1', '-1' and '0'.

matically excluded from further considerations. The patterns that remain are:

$$-1 \ +1 \ 0 \ 0, \qquad 0 \ 0 \ -1 \ +1, \qquad -1 \ 0 \ 0 \ +1, \qquad 0 \ +1 \ -1 \ 0$$

The waveforms have fundamental frequency component which are in phase and subharmonic frequency components which have relative phases of $0°$, $90°$, $180°$ and $270°$. It is readilly recognisable that cyclic repetition of each group of symbols result in generation of one basic waveform as illustrated by Figure 4.5, in which each symbol corresponds to one-fourth of the fundamental period. The harmonic analysis of the inductor current i_{L_s} for anyone of the combinations with suitably chosen axis results in

$$i_{L_s}(t) = I_m \left(\frac{4}{3\pi} \cos\omega_r t - \frac{1}{2} \sin 2\omega_r t - \frac{4}{5\pi} \cos 3\omega_r t - \frac{4}{21\pi} \cos 5\omega_r t \ldots \right) \qquad (4.2)$$

where I_m is the peak value of the inductor current.

These coefficient will be used later in this chapter for power transfer calculations.

4.2.2 Circuit realisation

The one-port PST in its simplest form consists of an inductor, a capacitor and a single pole switch which can be configured in either the series or the parallel modes as
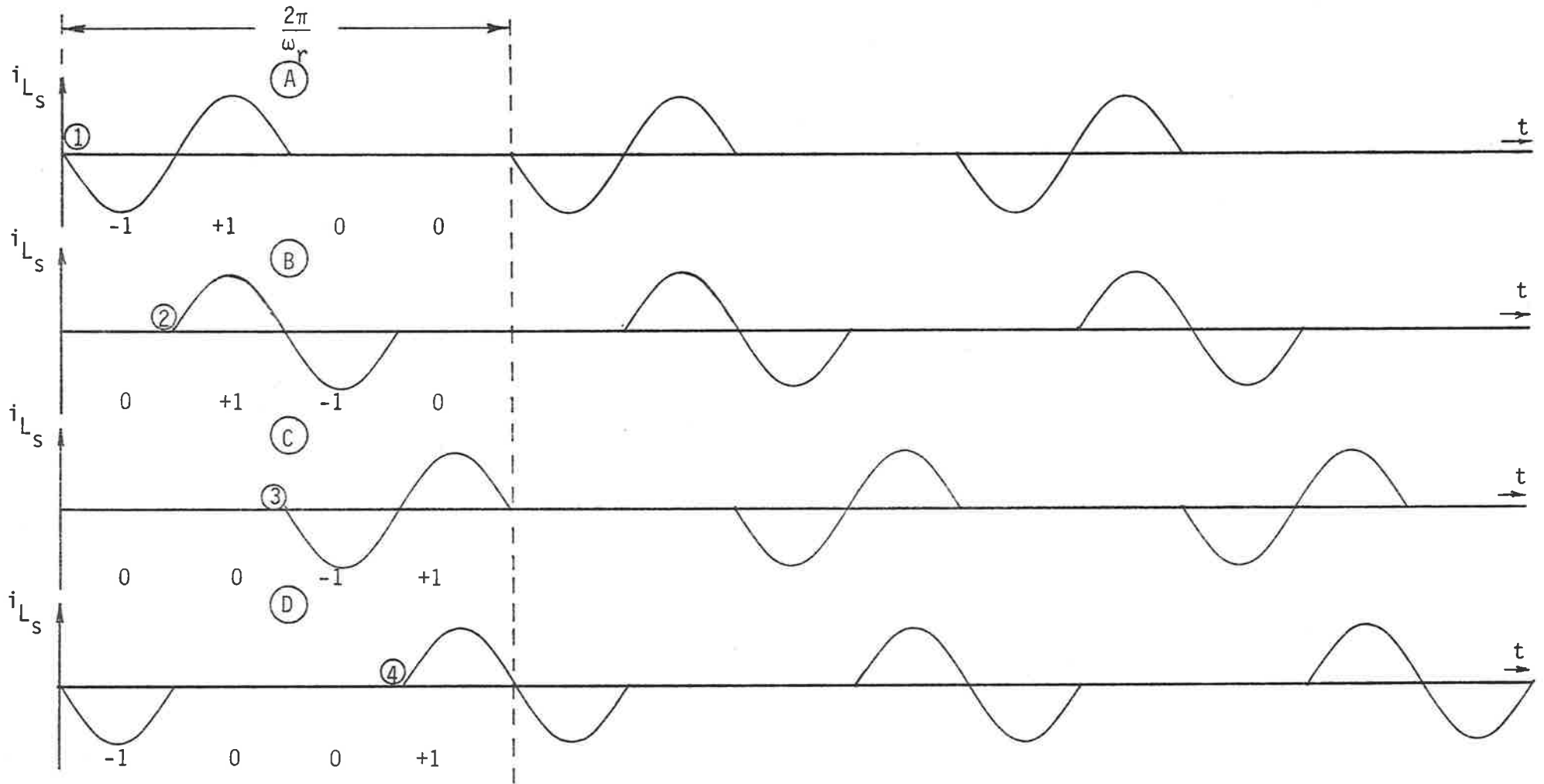
FIGURE 4.5. BASIC PATTERNS FOR GENERATION OF SUBHARMONIC FREQUENCY $\omega_r = \omega_t/2$.

shown in Figure 4.6. The generation of the desired inductor current is achieved by appropriate closure and opening of the switch in accordance with the rules established earlier.

For economy in the following analysis attention has been focussed towards the series mode of operation. However the approach can readily be extended to include the parallel mode of operation also.

If the transponder is intended to supply a reply code of more than 1 bit, some further variation of the switching sequence is required. As mentioned in Chapter 3, the maximum value of the quality factor associated with the transponder antenna is limited by the rate of information transfer resulting from the modulation of the subharmonic frequency. Therefore what is required with the reply code modulation is a method of changing the phase of the oscillation without first dissipating the energy in the tuned circuit. This objective may be accomplished, while still preserving the essential nature of the resonant circuit by varying the switching pattern at appropriate instants of time.

Thus, the next section explores the required switching patterns for the modulation process.
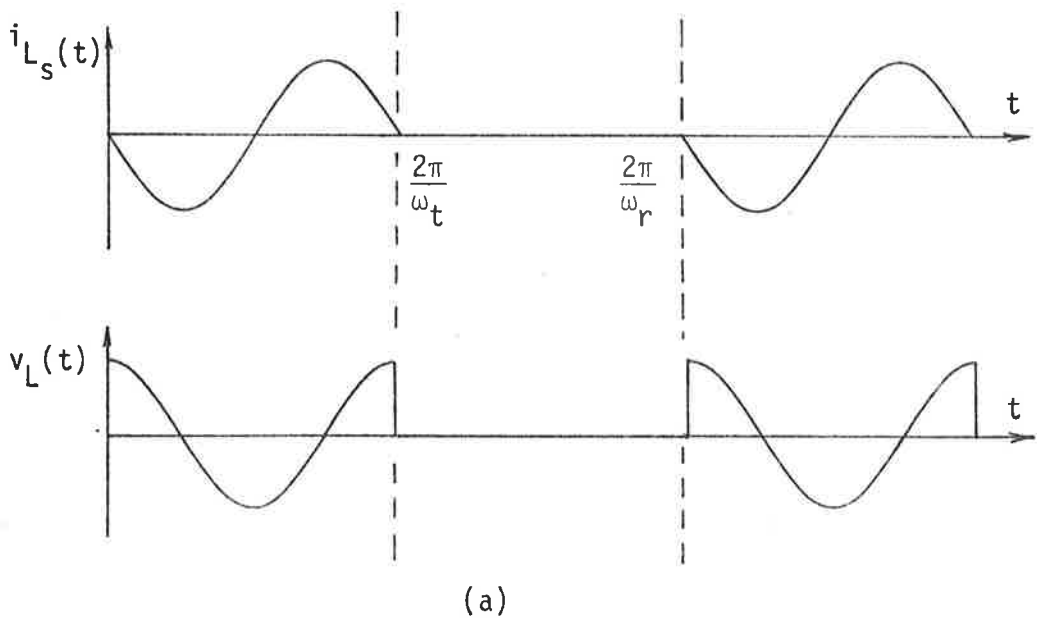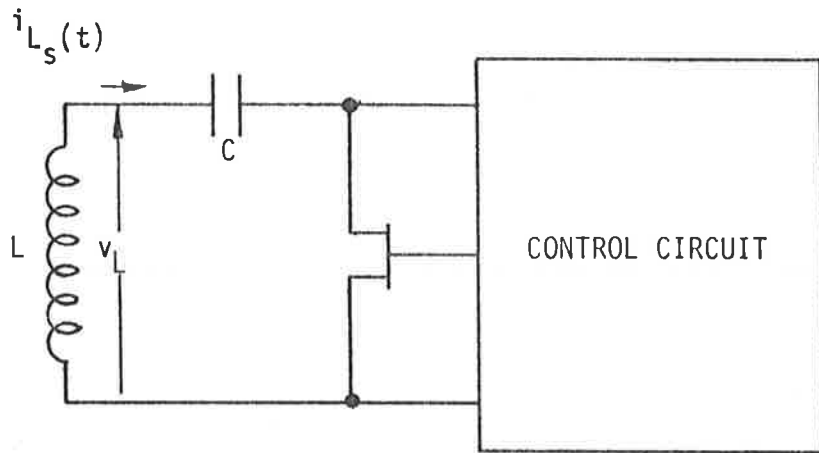
FIGURE 4.6. CIRCUIT STRUCTURE FOR SUBHARMONIC FREQUENCY SYNTHESIS.

(a) Series Mode.

157.
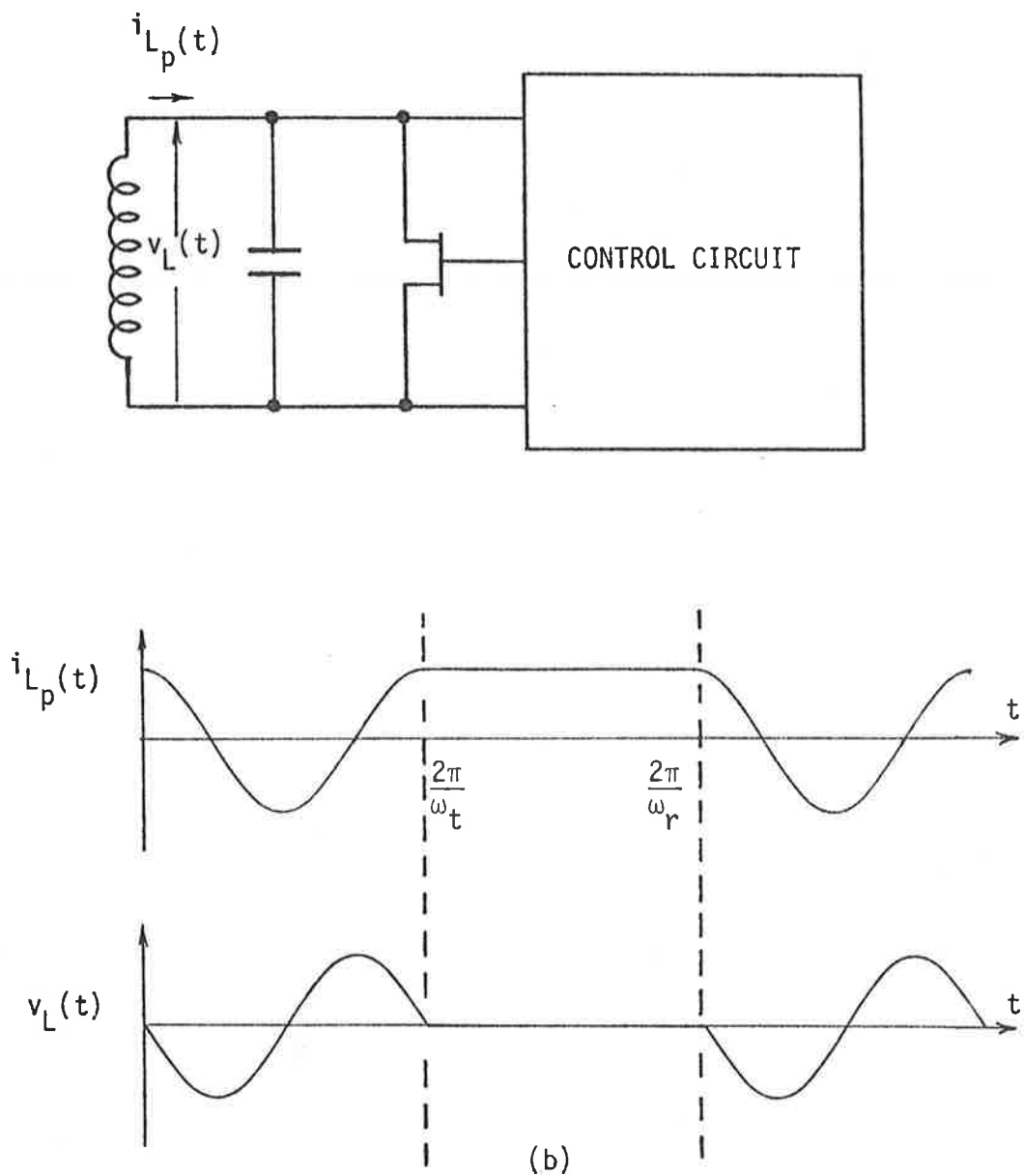
FIGURE 4.6.   CIRCUIT STRUCTURE FOR SUBHARMONIC FREQUENCY SYNTHESIS.

(b)   *Parallel Mode.*

4.3 Reply Code Modulation

Of the most common forms of modulation amplitude shift keying (ASK), frequency shift buying (FSK) and phase shift keying (PSK) the most efficient form from the point of view of error rate for a given signal-to-noise ratio is coherent PSK [100].

Initial exploratory analysis of various waveforms which effect the allowable changes between patterns indicated that PSK is a suitable method of imposing information on the reply signal and more importantly, it was discovered to be compatible with the one-port PST switching structure. PSK modulation becomes possible by displacing the switching intervals by an integer number of half periods of interrogation frequency ω_t. The waveforms A, B, C and D shown in Figure 4.5 result when the series switch is closed at points 1, 2, 3 and 4 respectively and that at periodically repeated intervals thereafter.

It is now appropriate to examine the methods by which transition between these steady state waveforms may be effected.

Once again the restrictions imposed previously on the circuit are required to be satisfied in this instant also. These are:

(i)   frequency components associated with the interrogation frequency must be present;

(ii)   the excitation source and the interrogation frequency component are required to be in phase;

(iii) no particular amplitude is required to be assigned to the
       interrogation frequency component;

(iv)   capacitor phase reversal is not permitted.

Conditions (i) - (ii) ensure that power flow at the interro-
gation frequency is maintained while restriction (iv) provides
for the minimisation of the losses associated with the switch and
permits a simple control circuitry to be realised.

Using the definitions given in Section 4.2.1, a comprehensive
investigation of various combinations of symbols for generation
and modulation of the first order subharmonic frequency, i.e. $s = 1$,
was performed.

The practical consequence of the above analysis resulted in
the following generalisation in which any transition are allowed
if one is given four cycles corresponding to the one-half period
of the interrogation frequency, to effect the transition and any
modulation phase can be reached from another phase. To establish
the transition region, from the knowledge of the preceeding and
succeeding patterns, it is possible to determine whether or not
capacitor phase changes are needed and subsequently insert either
even or odd number of capacitor phase changes as the case requires
while observing the requirements of maintaining the power trans-
fer and phase coherence with preceeding and succeeding patterns.
The latter demands the suspension for an even number of half
cycles.

Although there are various possibilities to define the relationship between the four basic patterns shown in Figure 4.5, it is convenient to describe these relationships in terms of shift and sign change. Thus the patterns shown in Figure 4.5 are transformed from one phase to another phase by simultaneous shift and sign change. The above process corresponds to no change in the fundamental frequency and 90° change to the subharmonic component for each shift.

A further point for consideration is that error rate for quad-phase modulation is higher than bi-phase modulation and in addition patterns are simpler to construct for the latter case. Therefore the patterns shown by Figure 4.7 are the only remaining patterns which fulfill all the switching requirements and provides bi-phase modulation of the reply frequency. The relationship between the above patterns are that two shifts are required.

To assist in describing the behaviour of the overall one-port PST system and in particular to show the build-up and decay times of the reply signal in the vicinity of the transitions a general purpose programme MOD was developed. The programme forms a modulated version of the transponder current waveform by cascading appropriate symbols, finds its Fourier transform in the frequency domain, generates a filtered spectrum using a Gaussian filter as the receiver, calculates the inverse Fourier transform, and finally plots the frequency spectrum and the time response of the original waveform. Details of the above programme is included in Appendix C.

161.
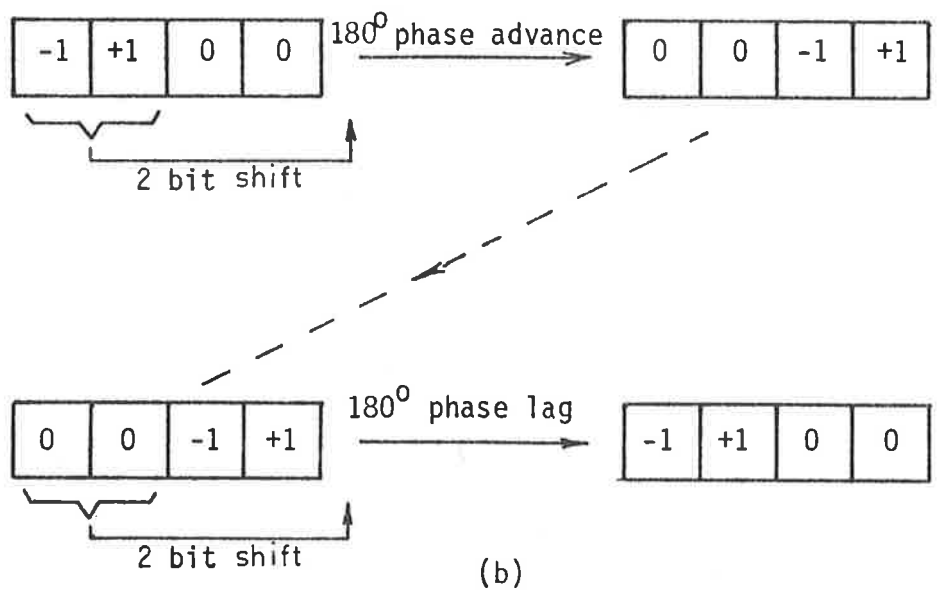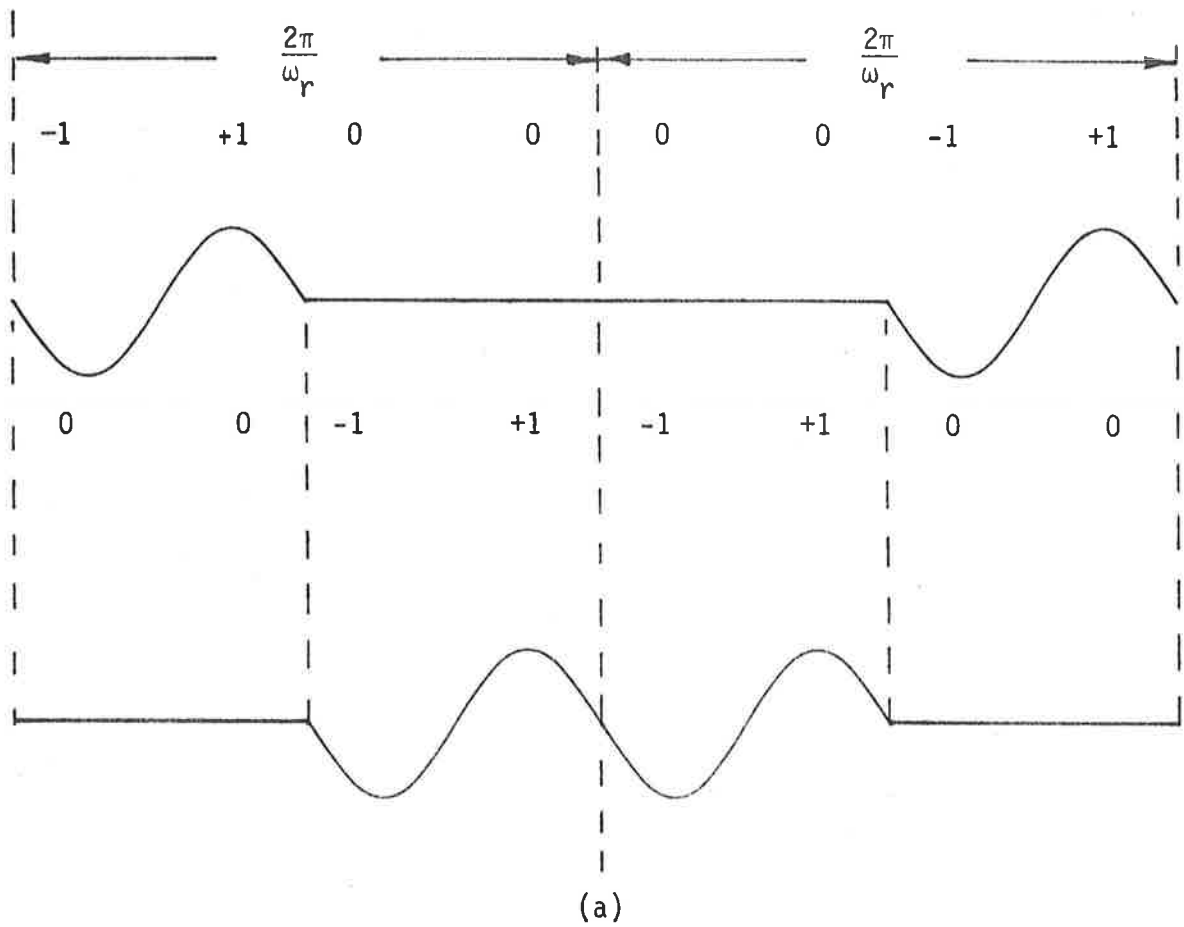
FIGURE 4.7. BI-PHASE MODULATION THROUGH SHIFT AND SIGN CHANGES.

(a) *Modulation through 2 bit rotation.*

(b) *Symbol representation.*

162.

The overall simulation using a Gaussian filter as the receiver with centre frequency of 50KHz and a quality factor of 8, is shown in Figure 4.8 - 4.9. As can be observed the 100KHz interrogation frequency remains undisturbed while the 50KHz reply signal is modulated.

The rotation and sign change presentation of the relationship between the waveforms is of particular interest as it enables easy prediction of the behaviours of the other harmonics present in the waveform.

A further result which could have an important influence on the structure of the receiver is that not only the subharmonic frequency ω_r is modulated but also all other higher order frequencies which are related to the interrogation frequency ω_t by

$$\omega_h = \left(\frac{2n + 1}{2}\right) \omega_t; \quad n = 1, 2, 3, \ldots \quad (4.3)$$

are also modulated. A typical time response corresponding to the patterns shown in Figure 4.8 when n = 2, i.e. 150KHz reply signal, is shown in Figure 4.10.

In the above operations the switching network is designed to be low loss and is controlled in such a way that excessively dissipative transients do not occur. In this way the reply code modulation can be provided while the energy required to maintain the oscillation is kept to the minimum which can be achieved con-

163.

Legend:

- - - - - Code
∙∙∙∙∙ Switched Waveform - 100KHz
∙∙∙∙∙∙∙ Modulated Reply Signal - 50KHz

Notes: Centre Frequency f_o = 50KHz
No. of cycles per bit = 8
Q = 8

'1' '0'

3.100E+00

1 DIV = 8.000E-02

700E+00

10   20   30   40   50   60   70   80   90   100

Time (μSec)
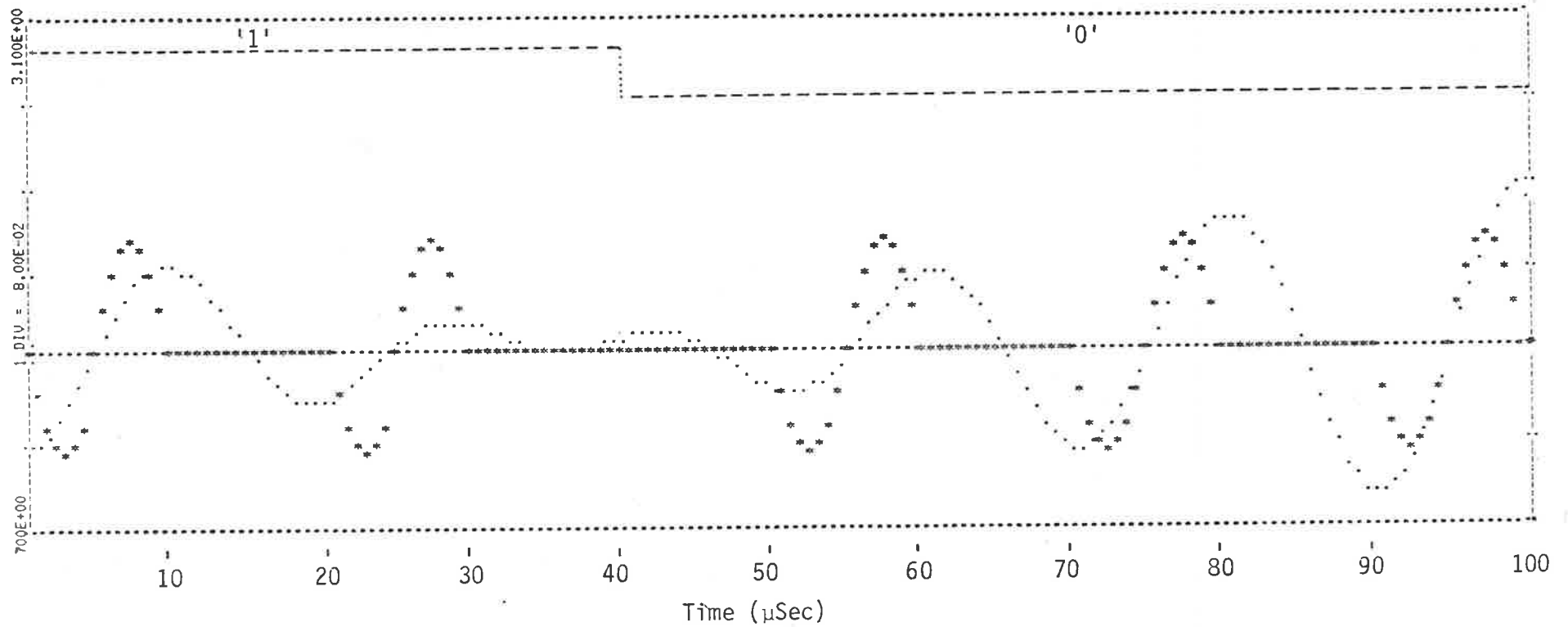
FIGURE 4.8(a). TIME RESPONSE CORRESPONDING TO BASIC BIT PATTERN -1 +1 0 0 → 0 0 -1 +1 WHEN PASSED THROUGH A

GAUSSIAN FILTER WITH CENTRE FREQUENCY OF 50KHz AND Q = 8.

Code -----

Switched Wqveform - 100KHz

Modulated Reply Signal 50KHz

'0'

'1'

165.

Time (μSec)
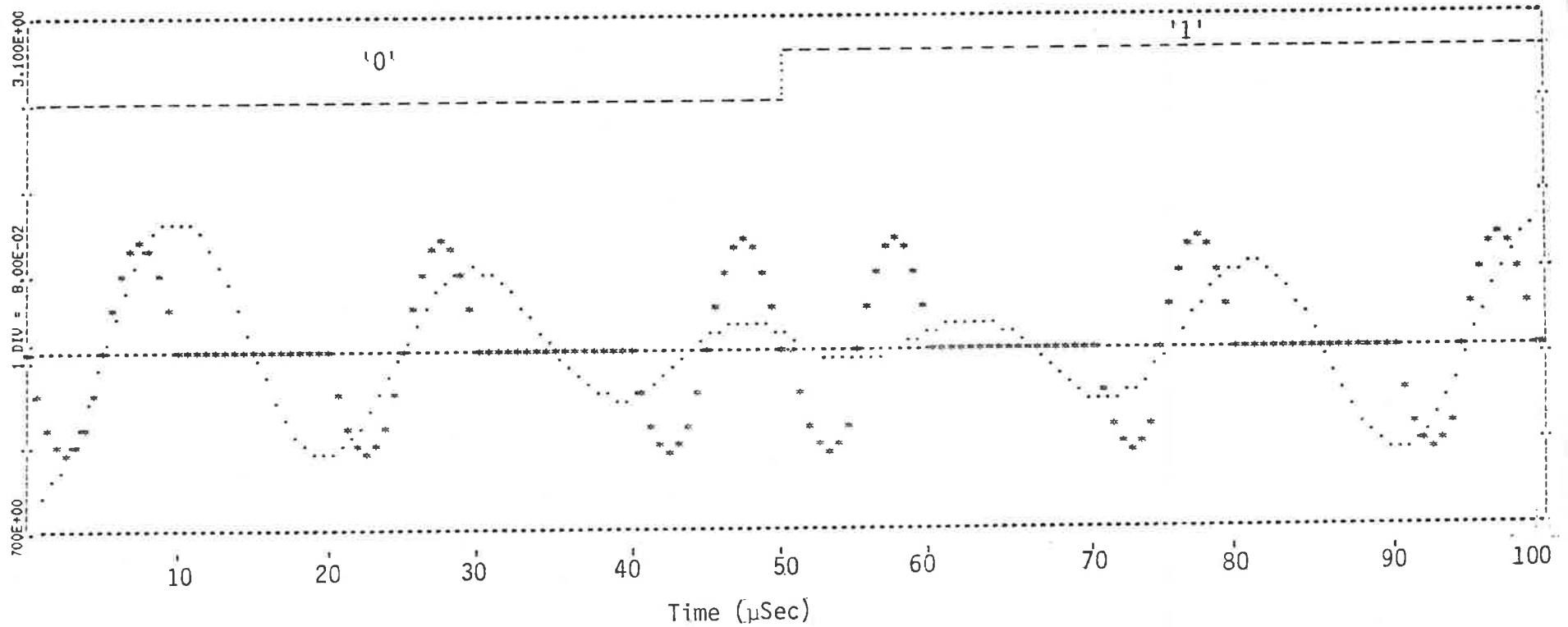
FIGURE 4.8(b).   TIME RESPONSE CORRESPONDING TO BASIC BIT PATTERN 0 0 -1 +1 → -1 +1 0 0 WHEN PASSED THROUGH A

GAUSSIAN FILTER WITH CENTRE FREQUENCY OF 50KHz AND Q = 8.
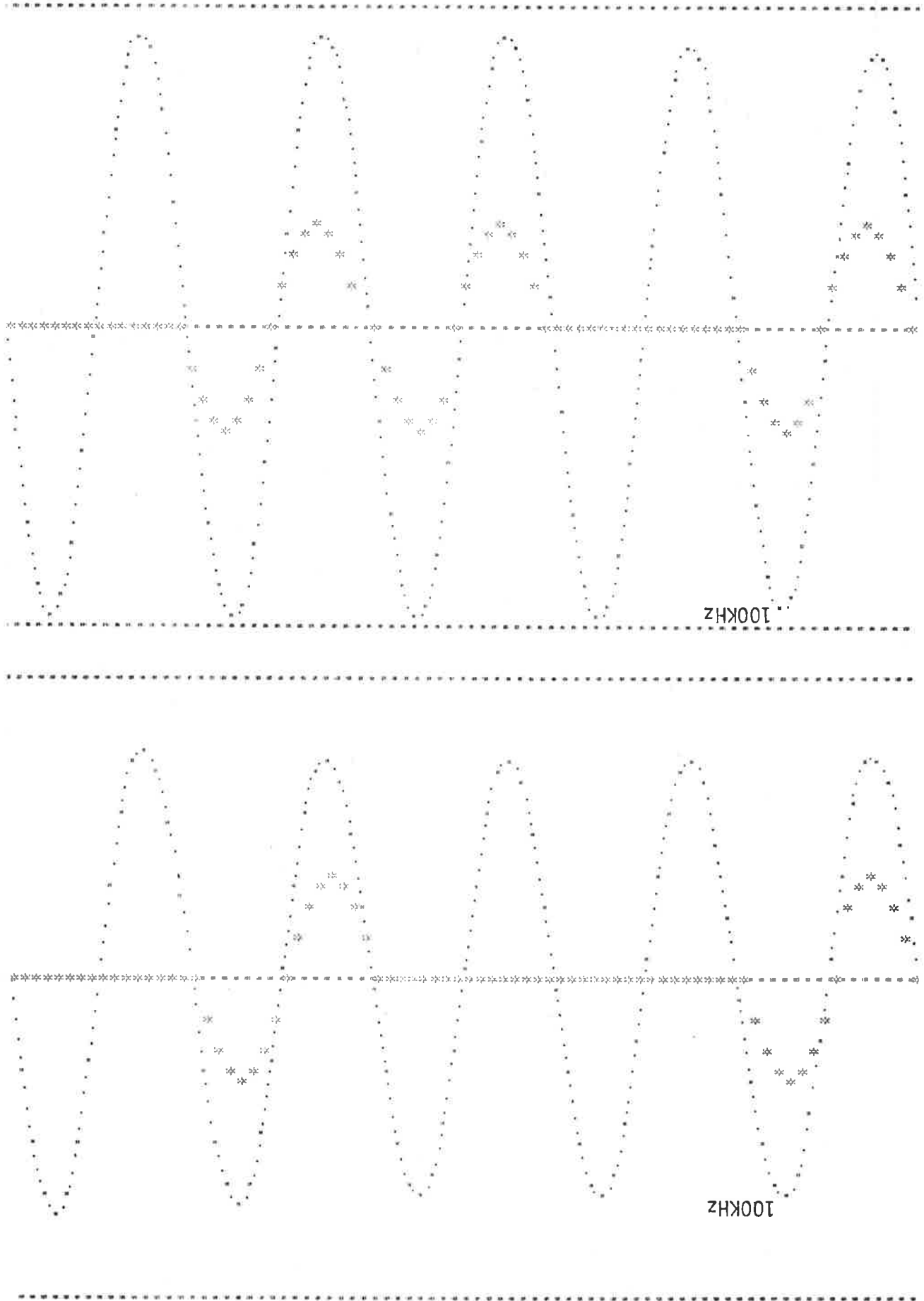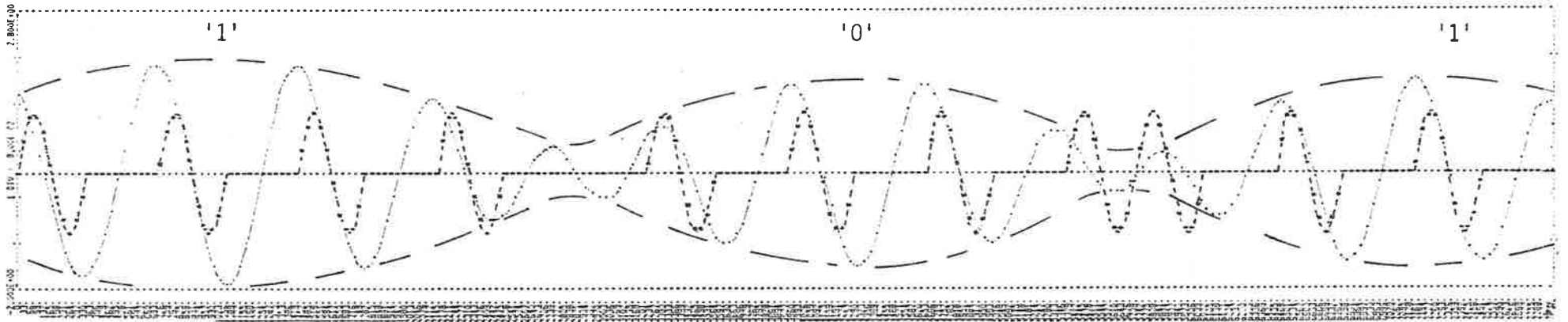
FIGURE 4.9. TIME RESPONSE CHARACTERISTICS FOR 3 BIT CODE WITH 4 CYCLES PER BIT.
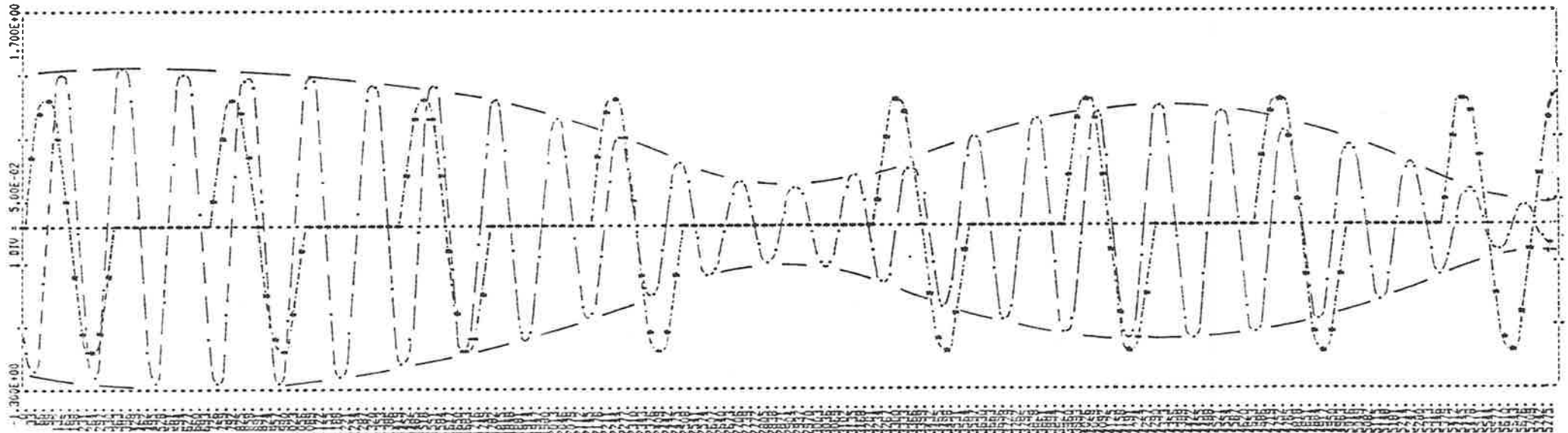
FIGURE 4.10. TIME RESPONSE CORRESPONDING TO BASIC BIT PATTERN +1 -1 0 0 → 0 0 +1 -1 WHEN PASSED THROUGH A GAUSSIAN

FILTER WITH CENTRE FREQUENCY OF 150KHz.

sistent with the quality factors of available components.

The significance of such modulation method is that while similar relationships between the quality factor of the resonant circuit and the electromagnetic losses as described by Equation (3.24) can be obtained, the requirements of the communication bandwidth and the quality factor of the transponder resonant circuit no longer exists due to switching technique used. Thus, the quality factor Q_2 of the transponder antenna can be made as large as practicable which enhances the power transfer across the electromagnetic link between the transmitter and the transponder.

4.4 Power Transfer Ratio Modelling

For the transfer of energy over the electromagnetic coupling links of the system, one is not concerned with the total stored energy in the transponder, but only that associated with the harmonics of the inductor current at ω_t and ω_r respectively. In view of the relation

$$Q = \frac{\omega L I^2}{P} \qquad (4.4)$$

between the quality factor Q, rms current I and mean rate of power dissipation P for a simple tuned circuit, effective quality factors

for the transponder coil at the transmitting and receiving frequencies can be defined as

$$Q_2' = \frac{\omega_r L I_r^2}{P}$$ (4.5)

and

$$Q_3' = \frac{\omega_r L I_r^2}{P}$$ (4.6)

where

I_t = rms value of transponder current at ω_t

I_r = rms value of transponder current at ω_r.

The importance of these quality factors are that they allow the transfer of powers across the two electromagnetic coupling links to be calculated by means of the simple formulae used in Section 3.4.1. Thus

$$\frac{P_2}{P_1} = k_t^2 \, Q_1 \, Q_2'$$ (4.7)

and

$$\frac{P_4}{P_3} = k_r^2 \; Q_3' \; Q_4 \qquad\qquad (4.8)$$

In practical realisation of the one-port PST it is not diffi-
cult to make the control power consumed within the transponder
negligible in relation to that power which sustains the oscilla-
tion and hence contributes to the transfer of energy. Furthermore,
to a good approximation $P_3 = P_2$ which results in the overall power
transfer from transmitter to receiver to be expressed as

$$\frac{P_4}{P_1} = k_t^2 \; k_r^2 \; Q_1 \; Q_2' \; Q_3' \; Q_4 \qquad\qquad (4.9)$$

It is possible to define a fundamental quality factor Q_F for
the transponder coil as

$$Q_F = 2\pi \; \frac{\text{Total stored energy in transponder}}{\text{Energy dissipated in fundamental period T}} \qquad (4.10)$$

where the fundamental period in this definition is given by
$T = 2\pi/\omega_r$.

The calculation of this quality factor requires a knowledge
of the detailed loss mechanism of the tuned circuit and their
allocation between the inductor, the capacitor and the switch.
However the particular point of defining the effective quality
factors Q_2' and Q_3' are each readily determined from Q_F by coeffic-
ients which depend only on waveshape and do not involve the details

171.

of the loss mechanism. Thus all complexities in the calculation of the latter are subsumed in the calculation of Q_F.

In view of the fixed relationships between the harmonics of the oscillation waveform and the fact that Q_F, Q_2' and Q_3' are all defined in relation to the same mean power dissipated in the circuit, Q_2' and Q_3' are given by

$$Q_2' = 4 \, \kappa_t^2 \, Q_F \qquad\qquad (4.11)$$

and

$$Q_3' = 2 \, \kappa_r^2 \, Q_F \qquad\qquad (4.12)$$

where κ_t and κ_r are waveform factors expressed as

$$\kappa_t = \frac{I_t}{I_m} \qquad\qquad (4.13)$$

$$\kappa_r = \frac{I_r}{I_m} \qquad\qquad (4.14)$$

The above values may be obtained from Equation (4.2).

The overall power transfer ratio between the transmitter and receiver antenna become

$$\frac{P_4}{P_1} = \chi_p \; k_t^2 \; k_r^2 \; Q_1 \; Q_F^2 \; Q_4 \tag{4.15}$$

where

$$\chi_p = 8 \; \kappa_t^2 \; \kappa_r^2. \tag{4.16}$$

In the one-port structure no power matching is required, and only a small fraction of the power delivered to the transponder is required to drive the electronic circuitry. Therefore to take such a loss into consideration, the efficiency factor η' is incorporated in Equation (4.15) resulting in

$$\frac{P_4}{P_1} = \eta' \; \chi_p \; k_t^2 \; k_r^2 \; Q_1 \; Q_F^2 \; Q_4 \tag{4.17}$$

4.4.1 Fundamental quality factor description

The main task in this section is to formulate a mathematical model for the effective quality factor Q_F defined by Equation (4.10). The calculation of this quality factor re-

173.

quires a knowledge of the detailed loss mechanisms of the tuned circuit and their allocation between the coil, the capacitor and the control switch.

In practical situations where field effect transistors are used as the switching element, the switch losses may be modelled by a forward resistance R_f when the switch is 'on' and a leakage resistance R_b when the switch is 'off'. The capacitor and inductor losses may be represented by R_p and R_s' respectively. These losses correspond to the two switching periods as shown in Figure 4.11. In practice the leakage resistance R_b is very large and therefore its influence on the circuit operation can be neglected. Furthermore, by suitable choice of capacitor, the capacitor losses may also be made very small such that negligible change in the capacitor voltage occurs during the period in which the oscillation is suspended.

The energy dissipated in one fundamental cycle is

$$E_d = W_1 T_1 + W_2 T_2 \qquad (4.18)$$

where W_1 and W_2 are the average powers dissipated over times T_1 and T_2. With R_b being in the order of 10^{10} - 10^{12} ohms, and using good quality capacitor it is possible to make the losses in the period during which the oscillation is suspended small. Therefore Equation (4.18) can be described to a good approximation by
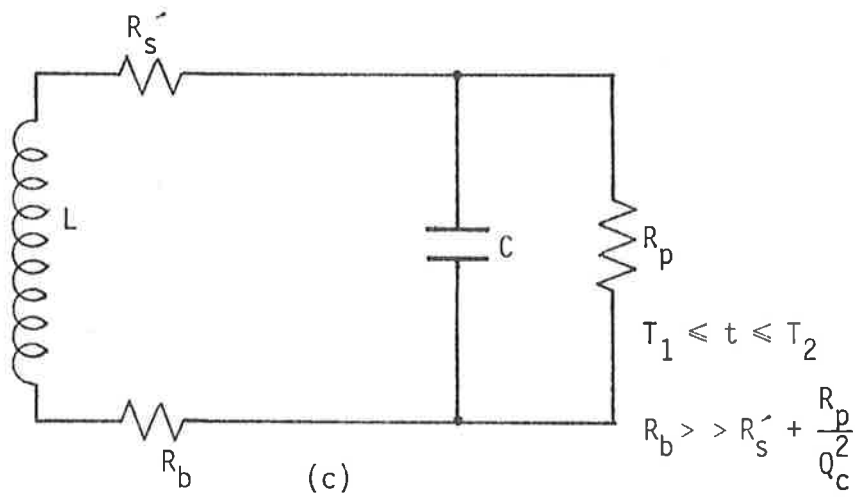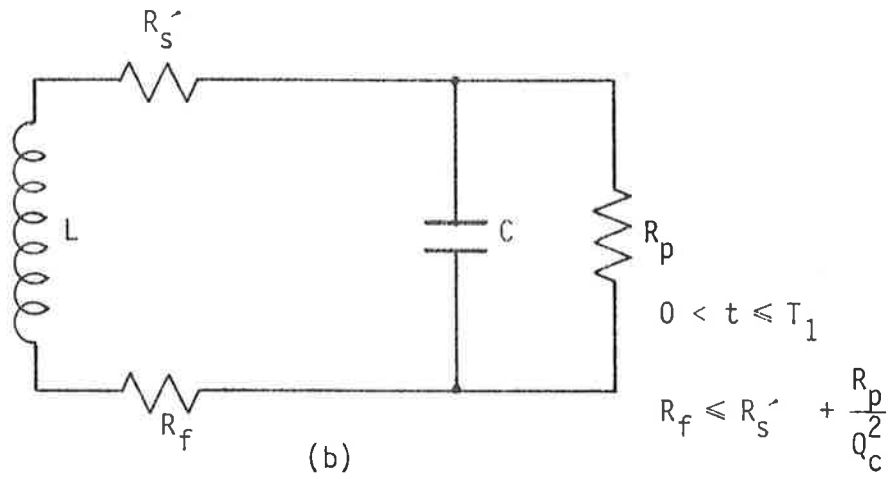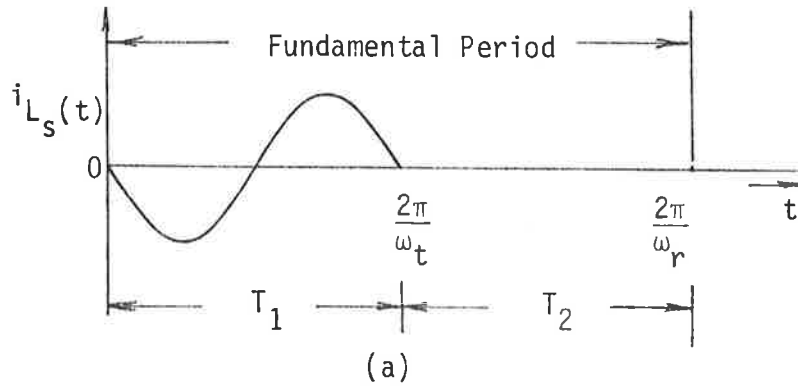
FIGURE 4.11. MODELLING OF THE LOSS MECHANISM.

(a) *Current waveform.*

(b) *Series switch ON.*

(c) *Series switch OFF.*

175.

$$E_d = \frac{1}{2} T_1 I_m^2 R_t' \qquad (4.19)$$

where R_t' is series equivalent resistance given by

$$R_t' = R_s' + R_f + R_c \qquad (4.20)$$

and

$$R_c = \frac{R_p}{Q_c^2}$$

$$Q_c = \omega R_p C \qquad (4.21)$$

The fundamental quality factor Q_F from definition can now be expressed as

$$\frac{1}{Q_F} = \frac{1}{Q_2} + \frac{1}{Q_s} \qquad (4.22)$$

where Q_2 takes into consideration the losses associated with the capacitor and Q_s is the losses due to the switching element. Thus

$$Q_2 = \frac{\omega_t L}{R_t} \qquad (4.23)$$

where $R_t = R_s' + R_c$, and

$$Q_s = \frac{\omega_t L}{R_f} \qquad (4.24)$$

The model for the power transfer ratio can now be expressed in a more convenient form

$$\frac{P_4}{P_1} = \eta' \chi_p \left(\frac{1}{1 + R_f/R_t}\right)^2 k_t^2 k_r^2 Q_1 Q_2^2 Q_4 \qquad (4.25)$$

With an interrogation frequency of ω_t and a reply signal $\omega_r = \omega_t/2$, the value of χ_p from Equation (4.2) is $8/9\pi^2$.

The consequence of the above assumptions are that if the losses during the period in which the oscillation is suspended are made small, the power transfer across the electromagnetic link may be described in terms of the unswitched transponder tuned circuit quality factor Q_2.

This model is of particular significance since it provides a simple method for predicting the power transfer within the one-port PST system.

177.

It should further be noted that is is not difficult to obtain switching elements which have very low 'on' resistances in the order of 1-5 ohms and large 'off' resistances in the order of 10^{10} - 10^{13} ohms. For example the N-channel enhancement type field effect transistor (VMP2) has typical $r_{ds(on)}$ = 2 ohms, and $r_{DS(off)}$ = 10 Gohms. The validity of the above assumptions were confirmed through experiments by using several coil structures and different FETs having "on" resistances in the range 2-18 ohms.

There are two limiting cases of practical interest. The first being the situation in which $R_f \ll R_t$. The power transfer ratio becomes

$$\frac{P_4}{P_1} = \eta' \frac{8}{9\pi^2} Q_1 Q_2^2 Q_4 k_t^2 k_r^2 \qquad (4.26)$$

The second case is when $R_f = R_t$ which results in

$$\frac{P_4}{P_1} = \eta' \frac{2}{9\pi^2} Q_1 Q_2^2 Q_4 k_t^2 k_r^2 \qquad (4.27)$$

It can readily be recognised that by suitable choice of the switching element and coil losses, with all other parameters kept constant, it is possible to maximise the power transfer. When the ratio R_f/R_t is varied within the range 0-1, the corresponding change in the power transfer also

178.

varies between 0 and 6dB. Thus one seeks to minimise the above ratio by suitable selections of FET switch and the transponder coil.

4.5 Signal-to-Noise Estimation

To illustrate the practical use of the above results and the level of performance achievable in an operational system, the overall power transfer ratios for both the transmitting and receiving links in a typical one-port subharmonic system are evaluated using the model defined by Equation (4.26).

In this system the transmitter and receiver antennas are provided by a square single turn of planar coil of side 1.0m with respective quality factors Q_1 = 50 at the transmitter frequency and Q_4 = 8 at the receiver frequency. The transponder antenna takes the form of square planar coil with sides of 0.10m. The quality factor Q_2 of the transponder is taken as 50. In this case no power matching is required and only 10% of the available transponder power is required to drive the electronic control circuitry. With a transmitter power of 10 watts and using the same peak noise amplitude of -88.6dBW as in Chapter 3, a plot of signal-to-peak impulsive noise ratio as a function of sensing distance can be constructed. The result of this analysis is shown in Figure 4.12 which illustrate that for the kind of antenna structures used, the one-port PST is marginally better than the equivalent two-port system. However the significant factor is that the one-port PST occupies only half the space as that required by the two-port PST. Thus for an equivalent antenna size, significant improvement can be expected from the one-port structure.

179.
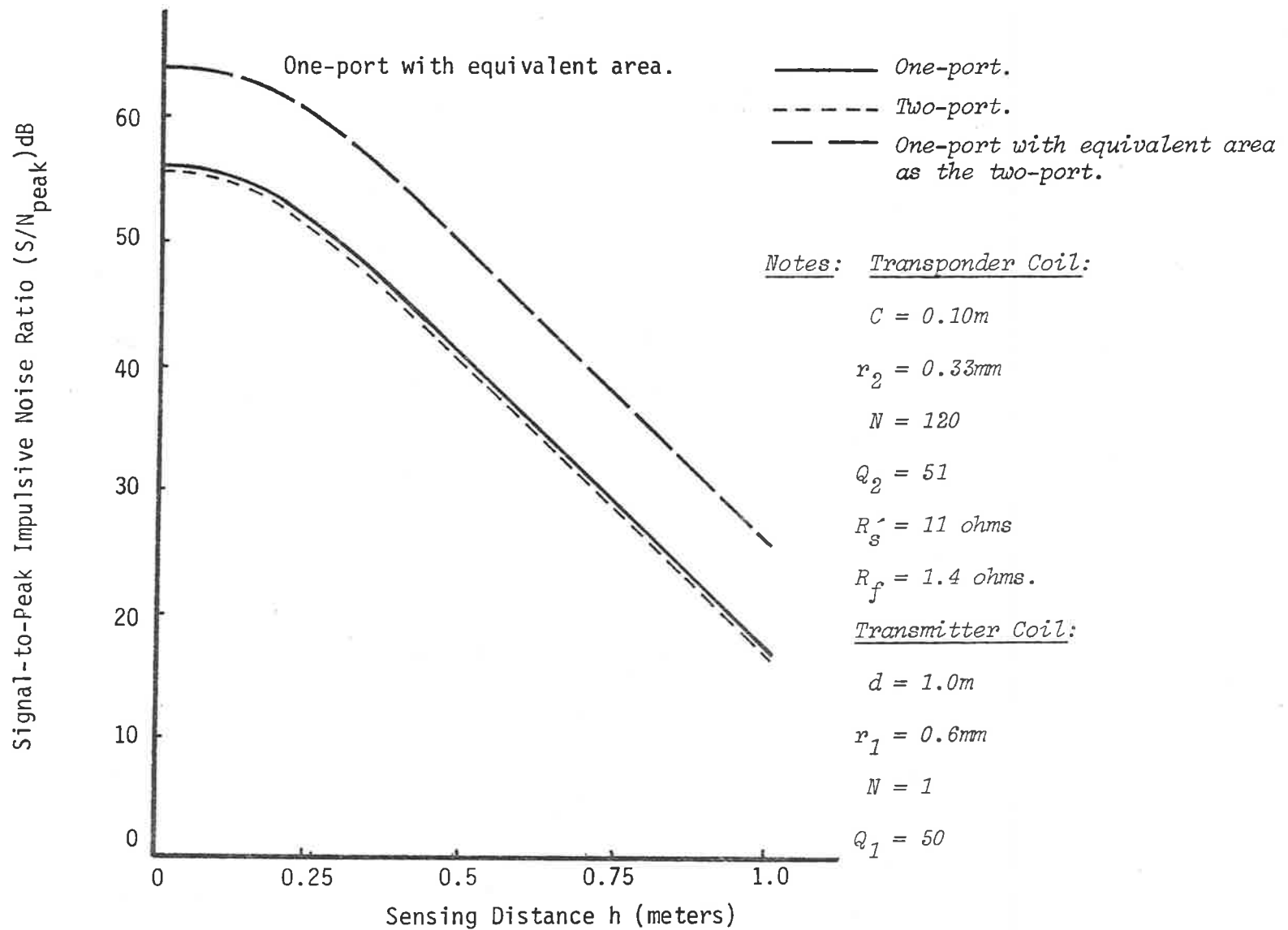
FIGURE 4.12. PLOTS OF SIGNAL-TO-PEAK IMPULSIVE NOISE RATIO AS A FUNCTION OF SENSING

DISTANCE h(m) FOR THREE PST STRUCTURES.

4.6 Transponder Control Circuit Realisation

In order for the switching element in the transponder to operate at correct instants of time, it is necessary for the control circuitry within the transponder to extract timing information from the incoming interrogation signal and must further be able to reintroduce this timing during the interval in which the oscillation is suspended. Of the several possibilities such as fixed timing circuit, phase locked loop (PLL) and auxilliary oscillation the later two were considered for further investigations.

The configuration utilizing the PLL[131] provides the basis for realisation of an intelligent controller with the ability to adjust to variations in the interrogation frequency. However the discrete realisation of such an approach consumes relatively large portions of the available power in the transponder, i.e. 5mW at 3 volts.

It should be recognised that through integration using either I^2L or the alternative LOCMOS process significant reduction in the power consumption can be realised. This is discussed more fully in Chapter 7.

The basic structure of the alternative circuit arrangement which permits very low power consumption is shown in Figure 4.13. In this approach the energy exchange process continues between the timing capacitor C and the two inductors L and L_a at appropriate instants of time. The auxilliary inductor L_a is shielded from the interrogation source and serves to produce the time interval during the period in which this information is unavailable. This is achieved by making $L = L_a$.
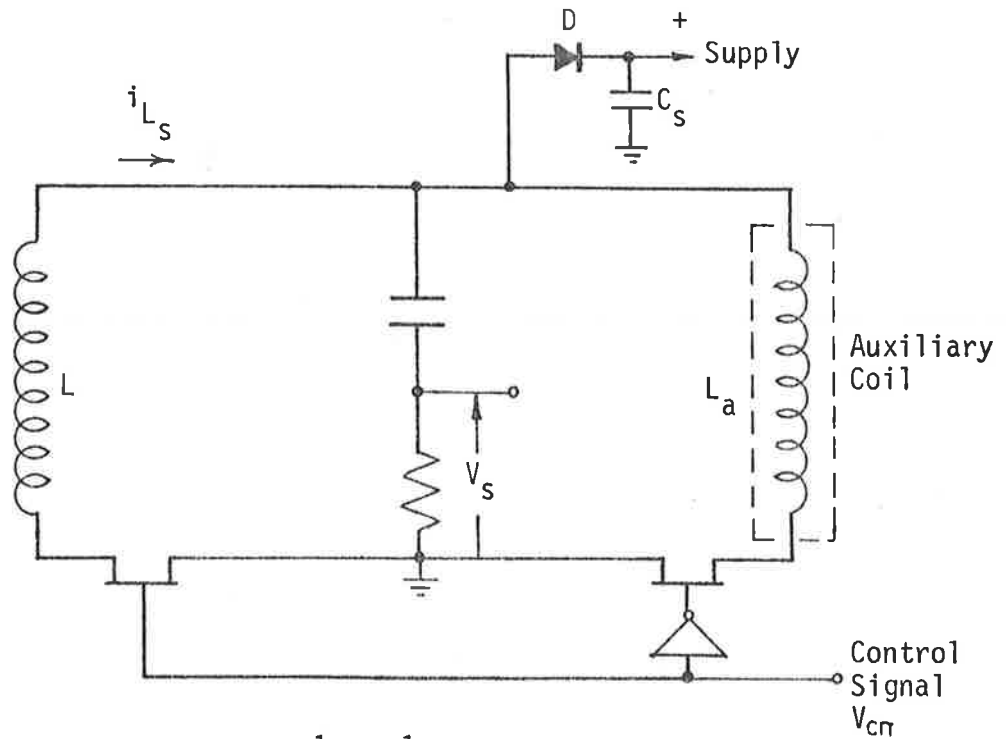
$$\omega_t = \frac{1}{LC} = \frac{1}{L_a C}$$

(a)
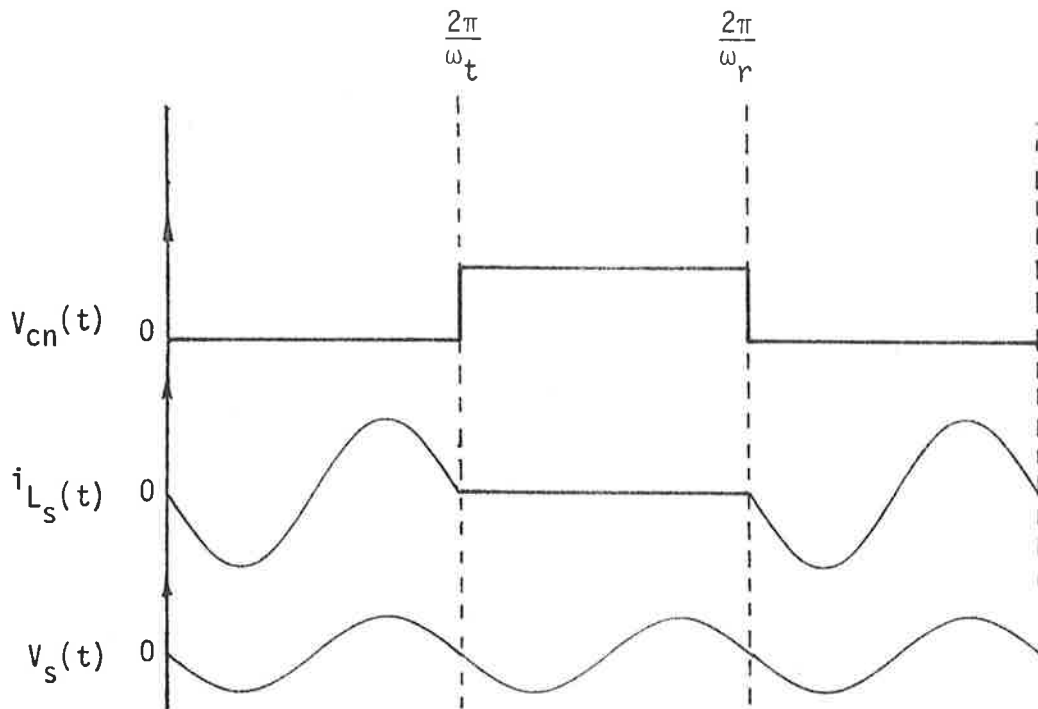
(b)

FIGURE 4.13.   ONE-PORT PST.

(a) *Basic Structure.*
(b⊥ *Waveforms.*

182.

Diode D in conjunction with capacitor C_s provides the necessary voltage to operate the control circuitry.

Figures 4.14 - 4.17 illustrate the structures and the relevant waveforms for a one-port PST which was constructed. This configuration was operated at an interrogation frequency of 100kHz, and returned a continuously recycled reply code of length 64 bits in the form of a BPSK modulated carrier frequency at 50kHz. Eight carrier cycles were allocated to each bit of the reply code to improve the S/N ratio performance of the system. For the circuit illustrated above the total power consumption is approximately 100μW at 3 volts. Incorporation of a FET regulator extends the range to 15 volts for approximately the same dissipation. Evaluation of the circuit indicated a close correlation between the general results and those predicted through modelling.

A further point of interest is that the amplitude of the transponder oscillation builds up over a period T_d given by

$$T_d = \frac{Q_F}{\omega_r} \qquad (4.28)$$

which is normally relatively large compared with the period of the reply code modulation. Therefore it is desirable to delay the commencement of the modulation when the transponder is first energised until the transponder stored energy has reached a reasonable fraction of its steady state. Using the circuit configuration shown above this can readily be realised through appropriate time constants associated with the supply source.

$$L = L_c$$

$$f_o = \frac{1}{2\pi\sqrt{LC}}$$
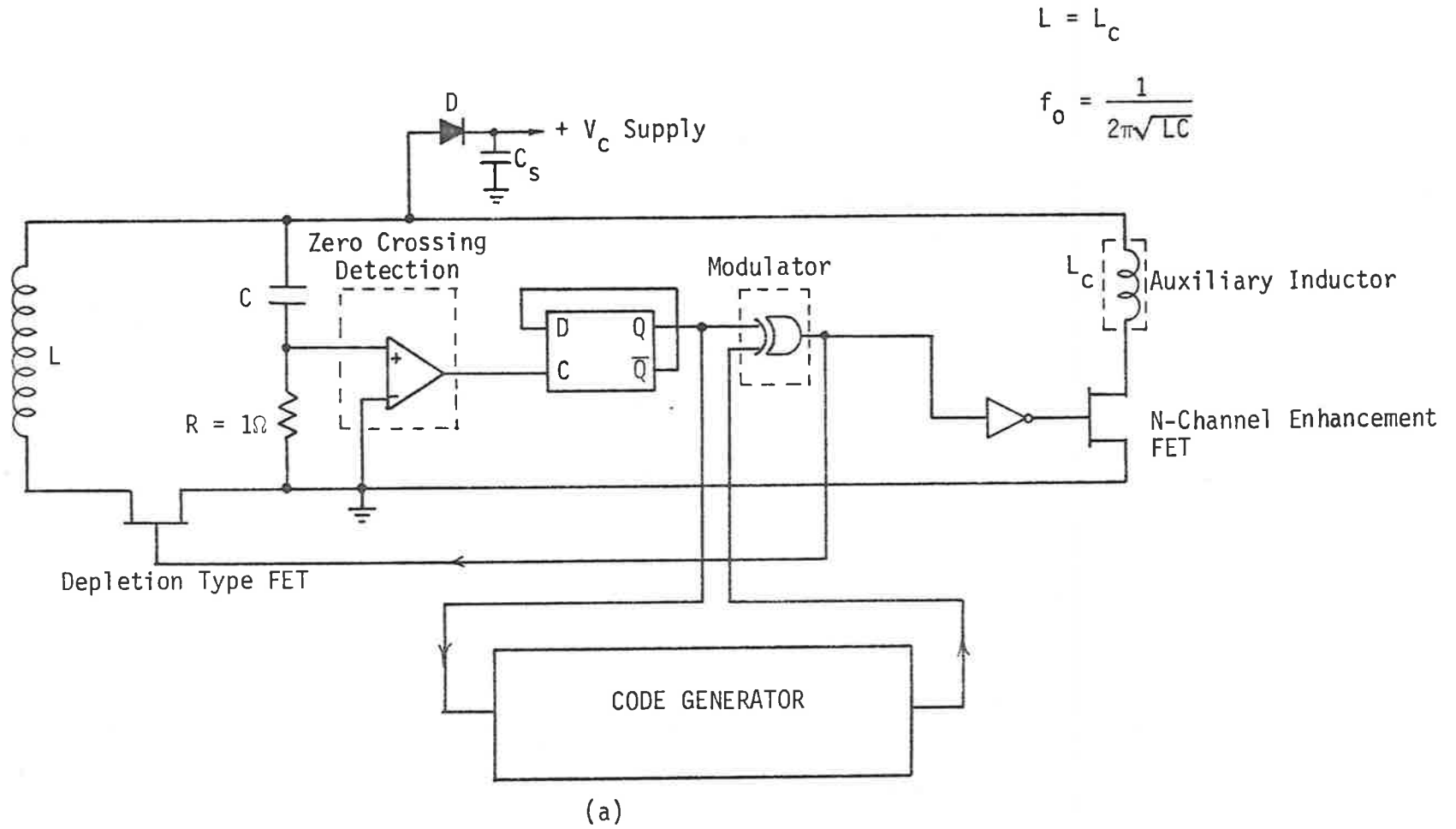
FIGURE 4.14.   ONE-PORT PASSIVE SUBHARMONIC TRANSPONDER.

(a) Basic Structure.

(b)
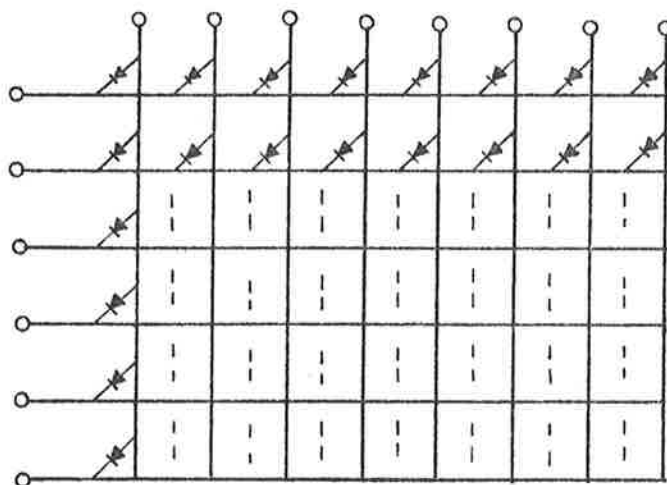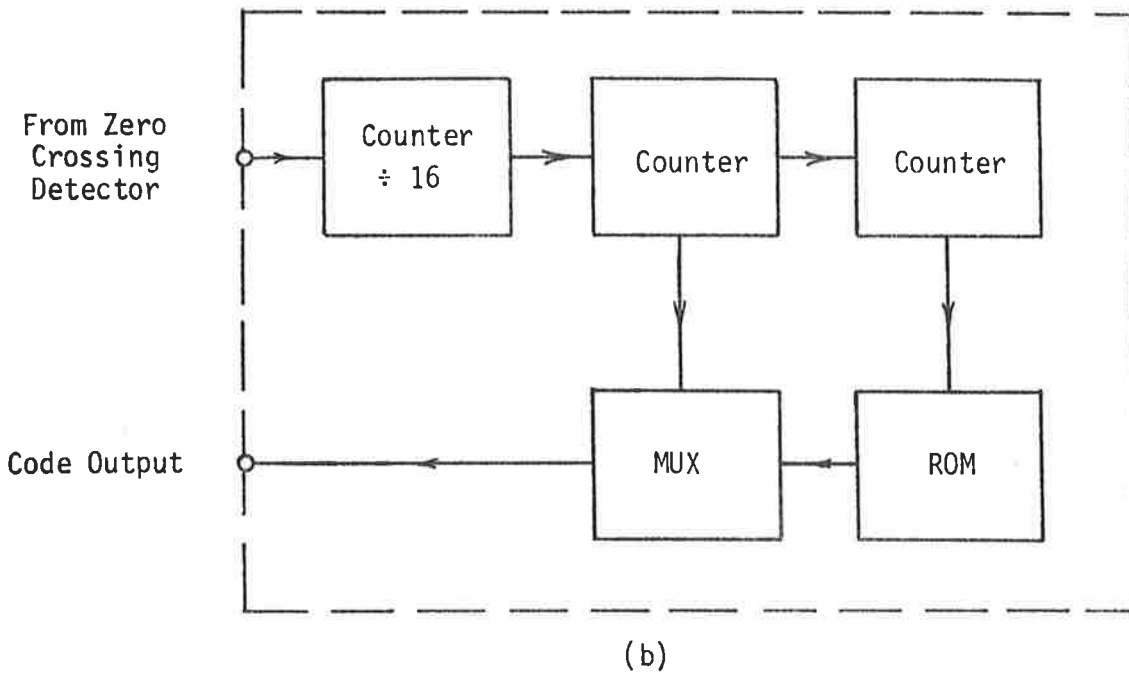
ROM: Type HM-0186-5 with Fusiable Links.

(c)

FIGURE 4.14.   ONE-PORT PASSIVE SUBHARMONIC TRANSPONDER.

(b)   *Code Generator.*

(c)   *Field Programmable ROM.*

185.
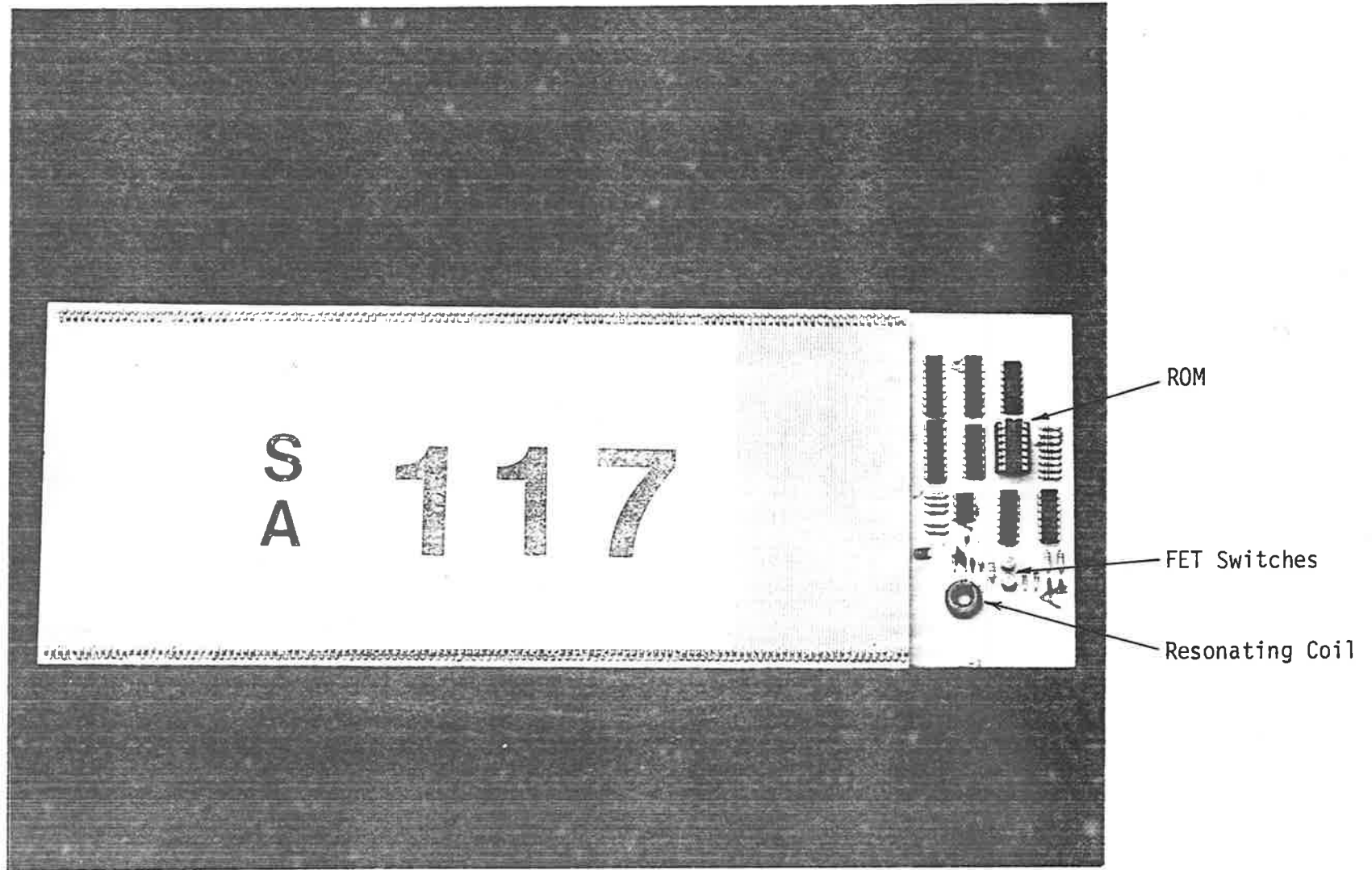
FIGURE 4.15.   A TYPICAL ONE-PORT PST STRUCTURE USED AS A NUMBER PLATE.
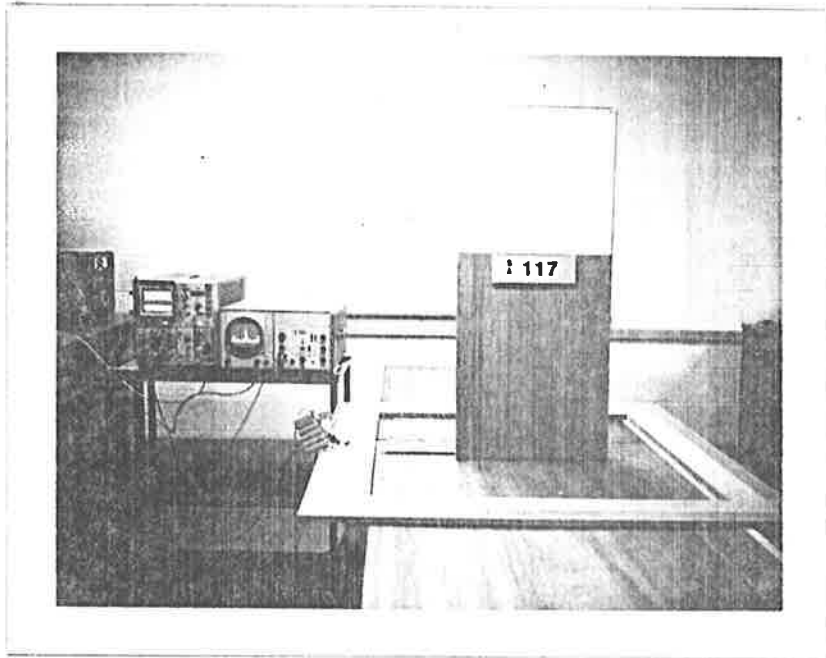
FIGURE 4.16.   MEASURING SET UP SHOWING THE RELATIONSHIP
BETWEEN THE TRANSPONDER AND THE INTERROGATION ANTENNA.

Transmitter
Frequency

Transponder
Current

Received
Frequency

(a)

Modulated
Reply Signal

Code
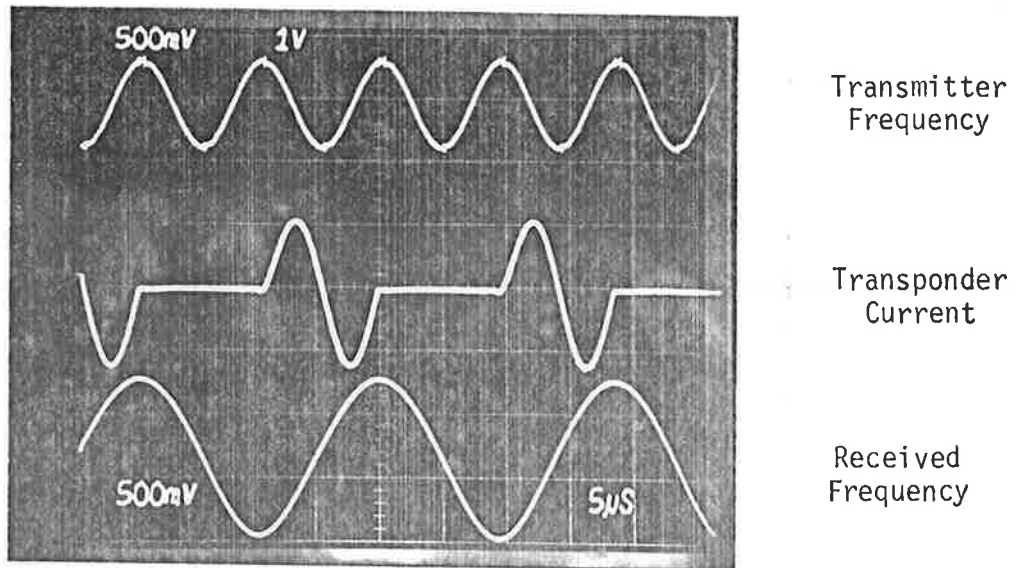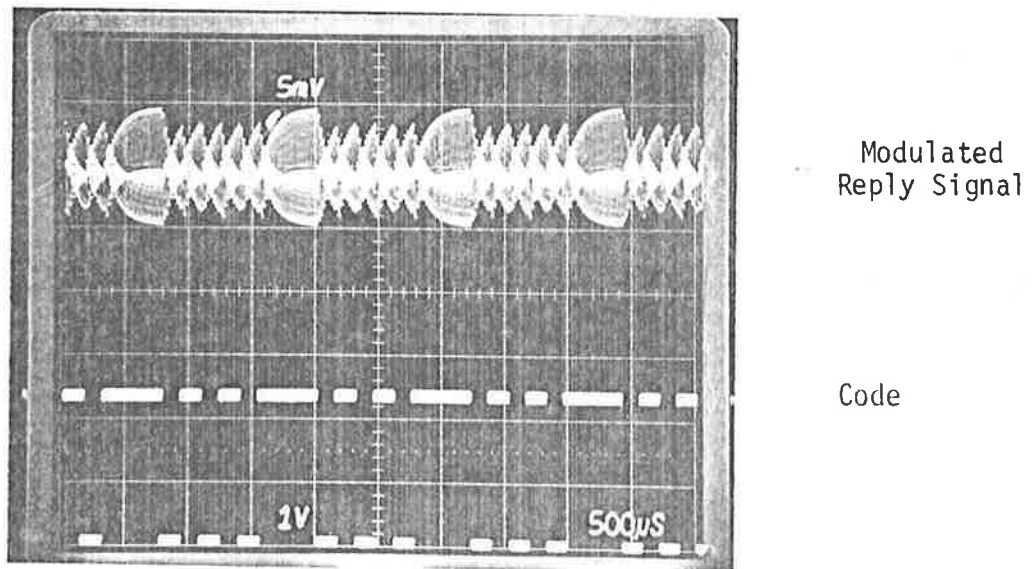
(b)

FIGURE 4.17.   PST WAVEFORMS.

(a)   Unmodulated.

(b)   Binary phase modulated waveform at the receiver
      antenna.

188.
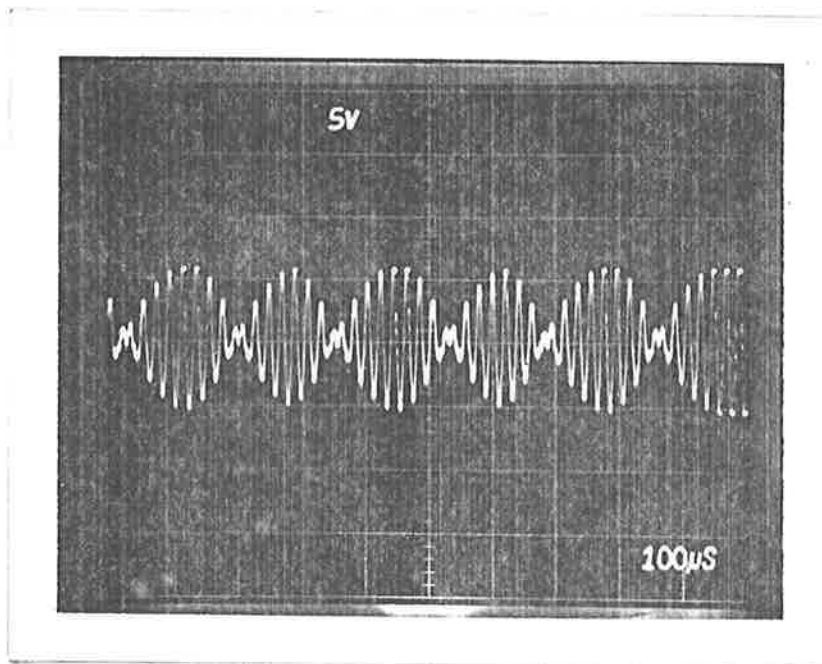
Note: Amplifier Gain = 1000

$Q_r = 9$

FIGURE 4.17 (c). 50kHZ BPSK WAVEFORM AFTER FILTERING AND AMPLIFICATION.

For the kind of parameters described previously T_d may vary between approximately 0.5 - 1.0mSec.

Before proceeding with overall system description and performance estimation it is desirable to present modelling principles which enable appropriate local optimizations of the transponder parameters to be performed. Therefore the next two chapters explore the above possibilities.

4.7 Conclusions

In this chapter a novel and original principle relating to frequency synthesis and PSK modulation associated with a one-port passive subharmonic transponder has been demonstrated. The important characteristic of the approach is that the reply signal energy is not injected into the coupling element from a dc reservoir as in the prior cases but rather it is synthesized, without prior conversion to dc, by switches and control elements which operate at appropriate instants of time to modulate the energy exchange process between the transponder near-field coupling element and its complementary energy storage element with which it is resonated.

The principle outlined in relation to reply code modulation has shown that the energy exchange process between the elements of the transponder is not disturbed by the modulation process and therefore constraints relating the communication bandwidth required by the

signal and the quality factor of the transponder tuned curcuit are broken. Therefore the power transfer across the electromagnetic links between transmitter- transponder-receiver can further be enhanced by making the quality factor of the transponder antenna as large as practicable and only the quality factor of the receiver antenna need be limited by the modulation bandwidth considerations.

A further point of interest which has been demonstrated is that when resonance process is interrupted on a cyclic basis in the kind of structures discussed, the resonance phenomenon is independent of the interruptions, provided the switching occurs at the zeros of the inductor current.

Through analysis a simple model describing the power transfer in the electromagnetic links was developed. This enabled a direct comparison between the one-port and two-port structure to be made. The significance of the above result is that although the operational characteristics are similar for both PST structures, for the kind of practical system parameters considered, the one-port PST achieves the same results through half the amount of antenna space as that required by the two-port structure. However if the one-port antenna dimensions is arranged to occupy the same area as that of the two-port then approximately 12dB gain becomes available.

The modulation principles developed has led into realisation of simple switching and control circuitry such that the losses in the tuned circuit could be kept to a minimum.

CHAPTER 5

COUPLING VOLUME THEORY

5.1 Introduction

In Chapter 3, Equation (3.22) gave an indication of the importance of high quality and coupling factors but failed to provide sufficient insight into the separate influences of the individual antenna geometries in establishing the level of coupling achieved. For this reason the concepts of coupling and dispersal volumes are introduced. These concepts enable the separation of the influence of different antenna parameters on the coupling and hence permit appropriate local optimization to be performed.

The desired separation of the effects of different sets of antenna* dimensions on power transfer ratio is achieved by recognising that in the weak coupling situation the basic excitation mechanism for the transponder antenna is the magnetic field created by

---

* *Since the wavelength is much larger than the distances involved between the transponder and interrogation unit the coupling elements are not antennae in the true sense. However in order to keep the generality of the description this term is used interchangeably with coils.*

the transmitter antenna. This magnetic field is in a weak coupling situation determined by the transmitter antenna parameters and excitation level alone, and is not influenced by the small power level established in the receptor coil. Furthermore, the magnetic field may be regarded as uniform over the comparatively small volume occupied by the transponder.

In the first part of this chapter some preliminary analysis is carried out in order to have an insight into the kind of variation of the power transfer that one could expect when the orientation and position of the two antennas are varied. The second section deals with development of principles on which local optimization based on individual antenna parameters can be performed.

5.2 Power Transfer Factor

For this analysis it is assumed that the coupling between the transmitter and transponder antennae is once again by magnetic fields alone, and further, the transponder coil is in the most favourable orientation for coupling to the magnetic field at the point in question. The energy density U_m stored in the magnetic field at the transponder position due to the transmitter antenna can be written as

$$U_m = \mu_o H^2 \qquad\qquad (5.1)$$

where

H = rms value of magnetic field at the transponder position produced by rms current I_1 in the transmitter antenna.

The rms value of stored magnetic energy W_2 in receptor coil self inductance when the receptor coil is short circuited can be expressed as

$$W_2 = L_2 \ I_2^2 \qquad\qquad (5.2)$$

where I_2 is the rms value of current in the receptor coil.

The power available when the receptor coil is tuned to resonance can be written as

$$P_2 = \omega_t \ W_2 \ Q_2 \qquad\qquad (5.3)$$

in which Q_2 is the quality factor associated with the receptor coil.

If the transmitter coil is resonated then the quality factor can be expressed as

$$Q_1 = \frac{\omega_t \ W_1}{P_1} \qquad\qquad (5.4)$$

194.

where

Q_1 = quality factor associated with transmitter coil

W_1 = rms value of magnetic energy in transmitter coil

P_1 = power dissipated in the transmitter coil resistance.

The power transfer between the transmitter coil and the receptor is then given by

$$\frac{P_2}{P_1} = Q_1 \ Q_2 \ \left(\frac{W_2}{W_1}\right) \tag{5.5}$$

where the ratio (W_2/W_1) is now referred to as power transfer factor F_p.

There are two cases of interest: first, when the axis of the antennae are parallel to each other; the second when the axes are orthogonal. The co-ordinates associated with the above configurations are shown in Figure 5.1.

5.2.1 Parallel antenna configuration

For the parallel configuration shown in Figure 5.1(a) the induced voltage E_2 in the receptor coil for a single turn is given by
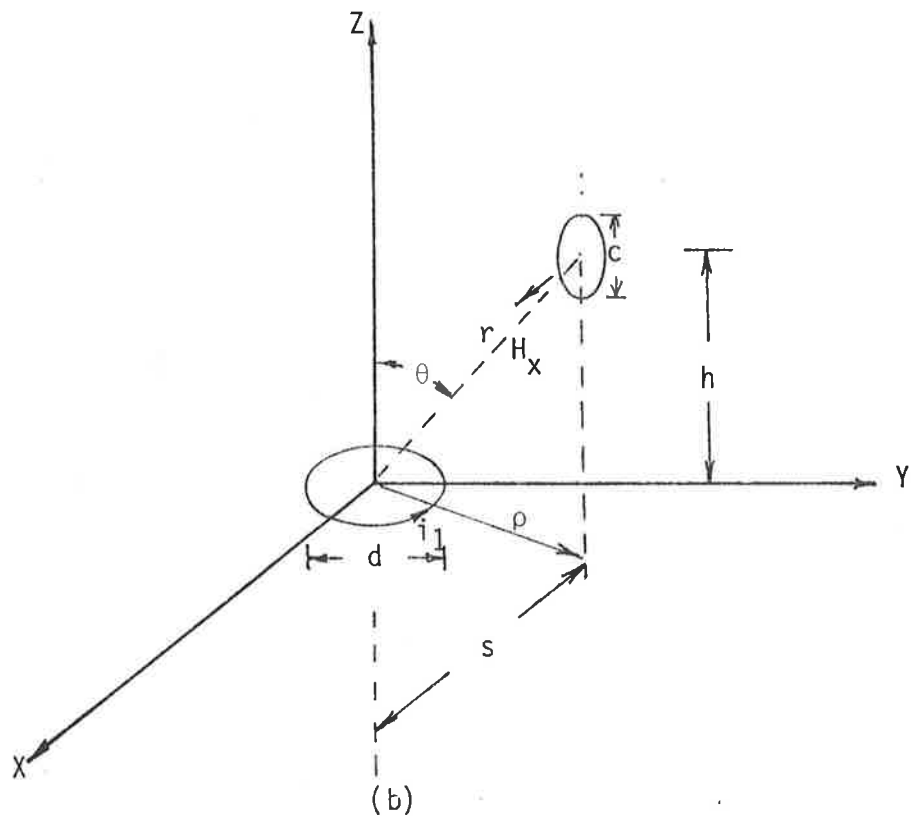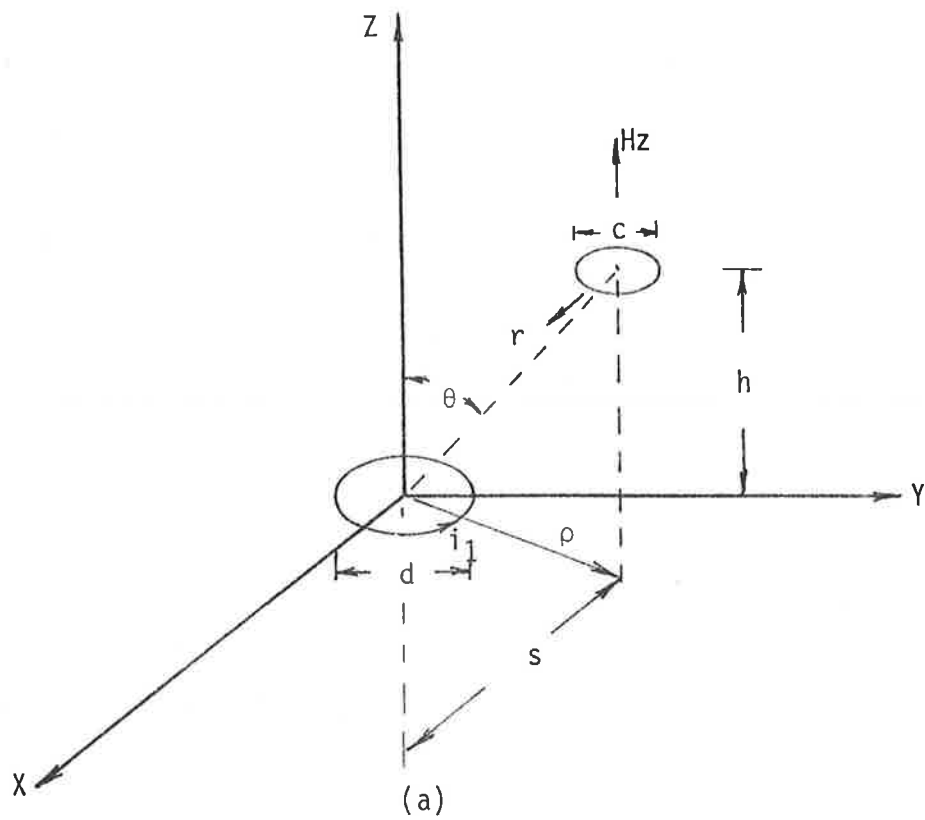
FIGURE 5.1. CO-ORDINATE SYSTEM SHOWING THE RELATIONSHIP BETWEEN
TRANSMITTER AND TRANSPONDER.

(a) Parallel Coils.
(b) Orthogonal Coils.

196.

$$E_2 = - \mu_0 \, \omega \, H_z \, A_r \qquad\qquad (5.6)$$

where H_z is the z component of the magnetic field and A_r is the area of receptor coil having diameter c. From Appendix D, H_z can be expressed as

$$H_z = \frac{I}{\pi d} \left[(1+m)^2 + n^2 \right]^{-\frac{1}{2}} \left[\frac{1 - m^2 - n^2}{(1-m)^2 + n^2} E(\alpha) + K(\alpha) \right] \qquad (5.7)$$

where

$$m = \frac{2s}{d}$$

$$n = \frac{2h}{d} \qquad\qquad\qquad (5.8)$$

$$\alpha = \sqrt{\frac{4m}{(1+m)^2 + n^2}}$$

s = axial displacement between the centres of the coils in the x-direction

h = separation between the coils in the z-direction

K(α) = Elliptic integral of the first kind

E(α) = Elliptic integral of the second kind

In order to calculate the power transfer factor F_p, the self inductances associated with the transmitter and receptor coils are taken as

197.

$$L_1 = \frac{\mu_o\, d}{2} \left(\log_e \frac{4d}{r_1} - 2 \right)$$

$$L_2 = \frac{\mu_o\, c}{2} \left(\log_e \frac{4c}{r_2} - 2 \right)$$

(5.9)

where r_1 and r_2 are the radii of the wires associated with the transponder and receptor coils respectively.

By noting that the stored energy in the transmitter coil is $L_1\, I_1^2$, then F_p can be expressed as

$$F_p = \frac{\gamma^3}{4\left[\left(\log_e \frac{4d}{r_1} - 2\right)\left(\log_e \frac{4c}{r_2} - 2\right)\left((1+m)^2 + n^2\right) \right]} \left[\frac{1-m^2-n^2}{(1-m)^2 + n^2} E(\alpha) + K(\alpha) \right]^2 \quad (5.10)$$

where

$$\gamma = \frac{c}{d} \qquad\qquad (5.11)$$

Plots of the power transfer factor F_p as a function of m for several values of n are shown in Figure 5.2. In these plots the value of wire radii is taken as $r_1 = r_2$. It is interesting to note that for the range of values of n shown the axial displacement between the centres of the coils by 83% results in a maximum of 3dB change in the power transfer factor.

198.
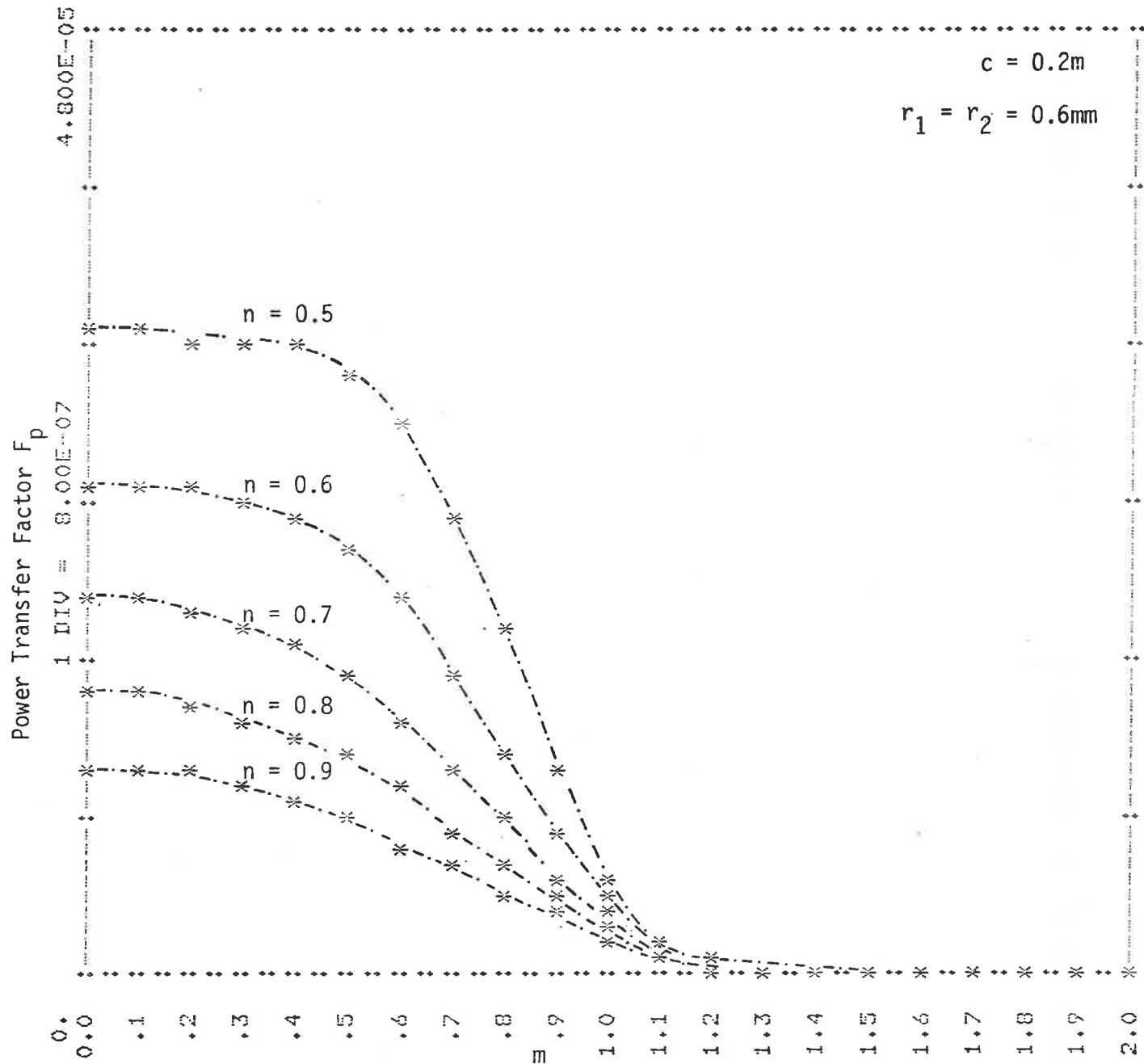
FIGURE 5.2(a). PLOT OF POWER TRANSFER FACTOR F_p AS A FUNCTION OF m FOR SEVERAL VALUE OF n WITH C = 0.2m USING PARALLEL COILS.
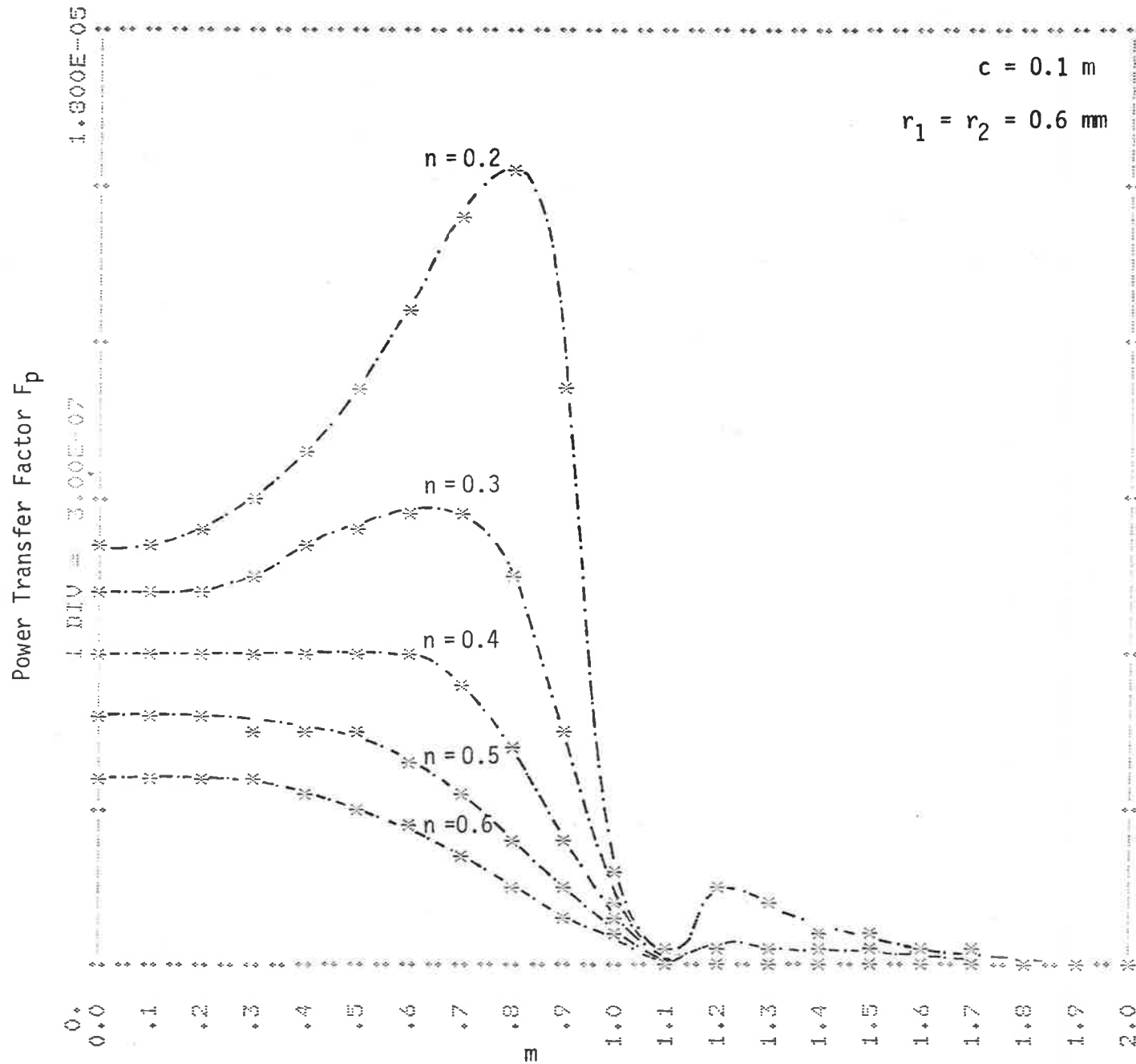
FIGURE 5.2(b). PLOT OF POWER TRANSFER FACTOR F$_p$ AS A FUNCTION OF m FOR SEVERAL VALUES OF n WITH c = 0.1m USING PARALLEL COILS

5.2.2 Orthogonal antenna configuration

In the orthogonal mode as shown in Figure 5.1(b), the x component of the magnetic field H_x, from Appendix D is

$$H_x = \frac{nI}{2\pi s\left[(1+m)^2 + n^2\right]^{\frac{1}{2}}} \left[\frac{1+m^2+n^2}{(1-m)^2+n^2} E(\alpha) - K(\alpha)\right] \qquad (5.12)$$

where

$$\alpha = \sqrt{\frac{4s}{(1+m)^2 + n^2}} \qquad (5.13)$$

The power transfer factor can be written as

$$F_p = \frac{\gamma^3 \sigma^2}{4\left[\log_e \frac{4d}{r_1} - 2\right]\left[\log_e \frac{4c}{r_1} - 2\right]\left[(1+m)^2 + n^2\right]} \left[\frac{1+m^2+n^2}{(1-m)^2+n^2} E(\alpha) - K(\alpha)\right]^2 \qquad (5.14)$$

where $\sigma = \frac{h}{s}$.

Plots of the power transfer factor F_p as a function of m for several values of n are also shown in Figure 5.3 for the orthogonal coils where wire radii $r_1 = r_2$.

The significance of these curves are that they provide a direct means to calculate the amount of power delivered to the transponder coil for a given transmitter power when practical quality factors are assigned to each of the coils.
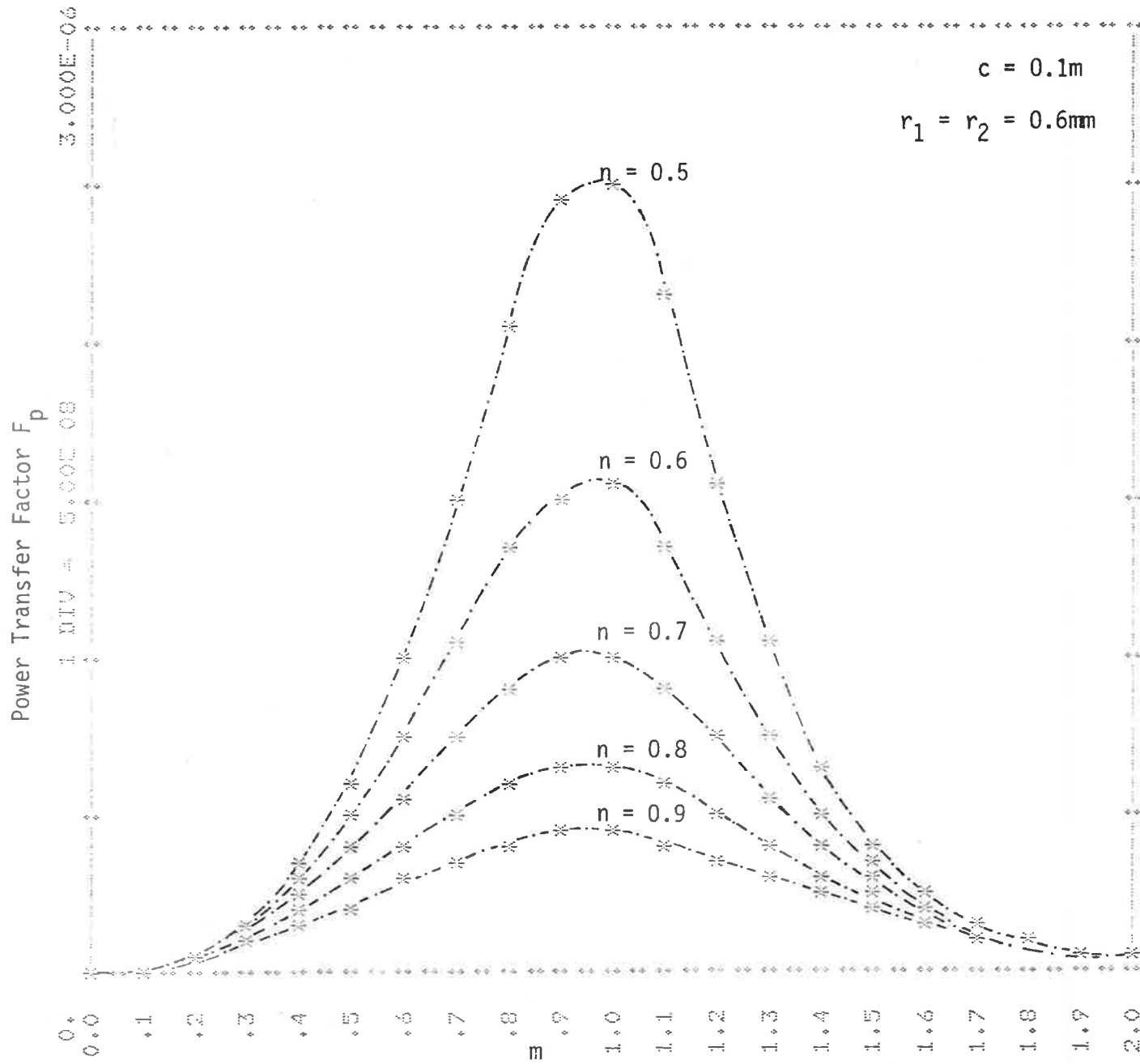
FIGURE 5.3(a). PLOT OF POWER TRANSFER FACTOR F_p AS A FUNCTION OF m FOR SEVERAL VALUES OF n USING ORTHOGONAL COILS.
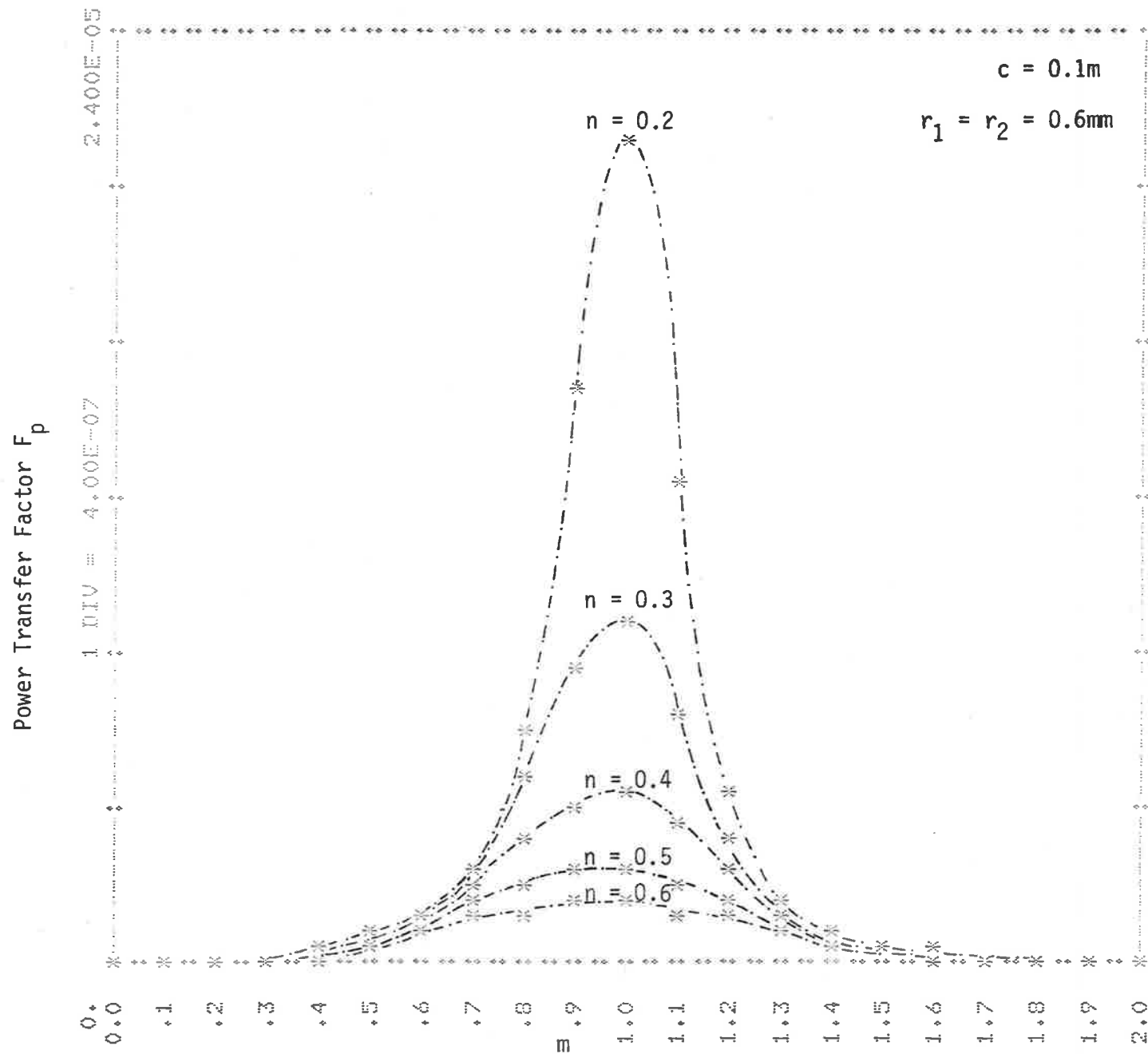
FIGURE 5.3(b). PLOT OF POWER TRANSFER FACTOR F_p AS A FUNCTION OF m FOR SEVERAL VALUES OF n USING ORTHOGONAL COILS.

Further insight is also gained into the variation of power transfer for various separations and longitudinal displacements.

5.3 Coupling Volume Theory

Examination of power transfer factor F_p indicate that if this relation is rearranged in terms of the magnetic energy density U_m produced at the transponder position, some interesting relations could emerge. Introducing the term U_m in the power transfer factor F_p results in the expression

$$F_p = \frac{(W_2/U_m)}{(W_1/U_m)} \qquad (5.15)$$

The ratio $\left(\frac{W_2}{U_m}\right)$ has the dimensions of volume and is denoted by coupling volume V_c. For the receptor antenna this is defined as the ratio:

$$V_c = \frac{\left(\begin{array}{c}\text{Peak value of stored magnetic energy}\\ \text{in receptor self inductance when}\\ \text{receptor is short circuited}\end{array}\right)}{\left(\begin{array}{c}\text{Peak value of the magnetic energy}\\ \text{density produced at the transponder}\\ \text{position by the transmitter}\end{array}\right)} \text{(metre}^3) \qquad (5.16)$$

Use is now made of the relation that the power to the receptor coil loading resistance when it is tuned to resonance is $\omega_o\, Q_2$ times

the peak value of the stored magnetic energy in the receptor coil
self inductance when it is short circuited, to obtain the results

$$\begin{pmatrix} \text{Power to} \\ \text{receptor} \\ \text{loading} \\ \text{resistance} \end{pmatrix} = \omega_o \, Q_2 \, V_c \begin{pmatrix} \text{Peak value of energy density per} \\ \text{unit volume produced at the} \\ \text{transponder by the transmitter} \end{pmatrix} \qquad (5.17)$$

This relation shows clearly that the coupling volume V_c serves
as a figure of merit for various antennas all loaded to give the
same quality factor.

It is now necessary to provide a relation between the energy
density at the transponder position and the transmitter power.
Clearly for a given transmitter antenna geometry, this density is
proportional to the total stored energy of the antenna as shown by
the ratio $\left(\dfrac{W_1}{U_m}\right)$. The use of this fact can be made to define the
dispersal volume V_d for the transmitter antenna as the ratio

$$V_d = \frac{\begin{pmatrix} \text{Peak value of the total stored magnetic} \\ \text{energy in the transmitter antenna} \end{pmatrix}}{\begin{pmatrix} \text{Peak value of the magnetic energy density} \\ \text{produced at the transponder position by} \\ \text{the transmitter} \end{pmatrix}} \quad (\text{meter}^3) \qquad (5.18)$$

It is further possible to make use of the relation that power
to the transmitter antenna loading resistance is (ω_o/Q_1) times the
peak value of the stored mangetic energy in the transmitter self
inductance to establish in conjunction with the preceding results,
the principal results of this analysis, which is an expression for
the power transfer ratio between transmitter and receptor antennas.
This result is:

205.

$$\frac{P_2}{P_1} = Q_1 \, Q_2 \left(\frac{V_c}{V_d}\right) \tag{5.19}$$

Similarly, with reference to Figure 3.14 the power transfer ratio P_4/P_3 in the link from the transponder antenna to receiver antenna can be calculated by using the expression

$$\frac{P_4}{P_3} = Q_3 \, Q_4 \left(\frac{V_c'}{V_d'}\right) \tag{5.20}$$

where V_c' is the coupling volume of the transponder antenna and V_d' is the dispersal volume of the receiver antenna. The structure of the above relation makes it appear that the direction of the power flow is from the receiver to the transponder antenna. However the electromagnetic reciprocity theorem ensures that the same expression describes power flow in the reverse direction.

Application of these analyses to the one port PST structure in which $V_c' = V_c$ and $V_d' = V_d$ results in

$$\frac{P_4}{P_1} = \eta' \chi_p \left(\frac{V_c}{V_d}\right)^2 Q_1 \, Q_F^2 \, Q_4 \tag{5.21}$$

where χ_p is the shape factor as defined by Equation (4.16) in Chapter 4.

These results show that for strong coupling there is a need for a large coupling volume in the transponder and a small dispersal volume in the transmitter. The transmitter antenna behaves, in so far as the transponder is concerned, as if the transmitter antenna stored energy were uniformly distributed over the volume equal to the transmitter dispersal volume.

A further contrast between the coupling volume and the dispersal volume which should be noted is that while the former depends only upon the characteristics of the receptor antenna, the dispersal volume depends not only upon the antenna dimensions but also on the position of the transponder within the transmitter antenna's field. The dispersal volume increases substantially with increase of separation of the two antennas.

The significance of these results are that the ratio V_c and V_d are dependent on the geometries of the coils which are individually subject to optimization while the quality factors indicate how efficient the transfer of power can be made.

In order to gain further insight into these concepts in the following sections expressions are derived for the coupling volume and the dispersal volumes associated with several practical antenna structures.

5.4 Coupling Volume Calculations

Several types of near field magnetic antennas which are of interest in the realization of the passive subharmonic transponder are shown in Table 5.1. The diagrams in the table illustrate round and square perimeter planar coiles, round or square cross-section solenoidal coils, and a slab solenoidal coil. In each case the coil is assumed to be uniformly close wound over the indicated perimeter or surface; in none of the cases however does the number of turns enter final expressions obtained for coupling volume.

In the results to be presented the coils are assumed in the first instance to be air cored, with the effects of providing high permeability cores to be presented in the later section.
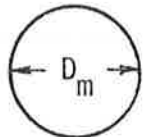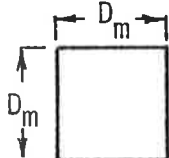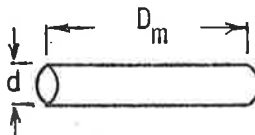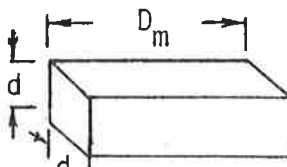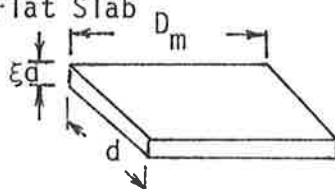
In order to obtain results which are of sufficient algebraic simplicity to enable effective comparison between coils of different style, a number of approximations are made. These are that the internal inductance of the wire may be neglected, and that the dimensions of the solenoid and slabs are such that long solenoid formulae may be used.

Further, the calculations are based on the shape which is most convenient mathematically, viz. a circle. Such an approach can also be extended to a square antenna where the dimensions are chosen such that $D = d\sqrt{\frac{\pi}{4}}$, where D is the length of the side of a square antenna having the same area as a circular antenna with diameter d.

For a flat coil, from definition the coupling volume can readily be shown to be

TABLE 5.1. TABULATION OF COUPLING VOLUME FOR SEVERAL STRUCTURES

$$V_c = \chi_c D_m^3$$

Shape	χ_c	η_s
Circular Coil $\leftarrow D_m \rightarrow$ r = radius of wire	$\dfrac{\pi^2}{8\left[\log_e \dfrac{4D_m}{r} - 2\right]}$	$\chi_c\left(\dfrac{2D_m}{\pi r}\right)$
Square Coil $\leftarrow D_m \rightarrow$ D_m r = radius of wire	$\dfrac{\pi}{2\left[\log_e\left(\dfrac{4D_m}{r}\right)+\dfrac{r}{D_m} - 2.16\right]}$	$\chi_c\left(\dfrac{D_m}{2r}\right)$
Solenoid $\leftarrow D_m \rightarrow$ d $D_m > d$	$\dfrac{\pi}{4}\left(\dfrac{d}{D_m}\right)^2$	1
Solenoid $\leftarrow D_m \rightarrow$ d d $D_m > d$	$\left(\dfrac{d}{D_m}\right)^2$	1
Flat Slab D_m ξd d $D_m > \xi d$	$\dfrac{\xi}{K}\left(\dfrac{d}{D_m}\right)^2$	$1/K$

209.

$$V_c = \frac{\mu_0 \ A^2 \ N^2}{L} \quad (\text{metre}^3) \tag{5.22}$$

where A is the flux collecting area, L is its self inductance, N is the number of turns and μ_0 is the permeability of free space.

Similarly for an air cored solenoid having length ℓ, with either a round or rectangular cross-section the coupling volume is described by the relation

$$V_c = \frac{A\ell}{K} \quad (\text{metre}^3) \tag{5.23}$$

where A is the cross-section area and K is a correction factor[103] to take into consideration the end effect. When the angular aperture of the solenoid at the centre is less that 45^0, K can be represented by

$$K = 1 - \frac{4k}{3\pi k'} + 2q + 12q^2 + 44q^3 + 116q^4 + 260q^5 + \ldots \tag{5.24}$$

where

$$q = \frac{x}{2} + 2\left(\frac{x}{2}\right)^5 + 15 \left(\frac{x}{2}\right)^9 + \ldots \tag{5.25}$$

210.

and

$$x = \frac{1 - \sqrt{k'}}{1 + \sqrt{k'}}$$

$$k^2 = \frac{\ell^2}{\ell^2 + d^2}$$

$$k'^2 = \frac{d^2}{\ell^2 + d^2}$$

and d is the diameter or alternatively the width of the coil as the case may be.

For long solenoids Equation (5.23) reduces to

$$V_c = A\ell \quad (\text{meter}^3)$$

which simply corresponds to the physical volume of the solenoid.

The overall results of these analyses can be expressed by a general relation given in terms of the maximum dimension of the antenna structures denoted by D_m. The model describing the coupling volume becomes

$$V_c = \chi_c D^3 \tag{5.26}$$

where value of χ_c is defined in Table 5.1 for several structures

211.

of interest.

Theoretical calculations based on the model defined by Equation
(5.26) and corresponding measured values for several solenoids having
different cross-sectional areas are also shown in Table 5.2. Pro-
vided the length of the solenoid is greater than the smallest cross-
sectional axis, the model provides an accurate representation for
the coupling volume.

In order to have an insight into the effectiveness of the struc-
tures in terms of the physical volume V_p the antennas occupy, the
space efficiency factor η_s defined as
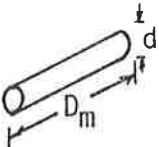
$$\eta_s = \frac{\text{Coupling Volume } (V_c)}{\text{Physical Volume } (V_p)} \qquad (5.27)$$
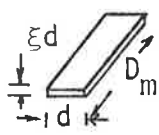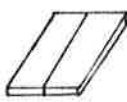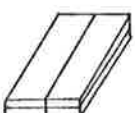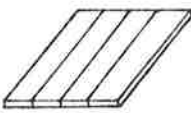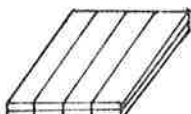
is introduced. The above expression is a good indicator of the
effectiveness of an antenna in which dimensional constraints are
imposed on the structure.

Values of η_s for several structures of interest are also shown
in Table 5.1. The table illustrates the superiority of large area
planar coils as near field magnetic antennas when the operative con-
straint is the largest dimension or the objective is maximization
of the space efficiency factor η_s. Therefore this structure will
be analysed in more detail in Chapter 6.

* *The measurements for the coupling volume were conducted using
a search coil for determination of the magnetic field.*

TABLE 5.2. COMPARISON BETWEEN MEASURED AND COMPUTED
VALUES FOR COUPLING VOLUMES

Shape \ Parameter	N	D_m mm	d mm	-	L_{meas} μH	L_{th} μH	K	$V_{C_{meas}}$ $m^3 \times 10^{-6}$	$V_{C_{th}}$ $m^3 \times 10^{-6}$
(rod)	52	33.3	12.5	–	11.8	11.7	0.852	5.19	5.26
	105	66.0	12.5	–	26.0	25.9	0.921	9.60	9.71
	219	12 9	12.5	–	53.3	55.3	0.958	19.01	18.1

Shape \ Parameter	N	D_m mm	d mm	ξd mm	L_{meas} μH	L_{th} μH	K	$V_{C_{meas}}$ $m^3 \times 10^{-6}$	$V_{C_{th}}$ $m^3 \times 10^{-6}$
	44	26.9	14.4	7.8	7.9	8.2	0.807	3.9	3.7
	88	55.0	14.2	7.8	16.9	17.6	0.898	7.1	6.8
	176	109.6	13.8	7.8	34.8	35.3	0.949	12.5	12.1
	44	26.4	14.2	14.1	13.7	14.9	0.807	6.9	6.6
	88	54.5	14.4	14.2	30.7	32.7	0.897	12.8	12.4
	176	107.0	15.4	14.4	72.6	76.0	0.941	26.1	25.2
	44	27.2	28.5	7.6	13.0	13.1	0.678	8.7	8.7
	88	53.8	28.3	7.6	30.1	31.5	0.810	14.9	14.3
	176	111.4	26.6	7.6	61.3	64.0	0.906	25.5	24.9
	44	27.8	27.0	14.4	23.8	23.6	0.695	15.3	15.6
	88	54.7	28.0	14.4	56.9	58.4	0.815	27.9	27.0
	176	108.0	28.3	14.6	129.2	133.6	0.897	52.3	49.7
	44	28.2	56.0	7.8	28.2	–	–	17.8	–
	88	55.7	51.7	7.8	57.3	49.6	0.704	26.5	31.9
	176	110.9	54.0	7.5	128.0	116.9	0.822	51.7	54.6
	44	26.6	53.4	4.4	46.1	–	–	32.4	–
	88	54.4	53.0	3.9	101.5	91.5	0.694	51.1	57.7
	176	110.2	53.5	4.4	235.6	223.9	0.823	97.9	103.2

$V_{C_{meas}}$ = measured value of coupling volume.

$V_{C_{th}}$ = theoretical value of coupling volume.

N = number of turns.

K = inductance correction factor.

5.5 Dispersal Volume Calculations

The analysis of the dispersal volume V_d of a near field magnetic antenna requires consideration of not only the antenna shape and dimensions but also the distance and direction to the field point to be energized by the antenna. In view of the number of variables involved it is not practicable to consider all cases. However, results for a sufficient range of variation of parameters is presented which allows for useful conclusions to be drawn.

Once again the coils are assumed to be air cored with the results of ferrite cores to be considered later. The coils are further assumed to be uniformly close wound, internal inductance of the wires is neglected, and the dimensions and distance to the point of excitation are such that long solenoid formulae may be used. The results do cover the case when the distance to the excitation point is comparable with the antenna dimensions, as this positioning is frequently necessary for practical transponders, as well as the far field case wherein the antenna acts as a simple dipole. The later however provides, in conjunction with the assymptotic relation discussed later between coupling volume and dispersal volume at large distances, a useful check in the validity of the present results.

The dispersal volume for several geometrics can be calculated as follows:

(i) Flat Planar Coil

The dispersal volume V_d for a flat coil can be derived by noting that the magnetic field H at a distance h along the axis from the centre of a circular coil of diameter d having N turns and carrying a current I_t is given by (Appendix D)

214.

$$H = \frac{N\,I_t}{d\left[1 + \left(\frac{2h}{d}\right)^2\right]^{3/2}} \tag{5.28}$$

From definition, the dispersal volume for the transmitter antenna can be expressed as

$$V_d = \frac{I_t^2\,L_t}{\mu_o\,H^2} \quad (\text{metre}^3) \tag{5.29}$$

For a circular antenna of diameter d and wire radius r_1, the expression becomes

$$V_d = \frac{1}{2}\left[\log_e \frac{4d}{r_1} - 2\right] P\,d^3 \tag{5.30}$$

where

$$P = \left(1 + \phi^2\right)^3 \tag{5.31}$$

and

$$\phi = \sqrt{\pi}\,(h/D) \tag{5.32}$$

For a square coil having sides D with an area equivalent to that of a circular planar coil, the dispersal volume is approximated by

$$V_d = \frac{8}{\pi^2} \left\{ \log_e \frac{4D}{r_1} + \frac{r_1}{D} - 2.16 \right\} \left[1 + (\sqrt{\pi}h/D)^2 \right]^3 D^3 \qquad (5.33)$$

(ii) Logitudinal Solenoid

The dispersal volume for a longitudinal solenoid having N turns with length ℓ and diameter d can be expressed as

$$V_d = \frac{2}{\sqrt{\pi}} \left(\frac{\ell}{d}\right)^5 \left(1 + \frac{2h}{\ell}\right)^6 D^3 \qquad (5.34)$$

In the above derivation use is made of the self inductance formula for long and thin solenoid.

(iii) Transverse Solenoid

The structure of the solenoid is similar to that of (ii). However in this instant the sensing distance is orthogonal to the direction of the major axis of the solenoid. The dispersal volume can be readily shown to be described by

$$V_d = \frac{2}{\sqrt{\pi}} \left(\frac{\ell}{d}\right)^2 \left[1 + \left(\frac{2h}{\ell}\right)^2 \right]^3 D^3 \qquad (5.35)$$

216.

The results of the above analysis once again is modified in terms of the maximum dimension D_m associated with each antenna geometry and is represented by a general expression

$$V_d = \beta\ P\ D_m^3 \quad (\text{meter}^3) \hspace{2cm} (5.36)$$

where β is a shape dependent factor and P is the position dependent factor. Table 5.3 shows the values associated with the above parameters for several antenna structures.

The structure of the relation given by Equation (5.36) is of particular interest. The term $\beta\ D_m^3$ gives the value of dispersal volume at the centre of the antenna, i.e. $h = 0$. The second term P indicates the extent to which the dispersal volume is increased as the separation h from the centre of the antenna is increased.
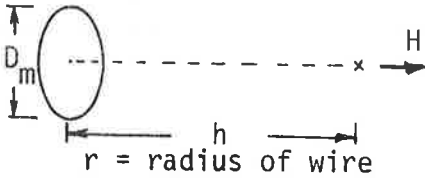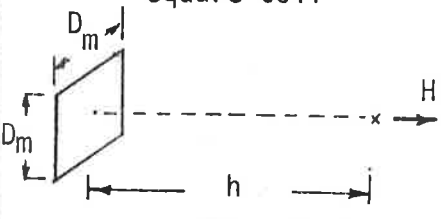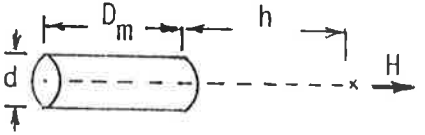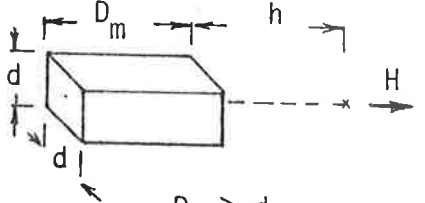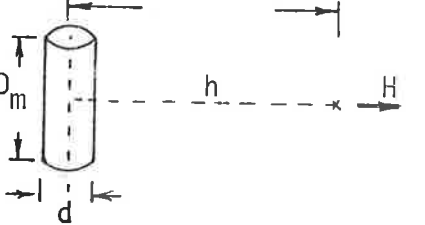
Plots of P in terms of the ratio (h/D_m) for the three main structures namely plannar coil, solenoid with sensing distance along the major axis and solenoid with sensing distance orthogonal to the major axes are shown in Figure 5.4.

These results demonstrate the general similarity of the position dependence of all antennas of a given maximum dimension, and the superiority of the flat coil over the air cored solenoid and slab coils.

For the flat coil in minimizing the dispersal volume with respect to D_m the minimum V_d occurs at $D_m = 2h$ and has the value

217.

TABLE 5.3.   TABULATION OF DISPERSAL VOLUME FOR SEVERAL STRUCTURES

$$V_d = \beta P D_m^3$$

Shape	β	P	ϕ
Circular Coil r = radius of wire	$\dfrac{1}{2}\left[\log_e \dfrac{4D_m}{r} - 2\right]$	$\left[1 + \phi^2\right]^3$	$\dfrac{2h}{D_m}$
Square Coil r = radius of wire	$\dfrac{8\left[\log_e \dfrac{4D_m}{r} + \dfrac{r}{D_m} - 2.16\right]}{\pi^2}$	$\left[1 + \phi^2\right]^3$	$\sqrt{\pi}\left(\dfrac{h}{D_m}\right)$
Solenoid $D_m > d$	$\dfrac{\pi}{4}\left(\dfrac{D_m}{d}\right)^2$	$\left[1 + \phi\right]^6$	$\dfrac{2h}{D_m}$
Solenoid $D_m > d$	$\dfrac{\pi^2}{16}\left(\dfrac{D_m}{d}\right)^2$	$\left[1 + \phi\right]^6$	$\dfrac{2h}{D_m}$
Solenoid	$\dfrac{\pi}{4}\left(\dfrac{D_m}{d}\right)^2$	$\left[1 + \phi^2\right]^3$	$\dfrac{2h}{D_m}$
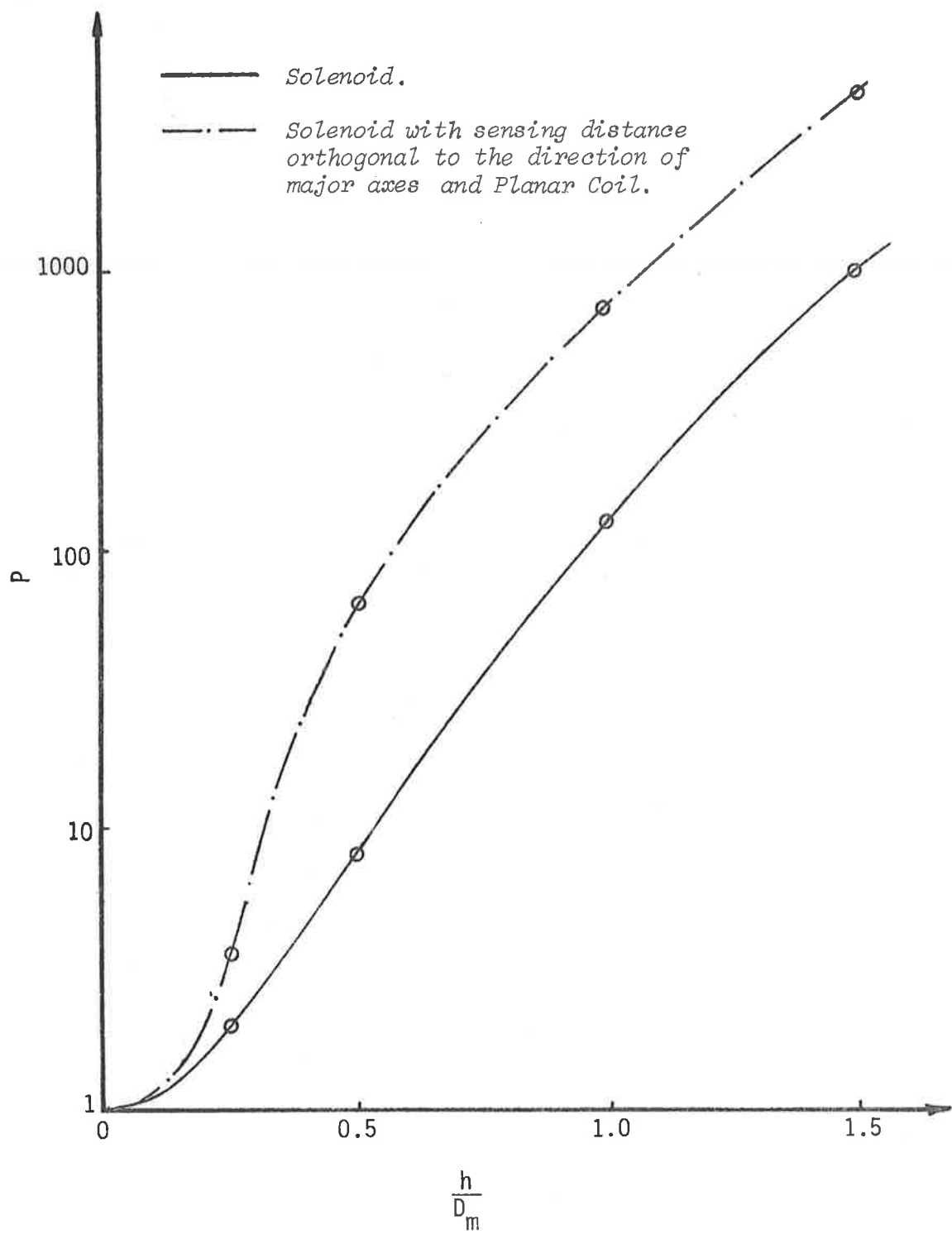
FIGURE 5.4. PLOT OF P AS A FUNCTION OF THE RATIO (h/D_m) FOR

SOLENOIDS AND PLANAR COILS.

$$V_{d_{min}} = 32 \ h^3 \left[\log_e \left(\frac{8h}{r} \right) - 2 \right] \qquad (5.37)$$

Similar results can readily be obtained for other geometrics. However these derivation are not as important since for vehicle identification systems and signpost implementation it is very difficult to maintain the relationship between the diameter and the sensing distance.

5.5.1   Asymptotic relations

In the discussion so far the coupling volume and dispersal volume have been defined as independent parameters. A general reciprocity argument indicates however that these quantities should be related.   Detailed analysis of the results of Table 5.1 and Table 5.3 indicate that at sufficiently large distances to the point of excitation the coupling and dispersal volumes of a given antenna bear the assymptotic relation given by

$$V_d = \frac{4 \ \pi^2 \ h^6}{V_c} \qquad (5.38)$$

The above expression may serve as a check to the validity of simple models obtained for different antenna structures.   A further relation which is of interest is the

power transfer ratio between the transmitter and transponder
antennas when the separation between the two antennas is
large compared with their dimensions.

The magnetic field created by the transmitter antenna
as the result of current I_t is

$$H = \frac{2m'}{4\pi \mu_o h^3} \tag{5.39}$$

where m' is the magnetic moment given by $\mu_o I_t A$, and A is
the flux collecting area. Using the results of Equation
(5.37) the power transfer ratio can be shown as

$$\frac{P_2}{P_1} = \left(\frac{1}{4\pi^2}\right) \frac{Q_1 Q_2 V_{c1} V_{c2}}{h^6} \tag{5.40}$$

where

V_{c1} = coupling volume of transmitter antenna

V_{c2} = coupling volume of transponder antenna

h = separation between the antennae.

5.6 Influence of Ferromagnetic Materials

The results of coupling volume and dispersal volume shown in Table 5.1 and Table 5.3 which apply to air cored antennas are modified substantially if a high permeability ferrite core is introduced.

When such a material is introduced into the transponder coil, the magnetic field associated with the coil causes the ferromagnetic body to be magnetized with poles on its surface. The magnetizing force $\tilde{H}_i$ inside the material differs in magnitude from the applied field $\tilde{H}$.

For an ellipsoid[105] magnetized along one of the principle axis the component of the magnetic field can be described by

$$\tilde{H}_i = \tilde{H} - N_d \tilde{M}_p \qquad (5.41)$$

where N_d is the demagnetization factor[106] determined by the ratios of the semipole axes of the ellipsoid, and $\tilde{M}_p$ is magnetic polarization. Therefore, if the magnetization components and the lengths of the axes of the ellipsoid are known, then the internal field $\tilde{H}_i$ may be predicted.

A precise calculation of magnetic field for other shapes results in complicated expressions which fail to highlight the major features for optimizations. However considerable simplification can be made if the antenna structures of interest are approximated by an ellipsoid. This assumption permits calculations

222.

to proceed on the basis of uniform magnetization.

The self inductance L of a coil is given by:

$$L = \frac{\int \tilde{B}.d\tilde{S}}{I} \tag{5.42}$$

where I is the rms current and $\tilde{S}$ is any surface over which the integration is carried and $\tilde{B}$ is the flux density over that surface.

For an air cored solenoid the inductance L_a can be expressed in terms of the magnetic field $\tilde{H}$. Thus,

$$L_a = \frac{\mu_0}{I} \int \tilde{H}.d\tilde{S} \tag{5.43}$$

where μ_0 is the permeability of the free space.

When a ferrite material is introduced into a current carrying coil, for uniform magnetization it is readily shown that the inductance can be approximated by[105]

$$L_f = \frac{\mu_0}{I} \left(\frac{1 + \chi_m}{1 + N_d \chi_m} \right) \int \tilde{H}.d\tilde{S} \tag{5.44}$$

where χ_m is the magnetic susceptibility.

Provided the introduced material into the coil is not saturated, the relative permeability μ_r of the material may be written as:
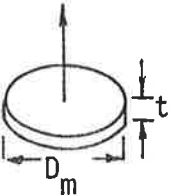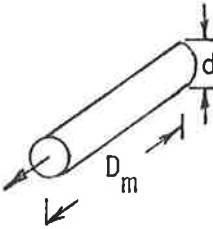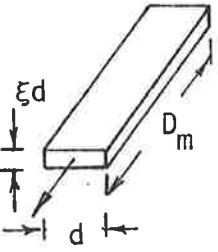
$$\mu_r = 1 + \chi_m \tag{5.45}$$

The ratio of Equation (5.44) and Equation (5.43) is denoted by μ_e and defines the improvements one can achieve when ferrite is introduced as a core. This relation is given by

$$\mu_e = \frac{\mu_r}{1 + N_d (\mu_r - 1)} \tag{5.47}$$

To provide a data base for optimization a theoretical and experimental study of effective permeability factor μ_e for ferrite cored coils of various types has been conducted. the experimental work was carried out for close wound coils on ferrite cores of two different permeabilities. The theoretical derivation was based on power series expansion of the demagnetization factors[109] shown in Table 5.4 derived from Appendix E. The approximation in the analysis are that the relative permeability of material is high and only geometries which can be approximated by an ellipsoid are considered. The example of results obtained is given in Figure 5.5 which illustrates for sensible geometrics the good agreement found between experimental and the simple analysis.

224.

TABLE 5.4. DEMAGNETIZATION FACTOR FOR SEVERAL STRUCTURES

Shape	Demagnetization Factor
$D_m \gg t$	$N_{d_3} = 1 - \left\{ \dfrac{4u}{\left(1 - u^2\right)^{3/2}} \left[\dfrac{\pi}{2} - \text{Arctan} \dfrac{u}{\left(1 - u^2\right)^{1/2}}\right] - \dfrac{u^2}{2\left(1 - u^2\right)} \right\}$ $u = \left(\dfrac{4t}{D_m}\right)^2$
$D_m > d$	$N_{d_1} = \dfrac{1 - \omega^2}{\omega^2} \left[\dfrac{1}{2\omega} \log_e \left(\dfrac{1 + \omega}{1 - \omega}\right) - 1\right]$ $\omega = \sqrt{1 - \left(\dfrac{d}{D_m}\right)^2}$
$\xi \leqslant 1$ $D_m > d$	$N_{d_1} = \dfrac{d_\xi^2 \, D_m}{\left(D_m^2 - d^2\right) \sqrt{D_m^2 - \xi^2 d^2}} \left[K(v,q) - E(v,q)\right]$ $v = \text{Arc Sin} \dfrac{\sqrt{D_m^2 - \xi^2 d^2}}{D_m^2}$ $q = \sqrt{\dfrac{D_m^2 - d^2}{D_m^2 - \xi^2 d^2}}$

$K(v,q)$ = Incomplete Elliptic Integral of the First kind.

$E(v,q)$ = Incomplete Elliptic Integral of the Second kind.
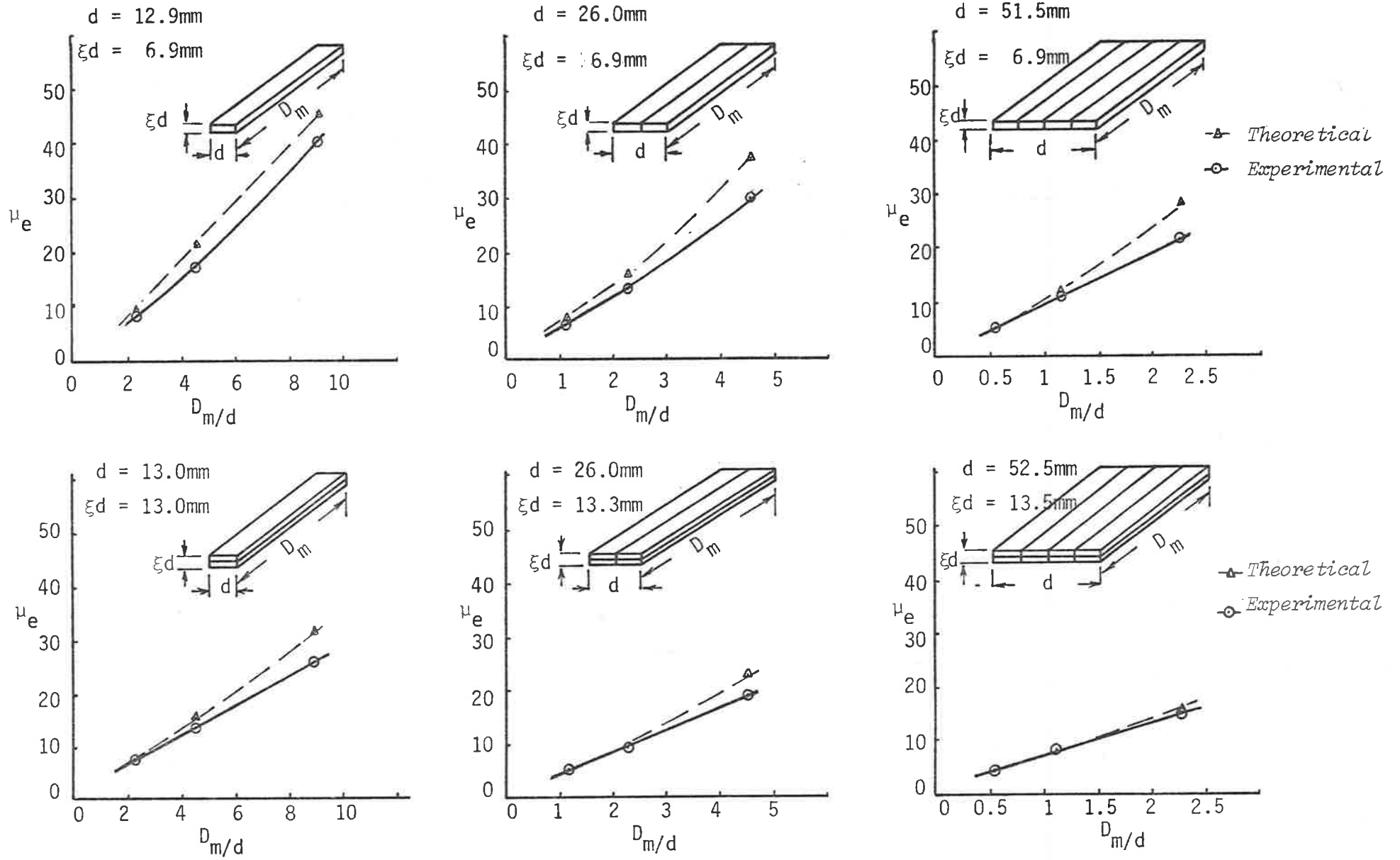
FIGURE 5.5. PLOT OF EFFECTIVE PERMEABILITY μ_e AS A FUNCTION OF $D_{m/d}$ FOR FERRITE SLABS.

5.6.1 Asymptotic behaviour

The asymptotic behaviour of the demagnetization in the direction of the magnetization for a circular thin disc from Table 5.4 can be written as

$$N_{d_3} = 1 - \frac{\pi}{2}\left(\frac{t}{D_m}\right) \tag{5.48}$$

with $D_m >> t$, Equation (5.44) reduces to unity. This case has been included to give an indication of the behaviour of demagnetizing factor for thin disc and thin square slab solenoids.

Similar asymptotic relation can also be derived for the rod magnetized along the major axis. This is given by

$$N_{d_1} = (d/D_m)^2 \log_e (D_m/d) \tag{5.49}$$

Putting $v = (d/D_m)$ and taking the first and second derivatives results in

$$\lim_{v \to 0} \frac{d\ N_{d_1}}{dv} = 0 \tag{5.50}$$

and

$$\lim_{v \to 0} \frac{d^2\ N_{d_1}}{dv} = \infty \tag{5.51}$$

Thus it can be seen that the curve has some kind of
singularity at v = 0. The tangent has zero slope but the
second derivative is infinite. Therefore a smooth curve
under these conditions is not practicable.

Predictions using these formulae agree well with those
of experimental results which are relevant.

5.6.2   Coupling volume approximations

Plots of experimental values of effective permeability
μ_e for slabs as a function of the ratio $\frac{1}{\sqrt{\xi}} \left(\frac{D_m}{d} \right)$ corresponding
to each of the previous structures is shown in Figure 5.6.
From the figure it is possible to derive an empirical
model for the effective permeability of a ferrite slab in
terms of its dimension.

This can roughly be approximated by

$$\mu_e \doteq \frac{3}{\sqrt{\xi}} \left(\frac{D_m}{d} \right) \tag{5.52}$$

Using the above empirical relationship the coupling
volume for ferrite slabs becomes

$$V_c = \frac{3\sqrt{\xi}}{K} \left(d \; D_m^2 \right) \quad (\text{meter}^3) \tag{5.53}$$

For practical dimensions the maximum error that can be
expected using Equation (5.53) in predicting the coupling
volume is in the order of 20%.

The significance of the above result is its simplicity
of structure which permits for easy evaluation of coupling

228.
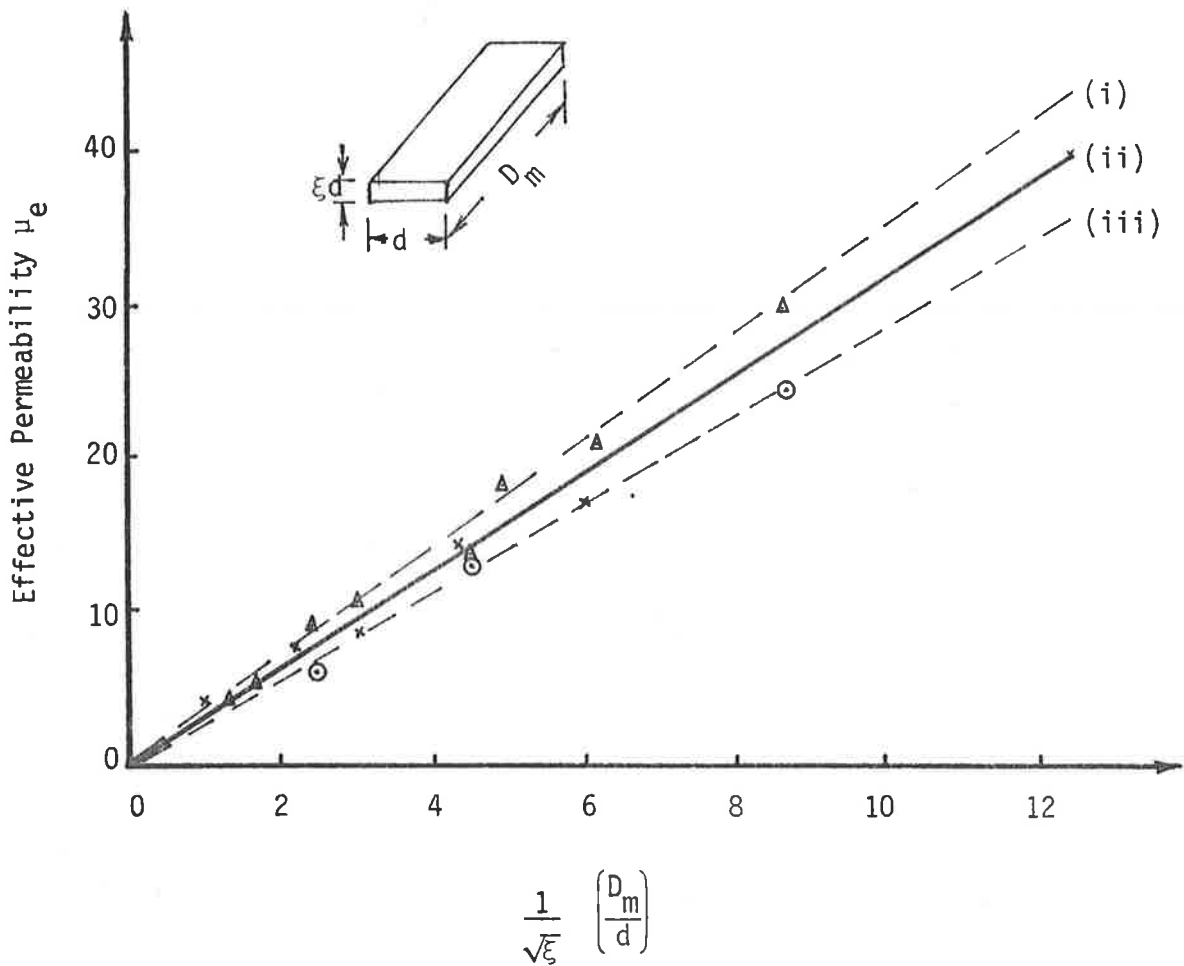
FIGURE 5.6.   EFFECTIVE PERMEABILITY μ_e OF FERRITE SLABS AS

A FUNCTION OF $\dfrac{1}{\sqrt{\xi}}\left[\dfrac{D_m}{d}\right]$.

(i)   *Slope (upper)* = *3.4.*

(ii)   *Slope (mean)*   = *3.2*

(iii) *Slope (lower)* $=$ *2.8.*

volume of ferrite slab antennas from purely the knowledge of dimensions.

5.6.3 Comparison of antenna structures

Given the multiplicity of geometrics it is of interest to compare the coupling and dispersal volumes of ferrite cored solenoid with flat coils.

The significance of the models which have been developed so far are that for flat coils no benefit is obtained when ferrite is introduced into the coil, while the introduction of high permeability ferrites into the slab coils or solenoids, improves the coupling volumes by the effective permeability μ_e. Similarly the dispersal volume for flat coils remain unaltered with the introduction of ferrite whereas dispersal volume for ferrite cored solenoids and slab coils is reduced by the value of the effective permeability.

Therefore for practical systems depending on the constraint imposed on the geometry an appropriate choice of antenna structure can be made based on the results of the tables and where necessary the asymptotic relations for demagnetising factors. In order to draw comparisons between the performance of different structures it is necessary to consider first any constraints placed upon the dimensions on orientations of the antennas by operational considerations. Taking   the coupling volume, the basic questions to consider are firstly whether the antenna can be made large in either one, two or three dimensions, and secondly whether the

230.

antenna must be oriented with its larger dimensions either
perpendicular to or parallel with the direction of the
exciting magnetic field. An example of the latter con-
straint is provided by the case when a flat plate or slab
antenna is required to be placed close to and parallel with,
rather than protruding from a flat conducting surface as for
example a body panel of a motor vehicle.

5.7 Transponder Operating Voltage

From the preceding theory developed it is evident that the
transfer of power to the transponder circuit is dependent upon the
physical volume assigned to the receptor antenna and the quality
factor which may be achieved when it is resonated but it is not
effected, except for second order effects, by the number of turns
associated with the coil. The number of turns serves merely to
establish the impedance level at which the power is obtained.

A further factor of importance in the design of the receptor
antenna is the fact that practical transponder circuits do not
operate as linear power converters, particularly at low power
levels, but rather show a threshold voltage, below which operation

of the circuit fails. Therefore the problem of deriving sufficient
voltage from the receptor coil for satisfactory operation of the
circuit must also be considered.

In order to maximise the available voltage the receptor coil
is always parallel tuned and the induced voltage available to the
transponder circuit is therefore greater than the induced voltage
by the quality factor of tuned circuit. The problem in practice
is therefore that of employing sufficient turns in the receptor
coil to obtain the necessary voltage at the transmitter power level
used.

The receptor coil induced voltage E_i from Equation (A.11),
Appendix A can be expressed in terms of the numbers of turns N_2,
the quality factor Q_2, flux collecting area A_r and the magnetic
field H created by the transmitter at the transponder position.
The expression is

$$E_i = \omega_t \, \mu_0 \, A_r \, N_2 \, Q_2 \, H \quad \text{(volts)} \tag{5.54}$$

The stored magnetic energy in the transmitter coil from
Equation (5.4) is given by

$$W_1 = \frac{Q_1 \, P_1}{\omega_t} \tag{5.55}$$

Therefore the dispersal volume from definition is

232.

$$V_d = \frac{Q_1 \, P_1}{\omega_t \, \mu_o \, H^2} \quad (\text{metre}^3) \qquad (5.56)$$

from which the magnetic field can be written as

$$H = \sqrt{\frac{Q_1 \, P_1}{V_d \, \omega_t \, \mu_o}} \qquad (5.57)$$

Substitution of Equation (5.57) in Equation (5.54) and subsequent re-arrangement results in the number of turns per volt to be

$$N_2 = \frac{1}{Q_2} \sqrt{\frac{V_d}{\mu_o \, \omega_t \, P_1 \, Q_1 \, A_r^2}} \quad (\text{turns volt}^{-1}) \qquad (5.58)$$

For ferrite cored coils Equation (5.58) is modified by the effective permeability factor μ_e. In this case the number of turns per volt is given by

$$N_{2f} = \frac{\mu_e}{Q_2} \sqrt{\frac{V_d}{\mu_o \, \omega_t \, P_1 \, Q_1 \, A_r^2}} \qquad (5.59)$$

In practice the necessary voltage levels can be obtained without recourse to the number of turns which lead to the coils becoming self resonant or unduly difficult to manufacture. A possible theoretical limit to the number of antenna turns could be reached if the strong capacitance of a high impedance winding became ex-

cessive but it is not common to encounter this limit in practical structures. Therefore using the above equation it is a simple matter to calculate the desired number of turns in order to achieve the necessary voltage.

5.8 Conclusions

The development of coupling volume and dispersal volume concepts in this chapter has provided the necessary means for separating the influence of different antenna parameters on the coupling. The physical significance of coupling and dispersal volumes are that for strong coupling a large coupling volume in the transponder and a small dispersal volume in the transmitter are desired. The transmitter antenna behaves in so far as the transponder is concerned, as if the transmitter antenna stored energy were uniformly distributed over a volume equal to the transmitter dispersal volume.

The contrast between the coupling volume and the dispersal volume is that while the former depends only upon the characteristics of the receptor antenna, the dispersal volume depends not only upon the antenna dimensions but also on the sensing position of the transponder within the transmitter antenna's field. The dispersal volume increases substantially with increase of separation of the two antennas, in fact at large separations the field approximates to that of a dipole and the dispersal volume increases as the sixth power of the distance.

The modelling principle has established the framework on which appropriate local omptimizations based on geometrics of individual antennas can be performed. The analysis provided an understanding of the effect of antenna parameters on system performance and has enabled conclusions on the general shapes that can be utilized for practical systems, to be drawn.

Analytical and empirical formulae for the performance of a range of antennas for use in practical PST system have also been derived. An interesting result for the flat ferrite cored slab solenoid is that, within the range of dimensions shown the effective permeability is determined principally by the shape rather than the intrinsic core material permeability.

The results of calculations of dispersal volumes for several geometrics of practical interest demonstrate the general similarity of the position dependence of all antennas of a given maximum dimension, and the superiority of the planar coil over the air cored solenoid and slab coils. Analysis, based on the assumption of uniform magnetisation of the effect of including high permeability ferrite cores again show that for the planar coils no benefit is obtained while the dispersal volume for the ferrite cored solenoids and slab coils is reduced by the effective permeability μ_e.

The fact that in practice it is frequently necessary to make the transmitter antenna dimensions comparable with the sensing distance and the cost of ferrite materials combine to make the air cored planar coil the only practicable design option.

The mathematical model developed for the coupling volume indicate the superiority of large area plannar coils as near field magnetic antennas. When dimensional constraints are relaxed on the physical area of the coils, the altnernative slab coils, or solenoids may be used. General conclusions which can be derived from the analysis are:*

(i)   When the antenna is required to be narrow in one dimension, flat coil or ferrite slab are better than ferrite rod.

(ii)   When the antenna requirements are that they should be narrow in two-dimension, ferrite rod has definite advantage.

(iii)   Antennas which are large in three dimension provide only slight gain at the expense of a massive amount of ferrite.

The significance of the above analysis in describing the power transfer are that the coupling and dispersal volumes are dependant on the geometrics of the antennas which are individually subject to optimization while the quality factors indicate how efficient the transfer of power can be made.

---

*   *The direction of magnetic field is in accordance with the direction of the arrow shown in Table 5.4.*

CHAPTER 6

POWER TRANSFER IN PROXIMITY OF CONDUCTING BODIES

6.1 Introduction

In vehicle identification and location systems the transponder
or alternatively the interrogation antenna are generally required
to be mounted in the vicinity of a mass of metal. Therefore it is
necessary to investigate the power transfer characteristics under
such conditions.

When a coil carrying a time-varying current is placed in the
proximity of a conducting surface, depending on the orientation of
the coil, eddy currents are induced in that surface. As a conse-
quence the impedance of the coil is modified. When conducting
boundaries are imperfect an exact solution for the impedance change,
would require solution of Maxwell's equation[107] in both the con-
ducting region as well as the region surrounding the material.

However the complexity of the analysis can be avoided if ad-
vantage is taken of the fact that most practical conductors are
good enough to cause only a slight modification of the ideal solution.
Therefore the method of images appear as a suitable approximation

for such investigations.

6.2 Analytical Modelling

If the interface is a perfect electrical conductor, the change in the impedance of the coil with its axis normal to the plane of the conducting surface, can be thought to be caused by the presence of an image coil as shown in Figure 6.1.

This approach can be analysed in terms of inductively coupled circuit, where the secondary, i.e. the image coil, couples into the primary a resistive component to account for the finite conductivity of the interface, and a reactive term. The input impedance as seen at the terminal of the transponder coil is[112]

$$Z_{in} = R_2 + j\omega L_2 + \frac{\omega^2 M^2}{R_i + j\omega L_i} \qquad (6.1)$$

where R_i and L_i are resistive and reactive components associated with the image coil.

For materials having large conductivities the resistive component of coupled impedance is small and therefore can be neglected. Thus, Equation (6.1) reduces to
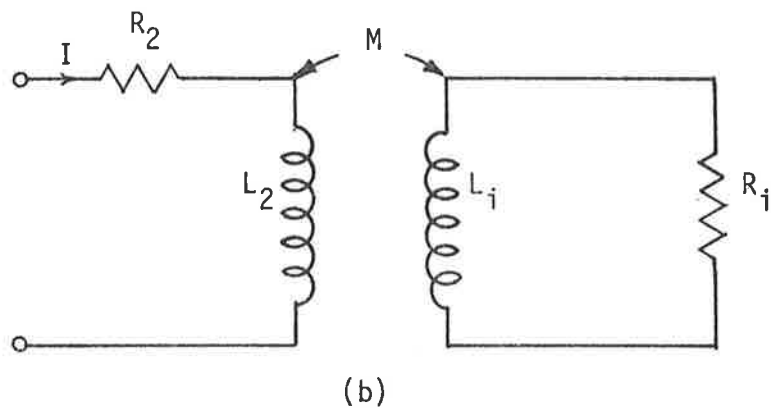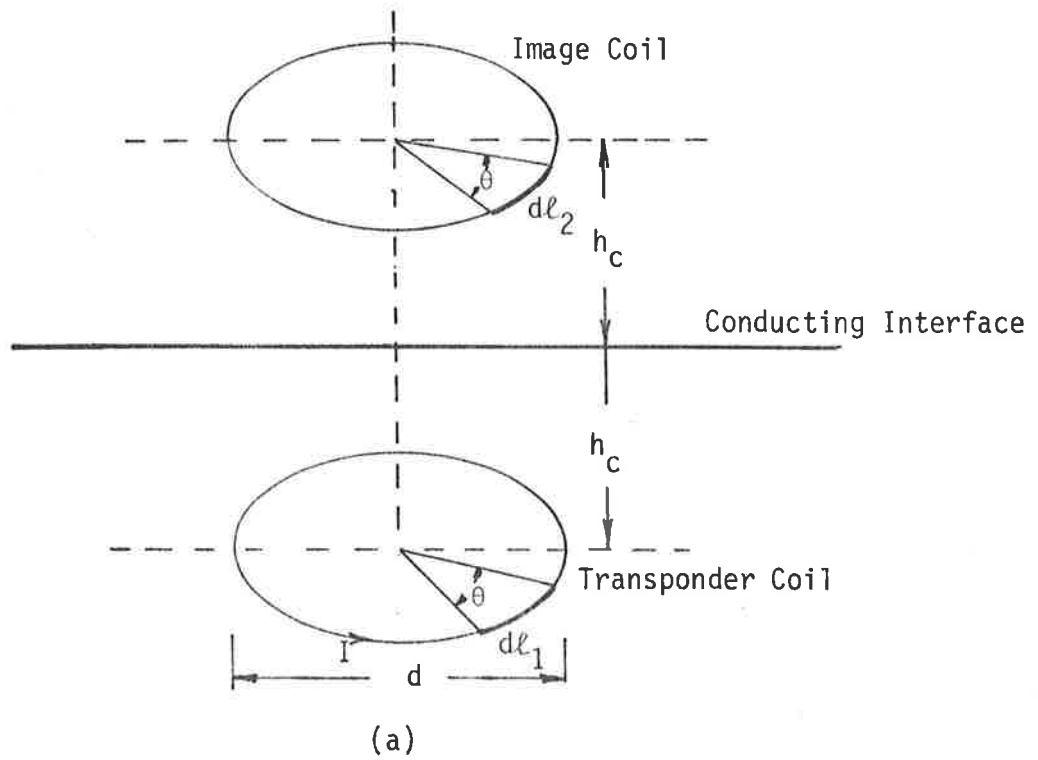
FIGURE 6.1. CURRENT CARRYING COIL IN PROXIMITY OF A CONDUCTING SURFACE.

(a) Structure.

(b) Equivalent Circuit Representation.

239.

$$Z_{in} = R_2 + j\omega \left[L_2 - \frac{M^2}{L_i} \right] \qquad (6.2)$$

The principal effect upon the transponder coil is the reduction in effective inductance L_e produced by the coupled reactance.

The change in inductance can be obtained using Newman's equation for mutual inductance of filamentary circuit given by[113]

$$M = \frac{\mu_0}{4\pi} \oint \oint \frac{d\vec{\ell}_1 \cdot d\vec{\ell}_2}{R} \qquad (6.3)$$

where $d\vec{\ell}_1$ and $d\vec{\ell}_2$ are differential elements of length about the actual and the image coils respectively. Thus after some manipulation and assuming that the radius of the wire $r << d$, the expression for the effective inductance L_e can be described by [113]

$$L_e = L_2 - \frac{\mu_0 d}{2} \left[\left(\frac{2}{\alpha} - \alpha \right) K(\alpha) - \frac{2}{\alpha} E(\alpha) \right] \qquad (6.4)$$

where

$$\alpha = \sqrt{\frac{1}{1 + \phi_c^2}}$$

$$\qquad (6.5)$$

$$\phi_c = \frac{2h_c}{d}$$

240.

and h_c is the spacing between the coil and the conducting surface.

The influence of the coupled negative reactance is to neutralize a portion of the receptor coil inductance. The reflected reactance becomes more significant as the spacing between the transponder and the interface is reduced.

The quality factor of the transponder coil is now modified to

$$Q_2 = \frac{\omega_t \, L_e}{R_2} \tag{6.6}$$

Equation (6.6) is sufficiently accurate for situations in which the interface has a high conductivity. However, when the interface consists of materials having relatively low conductivities such as steel substantial error in the value of Q_e can be expected. Therefore it is necessary to modify the model in order to take into consideration the effect of reflected resistance.

6.3 Reflected Resistance Calculations

At the boundary between a medium of high conductivity and free space, the electromagnetic field equation can be reduced to a simple form in which the surface current density $\tilde{J}$ is related to the magnetic field $\tilde{H}$ by the boundary condition[114]

$$\tilde{n} \times \ddot{H} = \tilde{J} \qquad (6.7)$$

where $\tilde{n}$ is a unit vector directed outward from the surface.

When the transponder coil is brought in the proximity of a semi-infinite conducting surface, at frequencies of interest, the average power loss per unit area can be shown to be[114]

$$W_L = \frac{1}{2} \text{ Real } |Z_S \; \tilde{J}.\tilde{J}*| \quad (\text{watt/m}^2) \qquad (6.8)$$

where Z_S is the surface impedance given in terms of surface resistivity R_S and inductance L_S and $\tilde{J}*$ is complex conjugate of current density $\tilde{J}$. The surface impedance is given by

$$Z_S = R_S + j\omega L_S \qquad (6.9)$$

where $R_S = \sqrt{\dfrac{\mu\omega}{2\sigma}}$ $\qquad (6.10)$

and ω is the frequency, μ is the permeability of the material and σ is the conductivity (mhos/meter). Equation (6.8) can now be written in a more convenient form:

$$W_L = \frac{1}{2} R_S |J_\phi|^2 \quad (\text{watt/m}^2) \qquad (6.11)$$

where J_ϕ is the ϕ component of the current density.

The magnetic field $\tilde{H}$ is further related to the surface current $\tilde{J}$ and in particular the ρ component of magnetic field H_ρ is numerically equal to the ϕ component of the current density J_ϕ. The dissipated power in the plane conductor can now be written in terms of the ρ component of the magnetic field H_ρ. Thus for any circle of constant radius ρ, the expression becomes

$$W_L = \frac{1}{2} \oint_0^\infty R_s \, 2\pi\rho |H_\rho|^2 d\rho \quad (\text{watt/m}^2) \tag{6.12}$$

From Appendix D the ρ component of magnetic field is

$$H_\rho = \frac{ih_c}{2\pi\rho \left[(d/2 + \rho)^2 + h_c^2\right]^{\frac{1}{2}}} \left[\frac{(d/2)^2 + \rho^2 + h_c^2}{(d/2 - \rho)^2 + h_c^2} E(\alpha) - K(\alpha)\right] \tag{6.13}$$

where

$$\alpha = \sqrt{\frac{4}{(d/2 + \rho)^2 + h_c^2}} \tag{6.14}$$

Substitution of Equation (6.14) in Equation (6.12) results in

$$W_L = \frac{R_s \, i^2 \, h_c^2}{\pi} \int_0^\infty \frac{1}{\rho \left[(d/2 + \rho)^2 + h_c^2\right]} \left[\frac{(d/2)^2 + \rho^2 + h_c^2}{(d/2 - \rho)^2 + h_c^2} E(\alpha) - K(\alpha)\right]^2 d\rho \tag{6.15}$$

243.

The reflected resistance R_r can now be estimated by noting that

$$W_L = I^2 R_r \qquad (6.16)$$

in which the values of current I is taken as $I = i/\sqrt{2}$. Therefore R_r may be obtained from the relation

$$R_r = \Gamma R_s \qquad (6.17)$$

where Γ is a geometric factor given by

$$\Gamma = \frac{2h_c^2}{\pi} \int_0^\infty \frac{1}{\rho\left[(d/2 + \rho)^2 + h_c^2\right]} \left[\frac{(d/2)^2 + \rho^2 + h_c^2}{(d/2 - \rho)^2 + h_c^2} E(\alpha) - K(\alpha)\right]^2 d\rho \qquad (6.18)$$

R_s in Equation (6.17) can be looked upon as a surface factor since the value of the reflected resistance is modified by the characteristics of the interface.

After appropriate transformation to change the limits of integration and by power series expansion of the elliptic integrals, the value of Γ was solved numerically. Plots of Γ as a function of the separation h_c for several values of coil diameter are shown in Figure 6.2.

244.

245.

Separation h_C (cm)
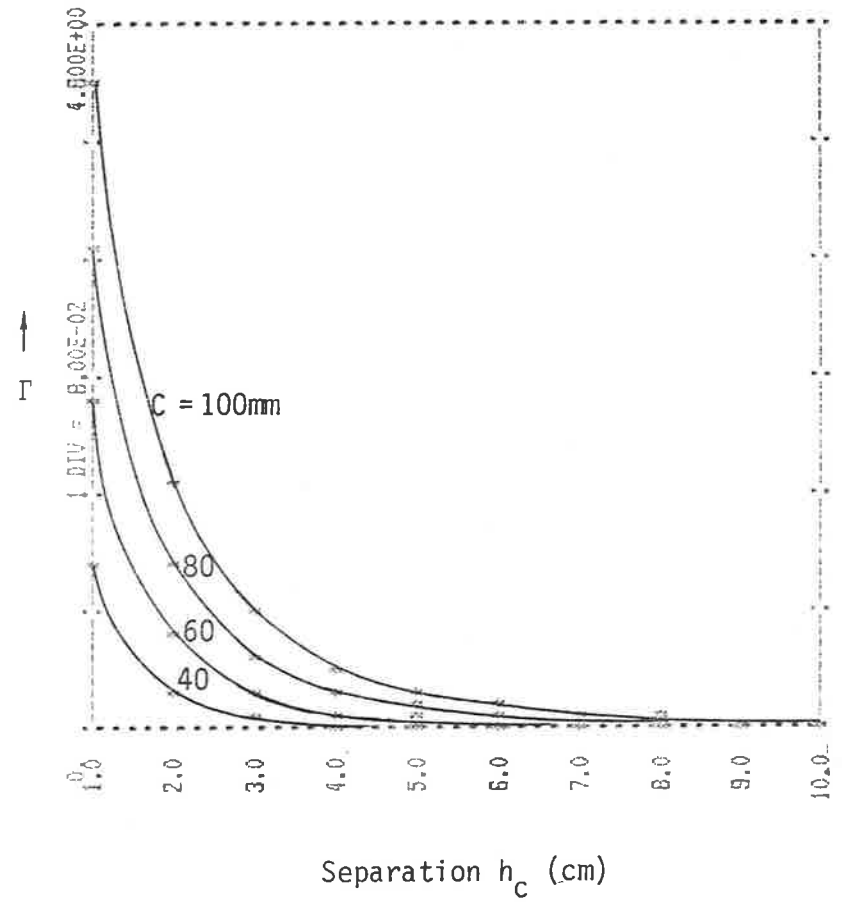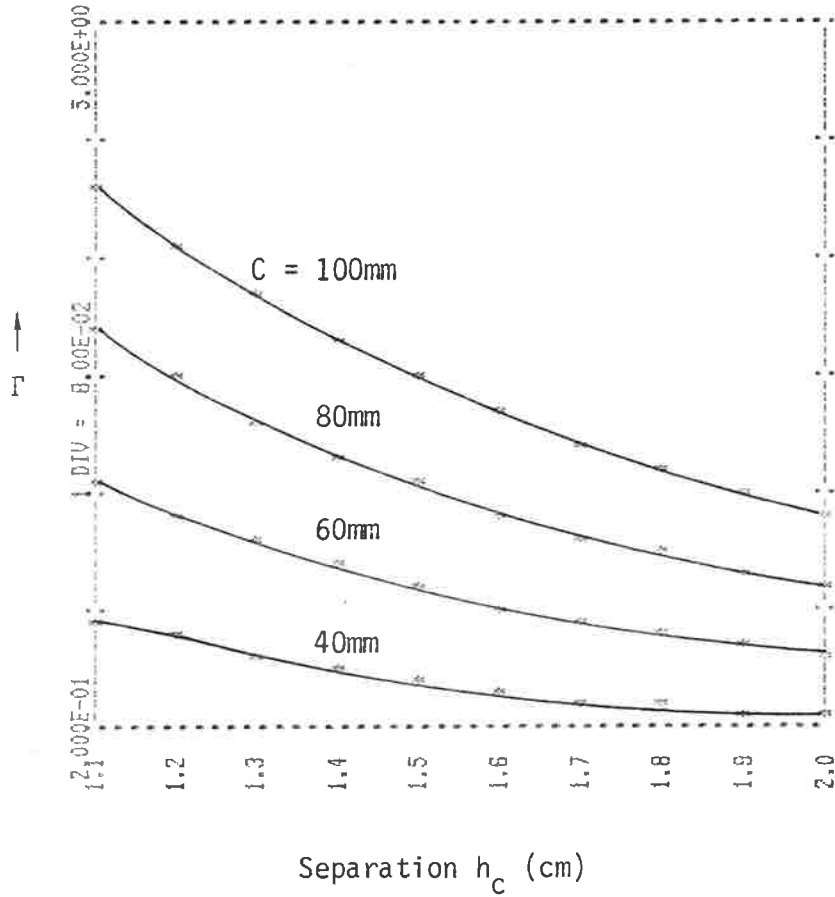
Separation h_C (cm)

FIGURE 6.2 (a).   PLOT OF GEOMETRIC FACTOR Γ AS A FUNCTION OF SEPARATION h_C (cm) FOR SEVERAL VALUES OF TRANSPONDER

COIL DIAMETER C (mm).

246.
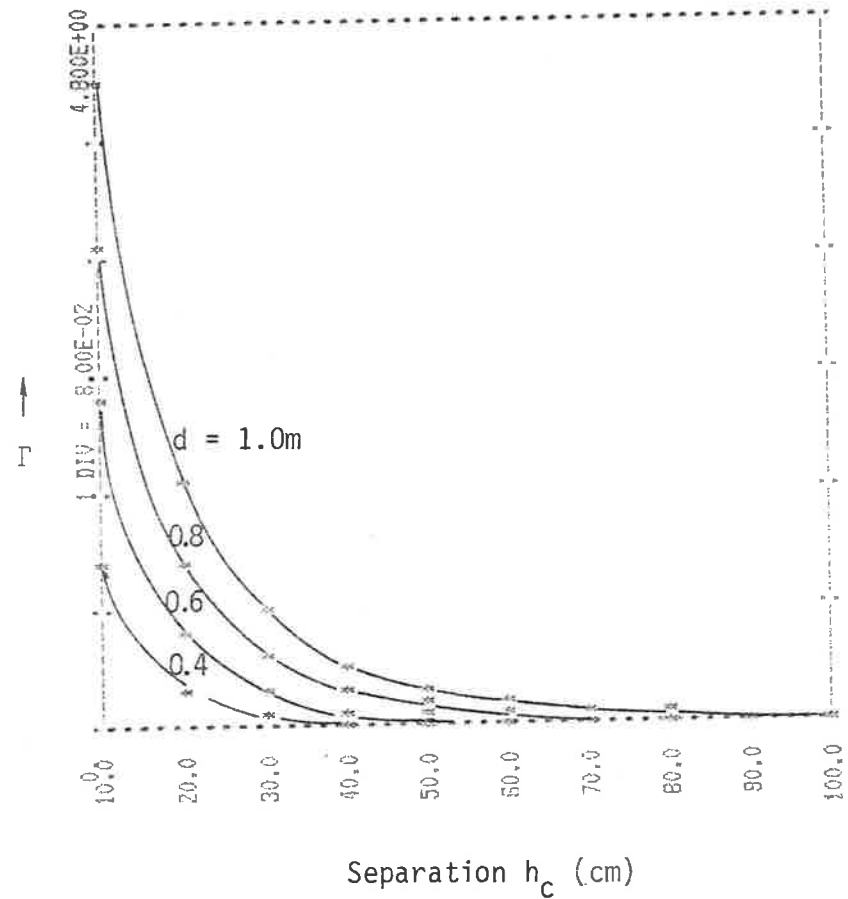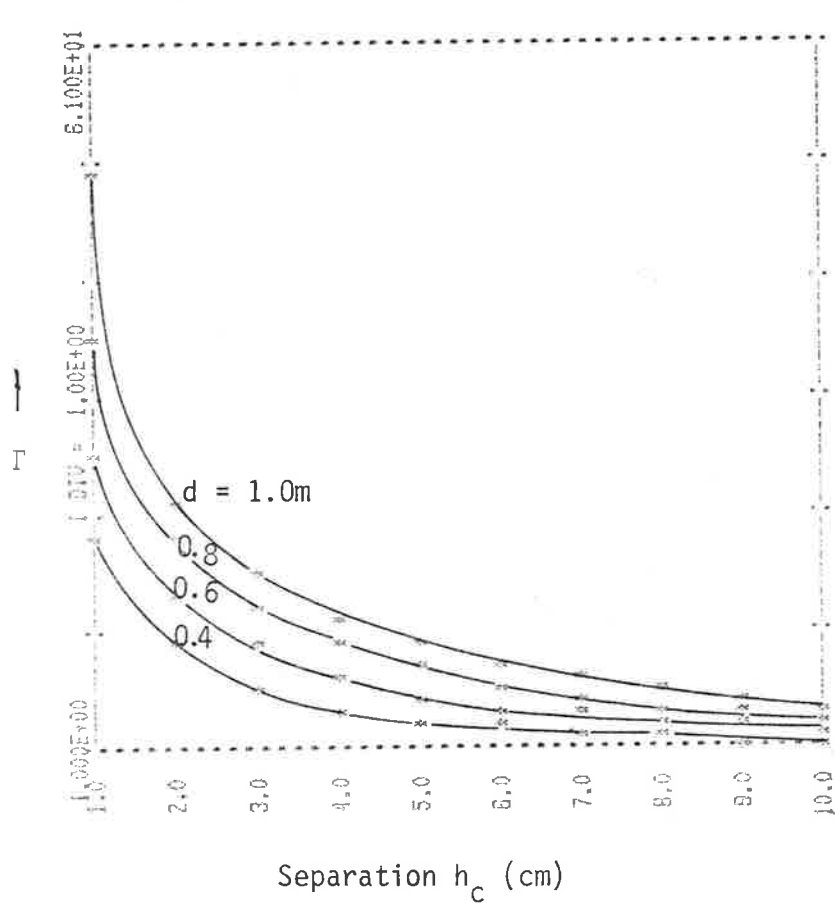
FIGURE 6.2 (b).   PLOT OF GEOMETRIC FACTOR Γ AS A FUNCTION OF SEPARATION h_c (cm) FOR SEVERAL VALUES OF TRANSMITTER

COIL DIAMETER d (CM).

The quality factor Q_{2c} for the transponder in the proximity of conducting body can now be obtained using Equation (6.4) and Equation (6.18). Thus

$$Q_{2c} = \frac{\omega L_e}{R_2 + \Gamma_2 R_s} \qquad (6.19)$$

Plots of this relation as a function of separation for several coil diameters and two different conductivities are shown in Figure 6.3. In these plots the ac resistance of a coil is used for analysis[113]. Experimental results for a coil having diameter d = 80mm is also shown on the same plots. For the range in which the separation $h_c \geqslant$ 5mm there is a close agreement between the theoretical prediction and the experimental values. As the separation h_c is made smaller the discrepancy between the experimental values and theoretical results increase. This variation is the result of using a perfect conductor in the calculation of the reflected inductance. However for the kind of transponder mountings that can be expected in practice for vehicle identification the model defined by Equation (6.19) is adequate in assisting with the description of the power transfer.

The significance of the curves shown in Figure 6.3 are that they provide an insight into the factors which limit the maximum value of quality factor of a planar coil when it is brought in the proximity of a conducting body. In addition they illustrate to gain the full benefit that is available in having high quality factors the separation of a planar coil from the conducting body should be > 30mm.

247.
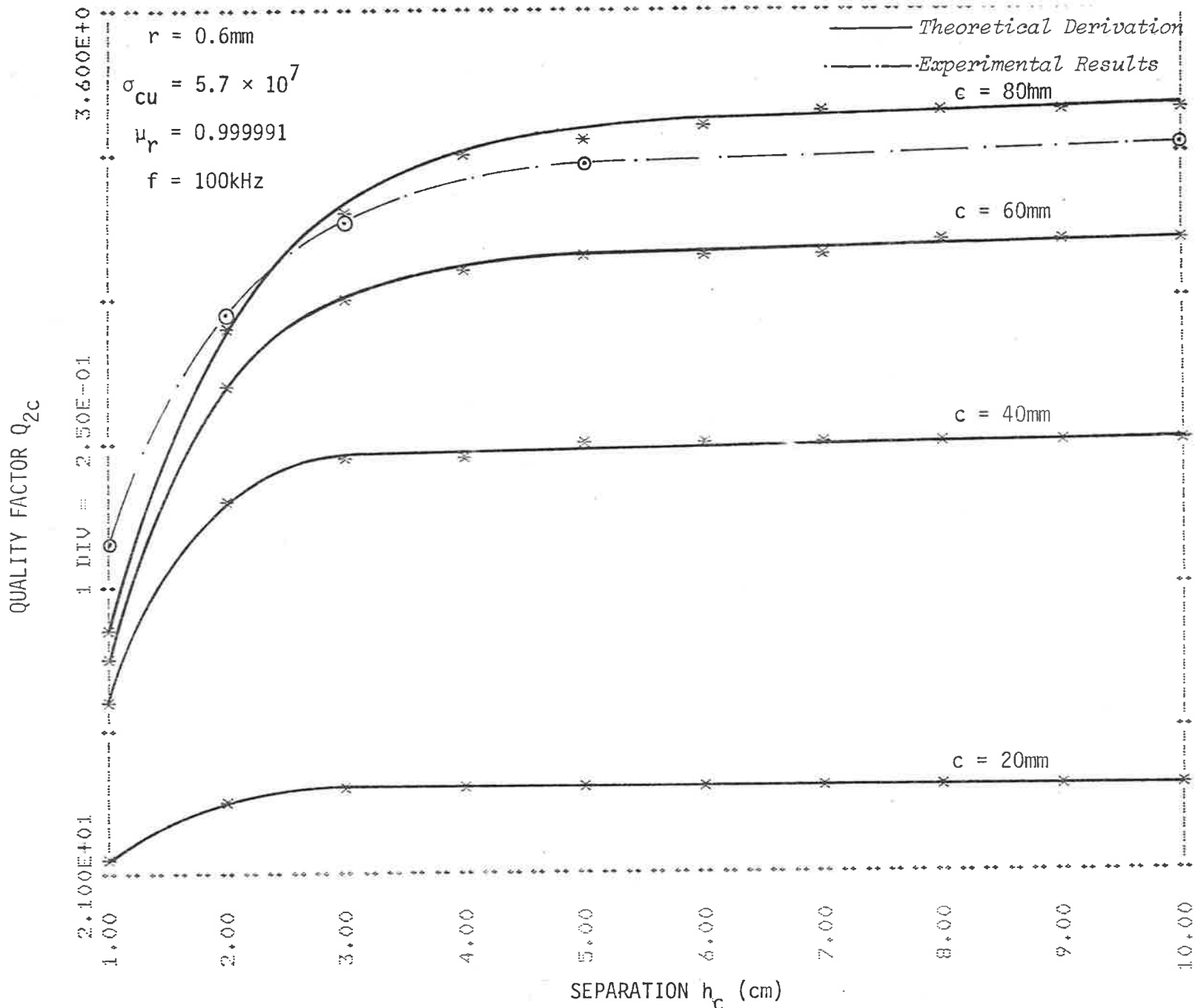
FIGURE 6.3 (a). PLOT OF QUALITY FACTOR Q_{2c} AS A FUNCTION OF SEPARATION FOR SEVERAL TRANSPONDER

COIL DIAMETERS USING COPPER AS INTERFACE.
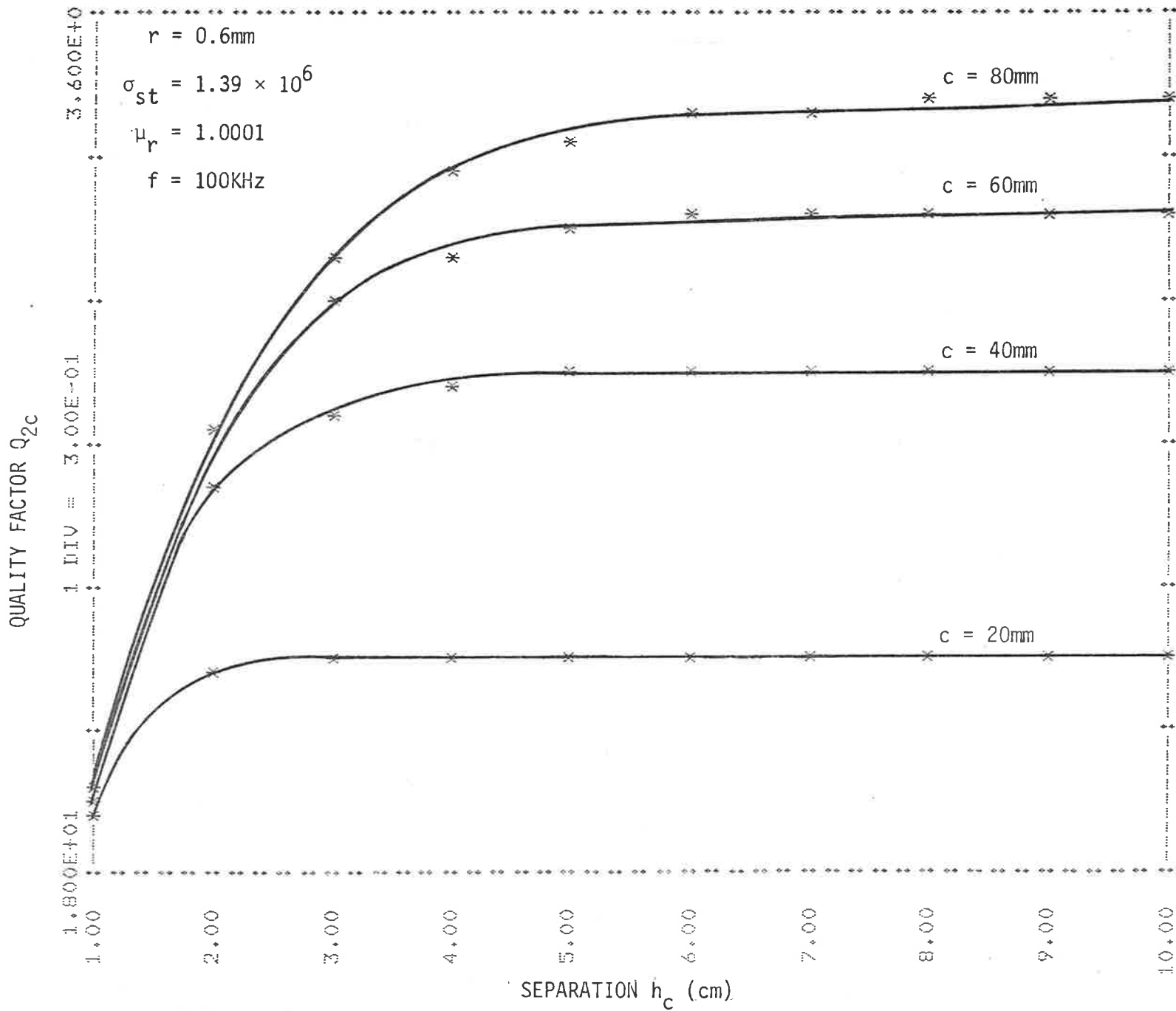
FIGURE 6.3 (b). PLOT OF QUALITY FACTOR Q_{2c} AS A FUNCTION OF SEPARATION FOR SEVERAL TRANSPONDER

COIL DIAMETERS USING 304 STEEL AS INTERFACE.

6.4 Power Transfer Considerations

In order to calculate the power transfer between the transmitter and transponder coils in the presence of a conducting body as shown in Figure 6.4, the following relations are defined.

The effective losses of the transmitter coil can be expressed by

$$R_{e1} = R_1 + \Gamma_1 (h_{c1}, d) R_s \qquad (6.20)$$

where $\Gamma_1(h_{c1}, d) R_s$ is the reflected losses associated with the transmitter coil as defined by Equation (6.18), h_{c1} is separation between the transmitter coil and the interface, and d is the diameter. Similarly the effective losses of transponder coil is given by

$$R_{e2} = R_2 + \Gamma_2 (h_{c2}, c) R_s \qquad (6.21)$$

where $\Gamma_2 (h_{c2}, c)$ is the reflected losses associated with the transponder coil, h_{c2} is separation between the transponder coil and the interface and c is the diameter.

From Equation (6.19), the quality factors of the transmitter and transponder coils in the presence of the conducting surface are further denoted by Q_{1c} and Q_{2c}.

Transmitter Image Coil

Transponder Image Coil

Conducting Plate

$h + 2h_{c2}$

Transponder Coil

h_{c2}

c

h

Transmitter Coil

d
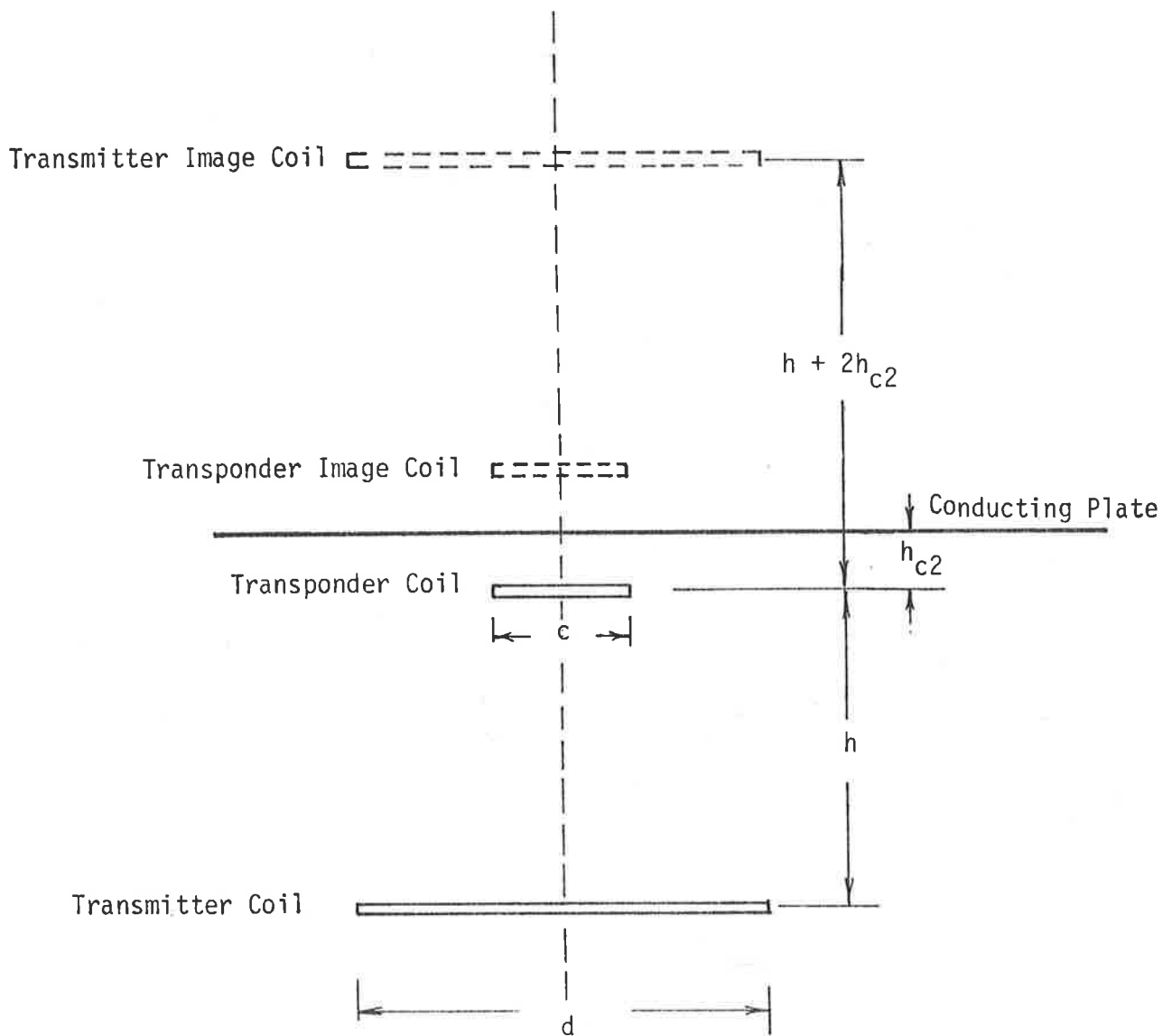
FIGURE 6.4.   RELATIONSHIP BETWEEN TRANSPONDER AND TRANSMITTER COILS

IN THE PRESENCE OF A CONDUCTING PLATE.

The power transfer in the proximity of the conducting body can be obtained by using the method of images once again. From Figure 6.4 and Appendix D, the resultant magnetic field H_r is

$$H_r = H - H_i \tag{6.22}$$

where H_i is the magnetic field due to the image coil and opposes the field H from the coil itself. The resultant magnetic field can be written as

$$H = \frac{I_t}{d} \left\{ \frac{1}{(1 + \phi_1^2)^{3/2}} - \frac{1}{(1 + \phi_2^2)^{3/2}} \right\} \tag{6.23}$$

where ϕ_1 is a parameter related to the separation between the transmitter and transponder coils and is given by

$$\phi_1 = \frac{2h}{d} \tag{6.24}$$

Similarly ϕ_2 is related to the separation between the transmitter and the transponder image coils and is written as

$$\phi_2 = \frac{2(h + 2h_{c2})}{d} \tag{6.25}$$

252.

The distances h and h_{c2} are further defined by

h = separation between the transmitter coil and the transponder

h_{c2} = separation between the transponder coil and the conducting
body.

The coupling volume of the transponder coil in the proximity
of the conducting body denoted by V_{cc} can now be described by the
expression

$$V_{cc} = \frac{\pi^2 c^3}{8\left[(\log_e \frac{4c}{r_2} - 2) - [(\frac{2}{\alpha_2} - \alpha_2) K(\alpha_2) - \frac{2}{\alpha_2} E(\alpha_2)]\right]} \quad (\text{metre}^3) \qquad (6.26)$$

where

$K(\alpha_2)$ = Elliptic integral of the first kind.

$E(\alpha_2)$ = Elliptic integral of the second kind.

and
$$\alpha_2 = \sqrt{\frac{2c \left(\frac{c}{2} - r_2\right)}{(c - r_2)^2 + (2h_{c2})^2}} \qquad (6.27)$$

Similarly the value of dispersal volume V_{dc} can be shown to be

$$V_{dc} = \frac{1}{2}\left\{(\log_e \frac{4d}{r_1} - 2) - \left[(\frac{2}{\alpha_1} - \alpha_1) K(\alpha_1) - \frac{2}{\alpha_1} E(\alpha_1)\right]\right\} P d^3 \quad (\text{metre}^3) \qquad (6.28)$$

where

$$P = \left[\frac{1}{(1 + \phi_1^2)^{3/2}} - \frac{1}{(1 + \phi_2^2)^{3/2}} \right]^{-2} \tag{6.29}$$

and

$$\alpha_1 = \sqrt{\frac{2d \, (d/2 - r_1)}{(d - r_1)^2 + (2[h + h_{c2}])^2}} \tag{6.30}$$

Plot of P as a function of separation h for several values of h_{c2} are shown in Figure 6.5.

For a sensing position at a fixed distance from a conducting plate the minimum value of P occurs when

$$h = \frac{d}{4} \tag{6.31}$$

For completeness, Figure 6.6 is also included to illustrate the variation of P as a function of diameter d for several values of h_{c2} when the separation h is held constant.
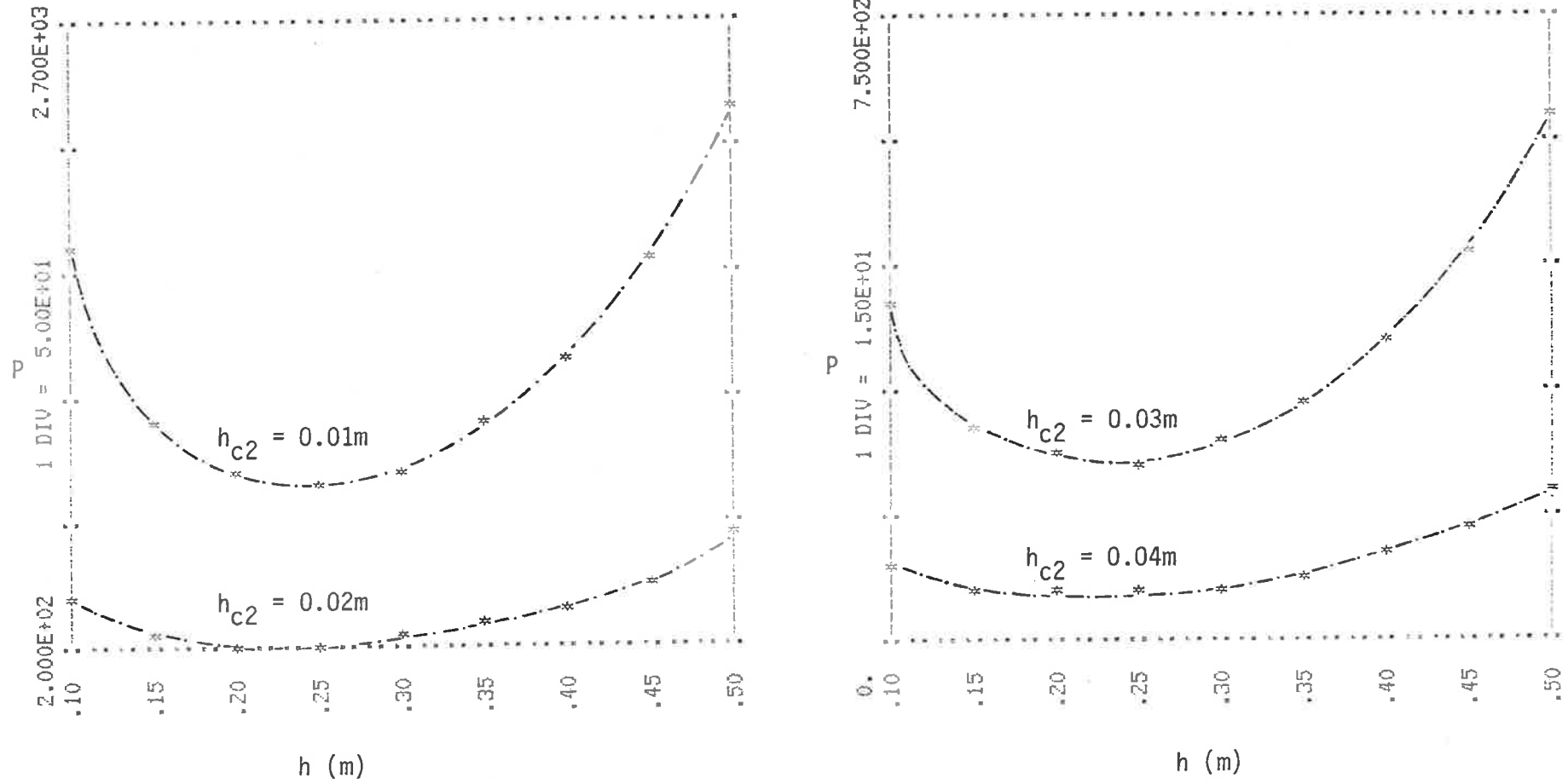
FIGURE 6.5.   VARIATION OF P AS A FUNCTION OF SEPARATION h FOR SEVERAL VALUES OF h_{c2} WITH TRANSMITTER COIL

DIAMETER d = 1.0m.
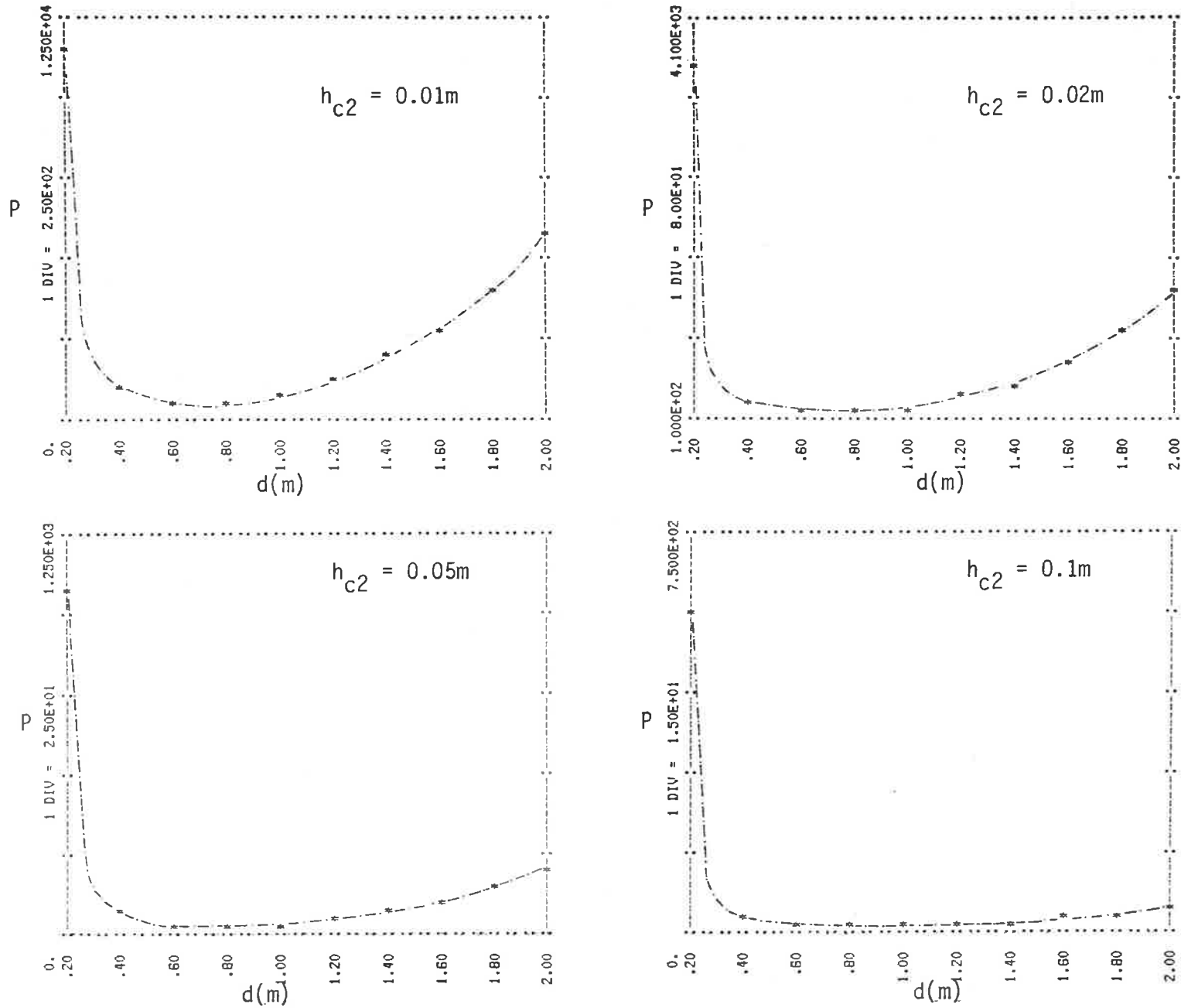
FIGURE 6.6.   VARIATION OF P AS A FUNCTION OF TRANSMITTER DIAMETER d FOR SEVERAL VALUES OF h_{c2} WITH SEPARATION h = 0.25m.

The complete power transfer relation in the proximity of a conducting body is now modelled by

$$\frac{P_4}{P_1} = \eta' \, X_p \left[\frac{1}{1 + R_f/R_t}\right] \, Q_{1c} \, Q_{2c}^2 \, Q_{4c} \left(\frac{V_{cc}}{V_{dc}}\right)^2 \qquad (6.32)$$

where Q_{4c} is the quality factor of the receiver coil in the proximity of the conducting body. Using the same planar coils as described in Chapter 4 the ratio (V_{cc}/V_{dc}) as a function of the separation h for several values of h_{c2} is illustrated in Figure 6.7.

The above analysis shows that the presence of a conducting interface marginally improves the coupling volume due to reduction in the self inductance of the coil, whereas for fixed values of coil dimension and separation h_{c2}, the dispersal volume has now a minimum value as the separation h between the transmitter and transponder is varied. For large values of h_{c2}, the results are similar to those obtained in Figure 3.16 in Chapter 3. However as the distance is reduced there is a significant degradation of the power transfer.

6.4.1 Performance evaluation

Although the inferior performance of planar coils in the proximity of a conducting body is recognised, the geometry is of sufficient practical interest due to low manufacturing cost which warrants further evaluation to establish the conditions under which satisfactory operation can be achieved.

257.
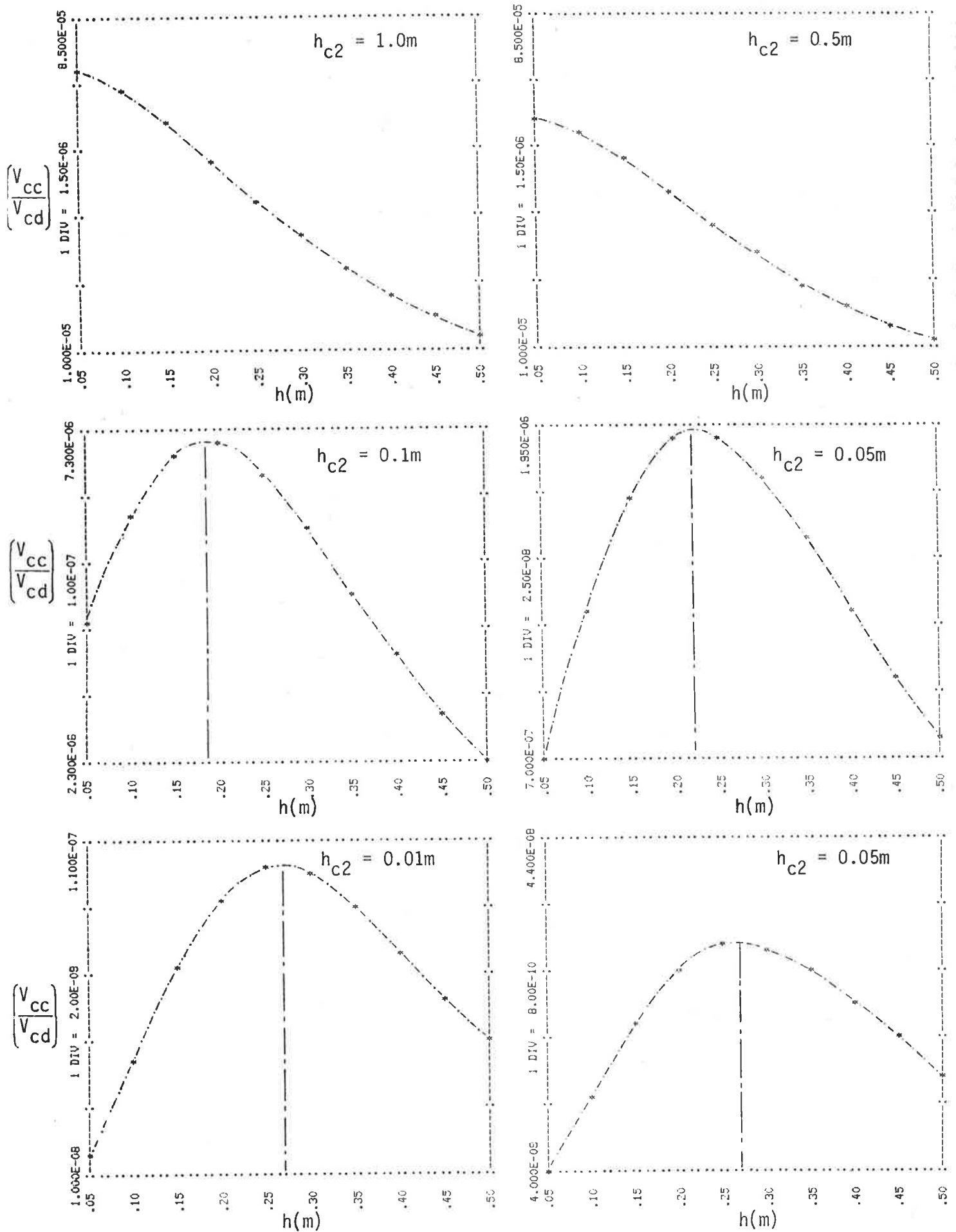
FIGURE 6.7.   PLOT OF (V_{cc}/V_{dc}) AS A FUNCTION OF SEPARATION h(m) FOR SEVERAL

VALUES OF h_{c2} WITH d = 1.129m, c = 0.113m, r_1 = r_2 = 0.6mm.

In a typical application such as that associated with identification of a motor vehicle it is desirable for the transponder to be located as close to the body of the vehicle as practicable. To estimate the operating range, the same antenna structures and parameters as specified in Table 3.3 (Chapter 3) are used. Using the above antennas and a fixed sensing distance h, the ratio (V_{cc}/V_{dc}) as a function of h_{c2} is shown in Figure 6.8. Similarly theoretical and experimental values for the transponder quality factors is also illustrated in Figure 6.9 when two different materials are used as interfaces. From these curves the power P_4 received by the receiver antenna as a function of separation h_{c2} at a sensing distance h = 0.5m and with the input power P_1 = 10 watts, is plotted in Figure 6.10 for both the two-port and the one-port transponders.

In order to obtain a virtually error free reception using PSK modulation a signal-to-noise ratio of 11dB is required. For this signal-to-noise ratio the probability of an error on any particular bit is less than 10^{-7}. From the curves shown in Figure 6.10, it can be observed that to achieve the above error rate at a sensing distance of 0.5m and for the given coil dimensions and peak noise power level of -88.6dBW, the separation h_{c2} between the transponder coil and the interface must be greater than 26mm for the one-port PST and greater than 39mm for the two-port PST. If the separation between the transponder and the interface is increased to 50mm an additional 12dB of noise margin becomes available.
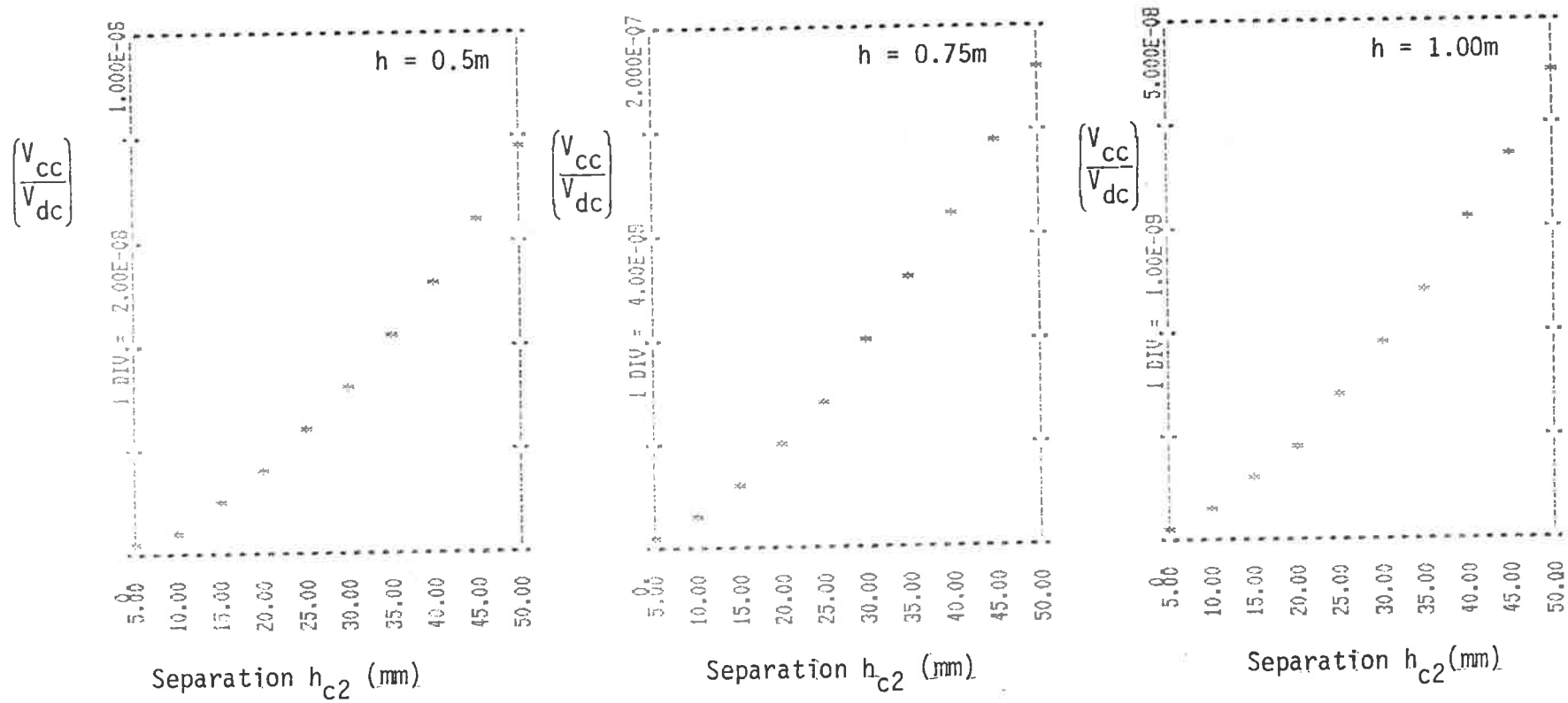
FIGURE 6.8. PLOT OF (V_{cc}/V_{dc}) AS A FUNCTION OF DISTANCE h_{c2} (mm) BETWEEN THE TRANSPONDER AND THE INTERFACE FOR SEVERAL VALUES OF SEPARATION h(m) WITH d = 1.129m AND c = 0.113m.

Figure content:

Q_{2c} (vertical axis) with values 0, 10, 20, 30, 40, 50

Separation h_{c2} (mm) (horizontal axis) with values 0, 10, 20, 30, 40

Al Plate
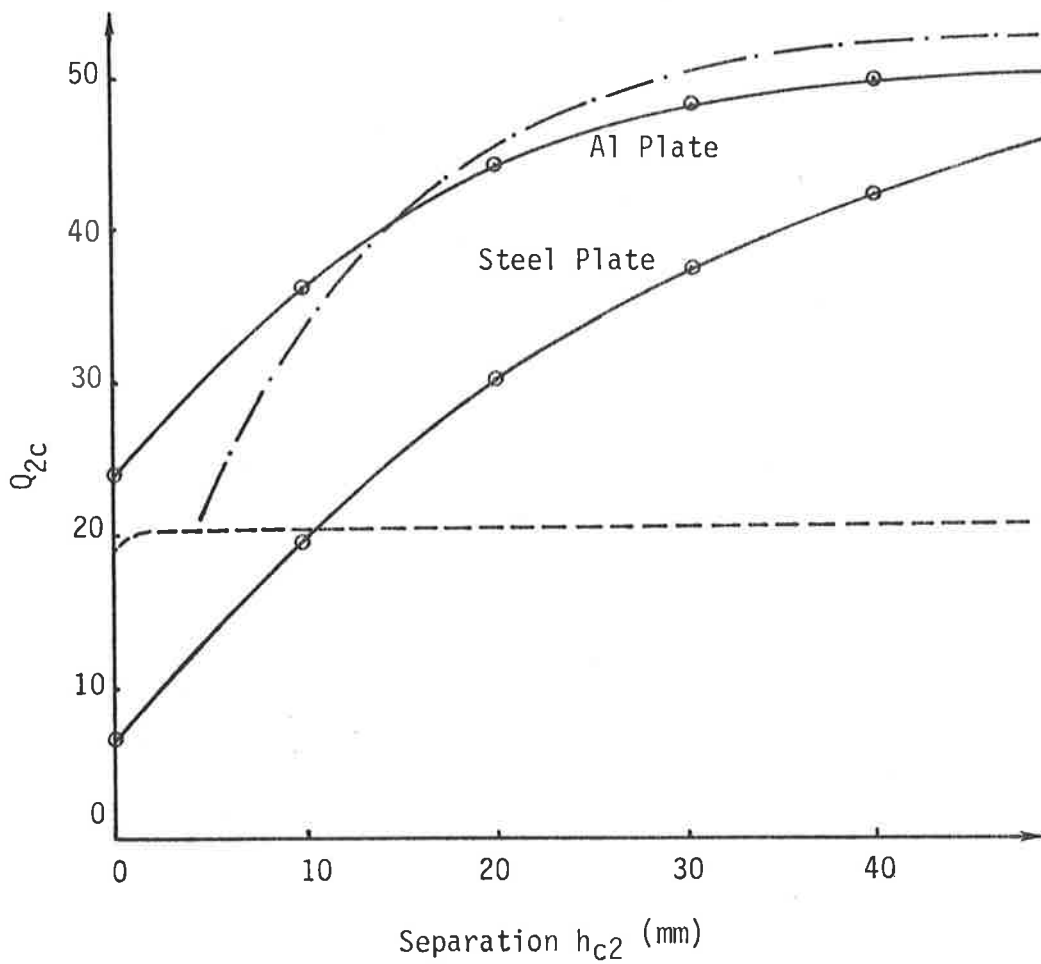
Steel Plate

―――――――― Experimental results.

―.――.―― Theoretical results when Al plate is used.

―――――― Transponder coil rested on a small Al plate (diam. = 0.12m) and brought in the proximity of steel interface.

Coil diameter = 0.113m

No. of turns = 30.

FIGURE 6.9.   PRACTICAL QUALITY FACTOR FOR TRANSPONDER COIL FOR CALCULATION

OF THE POWER TRANSFER.

261.
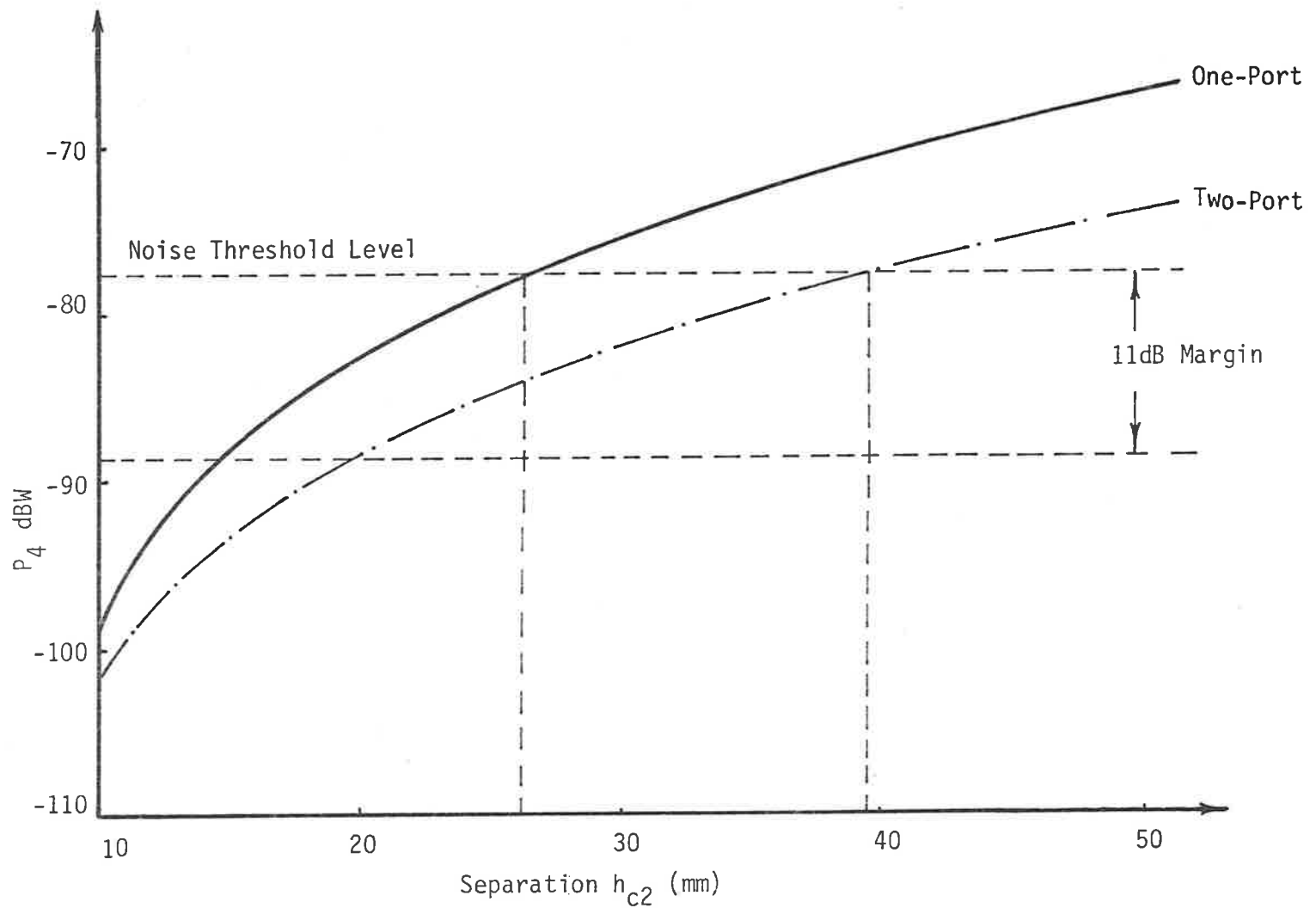
FIGURE 6.10.   COMPARISON BETWEEN THE POWER AVAILABLE AT THE RECEIVER AS A FUNCTION OF SEPARATION h_{c2}

BETWEEN TRANSPONDER AND A STEEL INTERFACE FOR ONE-PORT AND TWO-PORT TRANSPONDERS WITH h = 0.5m - NUMBER PLATE APPLICATION.

6.4.2 Virtual surface

The model defined by Equation (6.19) for the quality factor in the proximity of a conducting body indicated its dependence on the geometric factor Γ and the surface factor R_S. From Equation (6.18) it can be seen that for fixed dimensions, Γ cannot be changed. However it may be possible to reduce the surface factor R_S by using high conductivity material between the interface and the coil.

The resultant effect of this approach is included in Figure 6.9 in which an aluminium plate is placed between the steel surface and the transponder coil.

For this method to be effective the thickness t_S of the intervening material should be comparable with the skin depth δ_S. Results for various practical antenna dimensions using the above method will be presented in the next section.

6.4.3 Experimental results

The model defined by Equation 6.19 provided an insight into the kind of variation that one can expect when a current carrying coil is brought in the proximity of a con- ducting body. To provide a data base for the subsequent system evaluation the quality factors associated with several practical coils in proximity of both steel and aluminium plates were determined. The results for flat planar coils, air cored solenoids, ferrite slabs and rods having their major axes parallel to the conducting body are

263.

illustrated in Figures 6.11 - 6.13. These results enabled
for further exploratory analysis associated with practical
situations to be conducted. The significance of these
results is that for a given external magnetic field the
stored energy in a ferrite cored coil is less than in the
corresponding air cored coil. Therefore the ferrite cored
coil is more sensitive to external environment. Further,
the quality factors associated with ferrite cored coils are
generally higher than the corresponding air cored coils which
subsequently results in the external losses becoming more
noticeable.

From the results it can also be observed that for small
separations appreciable improvement can be obtained by intro-
ducing a high conductivity material such as aluminium between
the coil and the interface. In practice it is found that the
dimensions of the intervening material need only be marginally
larger than the dimensions of the transponder coil to achieve
the desired improvement in the quality factor.

6.5 Passive Sign-post Evaluation

The second case of interest is the situation where the PST
device is used as a sign post embedded under the road surface. The
transmitter and receiver antennas for this application are located
in the undercarriage of the vehicle. The geometry associated with

FIGURE 6.11. PLOT OF QUALITY FACTOR AND INDUCTANCE AS A FUNCTION OF

DISTANCE h_{c2} IN THE PROXIMITY OF AL AND STEEL CONDUCTING SURFACES.

(a)   Flat Rectangular Coil - 90mm × 60mm;   94 turns.

(b)   Flat Circular Coil - diam. = 100mm;   30 turns.

265.
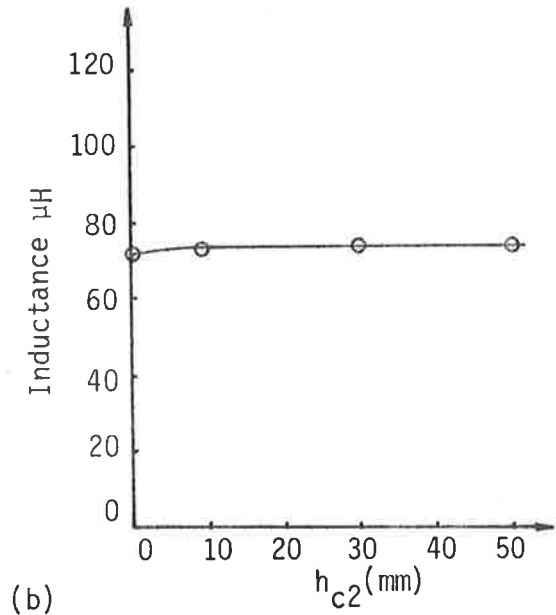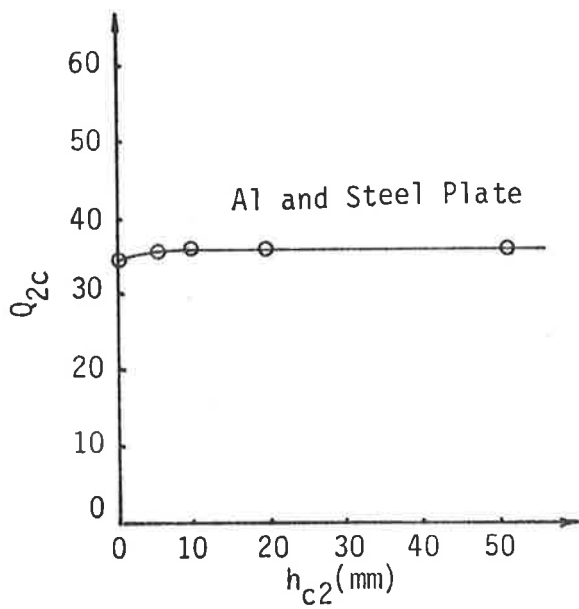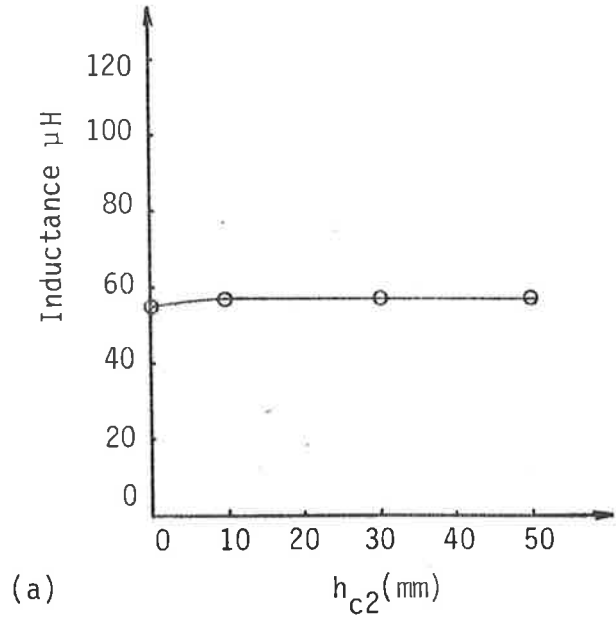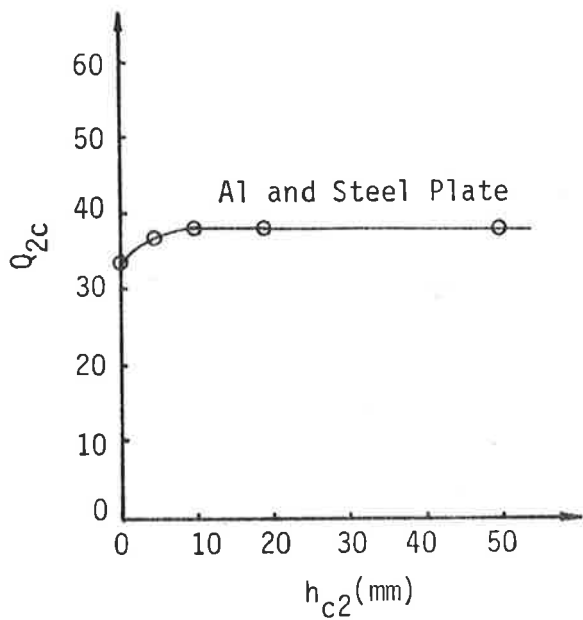
FIGURE 6.12.   PLOT OF QUALITY FACTOR AND INDUCTANCE AS A FUNCTION OF h_{c2}

IN THE PROXIMITY OF AL AND STEEL CONDUCTING SURFACES.

(a)   *Air Cored Slab 55 × 53 × 6.9mm;   80 turns.*

(b)   *Air Cored Solenoid 235 × 14 × 6.9mm;   233 turns.*
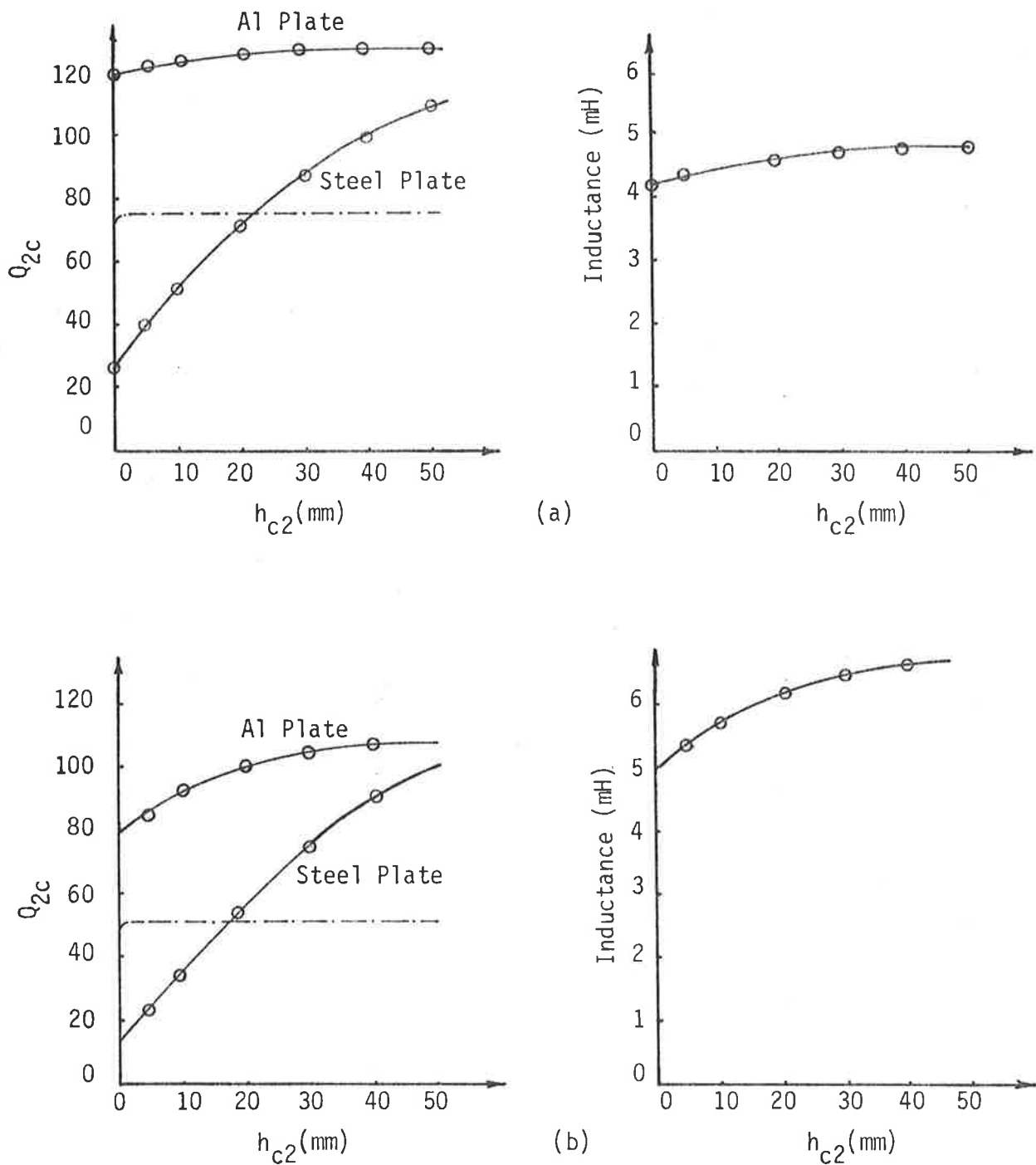
———·—·— *Coil rested on a small Al plate and brought in the proximity of steel interface.*

FIGURE 6.13.   PLOT OF QUALITY FACTOR AND INDUCTANCE AS A FUNCTION OF

OF DISTANCE FROM CONDUCTING PLATE.

(a)   *Ferrite Rod 233 × 14 × 6.9mm;   233 turns.*

(b)   *Ferrite Slab 53 × 55 × 6.9mm;   80 turns.*

267.

this configuration is shown in Figure 6.14.

The model describing the power transfer is similar to that obtained by Equation (6.32). However parameters α_1 and α_2 are now given by

$$\alpha_1 = \sqrt{\frac{2d\ (d/2 - r_1)}{(d - r_1)^2 + (2\ h_{c2})^2}} \tag{6.33}$$

and

$$\alpha_2 = \sqrt{\frac{2c\ (c/2 - r_2)}{(c - r_2)^2 + 2\ (h + h_{c2})^2}} \tag{6.34}$$

Figure 6.15 shows the reply level P_4 as a function of separation h_{c2} between the transmitter and steel interface for sign post applications when the sensing distance $h = 0.5$ meter. In this analysis similar square antennas structures as that used in Chapter 3 are used.

Similar analysis was also performed using a ferrite slab antenna having dimension 55.7mm × 51.7m × 6.9mm as the sign post. Comparison between the flat planar structure and the ferrite slab in terms of reply signal level P_4 as a function of sensing distance h when the transmitter is located 50mm from the undercarriage of a vehicle is shown in Figure 6.16. From the curves it can be observed that is is possible to choose dimensions of a ferrite slab in order to obtain an equivalent performance corresponding to a planar coil.

268.
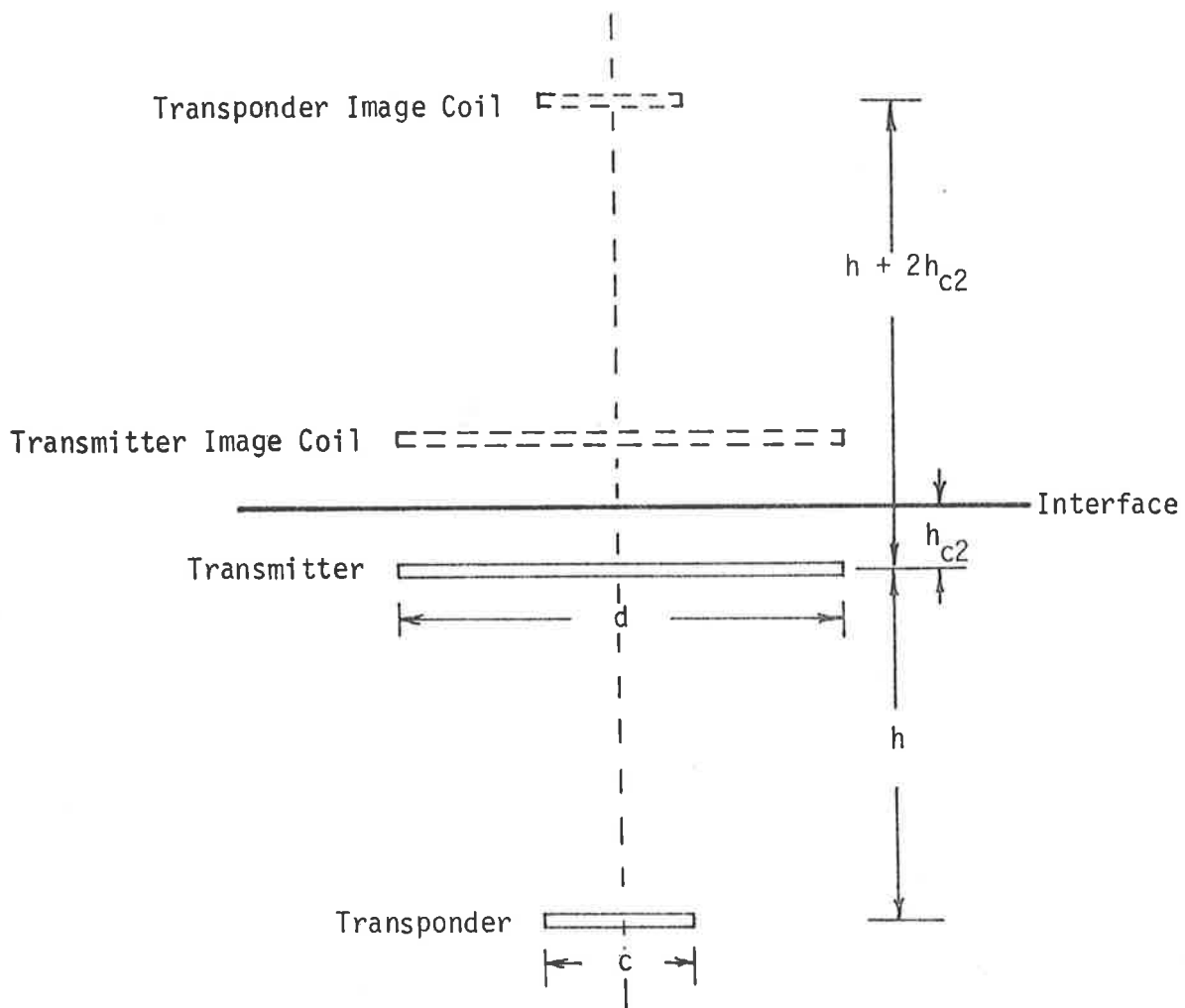
FIGURE 6.14. RELATIONSHIP BETWEEN THE TRANSPONDER AND TRANSMITTER WHEN USED AS A SIGN POST.
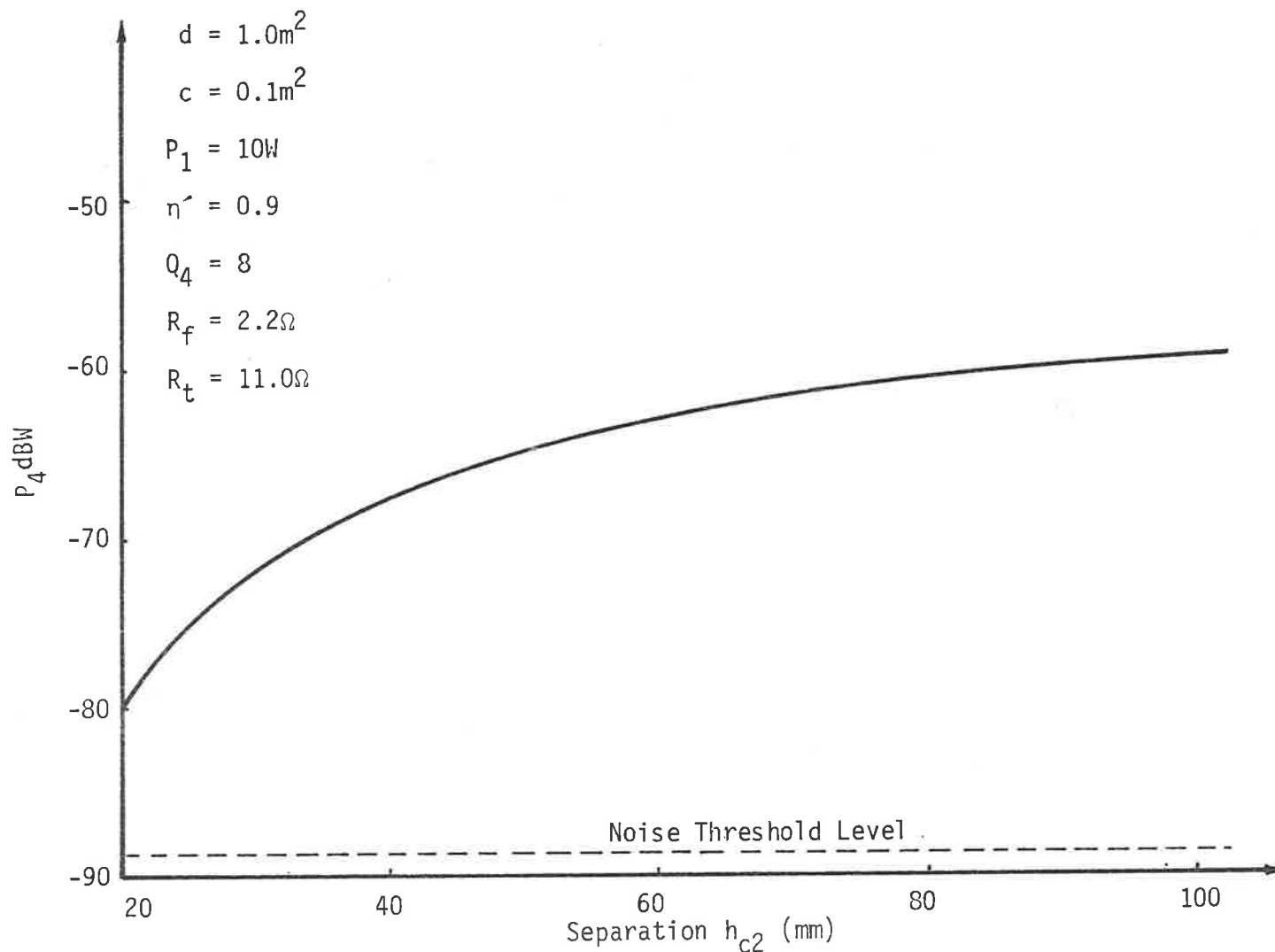
FIGURE 6.15. POWER AVAILABLE AT THE RECEIVER AS A FUNCTION OF THE SEPARATION h_{c2} BETWEEN TRANSMITTER COIL AND A STEEL INTERFACE WITH SENSING DISTANCE h = 0.5m – SIGN POST USING PLANAR COILS.
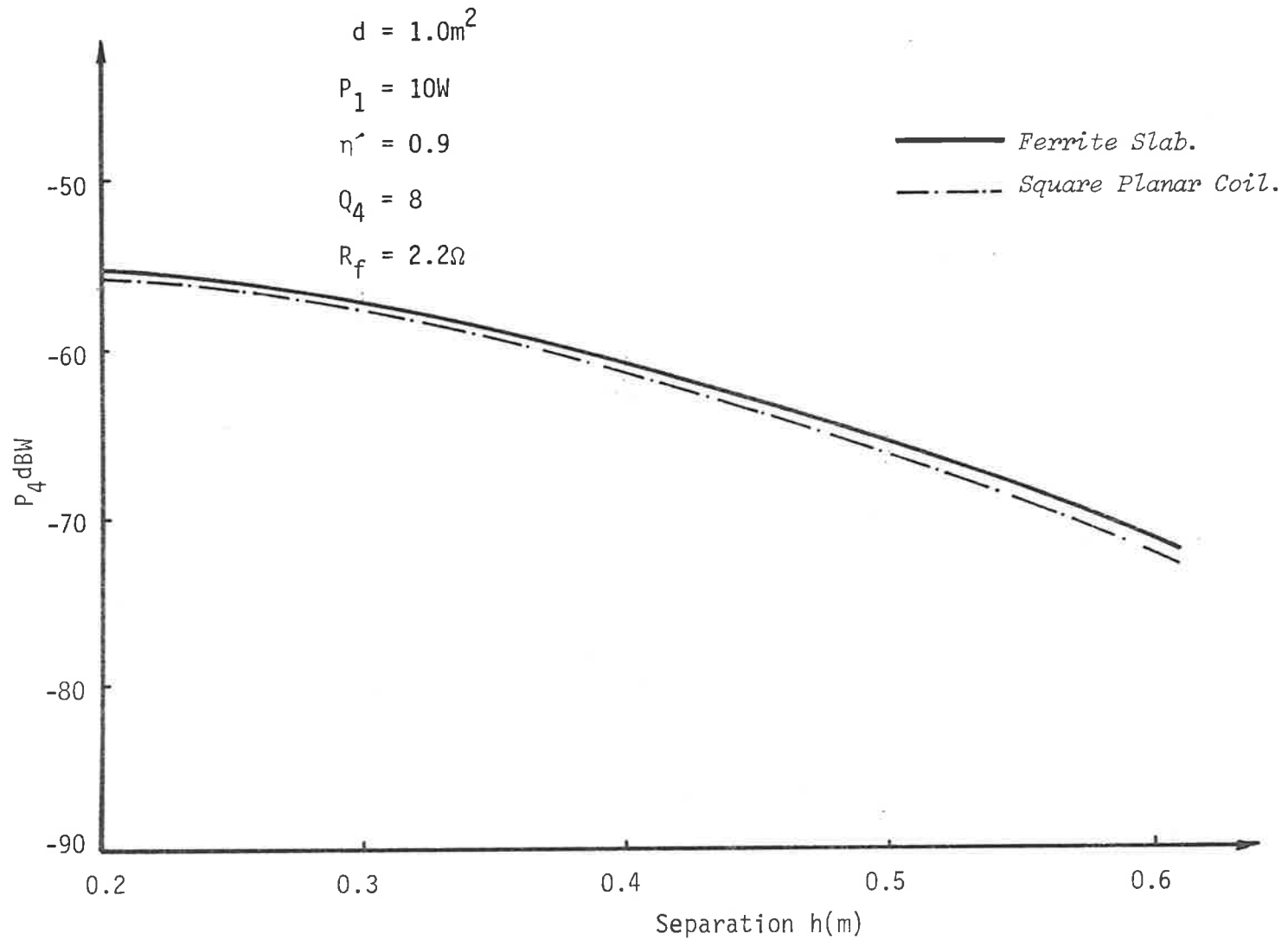
FIGURE 6.16.   COMPARISON BETWEEN SQUARE PLANAR COIL AND FERRITE SLAB WHEN USED AS A SIGN-POST WITH h_{c2} = 50mm.

In situations in which cost and material thickness are not issues for consideration the ferrite slab provides an advantage in terms of an overall reduction in the planar dimensions.

6.6 Conclusions

In this chapter particular emphasis was placed with the evaluation of the feasibility of PST devices in a practical application such as the number plate of a motor vehicle and sign post applications in which both dimensional constraints as well as manufacturing cost of the transponder antenna were major factors in the choice of the antenna structure.

The model developed to describe the power transfer in the proximity of an electrically conducting body has indicated the limitation which is encountered when attempts are made to maximise the quality factor and has illustrated the degradation of system performance for small separation between the transponder antenna and the interface. Through analysis it has been demonstrated that the coupling volume of the transponder antenna is marginally improved due to the reduction in the self inductance whereas there is a noticeable increase in the dispersal volume.

The interesting fact which has emerged from the above analysis is that for a fixed value of separation between the transponder and the interface there is an optimum value of sensing distance which maximises the power transfer across the electromagnetic links.

However it should be noted that the available power is substantially less than the corresponding case in which the interface is absent.

Introduction of a high conductivity material such as aluminium between the transponder and low conductivity magnetic material such as steel provide significant improvements in the quality factor. Experimentally it was found that sufficient improvement can be gained when the dimension of the introduced plate is in the same order as that of the transponder antenna.

The flat slab ferrite cored solenoid is of particular merit in the case when the antenna must be placed adjacent to a conducting plate, in which situation the planar coil becomes decoupled from the exciting field which is at useful operating frequencies constrained to lie parallel to the conducting plate.

Once again it is in such applications that the merits of the one-port PST are in evidence, as the inefficiencies of the two-port approach cannot be compensated for by increase of antenna size.

CHAPTER 7

PST SYSTEM CONSIDERATIONS

7.1 Introduction

In this chapter attention is focussed on practical implementation of the one-port PST system for two applications, namely:

(i) the identification of motor vehicles by means of buried transmitter and receiver antennas which interrogate a vehicle mounted transponder and process the reply signal; and

(ii) vehicle location systems in which the transponders are used as sign-posts embedded under the road surface, while the transmitter and receiver antennas are mounted underneath the vehicle.

The antennas considered for the transponder are the planar coil of sides 0.10m and the ferrite slab having dimension 55.7mm × 51.7mm × 6.9mm using 4B material. The dimensional choice is based on practical considerations in which it is required to keep the dimensions of the PST device as small as possible and yet to ensure that satisfactory performance is achievable at

274.

moderately low interrogation power levels and at sensing distance in the order of 0.5m. On the basis of the results obtained in Chapter 6, Figure 6.10 and Figure 6.16 it appeared that the above antenna structures satisfy the operational requirements and there-fore are suitable to be used for estimating the overall system performance.

In the following section practical considerations in the realisation of a typical interrogation system such as code structure, environmental noise, error rates, receiver design and integrated circuit development are presented.

7.2 Code Structure

At present there is no international standard which specifies either the technology or the required information content of vehicle identification systems. However several bodies including the American National Standards Institute are working to establish this standard which includes such factors as the code structure, the necessary information content, accuracy and transponder location on the vehicle.

A typical approach to the code structure and the information content by the Dutch National Standard format[110] is illustrated by Table 7.1. An alternative scheme used in the United States is also shown in Table 7.2, where the basic label contains 37 digit

TABLE 7.1.   CODE STRUCTURE – DUTCH NATIONAL STANDARD FORMAT.

			1	2	3	4	5	6	7	8	9	10	11	12	13	14	15	16	17	18
I		*Fixed route vehicles*	[1]																	
	1	Area or organisation code	1	[x	x]															
	2	Route numbers or line services	1	x	x	[x	x	x	x	x	x	x]								
	3	Route nos. for diversions	1	x	x	1	1	1	1	1	[x	x]								
	4	Running nos. of line services	1	x	x	x	x	x	x	x	x	x	[x	x	x	x	x	x]		
	5	Special trips	1	x	x	x	x	x	x	x	x	x	1	1	1	1	[x	x]		
	6	Nature of vehicle	1	x	x	x	x	x	x	x	x	x	x	x	x	x	x	x	[x	x]
II		*Variable route vehicles*	[0]																	
	1	Vehicle class – police	0	[0	0	1	x	0]												
		– fire brigade	0	[0	0	0	1	0]												
		– ambulance	0	[0	0	0	1	1]												
		– taxi	0	[0	0	0	0	1]												
	2	Priority class	0	0	0	x	x	x	[x	x]										
	3	Direction code	0	0	0	x	x	x	x	x	[x	x]								
	4	Vehicle number	0	0	0	x	x	x	x	x	x	x	[x	x	x	x	x	x	x	x]
III		*Spare*																		
	1	General reserve	[0	1]	x	x	x	x	x	x	x	x	x	x	x	x	x	x	x	x
	2	Spare for public transport/ 2nd vehicle-mounted unit	[0	0	1]	x	x	x	x	x	x	x	x	x	x	x	x	x	x	x
	3	Police spare	0	0	0	1	x	[1]	x	x	x	x	x	x	x	x	x	x	x	x
	4	Taxi spare	0	0	0	0	0	1	[1	0]	x	x	x	x	x	x	x	x	x	x
	5	Remaining reserve for police, fire brigade, ambulance, taxi	0	0	0	x	x	x	[1	1]	x	x	x	x	x	x	x	x	x	x

Explanation

I.1: 2 bits provide codes 0, 1, 2 and 3.

I.2: 7 bits provide capacity for up to 127 route nos.

I.3: Code "00" (route no. 124) for variable diversion route. At scheduled diversion point direction is given by bits 9-10 as in II.3 (route nos. 125-126-127).

I.4: 6 bits offer 63 nos. per route, nos. 60...63 being used for I.5.

I.5: Example: depot vehicles (00), instruction veh. (01). veh. on trial trip (10), maintenance veh. (11).

I.6: Typical uses: express service, stop skip, request for priority during stop procedure.

II.1: Bit 5 permits sistinction between 2 police categories.

II.2: No priority 00 / Conditional priority 01 / Absolute priority 10 / Spare 11

II.3: No direction info. 00 (cf. I.3 variable diversion route) / Right turn 01 / Left turn 10 / Straight on. 11

II.4: 255 vehicle nos. available per class.

III.1: Available for any vehicle types not covered by standard code (2^{16} options).

III.2: 001 indicates that a second vehicle mounted unit provides additional info. to that of 1st veh. mtd. unit (2^{15} options).

III.3: 2^{12} extra options.

III.4: Example: rented cars without priority.

III.5: For variable-route vehicles requiring no priority.

TABLE 7.2.   CODE STRUCTURE - U.S.A.

	1	2	3	4	5	6	7	8	9	10	11	12	13	14	15	16	17	18	19	20	21	22	23	24	25	26	27	28	29	30	31	32	33	34	35	36	37
1. Validity digits	[1]	x	x	x	x	x	x	x	x	x	x	x	x	x	x	x	x	x	x	x	x	x	x	x	x	x	x	x	x	x	x	x	x	x	x	x	[1]
2. Vehicle type	1	[x	x	x	x]	x	x	x	x	x	x	x	x	x	x	x	x	x	x	x	x	x	x	x	x	x	x	x	x	x	x	x	x	x	x	x	1
3. Owner digit	1	x	x	x	x	[x	x	x	x	x	x	x	x	x	x]	x	x	x	x	x	x	x	x	x	x	x	x	x	x	x	x	x	x	x	x	x	1
4. Vehicle number	1	x	x	x	x	x	x	x	x	x	x	x	x	x	x	[x	x	x	x	x	x	x	x	x	x	x	x	x	x	x	x	x	x	x	x	x]	x	1
5. Parity digit	1	x	x	x	x	x	x	x	x	x	x	x	x	x	x	x	x	x	x	x	x	x	x	x	x	x	x	x	x	x	x	x	x	x	x	[x]	1

277.

locations which represents one validity digit, four vehicle type digits (16 vehicle types), 10 owner digit (1024 owners), 20 vehicle number digits (1,048,576 vehicles), and one parity digit. This code structure is capable of uniquely representing all the vehicles in the United States.

However considering the total number of vehicles on the world wide basis, code words in the order of 2^{48} or longer may be necessary. Thus, the present choice of 64 bits allows 16 bits to be used for error detection and corrections if required.

In order to have an appreciation of errors associated with detection of the reply signal, for independent errors the probability of detecting (M-m) bits in a M bit code can be written as[111]

$$ P_{(M-m),M} = \frac{M!}{(M - m)! \; m!} \; p^{(M - m)} \; (1 - p)^m \qquad (7.1) $$

where

    p = probability of detecting a signal bit.

    M = number of bits in a code.

    m = 0, 1, 2, ..., M.

The main factor which emerges from Equation (7.1) is that the error is determined by the number of bits in a code and is dependent on the probability p of detecting a single bit in that code. To assess the performance of a code, it is necessary to know how often

a code word is corrupted by errors and how often the error detecting or correcting ability of the code is exceeded. Thus the characterisation of environmental noise is of particular significance in the above analysis.

7.3 Environmental Noise Modelling

The noise performance of low frequency transponders is mainly affected by electromagnetic interference introduced in the reply signal propagation path with receiver noise playing only a minor part. The noise normally encountered is of non-Gaussian impulsive type and do not readily provide for parametric description. The impulsive character of the noise is particularly effective in causing errors in data communication systems.

The usual sources of noise in low frequency communication systems are atmospheric noise and various forms of man-made noise, of which the principal contributors are power lines, industrial switching and automobile ignition. Environmental noise has been studied by several researchers largely from the point of view of VHF or UHF communications but some measurements relevant to LF region have been made. The emphasis in the literature has generally been on noise measurement and characterisation. The prediction of error rates in communication channel has been less often considered.

Various statistical measures for the description of environ-

mental noise have been proposed. These include amplitude probability distribution (APD) which shows the percentage of time noise amplitude exceeds a given level; the time probability distribution (TPD) which gives, for various noise amplitudes, the percentages of pulse spacings that exceed specified times; the noise amplitude distribution (NAD) which records the number of pulses per unit time that exceed specified levels; the pulse duration distribution (PDD) which shows, for various noise amplitudes the percentage of pulses which exceed various widths and the average crossing rate (ACR) which shows the average number of times the noise amplitude crosses various levels [91], [94], [98].

The most useful descriptions of the environmental noise for the prediction of system performance are the noise amplitude distribution (NAD) and the time probability distribution (TPD).

In order to provide the basis for a suitable parametric description of low frequency environmental noise, noise data was gathered from several environments including roadway surfaces with and without vehicles present[115]. The antenna structure used for the measurement was electrically balanced, magnetic dipole of approximately $1m^2$ cross-section, tuned with quality factor of the order of 10. The noise in this situation, is largely impulsive with periods much less than and separations much larger than the decay time of the antenna resonant circuit. The known passband characteristics of the antenna permits the use of envelope and phase rather than complete rf waveform detection without a loss of information. A typical noise characteristic and noise envelope is shown in Figure 7.1.
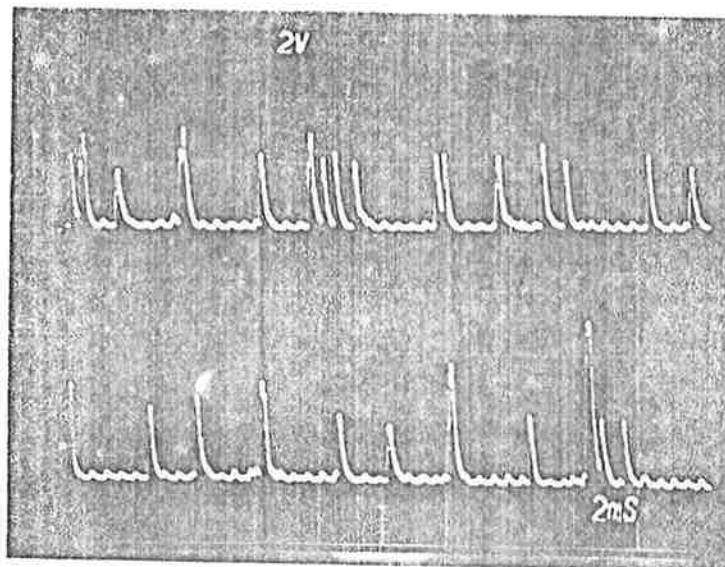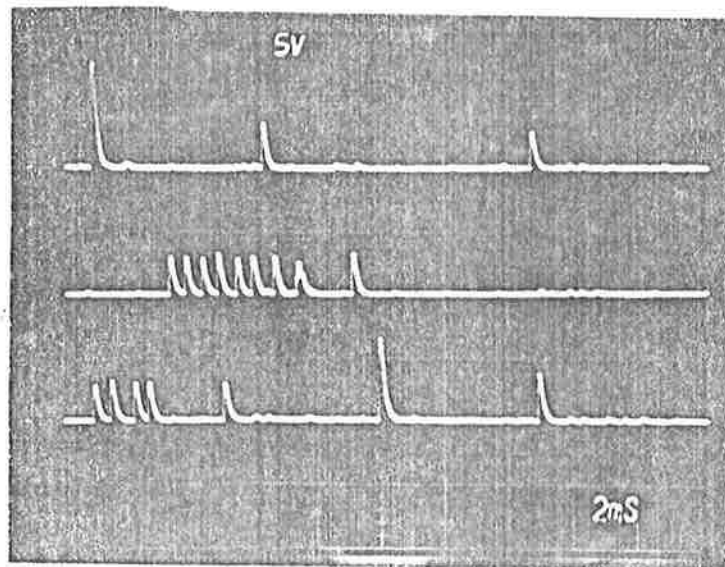
Notes: *(i)*   *Receiver Antenna Characteristics:*

> *Centre frequency*   *= 50kHz*
> *Bandwidth*   *= 6.25kHz*
> *Dynamic Resistance at resonance = 10 ohms*

     (ii) Antenna located on the road surface.

FIGURE 7.1 (a).   TYPICAL NOISE CHARACTERISTICS OBTAINED FROM THE

DETECTOR OUTPUT OF NOISE MEASURING DEVICE.

Calibration
Pulse

Signal at the
antenna
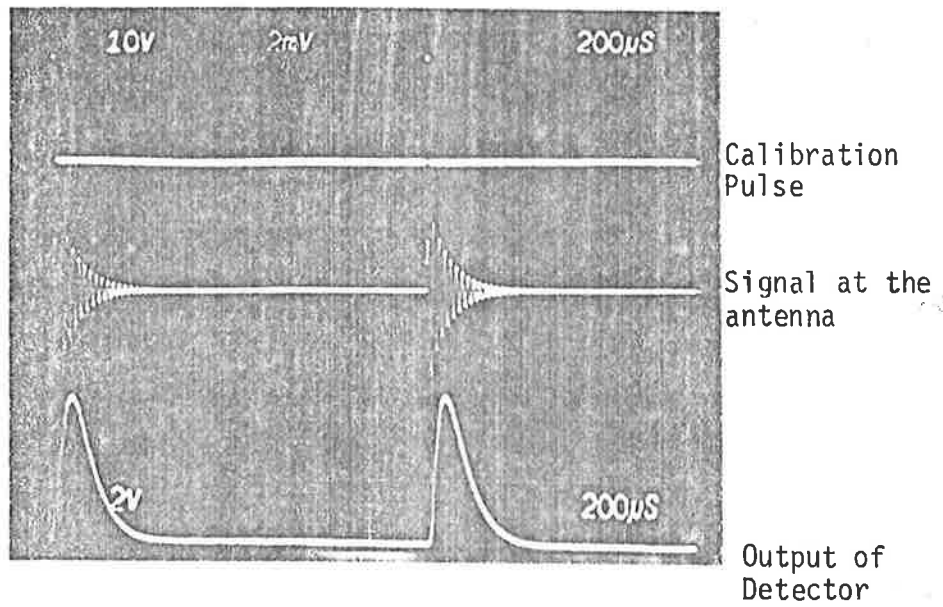
Output of
Detector

FIGURE 7.1 (b).   TYPICAL NOISE CHARACTERISTICS AT THE ANTENNA AND

DETECTOR OUTPUT.

Roy[121] performed detailed analysis of the stored noise data
and provided a mathematical model for calculating the system error
performance in terms of probability of an error bits per message.
This is expressed as:

$$P_e = \int\limits_0^\infty \int\limits_0^\infty N'(V)U\,[V_d\,(V,t') - V_s]\; dt'\; dV \qquad (7.2)$$

where

V_s = magnitude of reply signal.

U = unit step function.

$$V_d(V,\,t') = \frac{2}{T}\int\limits_0^T V_e^{-\alpha(t-t')}\,\text{Cos}\,\omega\,(t-t')\;U\,(t-t')\;dt \qquad (7.3)$$

N' (V) dV = number of pulses per unit time which have amplitude
lying in the range V and V + dV,

and α is time constant of receiver antenna circuit.

The result of the analysis is shown in Figure 7.2 in which
the predicted error for the passive subharmonic transponder
system for two different noise environment are plotted as a function
of the reply signal level. In these plots the noise pulses are
assumed to be uniformly distributed over the range $(-\pi, \pi)$.

283.
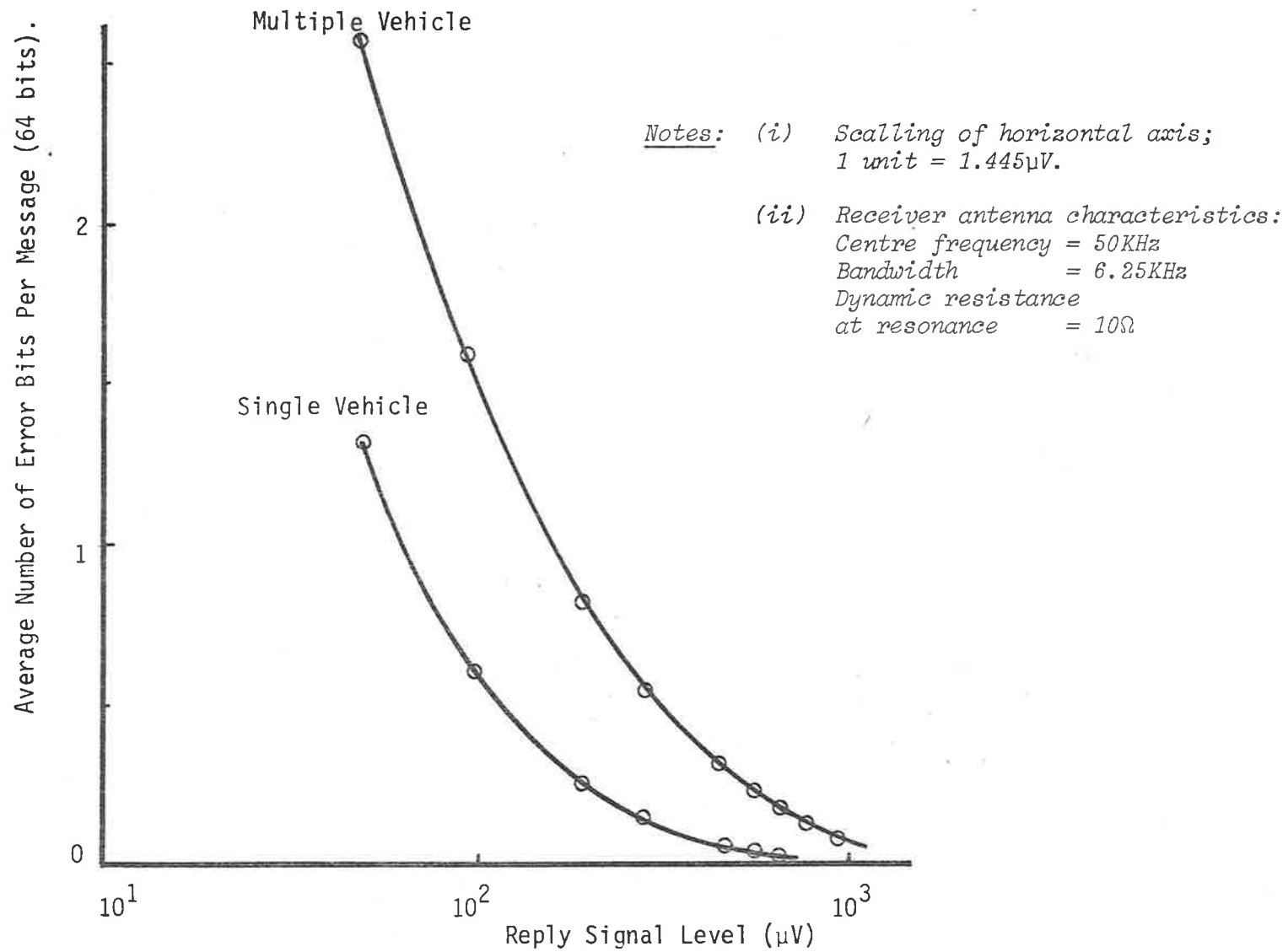
FIGURE 7.2.   AVERAGE NUMBER OF ERROR BITS PER MESSAGE AS A FUNCTION OF REPLY SIGNAL LEVEL FOR TWO DIFFERENT NOISE ENVIRONMENTS.

7.3.1 Error rate predictions

In order to estimate the error rates plots of the peak amplitude of the reply signal at the receiver antenna having dynamic resistance of 10 ohms at resonance and tuned to 50kHz is shown in Figure 7.3 (a) - (b) for the two applications, namely the number plate and sign post using planar square coils. The theoretical results are based on the modelling principles developed in the previous chapters.

A passive number plate constructed from a planar coil of sides 0.10m located at a distance of 50mm from the under-carriage and returning a 64-bit coherent PSK reply code with 8 carrier cycles per bit and operating at a sensing distance of 0.5 metre from a transmitter antenna energised with a power of 10 watts at 100kHz, will return a 50kHz reply signal level of -66.6 dBW to the receiver antenna having dynamic resistance of 10 ohms at resonance and tuned to 50kHz. The peak signal level in the antenna impedance of 10 ohms is 2.09mV which is substantially larger than the levels shown in Figure 7.2.

When similar transponder is used as a sign post with the transmitter and receiver antennas situated 50mm from the undercarriage, for similar power level and sensing distance as above, the PST will return a 50kHz reply signal level of -67.2dBW to the receiver antenna having dynamic resistance of 10 ohms. In this instant the peak signal level is 1.95mV. For this latter application it should be noted that from Figure 6.17 similar results are also achieved when the smaller

Steel Undercarriage

h_{c2} = 50mm

Transponder

|←0.1m→|

Road Surface

|————1.0m————|

h

Transmitter and
Receiver Antennas
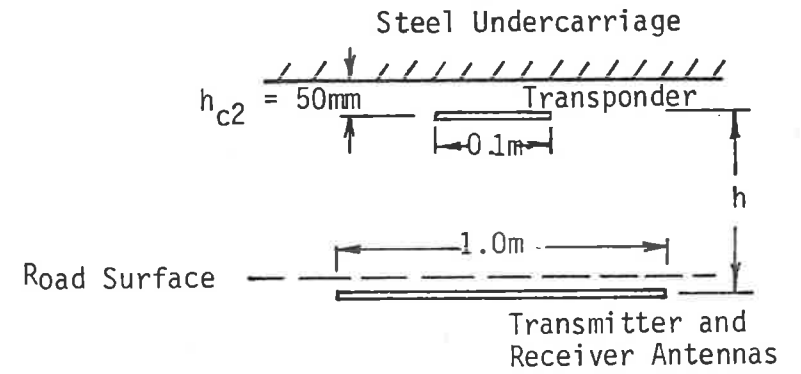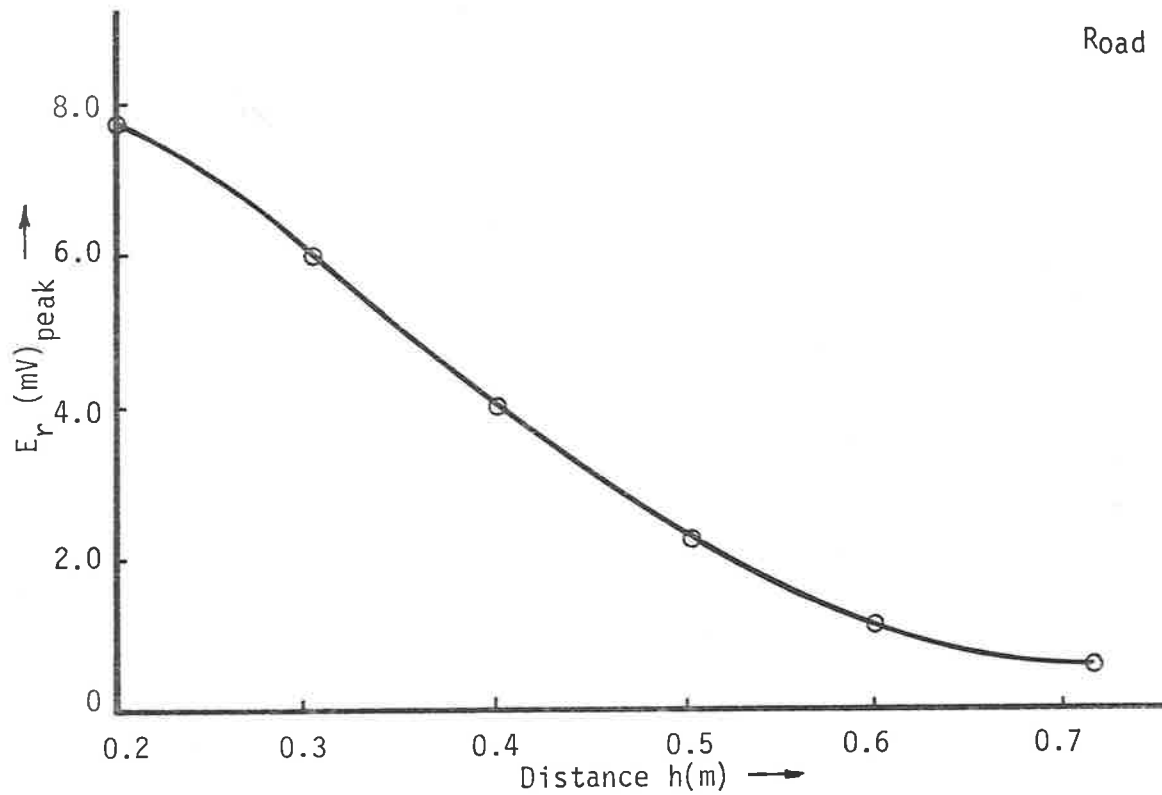
Q_{1c}	8
Q_{2c}	24
Q_{4c}	8
R_f	2.5Ω
η'	0.9
P_1	10 Watts

FIGURE 7.3 (a). PLOT OF SIGNAL LEVEL AT THE RECEIVER ANTENNA AS A FUNCTION OF DISTANCE h USING A FLAT SQUARE

COIL AS A NUMBER PLATE.

Legend:
—o— —o— *Planar Square Coil.*
—△— —△— *Ferrite Slab.*
—☐— —☐— *Experimental Results Using Ferrite Slab (55.7 × 51.1 × 6.9mm)*

Parameter	Flat Coil	Ferrite
Q_1	20	20
Q_{2c}	50	35*
Q_4	8	8
R_f	2.5	2.5
n'	0.9	0.9
P_1	10 watts	10 watts

* *The reduction in Q is to allow for losses encountered as the result of ferrite antenna being vertically buried under the road surface. Coil was loaded to give the desired Q.*
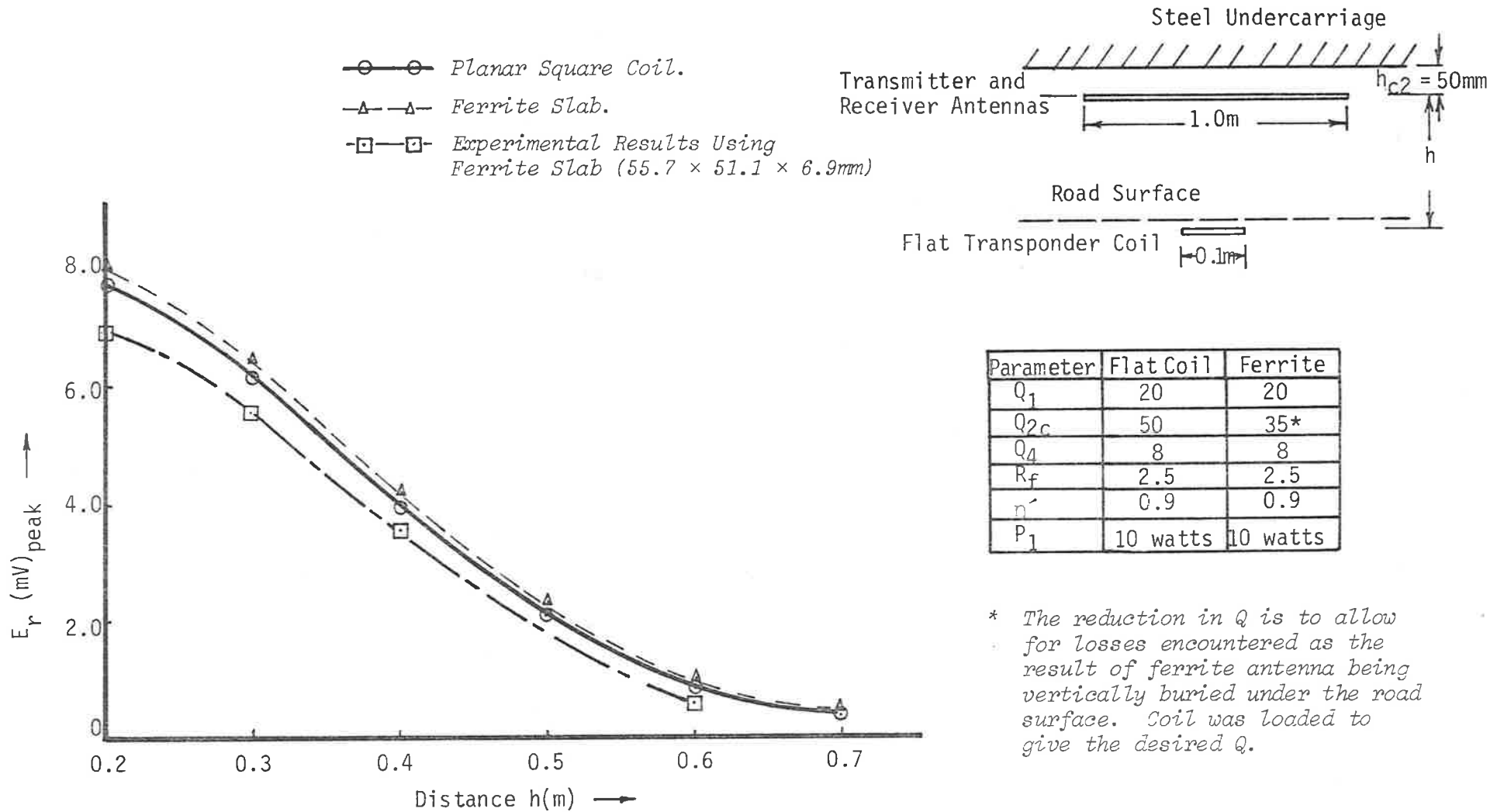
FIGURE 7.3 (b). PLOT OF SIGNAL LEVEL AT THE RECEIVER ANTENNA AS A FUNCTION OF DISTANCE h USING BOTH FLAT SQUARE COIL AND FERRITE SLAB AS A SIGN-POST EMBEDDED UNDER THE ROAD SURFACE.

ferrite slab having the dimensions of 55.7mm × 51.7mm × 6.9mm is used. Although the cost associated with ferrite slab is higher than the flat planar coil, for sign post applications it is easier to be installed by simply cutting a slot in the road surface.

A question of interest is whether buried PST devices can achieve the quality factors assumed in the theoretical modelling and laboratory experiments. On the basis of experience it is found by appropriate encapulation of the PST device the region of greatest energy density can be sufficiently isolated from the dissipative material and hence the assumed quality factors can be achieved. The quality factors used in the analysis have been empirically confirmed as achievable in the situations considered.

The results indicate that satisfactory performance may be obtained for transponder sizes that are likely to be acceptable in the two applications considered.

Using the above results in conjunction with error curves shown in Figure 7.2 it is possible to estimate the error rates. It is readily recognisable for the environment and the system parameters used, very low error rates are achievable. For a reply signal level of 1500μV, on the average one-bit error for every twelve 64-bit messages can be anticipated. Therefore for the reply signal levels that are achievable in a practical interrogation system complex decoding and error correction schemes is not necessary and

generally simpler methods become adequate.

However for systems operating under very noisy environment one may resort to the various error detection and correction techniques that are available[122 - 127]. The coding procedure generally consists of splitting the message into blocks and adding the information digits such that though errors occur, there is enough information so that the reply can be corrected.

7.4 Receiver Design

One of the major considerations in the receiver design is the ability of the receiver to separate the weak reply signal from the strong interrogation signal. The significant factor associated with subharmonic transponders is that the information in the reply code is transmitted in frequency ranges which differ from the interrogation frequency by factors of many times the bandwidth of the antenna tuned circuits. The wide spearation in the frequencies allow highly effective filtering of the interrogation energy from the receiver system, to the antenna of which the interrogation energy is normally strongly coupled as a consequence of the fact that both coupling elements scan the same region of space. Thus complex processing can be avoided.

Although a more general design principle of the receiver is

currently under investigations by another researcher, in order to have an appreciation of the overall system an arrangement which consisted of a combination of both analogue and digital sections as shown in Figure 7.4 was developed.

7.4.1 Receiver filter characterisation

A typical response that one is interested in separating the reply signal from the strong interrogation signal is shown in Figure 7.5. The transfer function which describes the above characteristics and has been normalised to give a resonance at 1 rad/sec and a notch at 2 rad/sec is given by

$$\frac{V_o}{V_i} = \frac{\alpha S^2 + 1}{(S^2 + \beta_1 S + 1)(\alpha S^2 + \beta_2 S + 1)} \qquad (7.4)$$

where

$$\left.\begin{array}{l} \alpha = 0.25 \\ \beta_1 = 1/Q_4 \\ \beta_2 = 2/Q_t \end{array}\right\} \qquad (7.5)$$
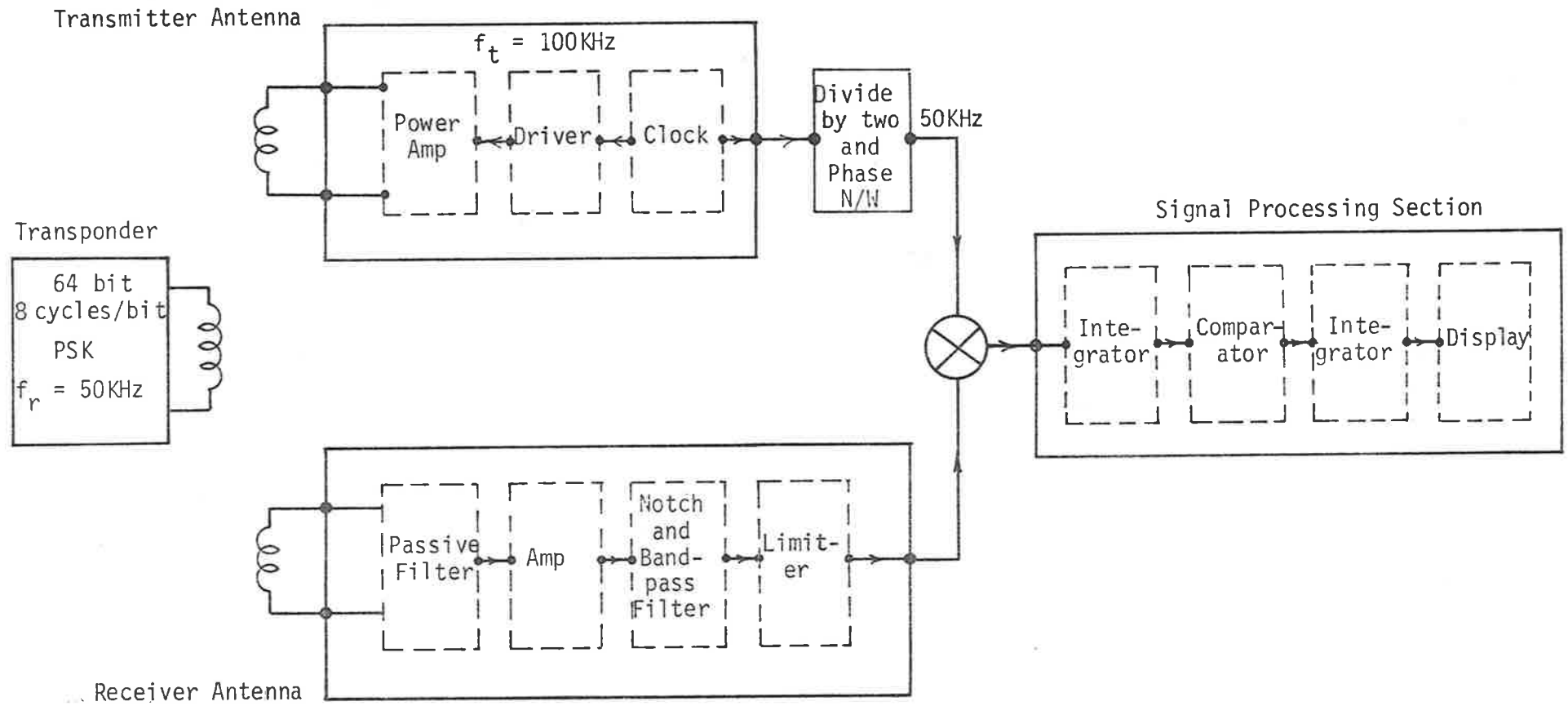
FIGURE 7.4.   BLOCK DIAGRAM - INTERROGATION SYSTEM.

291.

$$\omega_r = 50\text{KHz}$$
$$\omega_t = 100\text{KHz}$$
$$\Delta B = 6.25\text{KHz}$$
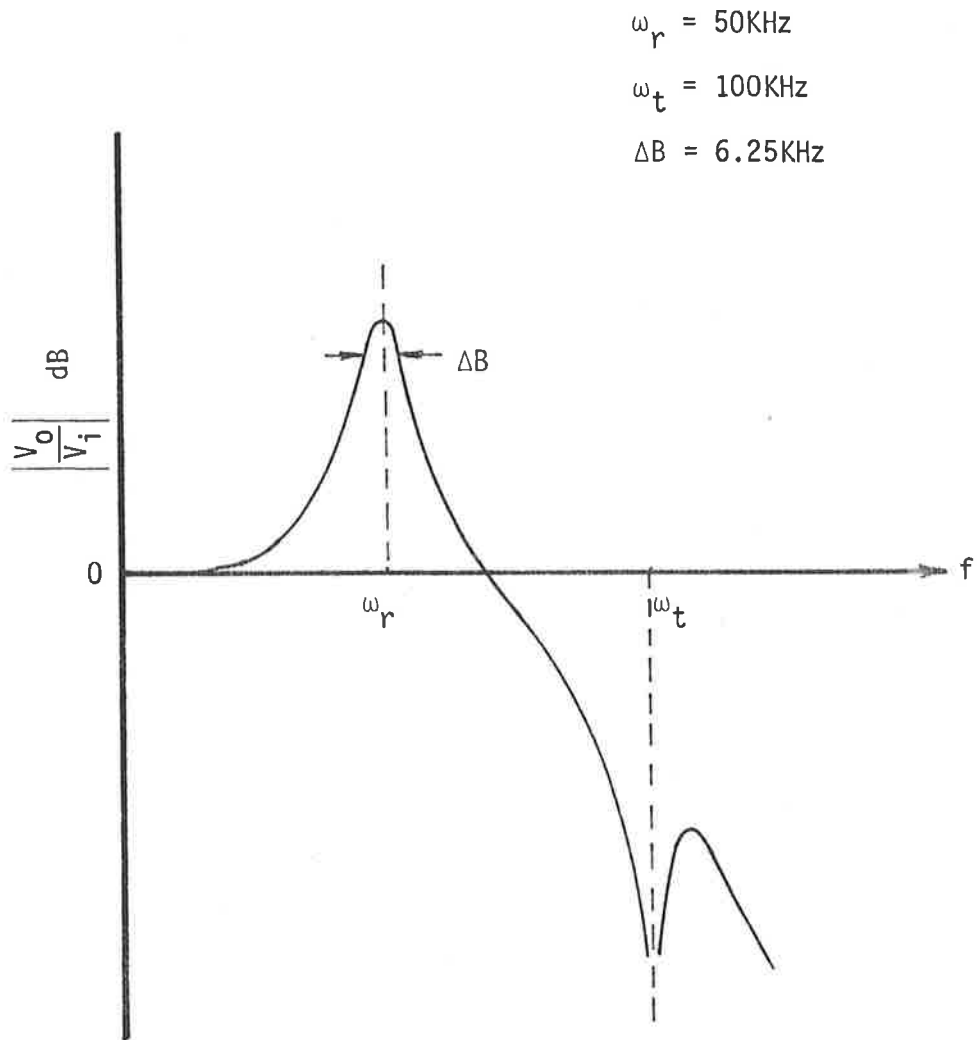
FIGURE 7.5.   DESIRED RESPONSE FOR THE RECEIVER TO SEPARATE THE WEAK

REPLY SIGNAL FROM THE STRONG   INTERROGATION SIGNAL.

and quality factor Q_4 determines the bandwidth of the resonance at ω_r. The value of Q_t may be chosen by noting the compromise necessary in ensuring that the notch at ω_t is as deep as practicable without influencing the rejection characteristics for slight variations in the interrogation frequency. In addition the notch should have little attenuation at ω_r.

With ω_r = 50kHz, ω_t = 100kHz and Q_r = 8, it is possible to satisfy the above condition when Q_t = 4. Thus the above transfer function can be written as:

$$\frac{V_o}{V_i} = \frac{s^2 + 4}{s^4 + 0.625\ s^3 + 5.0625\ s^2 + s + 4} \qquad (7.6)$$

Synthesis of the normalised form of a typical structure can be realised by Cauer Guillemin[128] method. This is shown in Figure 7.6 in which typical component values and the required load impedance (after appropriate frequency and impedance scalling) values are also given.

The theoretical and experimental response of the filter is illustrated in Figure 7.7 in which good agreement is observed. From the response it can be observed that approximately 56dB separation between the interrogation and reply frequencies are achieved.

In the practical realisation of the system further

293.
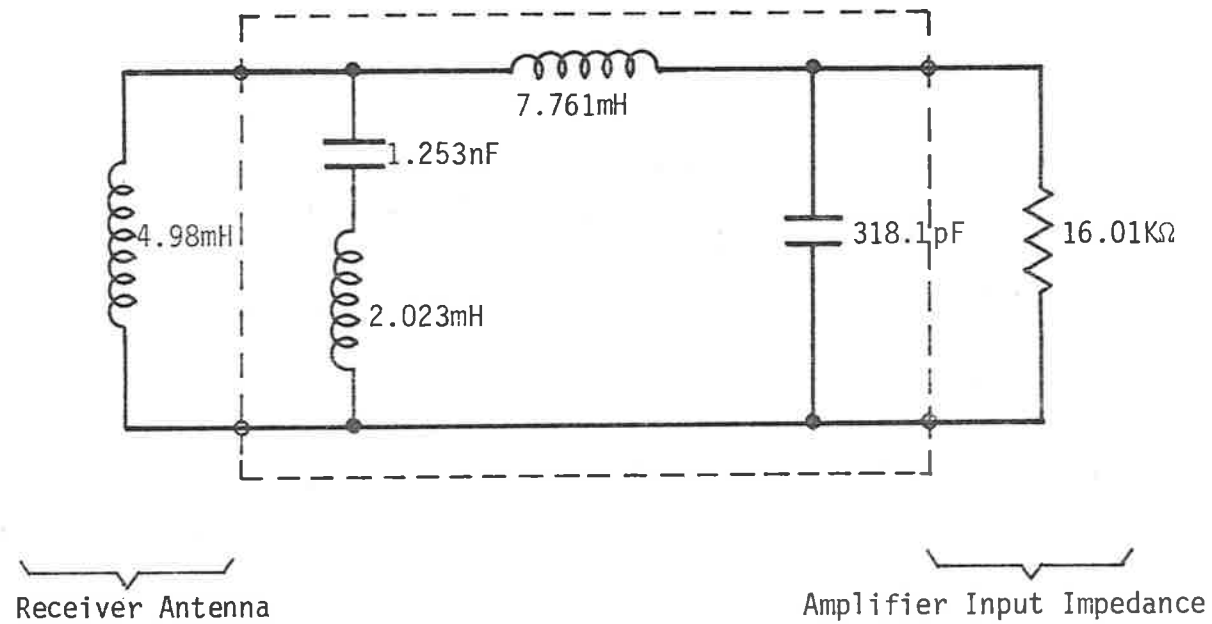
FIGURE 7.6.   RECEIVER FILTER DESIGN.
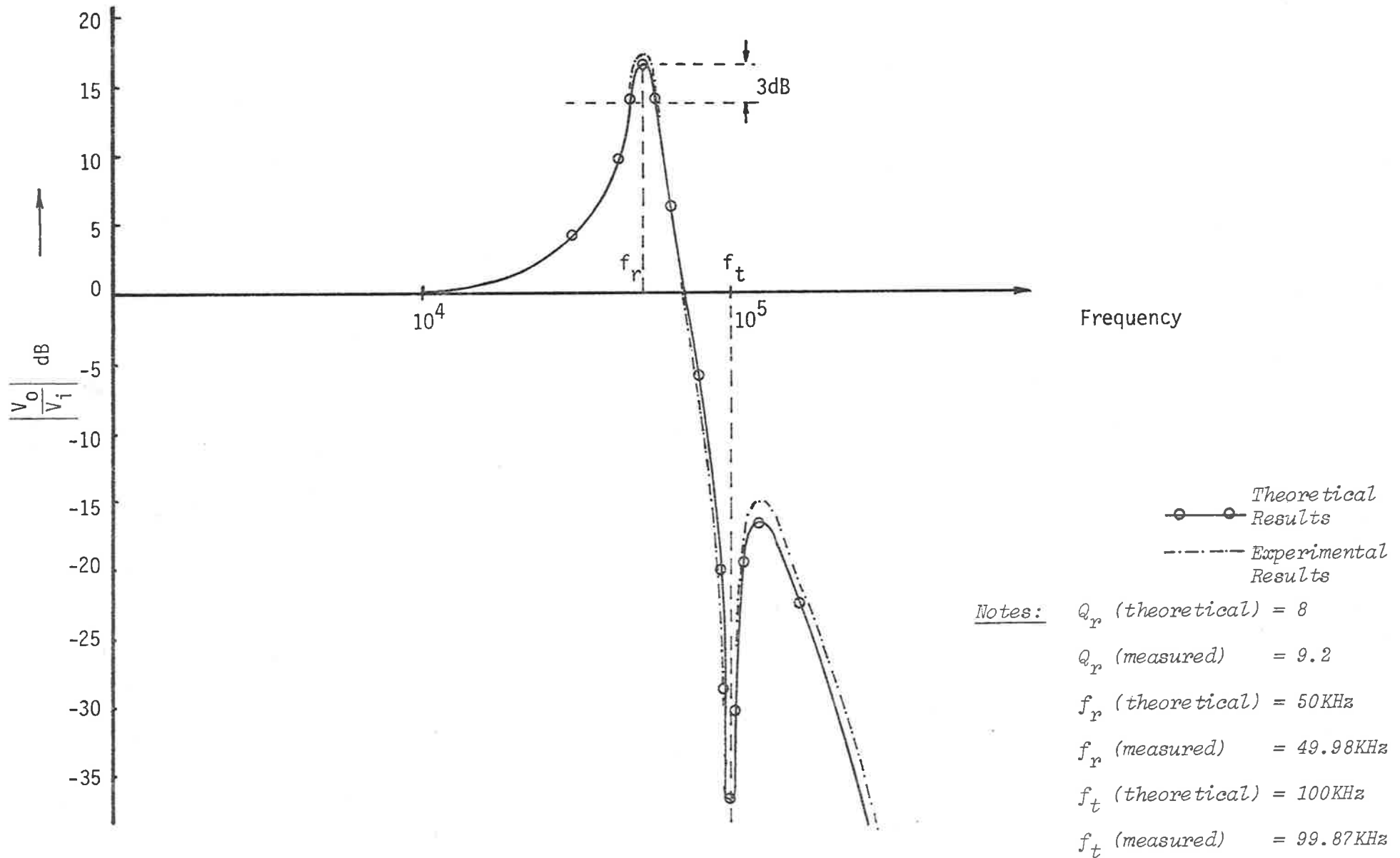
FIGURE 7.7.   FILTER CHARACTERISTICS.

Theoretical Results

Experimental Results

Notes: Q_r (theoretical) = 8

Q_r (measured)   = 9.2

f_r (theoretical) = 50KHz

f_r (measured)   = 49.98KHz

f_t (theoretical) = 100KHz

f_t (measured)   = 99.87KHz

attenuation at 100KHz was found necessary.   The structure

of the resultant filter and the overall response are shown

in Figures 7.8 and 7.9 respectively.   As it can be observed

approximately 90dB separation was achieved.

7.4.2 Signal processing section

There are several tasks the receiver must perform.   The

first being the ability to extract timing information from

the message in order to establish the cycle on which a

message bit commences.   Due to the availability of a direct

link between the transmitter and the receiver the 50kHz local

oscillator is available for synchronous detection.   Once bit

synchronization has been established integration of the mixer

product may be performed over several number of messages in

order to provide improvement in the signal-to-noise ratio.

To detect the start of the reply code a synchronizing

pattern is included at the start of each message.   Naturally

this reduces the number of data bits and restricts the over-

all code structure to avoid the repetition of the synchroniz-

ing pattern.

The second task that the receiver is required to perform

is to define the sign that can be assigned to the output.

Presence of a sufficient level of noise may cause the output

of the mixer to take either sign on any particular cycle.

It is possible to average out the noise by integrating the
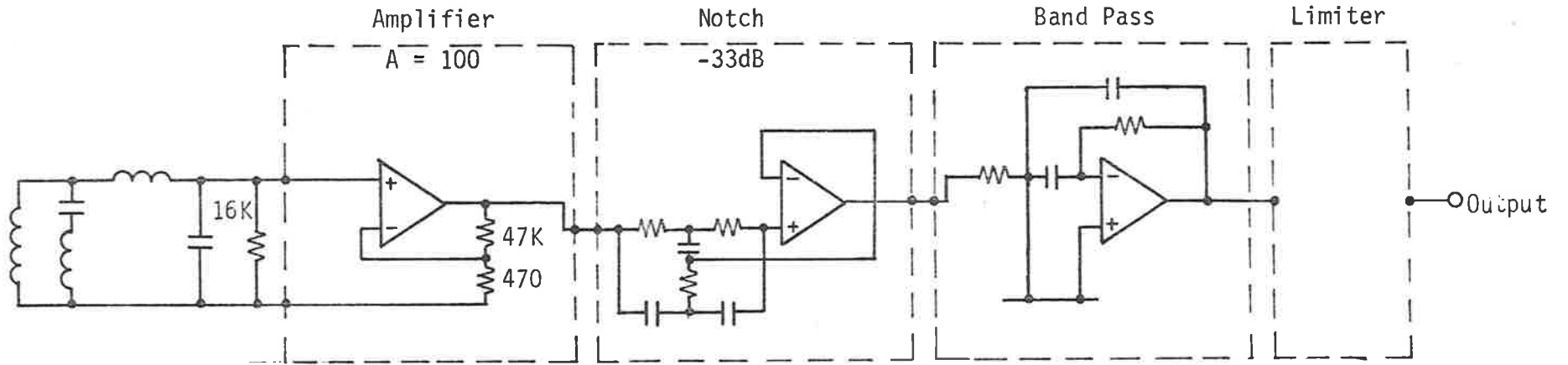
FIGURE 7.8.   RECEIVER FILTER STRUCTURE.
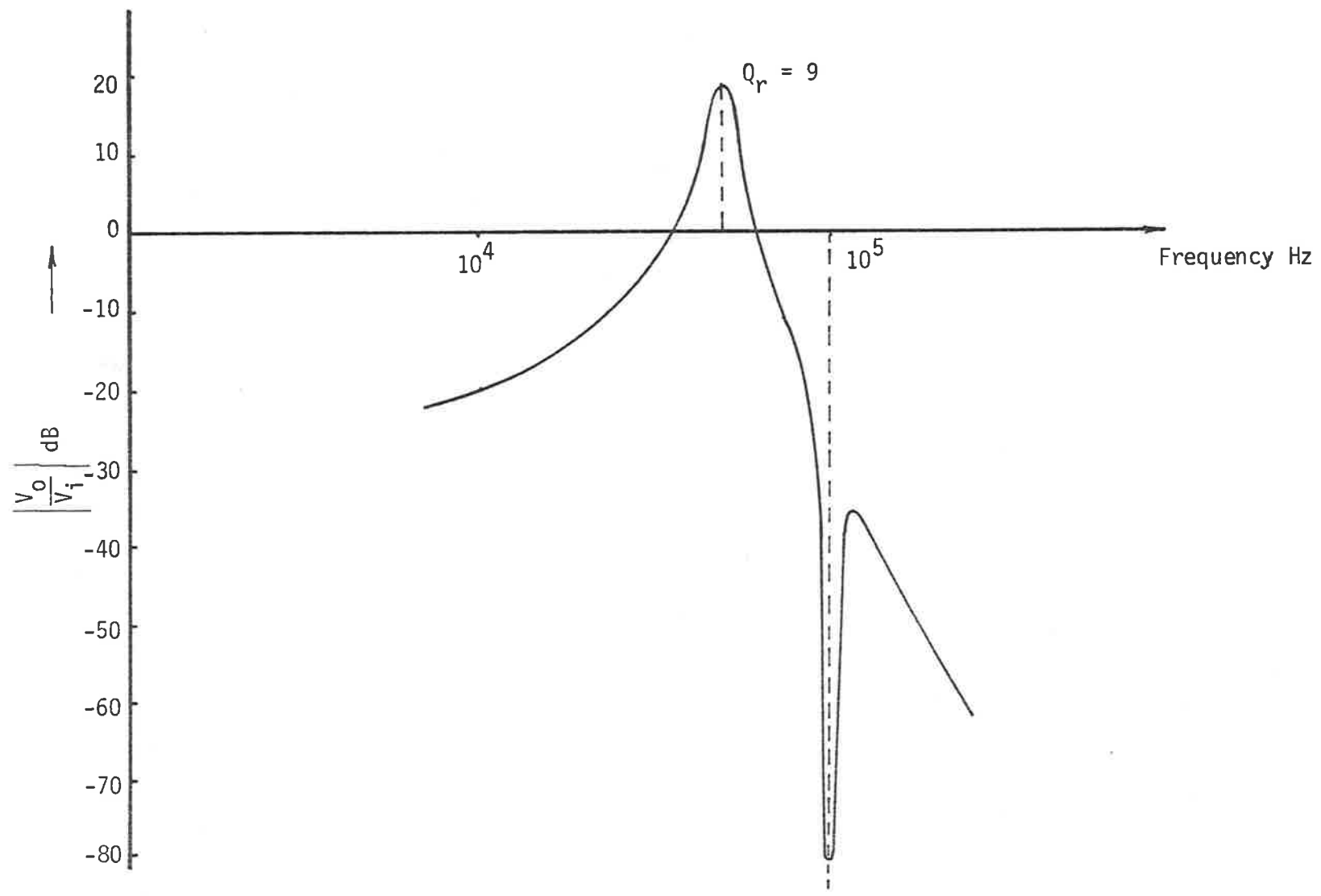
FIGURE 7.9. OVERALL RECEIVER RESPONSE.

multiplier output over several cycles of the reply signal which is pre-assigned to each bit.

The magnitude resulting from any particular bit increases as synchronization is approached. Therefore by varying the starting cycle over which integration occurs and looking for a maximum, synchronization can be achieved.

The main object of this portion of the work was the realisation of a flexable system such that not only the processing requirements discussed above could readily be met, but also to provide a working system for future development in this area of research. Therefore a general purpose data acquisition system suitable for on-site data recording and processing was designed and subsequently was constructed by Mr. N. Blockley. The receiver shown by Figure 7.10, incorporated Intel's SBC 80/30 microprocessor based system, DMA controller SBC 501, 32K of random access memory and the relevant interfacing units as illustrated.

In the system the number of cycles over which integration could proceed was set to 8. This was consistant with the requirement of the communication bandwidth and the information rate. However the number of samples that may be collected (which determines the number of messages) and the synchronization bit pattern were under programme control. The control commands which facilitates communication between the user and the system is shown in Figure 7.11. Once the appropriate parameters are entered and the transponder is

FIGURE 7.10. DATA ACQUISITION SYSTEM.
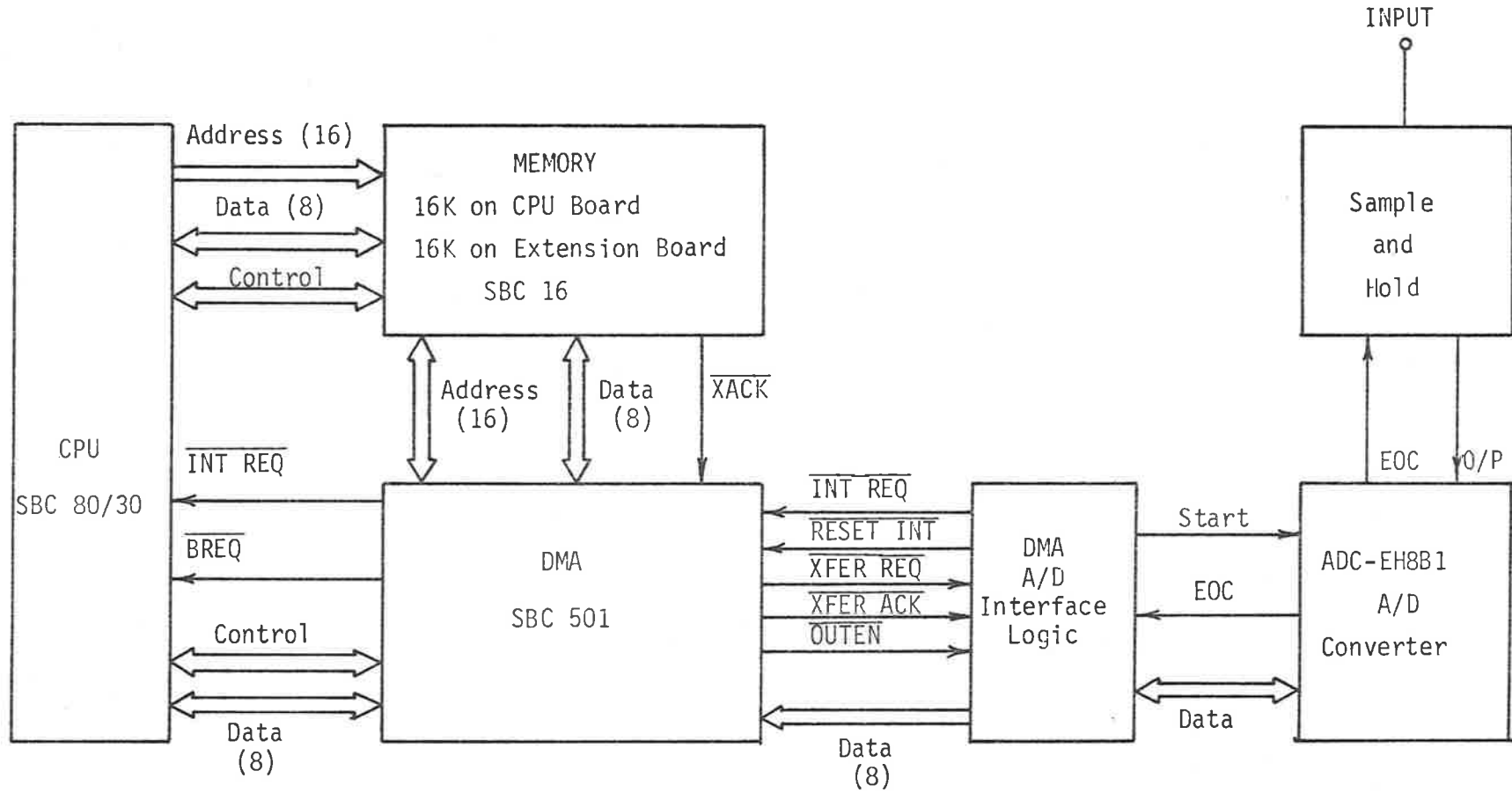
Notes: Sample time: 4.72 μS/sample.

Transfer rate: 211,667 samples/Sec.

```
*************************************************
                SYSTEM 90

         DATA ACQUISITION PROGRAM COMMANDS
*************************************************

         'A' - INSERT ADDRESS IN RAM WHERE
               DATA SAMPLES FROM DMA ARE TO
               BE STORED.

         'A' - 8000
=================================================

         'N' - SET NUMBER OF SAMPLES TO BE
               COLLECTED BY DMA.
=================================================

         'S' - START DMA AND A/D WORKING
=================================================

         'J' - INSERT STARTING STRING
               TO BE LOOKED FOR BY PROG.

         'J' 1010
=================================================

         'P' - PROCESS DATA RECEIVED FROM A/D
=================================================

         'D' - DISPLAY CODE AFTER PROCESSING
               IN 8 X 8 MATRIX
=================================================
```

FIGURE 7.11. DATA ACQUISITION SYSTEM PROGRAMME COMMANDS.

brought within the interrogation range collection of the
reply can be initiated either by software, or by manual
operation of a switch, or alternatively through detection
of a reply signal of sufficient strength. The results of
a typical response is subsequently displayed by an 8 × 8
matrix.

It should be noted that for a vehicle travelling at
100km/hr over a square loop of sides 1.11 meters for an
interrogation frequency of 100kHz and reply frequency of
50kHz with 64 bit message and 8 cycles per bit 4 messages
can be anticipated. At a sampling rate of 250K bit/sec
approximately 10K of memory is required.

The system has been applied to laboratory testing in
which the results are entirely satisfactory. Figure 7.12
illustrates the code structure for one of the PST devices
under test in which the pattern 1010 is used for synchron-
ization.

A typical PST interrogation system is shown in
Figure 7.13.

FIGURE 7.12.   TYPICAL PRINT-OUT OF AN OPERATIONAL SYSTEM DISPLAYING

THE REPLY CODE WITH 1 0 1 0 SYNCHRONIZATION PATTERN.

Microcomputer

Power Amplifier
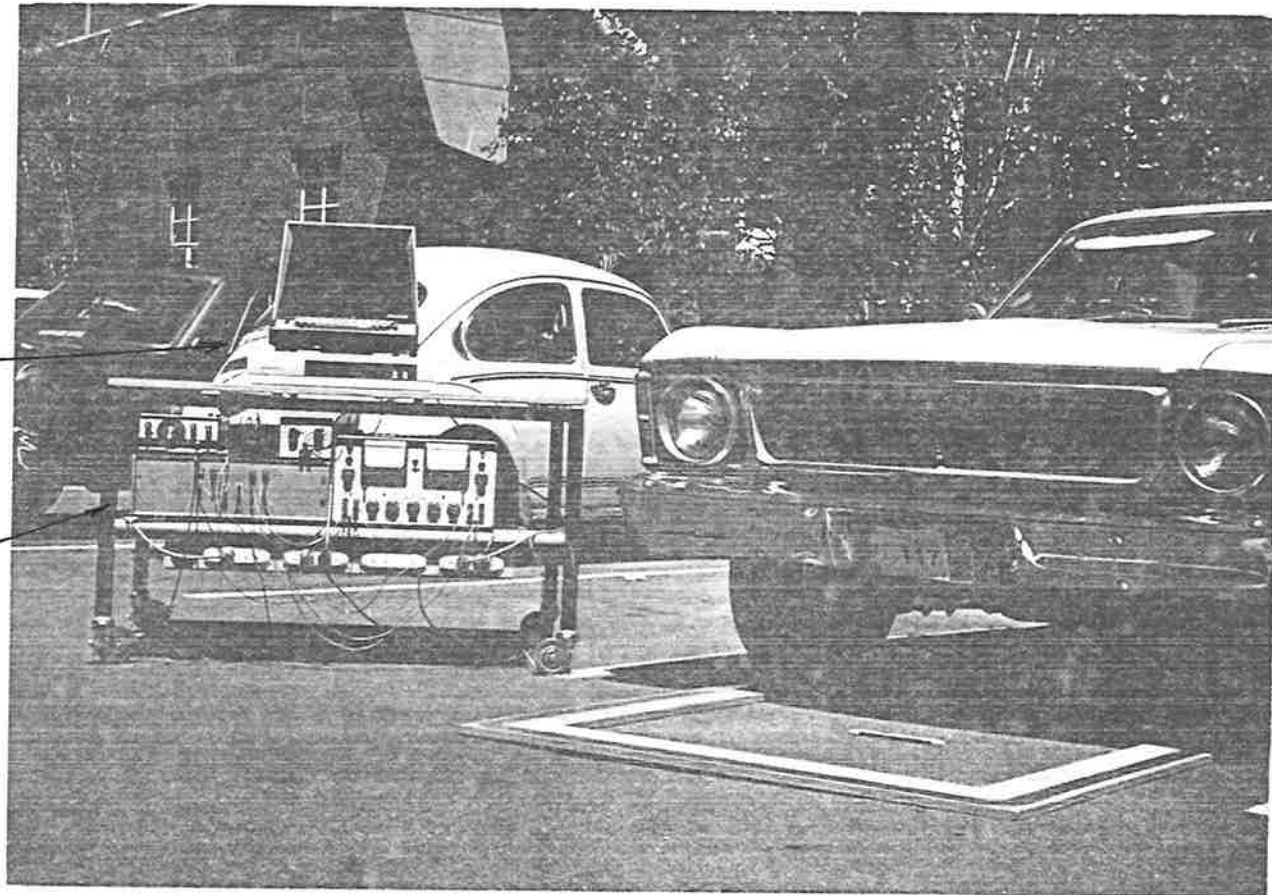
FIGURE 7.13. OVERALL PST INTERROGATION SYSTEM.

7.5 Transmitter Power Constraints

In practice the allowable values of transmitter power are limited by several factors. These include the power level which can be conveniently provided, statutory limitations on radiated or near fields produced by antennas, and considerations of electromagnetic compatability where other electronic instruments are installed within the field of the sensing apparatus.

Of the above list the most easily quantifiable are the statutory limitations required by licensing authorities. An important constraint is that provided by the United States Federal Communications Commission regulations[86], which is given in terms of maximum permissible power radiated to produce electric field strength ε at a distance of 305 meters (1000ft). This limit is 2.4/f (V/m) where f is the operating frequency. Thus at 100kHz the maximum allowable field strength at 305 meters is 24μV/m.

The radiated field strength ε for a dipole at a distance of R from the source is given by:

$$\varepsilon = \frac{120 \, \pi \, N}{R} \frac{AI}{\lambda^2} \, Cos \, \theta \qquad (7.7)$$

where A is the area enclosed by the loop, N is the number of turns and λ is the wavelength. For the transmitter structure discussed previously the field strength ε is below the specified limit at the 10 watt power level.

In the choice of the transmitter antenna size, if one takes as an objective the selection of antenna size which maximizes the magnetic field energy density at the transponder position, subject to the radiation field constraints but without regard to the transmitter power required, then the transmitter antenna becomes vanishingly small. Such structure cannot be used in practice because the power required to provide the interrogation energy density at the transponder position then tends to infinity. As a result of these considerations it can be concluded that an optimum situation is reached when the transmitter power is made as large as economic constraints allow, and the transmitter antenna is made small enough to meet the radiation constraint expressed by Equation (7.7).

7.6 Integration Approach

The last part of this research programme entailed studies of various low power technologies for integration of the passibe sub-harmonic device. Of the various possibilities considered the integrated injection logic (I^2L) showed the most promise.

The PST structure was designed using the layout diagrams shown in Figure 7.14 - 7.15 and was based upon minimum realisable photomech commensurate with manufacturability on the standard 7 mask bipolar process[129]. An integrated circuit layout was subsequently produced by R.C. Clarke using the software he developed
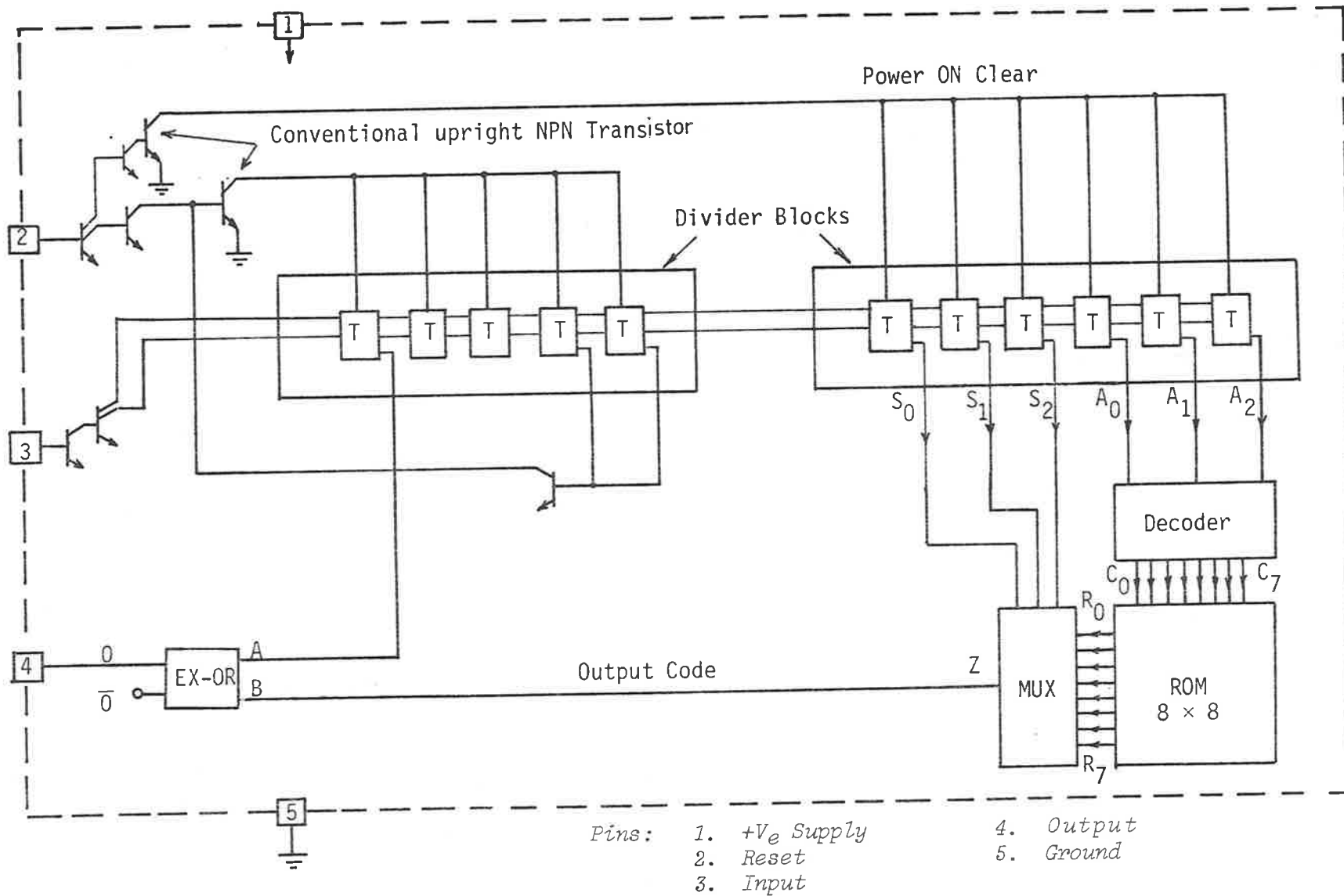
FIGURE 7.14. PST CIRCUIT USING INTEGRATED INJECTION LOGIC (I^2L).
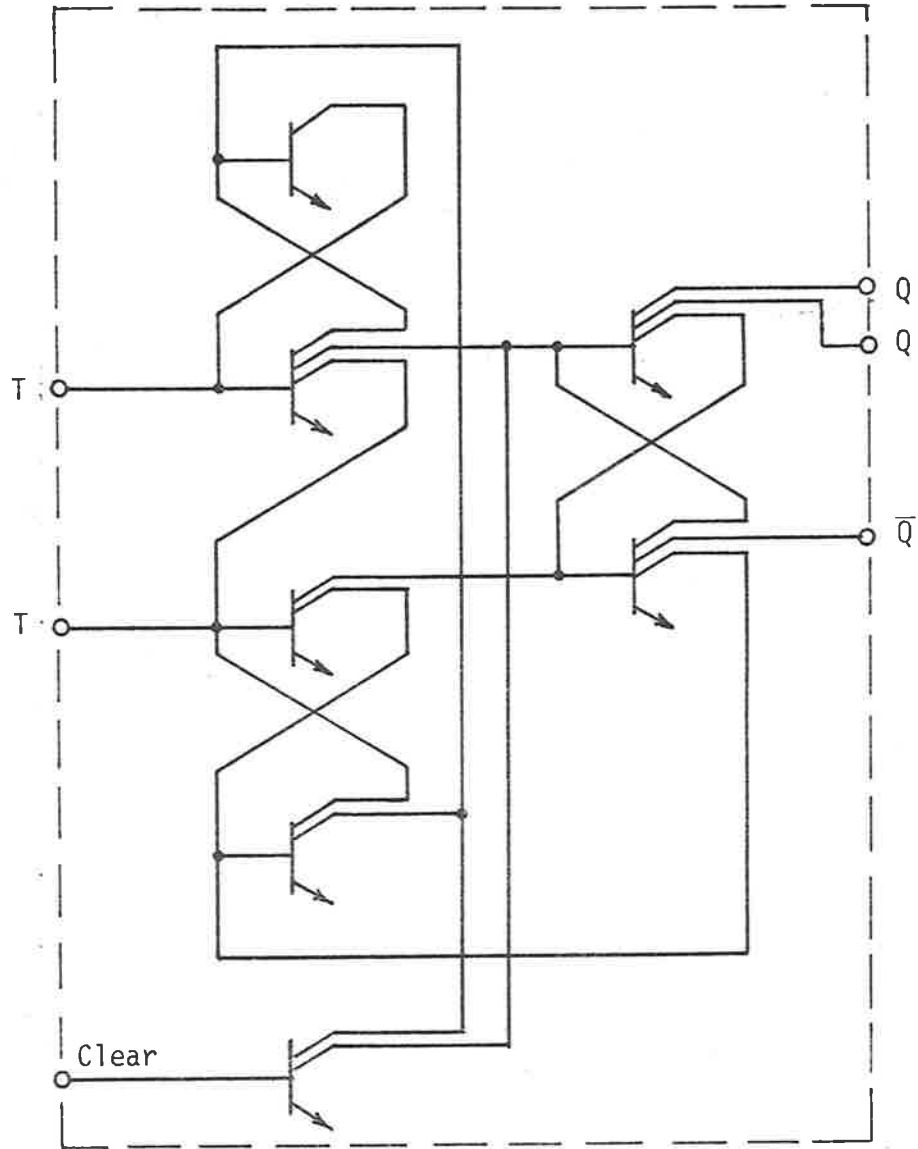
(a)
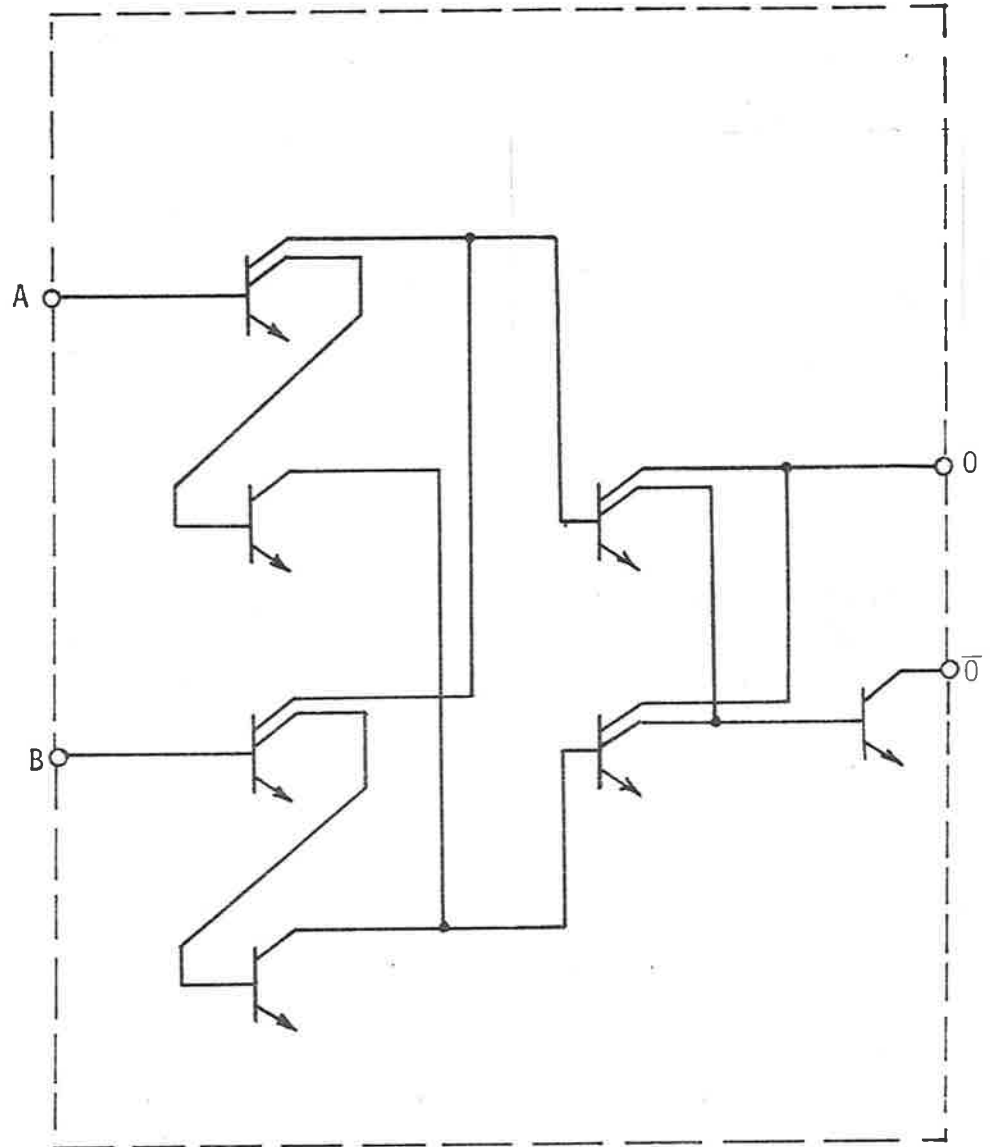
(b)

FIGURE 7.15. I^{2}L CIRCUIT DIAGRAM.

(a) Divide by Two D Flip-Flop.
(b) Exclusive OR.
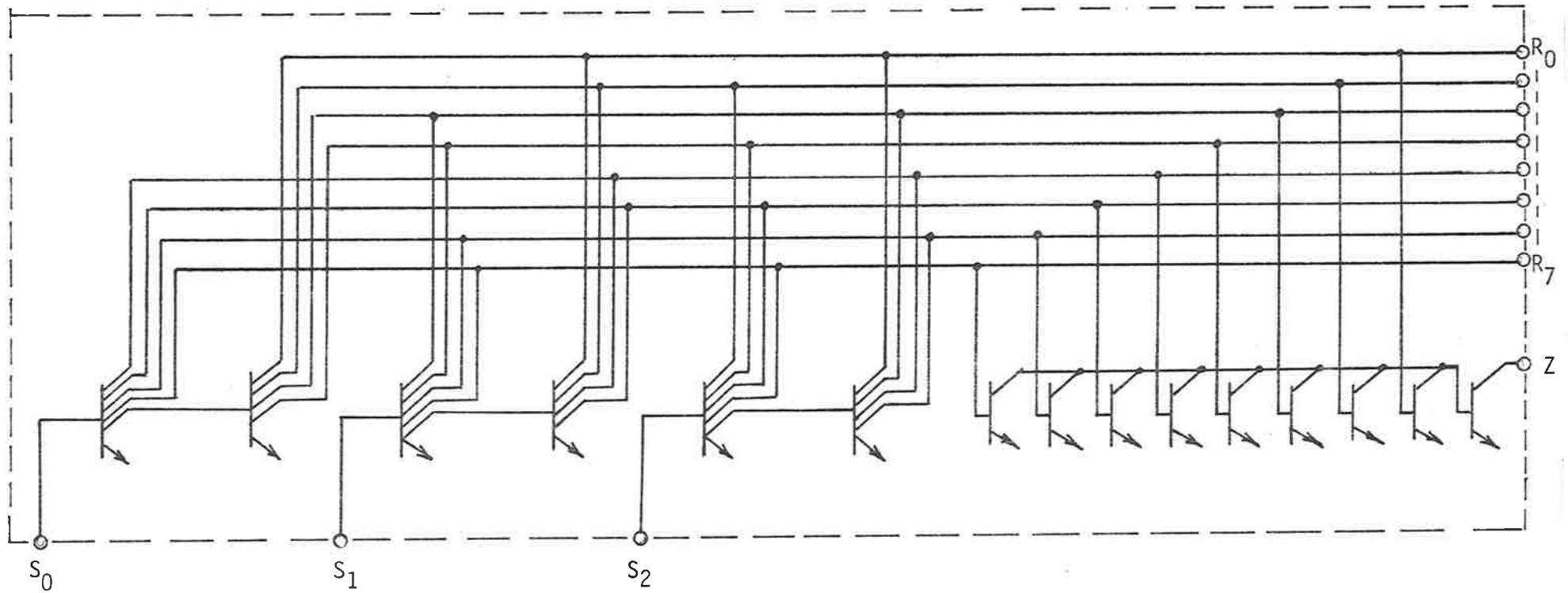
Note: 4 - 5 collector transistors are injected from both ends
to improve gain characteristics.

FIGURE 7.15 (c). I^2L CIRCUIT DIAGRAM FOR 8 LINE TO 1 LINE MULTIPLEXER.
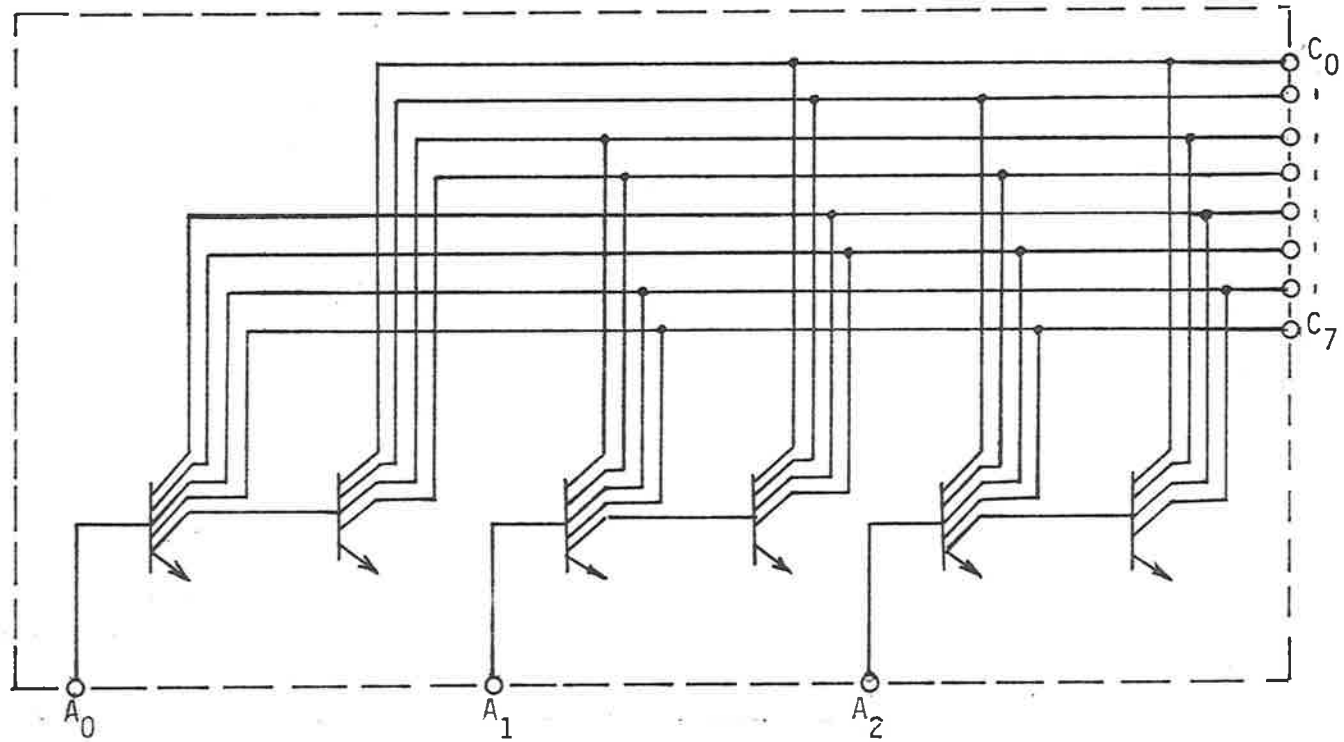
Note: *4 - 5 collector transistors are injected from both ends to improve gain characteristics.*

FIGURE 7.15 (d). I^2L CIRCUIT DIAGRAM FOR 3 LINE TO 8 LINE DECODER.

Note: <u>Read</u> <u>amplifiers</u> <u>enhanced</u> <u>PNP</u> <u>base</u> <u>width</u> <u>to</u> <u>reduce</u> <u>injected</u> <u>current</u> which permit 8 collectors in ROM section.
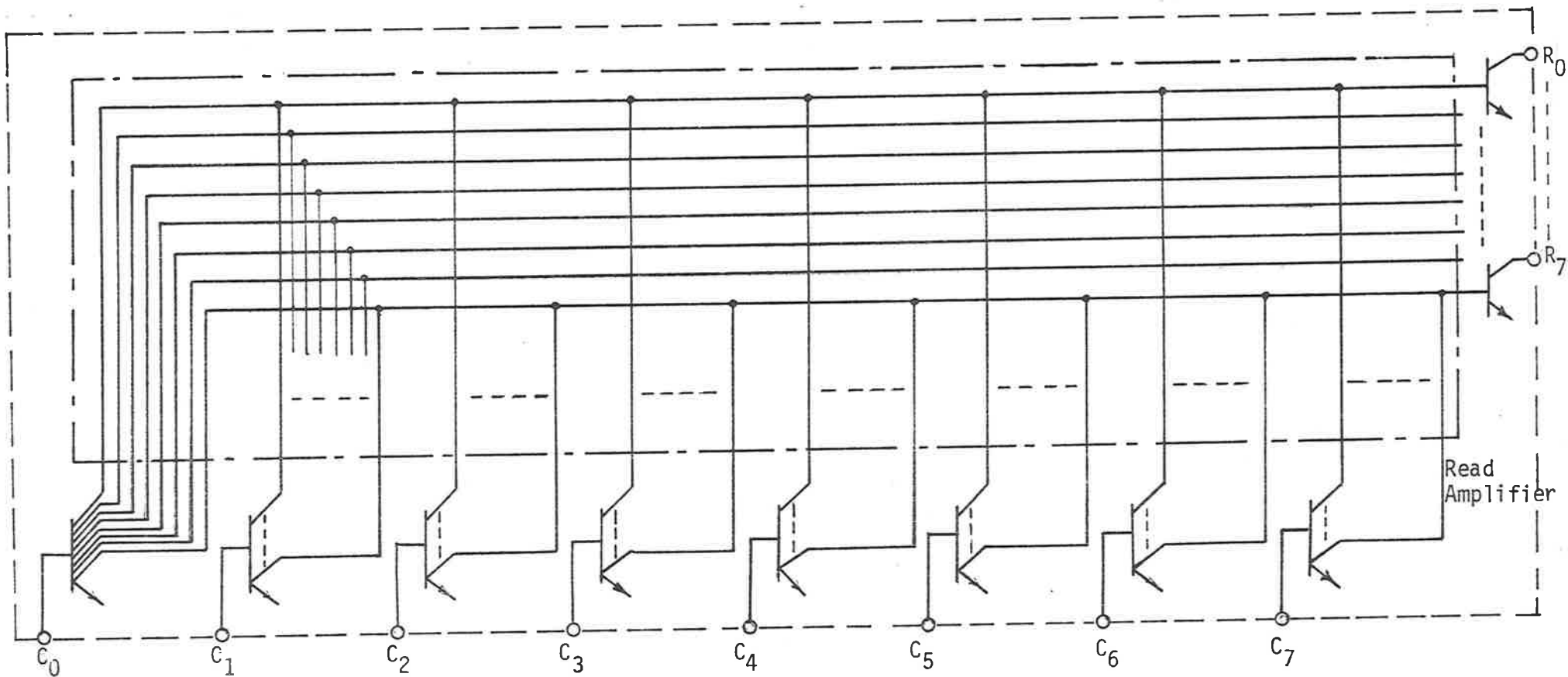
FIGURE 7.15 (e). I^2L CIRCUIT DIAGRAM FOR 64 BIT MASK PROGRAMMABLE ROM.

for mask productions. The chip layout is illustrated by Figure 7.16. The mask programmable 64-bit ROM section of the chip is also illustrated by Figure 7.17 and is based on Bergmann's work[130]. In order to estimate the power dissipated by the device one notes that only a very small number of gates operate at 100kHz. Thus for the above configuration an upper limit of approximately 20µW can be expected[139 - 140]. Therefore further improvement in the conversion factor η' can be realised.

Currently a field programmable version of the circuit is under development.

7.7 Summary and Conclusions

The investigation into the practical realisation of passive subharmonic transponders for vehicle identification and location determination, suitable for remote interrogation, was conducted in several phases. The first phase was concerned with gaining an insight into the general characteristic of power transfer and the constraints imposed on operational performance of the two-port passive subharmonic structure.

The results derivable from the analysis of the power transfer between resonated coupling elements acting in the near field region indicated that the power transfer is enhanced by having each tuned by connection to the complimentary storage element, and is in fact proportional to the product of the quality factors with which each
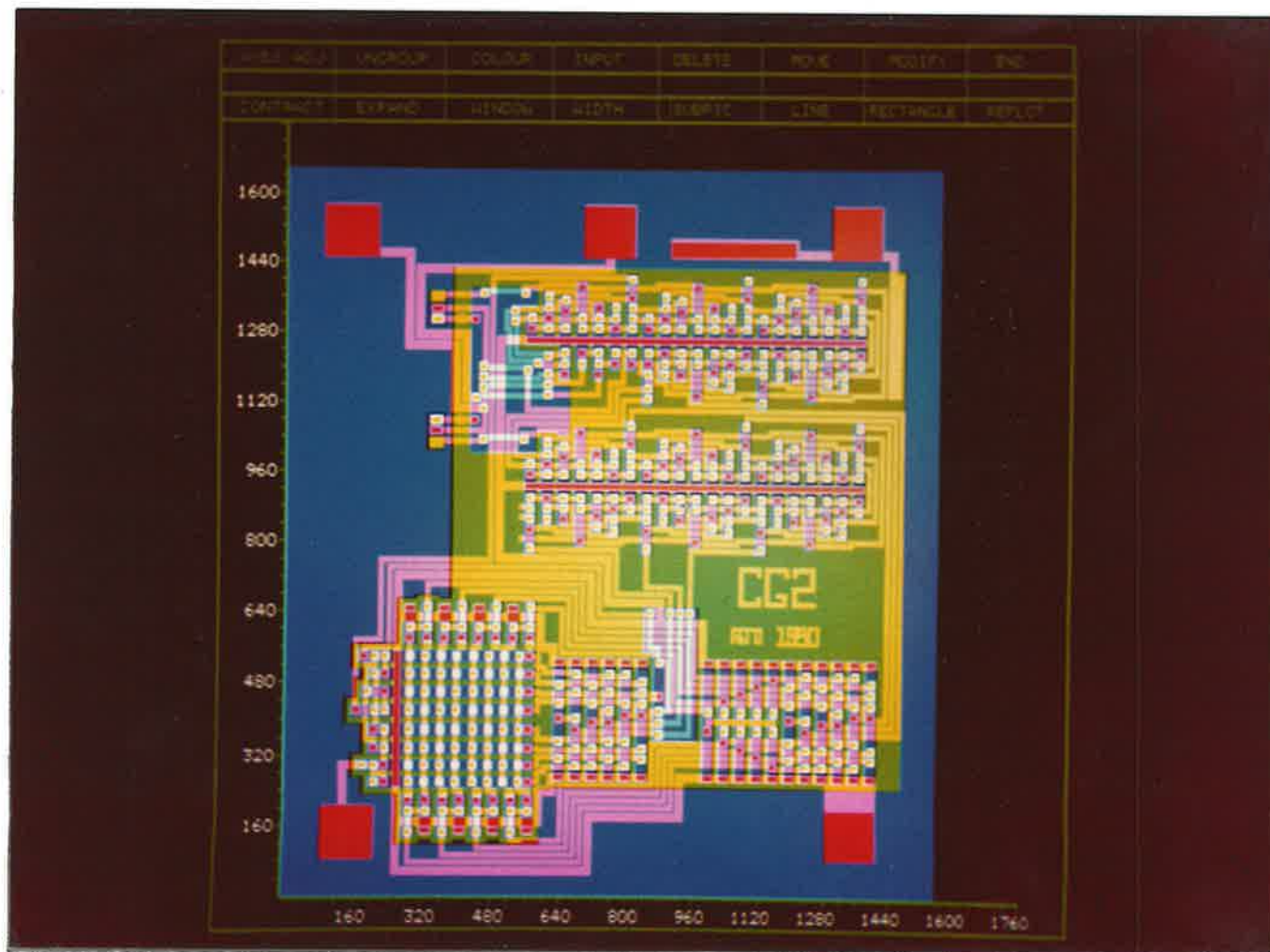
FIGURE 7.16.   INTEGRATED INJECTION LOGIC CHIP DETAIL OF PST.
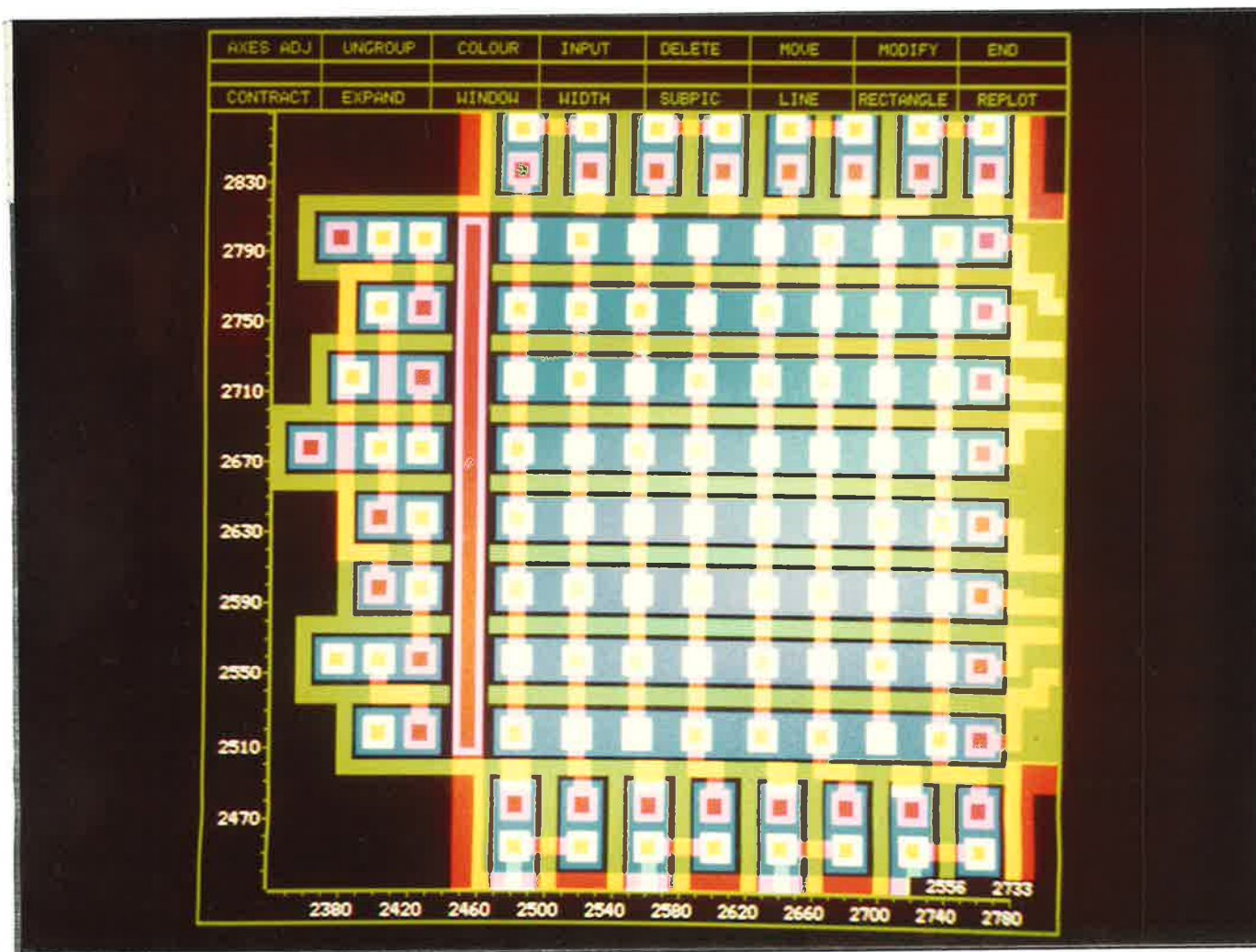
FIGURE 7.17.   CHIP DETAIL OF 64 BIT ROM.

of the two coupled elements is tuned. Applying the above results
to the problem of power transfer from the interrogation antenna
to the transponder it was observed that the real power available
in the transponder is maximized by forming a resonant circuit of
the highest possible quality factor at the energising frequency
between the transponder coupling element and its complimentary
energy storage element. A further basic result was that the ratio
of reactive power at the reply frequency in the tuned circuit con-
taining the transponder coupling element to the real power re-
quired to sustain the resonance is the well-known quality factor
of the resonance.

On the basis of the above analysis several factors which
limited the performance of the two-port PST were recognised. The
first being that the system performance was sensitiviely dependent
upon the total volume which could be allocated to the device
antennas. In applications where transponder volume must be kept
small the competition between the receptor and transponder antennas
for the available space is unwelcome.

The second factor which was noted related to the conversion
of the received power first to d.c. before being converted to the
subharmonic frequency. This was particularly relevant when low
levels of excitation voltage prevail. A third and very significant
limitation is that the quality factor of the transponder antenna is
frequently limited by considerations of communication bandwidth to
a value much less than can be achieved in resonant circuits of the
allowed size at the working frequency. This limitation was seen to
be inappropriate since the strength of coupling between near field

antennas is established by stored energy rather than the dissipated power within them, and operation of the transponder antenna at a higher quality factor would enhance the transfer of power across reply link. Based on these limitations a novel and original principle for subharmonic frequency generation and modulation using a one-port structure was developed.

In this structure the reply signal energy is not injected into the coupling element from a d.c. reservoir as in the previous cases but rather it is synthesized, without prior conversion to d.c., by switches and control elements which operate at appropriate instances of time to modulate the energy exchange process between the transponder near-field coupling element and its complimentary energy storage element with which it is resonated. In the present structure similar relationship between the quality factor of the resonance circuit and the electromagnetic losses can be obtained. However the requirements of the communication bandwidth and the quality factor of the resonance circuit no longer exists due to the switching technique used in the modulation process such that the energy exchange process between the energy storage elements of the transponder is not disturbed by the modulation.

The result of this approach is of particular significance since it is now possible to make the quality factor of the transponder as high as practicable and only the quality factor of the receiver need be limited by the modulation bandwidth considerations.

Based on the above finding the second phase entailed the development of simple modelling principles in order to describe

the performance of the one-port transponder. The consequence of this portion of the work resulted in following conclusions that if the losses during the period in which the oscillation in the transponder antenna is suspended are made small, the power transfer across the electromagnetic link may be described in terms of the unswitched transponder tuned circuit quality factor. The second factor which has emerged is that of all the possibilities that exist in the synthesis and modulation of the first subharmonic frequency there are only two basic patterns that remain which satisfy the requirements of continual power flow at the interrogation frequency, require only a single switching element (to ensure losses are minimised), and provide binary phase modulation through two rotations of the basic pattern.

The third phase was concerned with detailed analysis of various antenna structures in order to enable the separation of the influence of different antenna parameters on the coupling and hence permit appropriate local optimization to be performed. The desired separation of the effects of different antenna geometries on power transfer ratio was achieved by recognising that in the weak coupling situation the basic excitation mechanism for the transponder antenna is the magnetic field created by the transmitter antenna. This led into the development of the coupling volume and dispersal volume concepts. The modelling principles which were developed has established the framework on which appropriate local optimizations based on geometries of individual · antennas can be performed. The analysis provided an insight into the effect of antenna parameters on system performance and enabled conclusions on the general shapes that can be utilized for practical

systems to be drawn.

The coupling and dispersal volumes are dependant on the geometries of the antennas which are individually subject to optimization whereas the quality factors indicate how efficient the transfer of power can be made. The advantage of the above mathematical model is its analytical simplicity which provide for rapid computations in assessing the performance of a particular antenna structure and in estimation of the power transfer ratio.

The next phase was concerned with the practical considerations where the transponder was required to operate in the proximity of a conducting body. To expedite this approach a mathematical model for the power transfer was developed. Although it was recognised that planar coils do not perform as well as the corresponding ferrite slabs when brought near a conducting body it was decided to persue the matter in order to define the boundries for satisfactory operation. For this purpose a small square planar coil of sides 100mm and a ferrite slab of dimension 55.7 × 51.1mm × 6.9mm were chosen. Theoretical work supported by experimental results indicated that both structures were equivalent in terms of power transfer characteristics when used as sign post embedded in the road surface.

In the research programme it was recognised that perhaps the most pressing practical problem likely to be encountered was the achievement of an adequate signal-to-noise ratio at the receiver to permit sufficiently reliable code detection. To this end noise data were gathered and subsequently were used in estimating the overall system performance.

318.

The final phase included the construction of a one-port PST device based on discrete components, development of the interrogation system, and practical implementation of the PST for both vehicle identification and vehicle location systems. For the kind of geometries, power levels and environments described previously a one-port PST returning a 64-bit coherent PSK reply code with 8 carrier cycles per bit, an average of one-bit error can be expected for every twelve messages when operated at a sensing distance of 500mm from the interrogation source. This result is entirely satisfactory and provides for realisation of simple receiver structures.

The use of one-port passive subharmonic transponder for the kind of operating environment that may be encountered in traffic monitoring and surveillance systems has been successfully demonstrated. It has been shown that this technology is suitable and can be implemented effectively in both the vehicle identification and sign post applications.

APPENDIX A

IMAGE VOLTAGE

A.1   Derivation of Image Voltage V_p [20]

Referring to the co-ordinate system of Figure A.1 the magnetic field components for a small dipole can be expressed as[97]

$$H_\theta = \frac{m\ e^{-j\gamma r}}{4\pi} \left[\frac{1}{r^3} + \frac{j\gamma}{r^2} - \frac{\gamma^2}{r} \right] \text{Sin } \theta \qquad (A.1)$$

$$H_r = \frac{m\ e^{-j\gamma r}}{2\pi} \left[\frac{1}{r^3} + \frac{j\gamma}{r^2} \right] \text{Cos } \theta \qquad (A.2)$$

where

$m = NIA$

$A = \pi a^2$

$\gamma = \frac{\omega}{\sqrt{\mu t}}$

N = number of turns

For the frequency range of interest; i.e. at 100KHz,
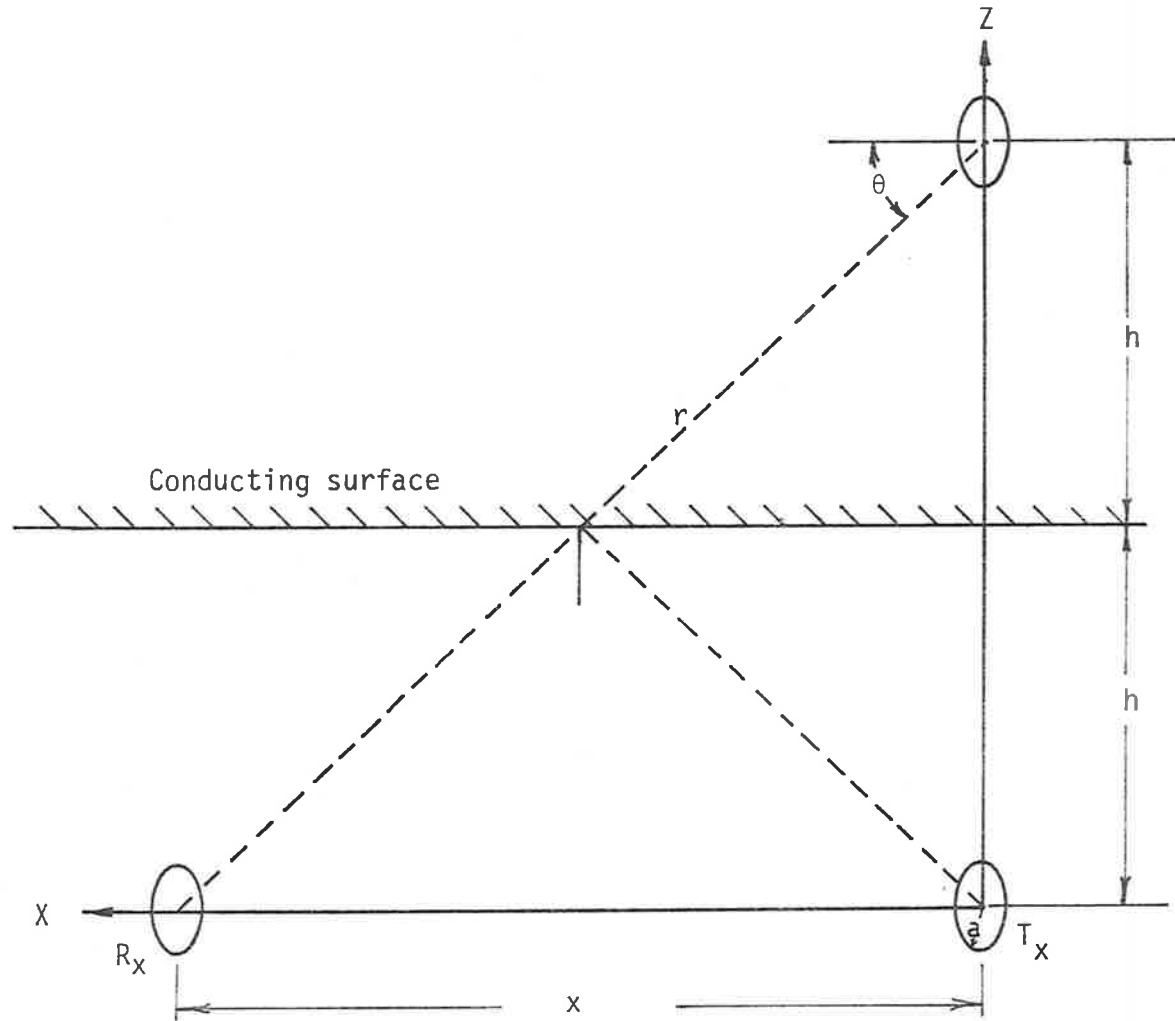
FIGURE A.1.   GEOMETRY ASSOCIATED WITH THE COORDINATE SYSTEM IN THE XZ PLANE

TABLE B.8. NORMALIZED DISTANCE MEASURE D_r USING FEATURE VECTOR ${}_b^i\tilde{x}$

D_r	Ford	Centura	Datsun	Volvo	Hillman	Valiant	Mazda	VW	Holden	Cortina	Lancer	Fiat	Escort	Ford Truck
Ford	0	0.97	0.68	1.0	1.07	0.61	1.58	0.93	1.07	1.22	0.86	1.03	1.32	1.39
Centura	0.97	0	1.31	1.32	1.25	1.14	1.32	1.46	1.46	1.60	1.03	0.76	1.14	1.58
Datsun	0.68	1.31	0	0.93	0.86	0.61	1.58	0.64	1.00	1.29	0.93	1.03	1.46	1.25
Volvo	1.0	1.32	0.93	0	0.93	0.97	1.42	0.71	0.64	1.22	0.71	1.10	0.68	0.61
Hillman	1.07	1.25	0.86	0.93	0	0.97	0.93	1.00	0.68	0.83	0.86	0.90	1.39	1.46
Valiant	0.61	1.14	0.61	0.97	0.97	0	1.68	0.91	1.19	1.03	0.68	0.93	1.29	1.36
Mazda	1.58	1.32	1.58	1.42	0.93	1.68	0	1.36	1.00	1.15	1.29	1.32	1.19	1.19
VW	0.93	1.46	0.64	0.71	1.00	0.97	1.36	0	0.78	1.14	0.86	1.03	1.19	1.10
Holden	1.07	1.46	1.00	0.64	0.68	1.19	1.00	0.78	0	0.90	0.93	1.32	0.75	0.90
Cortina	1.22	1.60	1.29	1.22	0.83	1.03	1.15	1.14	0.90	0	0.93	0.90	1.03	1.32
Lancer	0.86	1.03	0.93	0.71	0.86	0.68	1.29	0.86	0.93	0.93	0	0.90	0.88	1.03
Fiat	1.03	0.76	1.03	1.10	0.90	0.93	1.32	1.03	1.32	0.90	0.90	0	1.14	1.68
Escort	1.32	1.14	1.46	1.68	1.39	1.29	1.19	1.19	0.75	1.03	0.88	1.14	0	0.81
Ford Truck	1.39	1.58	1.25	0.61	1.46	1.36	1.19	1.10	0.90	1.32	1.03	1.68	0.81	0

$\gamma r \ll 1$, therefore Equation (A.1) and Equation (A.2) reduce to

$$H_\theta = \frac{m}{4\pi r^3} \, \text{Sin} \, \theta \tag{A.3}$$

$$H_r = \frac{m}{4\pi r^3} \, \text{Cos} \, \theta \tag{A.4}$$

Thus the field intensity is asymptotic to an inverse cubic law. The components H_z and H_x can be expressed as

$$H_z = \frac{m}{4\pi r^3} \left(3 \, \text{Cos}^2 \, \theta - 1 \right) \tag{A.5}$$

and

$$H_x = \frac{3m}{4\pi r^3} \, (\text{Sin} \, \theta \, \text{Cos} \, \theta) \tag{A.6}$$

With $\quad\quad\quad r^2 = 4h^2 + x^2 \tag{A.7}$

and

$$\text{Cos} \quad = \frac{x}{r} \tag{A.8}$$

322.

the magnetic field at the receiver coil due to the image coil is given by

$$H_{x_i} = \frac{N\,I\,a^2}{2} \left(\frac{x^2 - 2h^2}{\left[\left(4h^2 - x^2\right)\right]^{5/2}} \right) \qquad (A.9)$$

The induced voltage, e_i in a closed path in terms of the magnetic vector potential, $\tilde{A}$, is

$$e_i = - \frac{d}{dt} \oint_C \tilde{A}.d\tilde{\ell} \qquad (A.10)$$

$$e_i = - \frac{d}{dt} \oint_S \tilde{B}.d\tilde{S} \qquad (A.11)$$

where S is any surface bounded by the path, C, whose element is $d\tilde{\ell}$. For a circular loop of radius a, the rms value of e_i, corresponding to sinusoidal magnetic field intensity, $\tilde{H}$, is

$$E_i = -j\,\omega\,\pi\,a^2\,\mu_e\,H \qquad (A.12)$$

where $\omega = 2\pi f$, f being the frequency in Hz and μ_e the effective permeability of receiver coil. Therefore for a loop having N turns, the change in induced voltage, V_p, due to the presence of the conducting body can be expressed as

324.

$$V_p = K_i \left[\frac{x^2 - 2h^2}{\left(4h^2 + x^2\right)^{5/2}} \right] \qquad \text{(A.13)}$$

where

$$K_i = \frac{1}{2} \left[N^2 \, \omega \, I \, \pi \, a^4 \, \mu_e \right] \qquad \text{(A.14)}$$

The effective permeability μ_e used in Equation (A.14) takes into consideration the demagnetisation effect when ferrite material is used in the coils and its value is obtained empirically for a given structure.

APPENDIX B

VEHICLE SIGNATURE ANALYSIS

B.1 Frequency Domain Analysis

(a) Figure B.1 (a) - (c) illustrates signatures, differentiated signals and binary representation of the zero crossings of the differentiated signals for three different vehicles, i.e. 1972 Ford Futura, 1976 Chrysler Centura and 1976 Datsun 180B for several runs when the lateral displacement from the centre of the vehicle sensor is controlled within ±25cm.

(b) Table B.1 illustrates normalized Fourier components of the feature vector $\frac{i}{c}\tilde{X}$ for fourteen different vehicles, i.e. V_i, i = 1, 2, ..., 14. Only magnitudes which are greater than 0.1 are considered.

(c) Table B.2 (a) - (c) illustrates the normalized Fourier components of the feature vector $\frac{i}{c}\tilde{X}$ for several runs of three vehicles makes and models. The elements of the tables correspond to the signatures of Figure B.1 (a) - (c).
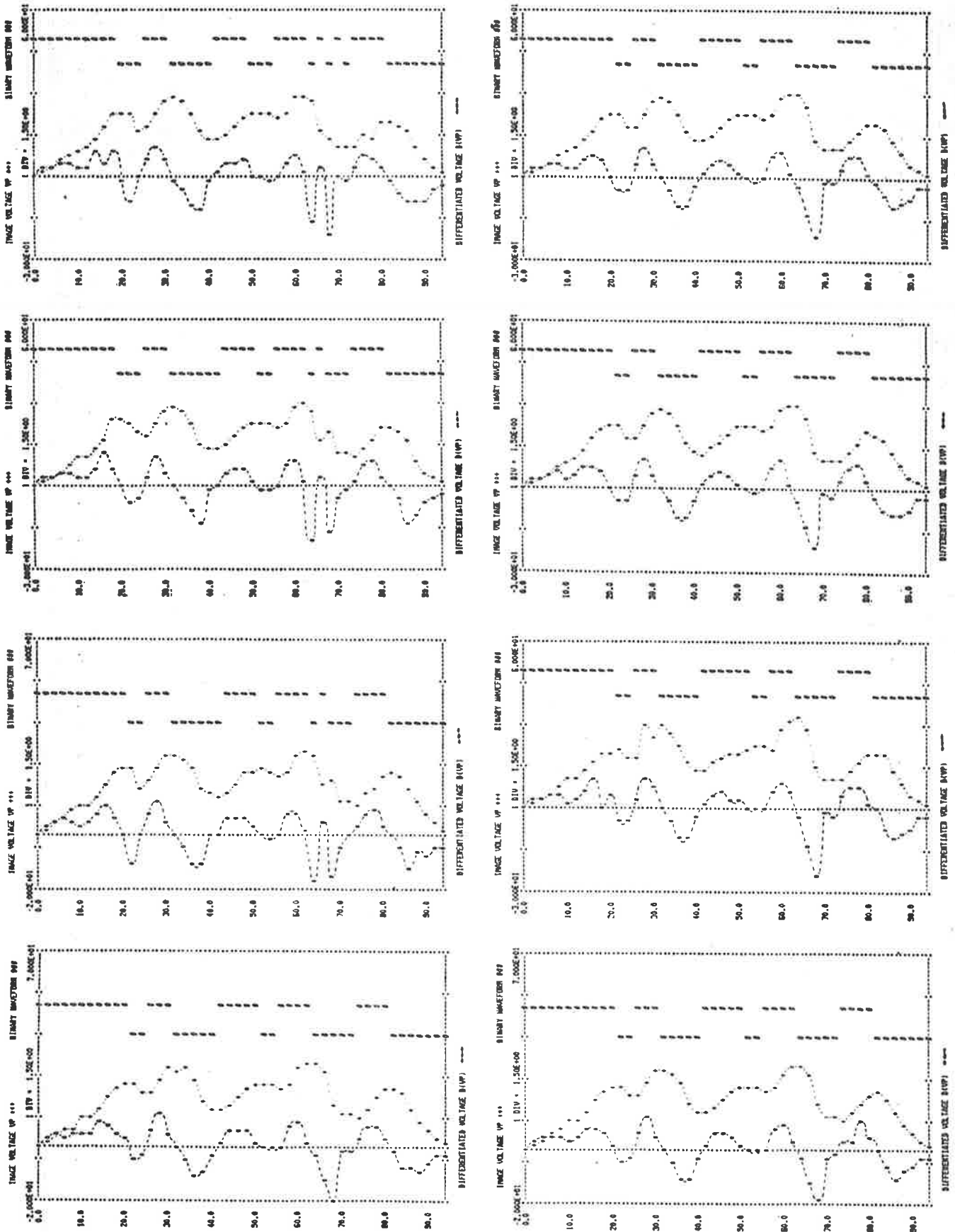
FIGURE B.1 (a). SIGNATURE, DIFFERENTIATED SIGNAL AND BINARY REPRESENTATION OF THE ZERO CROSSINGS OF THE DIFFERENTIATED SIGNAL FOR 1972 FORD FUTURE, CORRESPONDING TO 8 TRIALS WHEN THE LATERAL DISPLACEMENT IS CONTROLLED WITHIN ±25cm.
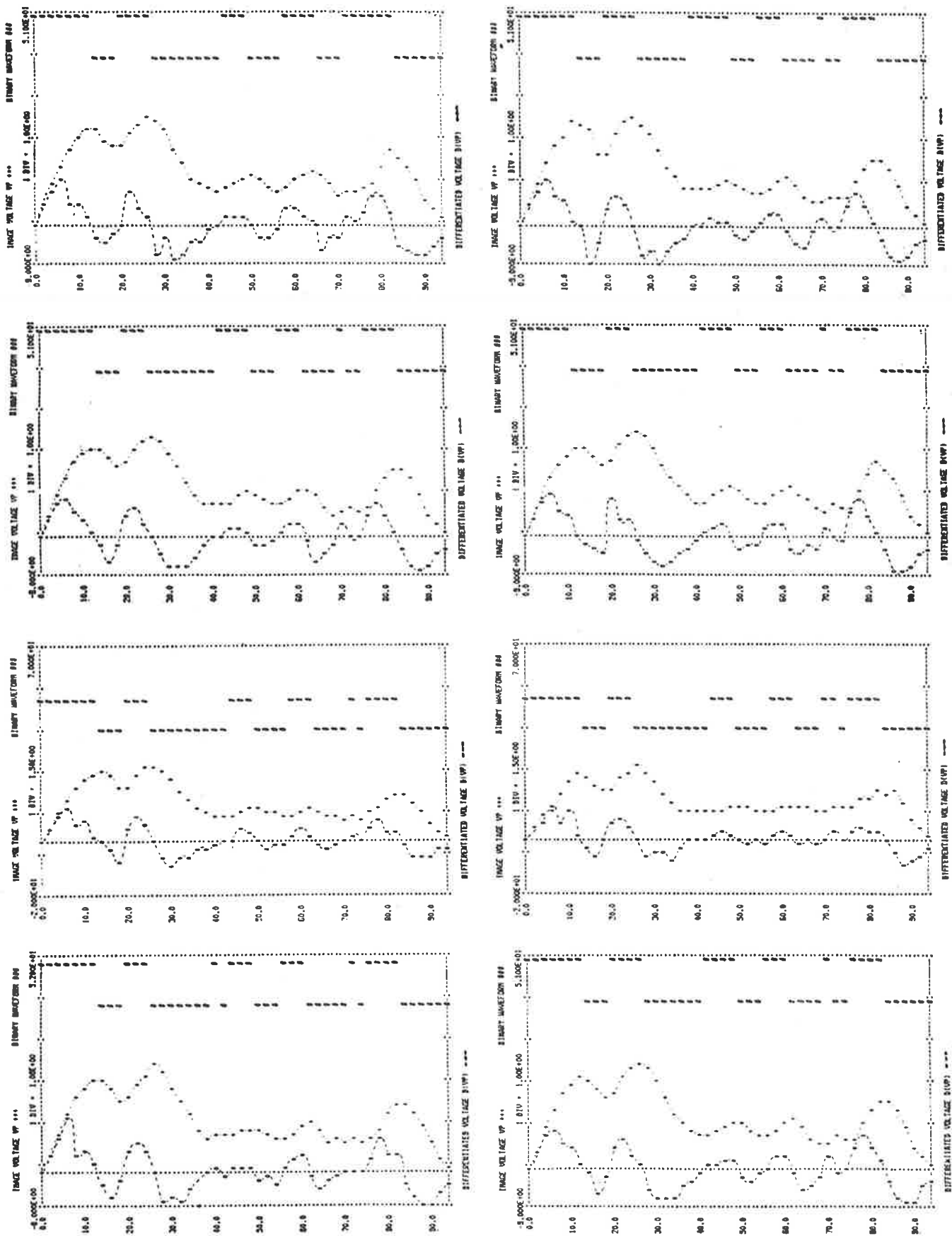
FIGURE B.1 (b). SIGNATURE, DIFFERENTIATED SIGNAL AND BINARY REPRESENTATION OF THE

ZERO CROSSINGS OF THE DIFFERENTIATED SIGNAL FOR 1976 CHRYSLER CENTURE CORRESPONDING

TO 8 TRIALS WHEN THE LATERAL DISPLACEMENT IS CONTROLLED WITHIN ±25cm.
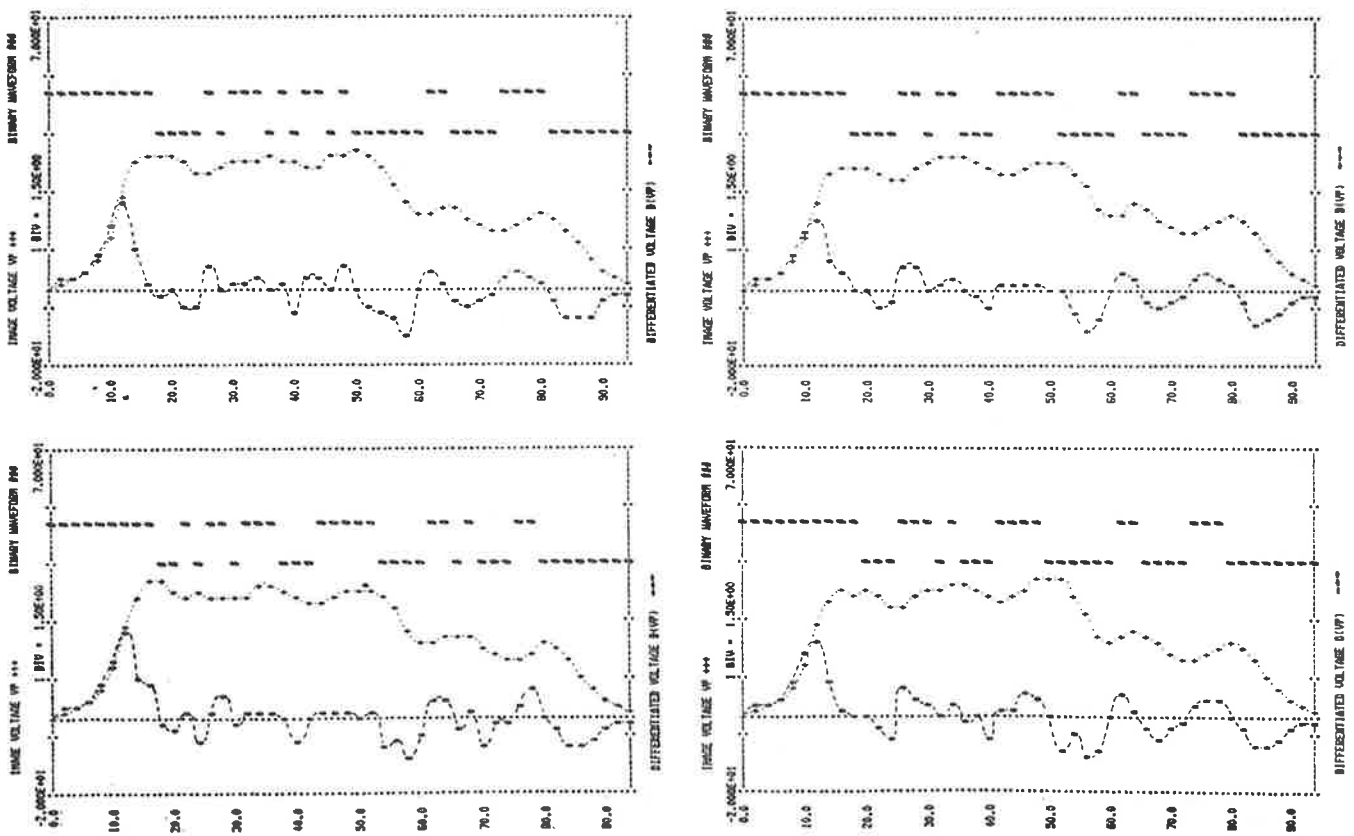
FIGURE B.1 (c).   SIGNATURE, DIFFERENTIATED SIGNAL AND BINARY REPRESENTATION OF THE

ZERO CROSSINGS OF THE DIFFERENTIATED SIGNAL FOR 1976 DATSUN 180B CORRESPONDING TO

4 TRIALS WHEN THE LATERAL DISPLACEMENT IS CONTROLLED WITHIN ±25cm.

TABLE B.1. NORMALIZED FOURIER COEFFICIENTS $\frac{i\tilde{x}}{c}$ FOR SEVERAL SIGNATURES

$\frac{i\tilde{x}}{c}$ $\tilde{V}$	NORMALIZED FOURIER COEFFICIENT											
	c_1	c_2	c_3	c_4	c_5	c_6	c_7	c_8	c_9	c_{10}	c_{11}	c_{12}
Ford	1.0	0.65	0.48	0.50	0.22	0.44	0.20	0	0.11	0	0	0
Centura	1.0	0.72	0.52	0.50	0.61	0	0	0.13	0	0.10	0	0
Datsun	1.0	0.33	0.40	0.15	0.11	0.16	0	0	0	0	0	0
Volvo	1.0	0.73	0.27	0.24	0	0	0	0.10	0	0	0	0
Hillman	1.0	0.41	0.78	0.13	0	0.22	0	0.10	0	0	0	0
Valiant	1.0	1.30	0.97	0.91	0.49	0.55	0.12	0	0.11	0	0	0
Mazda	1.0	0.84	0.86	0.15	0	0.16	0.11	0	0	0	0	0
VW	1.0	0.21	0.26	0	0	0	0	0	0	0	0	0
Holden	1.0	1.38	0.85	1.11	0.64	0	0.30	0	0.13	0.17	0	0.16
Cortina	1.0	0.36	0.44	0.19	0	0	0.19	0.12	0	0	0	0
Lancer	1.0	0.87	0.88	0.55	0	0.23	0.16	0	0	0	0	0
Fiat	1.0	0.14	0.25	0.23	0.23	0	0	0	0	0	0	0
Escort	1.0	0.49	0.10	0.16	0	0	0	0	0	0	0	0
Ford Truck	1.0	1.18	0.66	0.41	0.29	0.20	0.13	0	0	0	0	0

TABLE B.2. COMPONENTS OF FEATURE VECTOR $^i_c\tilde{X}$ FOR SEVERAL TRIALS WHEN LATERAL DISPLACEMENT IS CONTROLLED WITHIN ±25 cm

$^i_c\tilde{X}$ Norm Freq.	Ford (No. of Trials)								$\hat{C}$	σ_c
	0	a	b	c	d	e	f	g		
1	1.0	1.0	1.0	1.0	1.0	1.0	1.0	1.0	1.0	0.0
2	0.65	0.67	0.64	0.61	0.68	0.65	0.65	0.66	0.65	0.02
3	0.48	0.55	0.56	0.53	0.50	0.47	0.47	0.45	0.50	0.04
4	0.50	0.51	0.53	0.53	0.53	0.49	0.48	0.51	0.51	0.02
5	0.23	0.19	0.19	0.17	0.22	0.21	0.23	0.27	0.21	0.03
6	0.44	0.42	0.42	0.40	0.46	0.45	0.44	0.43	0.43	0.02
7	0.20	0.21	0.22	0.24	0.19	0.18	0.17	0.15	0.20	0.03
8	0.08	0.05	0.08	0.04	0.07	0.06	0.07	0.10	0.07	0.02
9	0.11	0.15	0.14	0.12	0.10	0.09	0.11	0.11	0.11	0.02
10	0.03	0.03	0.03	0.01	0.03	0.03	0.04	0.07	0.03	0.02
11	0.05	0.06	0.06	0.05	0.06	0.05	0.05	0.05	0.05	0.01
12	0.01	0.06	0.07	0.03	0.01	0.01	0.02	0.01	0.03	0.02

$^i_c\tilde{X}$ Norm Freq.	Centura (No. of Trials)								$\hat{C}$	σ_c
	0	a	b	c	d	e	f	g		
1	1.0	1.0	1.0	1.0	1.0	1.0	1.0	1.0	1.0	0.0
2	0.72	0.79	1.21	0.79	0.79	0.89	0.74	0.68	0.82	0.16
3	0.52	0.52	0.82	0.56	0.51	0.49	0.52	0.46	0.55	0.11
4	0.50	0.46	0.53	0.50	0.42	0.49	0.49	0.47	0.48	0.03
5	0.61	0.66	0.78	0.65	0.53	0.69	0.62	0.56	0.64	0.07
6	0.09	0.16	0.28	0.05	0.09	0.01	0.08	0.12	0.11	0.08
7	0.02	0.03	0.10	0.02	0.10	0.08	0.02	0.04	0.05	0.03
8	0.13	0.13	0.19	0.14	0.15	0.12	0.15	0.14	0.14	0.02
9	0.04	0.04	0.07	0.07	0.05	0.02	0.05	0.04	0.05	0.02
10	0.10	0.12	0.07	0.07	0.08	0.07	0.09	0.11	0.09	0.02
11	0.03	0.02	0.03	0.04	0.03	0.06	0.04	0.02	0.03	0.01
12	0.04	0.011	0.02	0.03	0.04	0.03	0.04	0.04	0.03	0.01

$_c^i\tilde{X}$ Norm Freq.	Datsun (No. of Trials)								$\hat{C}$	σ_c
	0	a	b	c	d					
1	1.0	1.0	1.0	1.0	1.0				1.0	0.0
2	0.33	0.31	0.30	0.34	0.36				0.33	0.02
3	0.40	0.43	0.40	0.37	0.40				0.40	0.05
4	0.15	0.14	0.12	0.15	0.14				0.14	0.03
5	0.11	0.12	0.12	0.10	0.12				0.11	0.03
6	0.16	0.16	0.19	0.17	0.15				0.17	0.02
7	0.09	0.09	0.08	0.08	0.11				0.09	0.03
8	0.03	0.04	0.04	0.04	0.02				0.09	0.02
9	0.03	0.03	0.02	0.03	0.04				0.04	0.02
10	0.01	0.02	0.01	0.02	0.03				0.02	0.01
11	0.05	0.04	0.05	0.04	0.03				0.04	0.02
12	0.04	0.03	0.02	0.03	0.01				0.03	0.02

(d) Table B.3 (a) - (c) show the normalized components of feature vector $_d^i\tilde{X}$ derived from the differentiated signatures corresponding to the signatures of Figure B.1 (a) - (c) for several runs under controlled lateral displacement.

B.2 Time Domain Analysis

(a) Tables B.4 and B.5 illustrate the components of the elements of the feature vector $_b^i\tilde{X}$ derived from the binary representation of the zero crossings of the differentiated signal corresponding to file 1 and file 2 respectively. The components of $_b^i\tilde{X}$ are obtained by dividing the binary waveform into N equally spaced segments and then allocating either a 'one' or a 'zero' to the components depending on the status of the binary waveform.

Several values of N were considered. It was found the minimum value of N that can be tolerated without introducing noticeable errors was 90. Therefore N was set to 96 corresponding to 12 × 8-bit words.

The data in the tables are given in hexadecimal format for ease of representation.

(b) Table B.6 shows the components of undercarriage vector $_u^i\tilde{X}$ derived from the relation

$$^i u_k = \frac{^i q_k}{t_p} \; ; \quad k = 1, 2, \ldots \tag{B.1}$$

333.

TABLE B.3. COMPONENTS OF THE FEATURE VECTOR $_d^i\tilde{x}$ DERIVED FROM
THE DIFFERENTIATED SIGNATURE WAVEFORMS

$_d^i\tilde{x}$ Norm Freq.	Ford (No. of Trials)								Mean
	0	a	b	c	d	e	f	g	
1	1.0	1.0	1.0	1.0	1.0	1.0	1.0	1.0	1.0
2	1.30	1.34	1.28	1.21	1.36	1.30	1.30	1.32	1.3
3	1.41	1.64	1.67	1.58	1.48	1.40	1.40	1.32	1.48
4	1.98	2.02	2.10	2.10	2.09	1.93	1.91	2.00	2.02
5	1.11	0.94	0.94	0.85	1.08	1.04	1.13	1.34	1.05
6	2.58	2.48	2.45	2.35	2.72	2.64	2.57	2.49	2.54
7	1.32	1.43	1.50	1.64	1.29	1.20	1.16	1.00	1.32
8	0.57	0.39	0.57	0.29	0.56	0.47	0.52	0.78	0.52
9	0.93	1.24	1.15	0.99	0.87	0.78	0.92	0.90	0.97
10	0.26	0.31	0.31	0.11	0.24	0.27	0.33	0.62	0.31
11	0.48	0.65	0.57	0.59	0.55	0.51	0.51	0.48	0.54
12	0.09	0.59	0.70	0.34	0.08	0.09	0.16	0.08	0.27

$_d^i\tilde{x}$ Norm Freq.	Centura (No. of Trials)								Mean
	0	a	b	c	d	e	f	g	
1	1.0	1.0	1.0	1.0	1.0	1.0	1.0	1.0	1.0
2	1.46	1.57	2.37	1.57	1.59	1.78	1.51	1.38	1.65
3	1.62	1.53	2.38	1.74	1.55	1.49	1.61	1.42	1.67
4	2.00	1.83	2.06	2.02	1.67	1.95	1.98	1.88	1.92
5	3.08	3.23	3.77	3.26	2.64	3.43	3.11	2.78	3.16
6	0.58	0.91	1.59	0.34	0.53	0.09	0.52	0.72	0.66
7	0.16	0.21	0.67	0.19	0.70	0.55	0.18	0.29	0.37
8	1.02	0.97	1.44	1.05	1.11	0.88	1.14	1.10	1.09
9	0.37	0.33	0.62	0.59	0.41	0.16	0.44	0.35	0.41
10	0.98	1.14	0.59	0.68	0.80	0.63	0.85	0.99	0.83
11	0.29	0.22	0.29	0.36	0.30	0.60	0.40	0.24	0.34
12	0.40	0.13	0.27	0.32	0.42	0.25	0.43	0.48	0.34

$_d^i\tilde{X}$ Norm Freq.	Datsun (No. of Trials)								Mean
	0	a	b	c	d				
1	1.0	1.0	1.0	1.0	1.0				1.00
2	0.66	0.60	0.59	0.67	0.71				0.65
3	1.16	1.27	1.19	1.08	1.19				1.19
4	0.60	0.54	0.48	0.58	0.53				0.55
5	0.51	0.92	0.59	0.50	0.55				0.61
6	0.96	0.59	1.12	0.99	0.89				0.91
7	0.57	0.32	0.53	0.54	0.71				0.53
8	0.25	0.28	0.29	0.30	0.13				0.25
9	0.28	0.13	0.15	0.25	0.32				0.23
10	0.12	0.39	0.08	0.13	0.28				0.20
11	0.45	0.27	0.44	0.44	0.26				0.31
12	0.39	0.29	0.26	0.30	0.13				0.77

Notes: Number of trials associated with each vehicle:

   (i)   Ford - 8 trials

   (ii)   Centura - 8 trials

   (iii)   Datsun - 5 trials

335.

TABLE B.4. BINARY REPRESENTATION OF THE ZERO CROSSINGS OF THE DIFFERENTIATED
SIGNATURE IN HEXADECIMAL FORMAT WITH N=96

$i\tilde{X}$ / b / $\tilde{V}$	COMPONENTS OF FEATURE VECTOR											
	1	2	3	4	5	6	7	8	9	10	11	12
Ford	FF	FF	F8	3F	00	3F	E0	FE	00	IF	C0	00
Centura	FF	F8	0F	80	00	3F	80	F8	02	0F	E0	00
Datsun	FF	FF	80	3F	E0	3F	80	03	80	3E	00	00
Volvo	FF	FF	FE	3F	00	00	40	00	71	FF	00	00
Hillman	FF	FF	80	00	03	FF	80	00	70	7F	00	00
Valiant	FF	FF	80	3E	00	07	F0	07	C0	7F	F0	00
Mazda	FF	FE	00	E0	0F	F4	00	E0	3F	E0	00	00
VW	FF	FE	E0	FF	F8	3E	00	00	03	E0	00	00
Holden	FF	FF	FC	3F	02	0F	80	00	FF	80	00	00
Cortina	FF	FF	E0	FE	00	F8	0E	00	00	E0	F8	00
Lancer	FF	FF	E1	FC	00	0F	FC	00	o1	FF	00	00
Fiat	FF	F8	0F	F8	03	FF	80	00	00	3F	E0	00
Escort	FF	FF	FF	F8	00	00	00	00	3F	80	80	00
Ford Truck	FF	FF	FF	FF	20	00	03	83	FF	F8	00	00

TABLE B.5. BINARY REPRESENTATION OF THE ZERO CROSSINGS OF THE DIFFERENTIATED SIGNATURE IN HEXADECIMAL FORMAT WITH N=96 AND LATERAL DISPLACEMENT CONTROLLED WITHIN ±25 cm

Ford $\begin{smallmatrix}i\tilde{X}\\b\end{smallmatrix}$	Components of Feature Vector
	1	2	3	4	5	6	7	8	9	10	11	12
0	FF	FF	F8	3F	00	3F	E0	FE	00	3F	80	00
a	FF	FF	F0	3F	00	IF	F0	FE	61	3F	C0	00
b	FF	FF	F8	7F	00	IF	F0	FE	61	3F	C0	80
c	FF	FF	F4	7F	00	FF	C4	FE	23	3B	C0	00
d	FF	FF	F4	3F	00	3F	F0	FE	00	3F	80	00
e	FF	FF	F8	3E	40	3F	E0	FE	00	3F	80	00
f	FF	FF	F8	3F	00	3F	F0	FE	00	3F	C0	00
g	FF	FF	EC	3B	00	3F	FC	3F	00	3F	80	00

Centura $\begin{smallmatrix}i\tilde{X}\\b\end{smallmatrix}$	Components of Feature Vector
	1	2	3	4	5	6	7	8	9	10	11	12
0	FF	F8	IF	C0	00	3F	80	FC	07	IF	E0	00
a	FF	F8	IF	C0	01	9E	C0	FC	21	9F	E0	00
b	FF	F8	IF	C0	00	0F	80	7E	43	9F	E4	00
c	FF	F0	IF	C0	00	3F	80	FC	03	IF	E0	00
d	FF	FC	0F	C0	00	0F	C0	3E	01	9F	E0	00
e	FF	FC	0F	E0	00	IF	C0	7F	81	BF	E0	00
f	FF	F8	IF	E0	00	3F	80	FC	07	IF	E0	00
g	FF	F8	0F	E0	01	BF	80	FC	0E	IF	E0	00

Datsun $\begin{smallmatrix}i\tilde{X}\\b\end{smallmatrix}$	Components of Feature Vector
	1	2	3	4	5	6	7	8	9	10	11	12
0	FF	FF	90	3F	F0	3F	C0	07	80	7F	00	00
a	FF	FF	80	67	F2	3D	C0	07	80	7F	80	00
b	FF	FF	D8	IF	V0	IF	E0	03	C0	3F	80	00
c	FF	FF	D0	7D	E0	3F	A0	07	80	7F	80	00
d	FF	FF	83	39	F8	IF	F8	07	88	0F	00	00

TABLE B.6. ELEMENTS OF UNDERCARRIAGE VECTOR $_u^i\tilde{X}$

$\tilde{V}$ \ $_u^i\tilde{X}$	ELEMENTS OF FEATURE VECTOR											
	1	2	3	4	5	6	7	8	9	10	11	12
Ford	23.0	4.0	7.5	9.0	11.0	5.0	7.5	11.0	8.0	14.0		
Centura	13.0	6.5	7.5	16.5	7.5	7.5	6.5	7.5	2.5	3.0	10.0	12.0
Datsun	19.5	8.0	11.5	6.0	9.0	10.5	4.0	9.5	7.0	15.0		
Volvo	24.5	2.5	6.0	17.5	2.5	14.5	3.0	1.0	10.0	16.5		
Hillman	19.5	21.5	12.0	14.5	3.5	4.5	7.5	17.0				
Valiant	20.0	5.5	7.5	13.5	9.5	7.0	6.0	8.0	11.5	11.5		
Mazda	18.0	6.0	3.5	9.0	12.5	10.0	2.5	6.5	9.5	23.0		
VW	21.5	4.5	15.5	3.0	8.0	22.0	8.0	17.5				
Holden	23.5	3.0	7.0	6.0	2.5	4.0	6.0	15.0	12.0	21.0		
Cortina	19.5	6.0	7.5	8.5	7.0	5.0	4.0	17.5	5.5	3.5	6.5	9.5
Lancer	20.0	3.0	8.0	14.0	11.0	17.0	12.0	15.0				
Fiat	14.5	6.5	10.5	7.0	13.0	25.5	9.5	13.5				
Escort	33.0	37.0	6.5	6.5	2.5	14.5						
Ford Truck	33.0	3.0	2.0	19.5	3.0	5.5	15.5	19.0				

where

$$^iq_k = \text{duration of the interval corresponding to the}$$

k^{th} section of the binary representation of the

zero crossings of the differentiated signal

associated with class i;

$$t_p = \text{total duration of the signal.}$$

In Table B.6 the value of t_p is taken as unity and the
magnitude of the components of $^i_u\tilde{X}$ are given in terms of the
percentage of t_p.

B.3 Distance Measure

(a) The proximity Table B.7 illustrates normalized values of
Euclidian distance D_E for the fourteen vehicle's signatures
when feature vector $^i_c\tilde{X}$ is used in the analysis.

(b) Table B.8 shows normalized proximity measure D_r when binary
feature vector $^i_b\tilde{X}$ is used in the analysis for the fourteen
vehicle signatures.

TABLE B.7. NORMALIZED DISTANCE MEASURE D_E USING FEATURE VECTOR ${}_c^i \tilde{X}$

D_E	Ford	Centura	Datsun	Volvo	Hillman	Valiant	Mazda	VW	Holden	Cortina	Lancer	Fiat	Escort	Ford Truck
Ford	0	0.75	0.76	0.81	0.84	1.2	0.84	1.11	1.53	0.75	0.70	0.99	0.95	0.79
Centura	0.75	0	1.04	1.09	1.05	1.24	1.03	1.24	1.31	1.01	1.00	1.00	1.09	0.81
Datsun	0.76	1.04	0	0.60	0.53	1.84	0.88	0.39	2.11	0.55	1.08	0.40	0.49	1.19
Volvo	0.81	1.09	0.60	0	0.81	1.69	0.89	0.73	1.81	0.75	0.95	0.80	0.40	0.91
Hillman	0.84	1.05	0.53	0.81	0	1.66	0.59	0.78	2.00	0.56	0.83	0.86	0.90	1.11
Valiant	1.20	1.24	1.84	1.69	1.66	0	1.38	2.20	0.85	1.91	1.19	2.10	2.00	0.91
Mazda	0.84	1.03	0.88	0.89	0.59	1.38	0	1.12	1.15	0.84	0.51	1.22	1.08	0.70
VW	1.11	1.24	0.39	0.73	0.78	2.2	1.12	0	2.34	0.48	1.48	0.44	0.45	1.56
Holden	1.53	1.31	2.11	1.81	2.00	0.85	1.15	2.34	0	2.01	1.50	2.18	2.09	1.30
Cortina	0.75	1.01	0.55	0.75	0.56	1.91	0.84	0.48	2.01	0	1.01	0.55	0.54	1.19
Lancer	0.70	1.00	1.08	0.95	0.83	1.19	0.51	1.48	1.50	1.01	0	1.35	1.24	0.63
Fiat	0.99	1.00	0.40	0.8	0.86	2.10	1.22	0.44	2.18	0.55	1.35	0	0.56	1.45
Escort	0.95	1.09	0.49	0.4	0.9	2.00	1.08	0.45	2.09	0.54	1.24	0.56	0	1.25
Ford Truck	0.79	0.81	1.19	0.91	1.11	0.91	0.70	1.56	1.30	1.19	0.63	1.45	1.25	0

TABLE B.8. NORMALIZED DISTANCE MEASURE D_r USING FEATURE VECTOR $_b^i \tilde{x}$

D_r	Ford	Centura	Datsun	Volvo	Hillman	Valiant	Mazda	VW	Holden	Cortina	Lancer	Fiat	Escort	Ford Truck
Ford	0	0.97	0.68	1.0	1.07	0.61	1.58	0.93	1.07	1.22	0.86	1.03	1.32	1.39
Centura	0.97	0	1.31	1.32	1.25	1.14	1.32	1.46	1.46	1.60	1.03	0.76	1.14	1.58
Datsun	0.68	1.31	0	0.93	0.86	0.61	1.58	0.64	1.00	1.29	0.93	1.03	1.46	1.25
Volvo	1.0	1.32	0.93	0	0.93	0.97	1.42	0.71	0.64	1.22	0.71	1.10	0.68	0.61
Hillman	1.07	1.25	0.86	0.93	0	0.97	0.93	1.00	0.68	0.83	0.86	0.90	1.39	1.46
Valiant	0.61	1.14	0.61	0.97	0.97	0	1.68	0.91	1.19	1.03	0.68	0.93	1.29	1.36
Mazda	1.58	1.32	1.58	1.42	0.93	1.68	0	1.36	1.00	1.15	1.29	1.32	1.19	1.19
VW	0.93	1.46	0.64	0.71	1.00	0.97	1.36	0	0.78	1.14	0.86	1.03	1.19	1.10
Holden	1.07	1.46	1.00	0.64	0.68	1.19	1.00	0.78	0	0.90	0.93	1.32	0.75	0.90
Cortina	1.22	1.60	1.29	1.22	0.83	1.03	1.15	1.14	0.90	0	0.93	0.90	1.03	1.32
Lancer	0.86	1.03	0.93	0.71	0.86	0.68	1.29	0.86	0.93	0.93	0	0.90	0.88	1.03
Fiat	1.03	0.76	1.03	1.10	0.90	0.93	1.32	1.03	1.32	0.90	0.90	0	1.14	1.68
Escort	1.32	1.14	1.46	1.68	1.39	1.29	1.19	1.19	0.75	1.03	0.88	1.14	0	0.81
Ford Truck	1.39	1.58	1.25	0.61	1.46	1.36	1.19	1.10	0.90	1.32	1.03	1.68	0.81	0

APPENDIX C

WAVEFORM SYNTHESIS AND MODULATION

C.1 Program Mod.

```
      PROGRAM MOD(INPUT,OUTPUT)
*
*     THIS PROGRAM FORMS A MODULATED TRANSPONDER CURRENT WAVEFORM.
*     IT THEN FINDS ITS FOURIER TRANSFORM IN THE FREQUENCY DOMAIN,
*     GENERATES A FILTERED SPECTRUM FROM A GAUSSIAN FILTER AND
*     FINALLY FINDS THE INVERSE FOURIER TRANSFORM IN THE TIME DOMAIN.
*
*
      DIMENSION FRN(32),FRM(32),ODATA(1024),FDATA(1024),NSCALE(15),
     .NPAT(14),MPAT(14)
      COMPLEX FR(1024)
      INTEGER TEMP
*
      EXTERNAL SIN,EXP
*
      PI=3.1415926536
      TWOPI=2.0*PI
*
*     SET TOTAL NUMBER OF POINTS NPT AND
*     NUMBER OF POINTS IN ONE SUBHARMONIC CYCLE OF WAVEFORM
*     (WE ARE USING 4 REPETITIONS OF 8 CYCLES OF THE SUBHARMONIC)
*
      NPT=1024
      NP=32
*
*
    2 CONTINUE
*
*     ZERO ALL ELEMENTS OF WAVEFORM VALUES
*
      DO 4 I=1,NPT
    4 FR(I)=0.0
      DO 5 I=1,NP
      FRN(I)=0.0
    5 FRM(I)=0.0
*
*     SET ORDER OF SUBHARMONIC REQUIRED
*
      PRINT 6
    6 FORMAT(//,1X,*TYPE ORDER OF SUBHARMONIC REQUIRED (MAX 6): *)
      READ *,LOS
*
*     SET UP SCALE AND DIVISIONS
*
      NSCALE(1)=1
      DO 10 I=2,15
   10 NSCALE(I)=0
      NSC=2*(LOS+1)
      NSC1=NSC+1
      SCALE=FLOAT(NP)/FLOAT(NSC)
      SC1=0.0
*
*     SET UP DIVISIONS ARRAY
```

```
      DO 20 I=2,NSC1
      SC2=SC1+SCALE
      NSCALE(I)=INT(SC2+0.5)
      SC1=SC2
   20 CONTINUE
*
*     SET UP PATTERN FOR SUBHARMONIC
*
      PRINT 30,NSC
   30 FORMAT(//,1X,*TYPE REQUIRED PATTERN(*,I2,* BITS): *)
      READ *,(NPAT(I),I=1,NSC)
*
*     FIND MODULATION REQUIRED
*
      PRINT 40,NSC
   40 FORMAT(//,1X,*TYPE REQUIRED MODULATION(*,I2,* BITS): *)
      READ *,(MPAT(I),I=1,NSC)
*
*     FILL ONE CYCLE OF WAVEFORM FOR EACH PATTERN
*
      DO 120 I=1,NSC
      RFAC=FLOAT(NSCALE(3))
      IS=NSCALE(I)
      IF=NSCALE(I+1)
      IF(NPAT(I).EQ.0) GOTO 100
      NFAC=NPAT(I)
      DO 90 K=IS,IF
        FRN(K)=FLOAT(NFAC)*SIN((FLOAT(K-IS)/RFAC)*TWOPI)
   90 CONTINUE
  100 IF(MPAT(I).EQ.0) GOTO 120
      MFAC=MPAT(I)
      DO 110 K=IS,IF
        FRM(K)=FLOAT(MFAC)*SIN((FLOAT(K-IS)/RFAC)*TWOPI)
  110 CONTINUE
  120 CONTINUE
*
*
*     FILL COMPLETE WAVEFORM
*
      K=1
      DO 170 L=1,2
*
      DO 140 I=1,8
      DO 130 J=1,NP
        FR(K)=CMPLX(FRN(J),0.0)
      K=K+1
  130 CONTINUE
  140 CONTINUE
*
      DO 160 I=1,8
      DO 150 J=1,NP
        FR(K)=CMPLX(FRM(J),0.0)
      K=K+1
  150 CONTINUE
  160 CONTINUE
*
  170 CONTINUE
*
      DO 195 I=1,NPT
  195 ODATA(I)=REAL(FR(I))
*
*     ..............................................................
*     SET UP CONSTANTS FOR FOURIER TRANSFORM AND GAUSSIAN FILTER
*
*        DT - SAMPLING INTERVAL IN THE TIME DOMAIN
*        DF - SAMPLING INTERVAL IN THE FREQUENCY DOMAIN
*        FP - PERIODIC FREQUENCY OF THE DISCRETE FOURIER TRANSFORM
*        RCF- RECEIVER FILTER BAND CENTRE FREQUENCY
*        SIGMA- SIGMA OF THE GAUSSIAN FILTER
*     ..............................................................
      PRINT 200
  200 FORMAT(//,1X,*TYPE RECEIVER BAND CENTRE FREQ.(KHZ): *)
      READ *,RCF
      PRINT 201
  201 FORMAT(//,1X,*TYPE Q OF RECEIVER CIRCUIT: *)
      READ *,Q
```

343.

```
      RCF=RCF*1.0E03
      FP=FLOAT(NP/(LOS+1))*1.0E05
      DT=1.0/FP
      DF=FP/FLOAT(NPT)
      RCFI=(RCF/DF)+1.0
      SIGMA=RCF/(G*2.0)
      SIG=SIGMA/DF
*
*     TRANSFORMATION TO FREQUENCY DOMAIN
*
      DXY=DT
      CALL BFAST(FR,10,-1.0,DXY)
*
*     OUTPUT OF THE TRANSFORMED SPECTRUM IF REQUIRED
*
      PRINT 205
  205 FORMAT(//,1X,*PLOT OF FREQ. SPECTRUM REQD.? (1=YES,2=NO): *)
      READ *,NPLT
      IF(NPLT.EQ.2) GOTO 207
*
      DO 206 I=1,NPT
  206 FDATA(I)=CABS(FR(I))
*
*     SET X-AXIS SCALE
*
      HS=0.0
      HDEL=DF
      IFMT=10HXF7.0,2X
*
      CALL PLTSYM(DUMMY,2,1H*,1H.)
      CALL PLTYHT(60)
      CALL PLTXLEN(+1)
      CALL PLTXNUM(DUMMY,IFMT,HS,HDEL)
      CALL PLT(1024,1,FDATA(1))
*
*
*     GENERATION OF THE FILTERED SPECTRUM
*
  207 DO 220 J=1,NPT
      GR=FLOAT(J)-RCFI
      GX=GR*GR/(2.0*SIG*SIG)
      IF(GX.GT.32.0) GOTO 210
      FILTER=EXP(-GX)
      FR(J)=FR(J)*FILTER
      GOTO 220
  210 FR(J)=CMPLX(0.0,0.0)
  220 CONTINUE
*
*     TRANSFORMATION BACK TO THE TIME DOMAIN
*
      DXY=DF
      CALL BFAST(FR,10,+1.0,DXY)
*
*     OUTPUT FILTERED WAVEFORM (RECEIVER INPUT) AND ORIGINAL SIGNAL
*
*     (SCALE FILTERED SIGNAL UP BY 10.0)
*
      DO 230 I=1,NPT
  230 FDATA(I)=10.0*FR(I)
*
      PRINT 240
  240 FORMAT(//,1X,*PLOT OF:*,/,10X,*(1)ORIGINAL SIGNAL (*,1H*,*)*,
     ./,10X,*(2)FILTERED RECEIVER SIGNAL (.)*)
*
*     SET X-AXIS SCALE
*
      HS=0.0
      HDEL=FLOAT(360/NP)
      IFMT=10HX,F7.0,2X
*
      CALL PLTSYM(DUMMY,2,1H*,1H.)
      CALL PLTXLEN(+1)
      CALL PLTYHT(60)
      CALL PLTXNUM(DUMMY,IFMT,HS,HDEL)
      CALL PLT(1024,2,DDATA(1),FDATA(1))
*
*     REPEAT FOR NEW WAVEFORM IF REQUIRED
*
      PRINT 250
  250 FORMAT(//,1X,*TYPE 1 TO REPEAT, 2 TO END: *)
      READ *,IRPT
      IF(IRPT.EQ.1) GOTO 2
*
*
      STOP
      END                        344.
```

```
*   .........................................................
*
        SUBROUTINE BFAST(Y,M,SIGN,DXY)
*
*
*       SUBROUTINE FOR CALCULATION OF EITHER FORWARD OR INVERSE
*       FOURIER TRANSFORM OF A COMPLEX SEQUENCE Y USING
*       THE FAST FOURIER TRANSFORM (FFT) ALGORITHM.
*
*                                       M
*       Y IS A COMPLEX ARRAY OF DIMENSION 2  AND IS BOTH THE INPUT
*       AND OUTPUT SEQUENCE OF THE SUBROUTINE.
*       PRESENT DIMENSIONS LIMIT=2**10
*
*       DXY = SAMPLE SPACING FOR THE INPUT ARRAY Y. THE CORRESPONDING
*       SAMPLE SPACING IN THE TRANSFORM DOMAIN IS OUTPUT IN DXY.
*
*       FOR TIME TO FREQUENCY TRANSFORMATION - SIGN = -1.0
*       FOR FREQUENCY TO TIME TRANSFORMATION - SIGN = +1.0
*
*       SUBROUTINE CON SETS UP A CONVERSION TABLE TO
*       REARRANGE THE INPUT ARRAY FOR PROCESSING.
*
*       SUBROUTINE TABLE SETS UP A TABLE OF ALL SINES
*       AND COSINES USED IN SUBROUTINE BFAST.
*
*
*
*
*
        COMPLEX A,U,W,T,Y
        DIMENSION A(1024),Y(2)
        COMMON / PERM/MM(1024)
        COMMON / TAB/TC(10),TS(10)
        DATA MSET/0/
*
        IF(MSET.EQ.M) GOTO 1
        CALL TABLE(M)
        CALL CON(M)
        MSET=M
      1 CONTINUE
*
        N=2**M
        DO 7 I=1,N
        J=MM(I)
      7 A(I)=Y(J)
*
        DO 20 L=1,M
        LE=2**L
        LE1=LE/2
        U=(1.0,0.0)
        W=CMPLX(TC(L),TS(L)*SIGN)
        DO 20 J=1,LE1
        DO 10 I=J,N,LE
        IP=I+LE1
        T=A(IP)*U
        A(IP)=A(I)-T
        A(I)=A(I)+T
     10 CONTINUE
        U=U*W
     20 CONTINUE
*
        DO 30 I=1,N
        Y(I)=A(I)*DXY
     30 CONTINUE
        DXY=1.0/(DXY*N)
*
        RETURN
        END
*
*
*   ...................................
*
        SUBROUTINE TABLE(M)
*
        COMMON /TAB/TC(10),TS(10)
        EXTERNAL SIN,COS
*
        PI=4.0*ATAN2(1.0,1.0)
        DO 1 I=1,M
        TC(I)=COS(PI/(2**(I-1)))
        TS(I)=SIN(PI/(2**(I-1)))
      1 CONTINUE
        RETURN
        END
```

```
*
*
*
      SUBROUTINE CON(M)
*
      INTEGER A,T
      COMMON /PERM/ A(1024)
*
      N=2**M
      NV2=N/2
      NM1=N-1
      J=1
      DO 1 I=1,N
    1 A(I)=I
      DO 7 I=1,NM1
      IF(I.GE.J) GOTO 5
      T=A(J)
      A(J)=A(I)
      A(I)=T
    5 K=NV2
    6 IF(K.GE.J) GOTO 7
      J=J-K
      K=K/2
      GOTO 6
    7 J=J+K
      RETURN
      END
*
*
*
*     ...................................................................
*
*
      SUBROUTINE PLT(NP,NFUNC,A1,A2,A3,A4,A5,A6)
*
*
*     THIS ROUTINE WILL PRODUCE A PLOT ON THE LINE PRINTER
*       NP       NUMBER OF POINTS
*       NFUNC    NUMBER OF FUNCTIONS TO BE PLOTTED
*       A1,...,A6 ARRAYS CONTAINING Y PARAMETERS OF FUNCTIONS TO BE
*                 PLOTTED(X VARIABLE INCREMENTS MONOTONICALLY)
*
*
*     DEFAULT PLOT PARAMETERS CAN BE CHANGED USING THE FOLLOWING CALLS
*
*     PLTYSC(DUMMY,N,FMIN,FMAX)
*        N = 0   SELF SCALING (DEFAULT)
*        N = 1   SCALING TO GIVE Y-AXIS LIMITS OF FMIN,FMAX
*     PLTYHT(NCHAR)
*        SETS PLOT HEIGHT TO NCHAR CHARACTERS (DEFAULT = 120)
*     PLTXLEN(NTH)
*        NTH POSITIVE - PLOT EVERY NTH POINT ONLY
*        NTH NEGATIVE - EXPAND PLOT TO NTH LINES PER POINT
*                (DEFAULT NTH = +1)
*     PLTXNUM(DUMMY,IFMT,X1,XDEL)
*        NUMBER X-AXIS BEGINNING WITH X1 AND INCREMENTING BY XDEL.
*        PRINT ACCORDING TO IFMT WHICH SPECIFIES A 10 PRINT CHARACTER
*                (DEFAULT X1=1.0  XDEL=1.0  IFMT=10HX,F7.2,2X  )
*     PLTSYM(DUMMY,NFUNC,A1,..A6)
*        SET THE FIRST NFUNC PLOT SYMBOLS
*        (DEFAULT A1=1H1,A2=1H2,..)
*     PLTYLAB(NCOL,NWDS,YLAB)
*        LABEL Y-AXIS WITH NWDS WORDS BEGINNING IN COLUMN NCOL,
*        WITH WORDS TAKEN FROM ARRAY YLAB
*     PLTXLAB(NOLINES,NWPL,XLAB)
*        LABEL X-AXIS WITH NOLINES LINES, NWPL WORDS PER LINE,
*        WITH WORDS TAKEN FROM ARRAY XLAB.
*
*
      REAL L
      DIMENSION L(121),A1(1),A2(1),A3(1),A4(1),A5(1),A6(1)
      DIMENSION XLAB(10),YLAB(10),SYMBOL(6),IFORM(5)
      DIMENSION PREFER(9)
      DATA NCHAR,NTH,X1,XDEL,IFMT,(SYMBOL(I),I=1,5),NOSCAL,NWDS,NOLINES
     1/120,+1,1.0,1.0,10HX,F7.2,2X ,1H1,1H2,1H3,1H4,1H5,1H6,0,0,0/
      DATA PREFER /1.0,1.5,2.0,2.5,3.0,4.0,5.0,8.0,10.0/
*
      F(X)=(X-FMIN)/CONST+1.5
*
      PRINT 200
  200 FORMAT(////)
```

346.

```
      NCHAR1=NCHAR+1
      IF(NOSCAL.EQ.1) GOTO 30
      FMAX=FMIN=A1(1)
      N1=1
      IF(NTH.GT.0) N1=NTH
      DO 7 M=1,NP,N1
      GOTO (6,5,4,3,2,1) NFUNC
    1 FMIN=AMIN1(A6(M),FMIN)
      FMAX=AMAX1(A6(M),FMAX)
    2 FMIN=AMIN1(A5(M),FMIN)
      FMAX=AMAX1(A5(M),FMAX)
    3 FMIN=AMIN1(A4(M),FMIN)
      FMAX=AMAX1(A4(M),FMAX)
    4 FMIN=AMIN1(A3(M),FMIN)
      FMAX=AMAX1(A3(M),FMIN)
    5 FMIN=AMIN1(A2(M),FMIN)
      FMAX=AMAX1(A2(M),FMAX)
    6 FMIN=AMIN1(A1(M),FMIN)
      FMAX=AMAX1(A1(M),FMAX)
    7 CONTINUE
*
*
      DIFF=FMAX-FMIN
      IF(DIFF.NE.0.0) GOTO 20
      PRINT 105,FMAX
  105 FORMAT(*1  Y-AXIS SCALING ERROR IN PLT*,/*  MAXIMUM=MINIMUM= *
     1,1PE10.3,//)
      RETURN
   20 YINC=DIFF/NCHAR
      AY=ALOG10(YINC)
      IY=INT(AY)
      IF(AY.LT.0.0) IY=IY-1
      Y=10.0**IY
      Y1=YINC/Y
      K=0
      DO 70 I=1,9
      IF(Y1.LE.PREFER(I))GOTO8
   70 CONTINUE
    8 J=I+K
      IF(J.LE.9)GOTO71
      J=2   $  Y=Y*10.0
   71 YINC=Y*PREFER(J)
      FM=INT(FMIN/Y/10.0)
      IF(FMIN.LT.0.0)FM=FM-1.0
      FMIN=FM*10.0*Y
      FM1=FMIN+NCHAR*YINC
      IF(FMAX.LE.FM1)GOTO9
      K=K+1   $  GOTO8
    9 FMAX=FM1
*
*
   30 CONST=(FMAX-FMIN)/NCHAR
      LZERO=1
      TZERO=FMIN*FMAX
      IF(TZERO.LT.0.0)LZERO=F(0.0)
      PRINT 93
   93 FORMAT(1H0)
*
      IF(NWDS.EQ.0)GOTO10
      NWD=(135-NCOL)/10
      NC=NCOL+1
      ENCODE(16,100,IFORM) NC,NWD
  100 FORMAT(5H(1H1,,I3,2HX,,I2,4HA10))
      PRINT IFORM,(YLAB(I),I=1,NWDS)
   10 NC=(NCHAR-30)/2
      ENCODE(46,101,IFORM) NC,NC
  101 FORMAT(12H(5X,1PE10.3,,I2,20HX,*1 DIV =*,1PE10.2,,I2,10HX,1PE10.3)
     1)
      PRINT IFORM,FMIN,CONST,FMAX
      ENCODE(18,103,IFORM) IFMT
  103 FORMAT(1H(,A10,7H,121A1))
*
      XDEL1=XDEL
      IF(NTH.GT.0)XDEL1=XDEL*NTH
      K=0
      X=X1
      IF(NTH.LT.0)K1=(1-NP)*NTH+1
      IF(NTH.GT.0)X1=(NP-1)/NTH+1
```

347.

```
   12 DO15 I=2,NCHAR
   15 L(I)=1H
   11 K=K+1
      IF(K.GT.K1)GOTO29
      IF(K.NE.1.AND.K.NE.K1)GOTO14
      DO13 I=2,NCHAR
   13 L(I)=1H-
      DO18 I=1,NCHAR1,10
   18 L(I)=1H:
   14 L(1)=L(LZERO)=L(NCHAR1)=1H:
      IF(NTH.LT.0)GOTO16
      II=(K-1)*NTH+1
      GOTO17
   16 II=(1-K)/NTH
      I2=1-II*NTH
      II=II+1
      IF(K.EQ.I2)GOTO17
      PRINT 102,(L(I),I=1,NCHAR1)
  102 FORMAT(10X,121A1)
      GOTO11
   17 GOTO(45,44,43,42,41,40) NFUNC
   40 M=F(A6(II))
      IF(M.LE.0.OR.M.GT.NCHAR1) GOTO41
      L(M)=SYMBOL(6)
   41 M=F(A5(II))
      IF(M.LE.0.OR.M.GT.NCHAR1) GOTO42
      L(M)=SYMBOL(5)
   42 M=F(A4(II))
      IF(M.LE.0.OR.M.GT.NCHAR1) GOTO43
      L(M)=SYMBOL(4)
   43 M=F(A3(II))
      IF(M.LE.0.OR.M.GT.NCHAR1) GOTO44
      L(M)=SYMBOL(3)
   44 M=F(A2(II))
      IF(M.LE.0.OR.M.GT.NCHAR1) GOTO45
      L(M)=SYMBOL(2)
   45 M=F(A1(II))
      IF(M.LE.0.OR.M.GT.NCHAR1) GOTO46
      L(M)=SYMBOL(1)
   46 PRINT IFORM,X,(L(I),I=1,NCHAR1)
      X=X+XDEL1
      GOTO12

   29 IF(NOLINES.EQ.0)RETURN
      J1=1   $  J2=NWPL
      DO39 I=1,NOLINES
      PRINT 104,(XLAB(J),J=J1,J2)
      J1=J1+NWPL
   39 J2=J2+NWPL
  104 FORMAT(1X,13A10)
      RETURN


      ENTRY PLTYSC
      NOSCAL=NFUNC
      FMAX=A2(1)
      FMIN=A1(1)
      RETURN
      ENTRY PLTYHT
      NCHAR=NP
      RETURN
      ENTRY PLTXLEN
      NTH=NP
      RETURN
      ENTRY PLTXNUM
      IFMT=NFUNC
      X1=A1(1)
      XDEL=A2(1)
      RETURN
      ENTRY PLTSYN
      GOTO(53,54,55,56,57,58) NFUNC
   58 SYMBOL(6)=A6(1)
   57 SYMBOL(5)=A5(1)
   56 SYMBOL(4)=A4(1)
   55 SYMBOL(3)=A3(1)
   54 SYMBOL(2)=A2(1)
   53 SYMBOL(1)=A1(1)
      RETURN
```

348.

```
      ENTRY PLTYLAB
      NWDS=NFUNC
      IF(NWDS.EQ.0)RETURN
      NCOL=NP
      DO59 I=1,NWDS
   59 YLAB(I)=A1(I)
      RETURN
      ENTRY PLTXLAB
      NOLINES=NP
      IF(NOLINES.EQ.0)RETURN
      NWPL=NFUNC
      N=NP*NFUNC
      DO60 I=1,N
   60 XLAB(I)=A1(I)
      RETURN
      END
```

349.

APPENDIX D

DERIVATION OF MAGNETIC FIELD

D.1 Derivation of Mangetic Field $\tilde{H}$

Let us consider a circular loop of constant current i and define co-ordinates as shown in Figure D.1.

The rectangular components of the vector potential $\tilde{A}$ can be obtained from[97]

$$A_x(r) = -\frac{\mu a i}{4\pi} \int_0^{2\pi} \frac{\text{Sin } \phi'}{|r - r'|} \, d\phi' \qquad (D.1)$$

$$A_y(r) = \frac{\mu a i}{4\pi} \int_0^{2\pi} \frac{\text{Cos } \phi'}{|r - r'|} \, d\phi' \qquad (D.2)$$

where the source co-ordinates are specialised to ($\rho' = a$, ϕ', $z' = 0$).

Since there is no z-directed current, then

$$A_z = 0 \qquad (D.3)$$
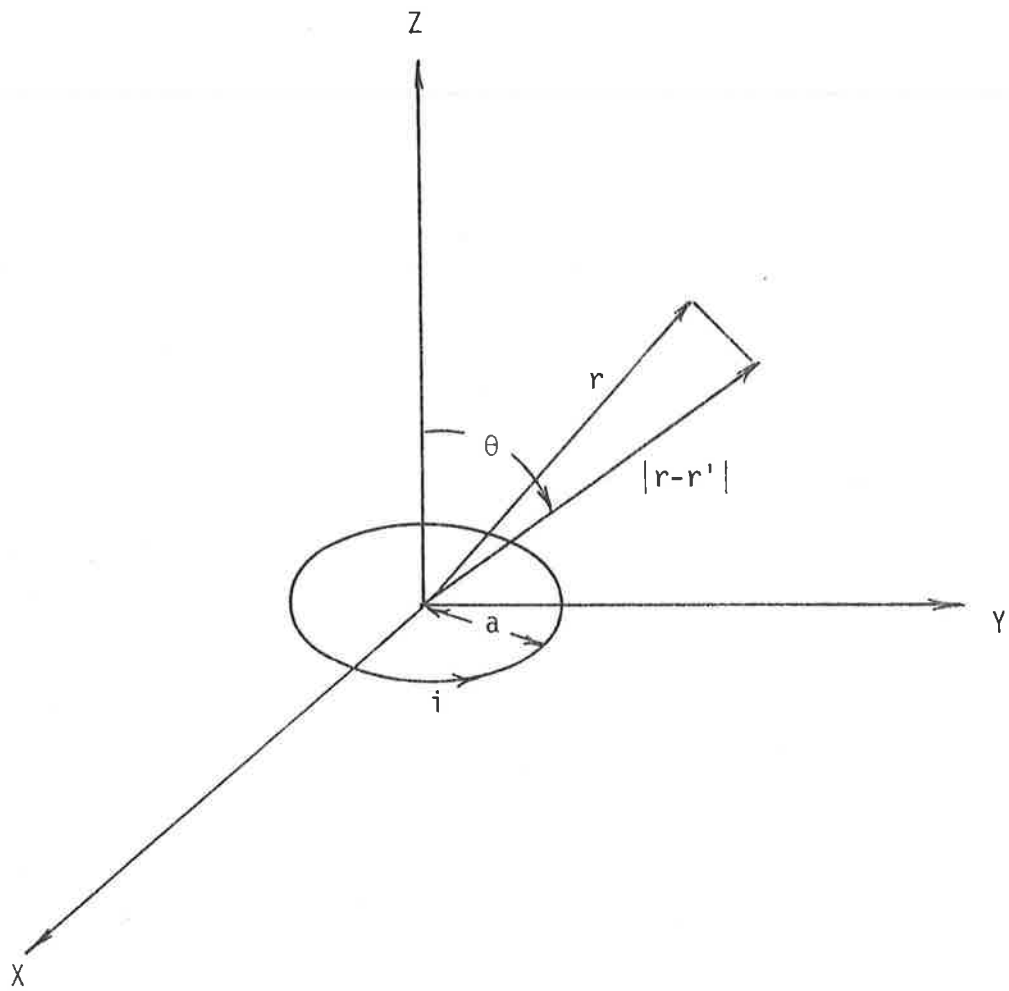
FIGURE D.1.   COORDINATES FOR A CURRENT CARRYING CIRCULAR LOOP.

where

$$|r - r'| = \left[(x - a \cos \phi')^2 + (y - a \sin \phi')^2 + z^2\right]^{\frac{1}{2}} \qquad (D.4)$$

or in cylindrical co-ordinates

$$|r - r'| = \left[\rho^2 + a^2 - 2 \rho a \cos (\phi - \phi') + z^2\right]^{\frac{1}{2}} \qquad (D.5)$$

and the field co-ordinates being (x, y, z) and (ρ, ϕ, z) respectively where

a = radius of the coil

ρ = radial distance from the cylinder axis.

From Figure D.1 it seems appropriate to use cylindrical co-ordinates.

The cylindrical components of vector potential $\tilde{A}$ can be obtained by noting that there is no A_z. Therefore only ϕ and ρ components exist.

The rotational symmetry about the z axis also make A_ρ and A_ϕ independent of ϕ.

Thus we need only to evaluate A_ρ and A_ϕ for one specific value of ϕ.

Further, we may pick a field point to lie in the y = 0 plane, i.e.

$$\phi = 0$$

then

$$A_x (\rho, 0, z) = A_\rho (\rho, \phi, z) \qquad (D.6)$$

and

$$A_y (\rho, 0, z) = A_\phi (\rho, \phi, z) \qquad (D.7)$$

We see in this case the x and ρ components and the y and ϕ components coincide in this plane.

We also note, equidistant from a field point in the y = 0 plane, there are equal but oppositely directed x components of current.

Thus, $\qquad$ A $\;= 0 \quad$ everywhere,

and we have only A ; with $\quad = 0$,

then

$$A_\phi(\rho, \phi, z) = \frac{\mu a i}{4\pi} \int_0^{2\pi} \frac{\cos \phi' \; d\phi'}{\sqrt{\rho^2 + a^2 - 2a\rho \cos \phi' + z^2}} \qquad (D.8)$$

we let

$$\phi' = \pi + 2\theta \qquad (D.9)$$

then

353.

$$A_\phi = \frac{\mu a i}{\pi} \int_0^{\pi/2} \frac{(2 \, \text{Sin}^2 \, \theta - 1)}{\sqrt{(a + \rho)^2 + z^2 - 4a\rho \, \text{Sin}^2 \, \theta}} \, d\theta \qquad (D.10)$$

If we also define

$$\alpha = 2 \left[\frac{a\rho}{(a + \rho)^2 + z^2} \right]^{\frac{1}{2}} \qquad (D.11)$$

then

$$A_\theta = \frac{\mu i}{\alpha \pi} \left(\frac{a}{\rho} \right)^{\frac{1}{2}} \left[\left(\frac{2 - \alpha^2}{2} \right) K(\alpha) - E(\alpha) \right] \qquad (D.12)$$

where

$$K(\alpha) = \int_0^{\pi/2} \frac{1}{\left(1 + \alpha^2 \, \text{Sin}^2 \, \theta \right)^{\frac{1}{2}}} \cdot d\theta \qquad (D.13)$$

$$E(\alpha) = \int_0^{\pi/2} \left(1 + \alpha^2 \, \text{Sin}^2 \, \theta \right)^{\frac{1}{2}} \cdot d\theta \qquad (D.14)$$

The field components can be obtained from

$$\tilde{B} = \tilde{\nabla} \times \tilde{A} \qquad (D.15)$$

Thus

354.

$$B_\rho = \frac{\mu i z}{2\pi\rho \left[(a + \rho)^2 + z^2\right]^{\frac{1}{2}}} \left[\frac{a^2 + \rho^2 + z^2}{(a - \rho)^2 + z^2} \cdot E(\alpha) - K(\alpha)\right] \qquad (D.16)$$

$$B_z = \frac{\mu i}{2\pi \left[(a + \rho)^2 + z^2\right]^{\frac{1}{2}}} \left[\frac{a^2 - \rho^2 - z^2}{(a - \rho)^2 + z^2} E(\alpha) + K(\alpha)\right] \qquad (D.17)$$

Letting

$$\tilde{B} = \mu\tilde{H} \qquad (D.18)$$

then the ρ and z components of the magnetic field becomes

$$H_\rho = \frac{i z}{2\pi\rho \left[(a + \rho)^2 + z^2\right]^{\frac{1}{2}}} \left[\frac{a^2 + \rho^2 + z^2}{(a - \rho)^2 + z^2} E(\alpha) - K(\alpha)\right] \qquad (D.19)$$

$$H_z = \frac{i}{2\pi \left[(a + \rho)^2 + z^2\right]^{\frac{1}{2}}} \left[\frac{a^2 - \rho^2 - z^2}{(a - \rho)^2 + z^2} E(\alpha) + K(\alpha)\right] \qquad (D.20)$$

$$H_\phi = 0 \qquad (D.21)$$

The components of the magnetic field in rectangular co-ordinates can be obtained by noting that

$$H_x = H_\rho \cos\phi - H_\phi \sin\phi \qquad (D.22)$$

$$H_y = H\rho \sin\phi + H_\phi \cos\phi \qquad (D.23)$$

355.

and

$$\rho = \sqrt{x^2 + y^2} \qquad (D.24)$$

$$\text{Sin } \phi = \frac{y}{\sqrt{x^2 + y^2}} \qquad (D.25)$$

$$\text{Cos } \phi = \frac{x}{\sqrt{x^2 + y^2}} \qquad (D.26)$$

Thus

$$H_x = \frac{ixz}{2\pi\left[x^2+y^2\right]\left[(a+\sqrt{x^2+y^2})^2+z^2\right]^{\frac{1}{2}}}\left[\frac{a^2+x^2+y^2+z^2}{(a-\sqrt{x^2+y^2})^2+z^2} E(\alpha) - K(\alpha)\right] \qquad (D.27)$$

$$H_y = \frac{iyz}{2\pi\left[x^2+y^2\right]\left[(a+\sqrt{x^2+y^2})^2+z^2\right]^{\frac{1}{2}}}\left[\frac{a^2+x^2+y^2+z^2}{(a-\sqrt{x^2+y^2})^2+z^2} E(\alpha) - K(\alpha)\right] \qquad (D.28)$$

$$H_z = \frac{i}{2\pi\left[(a + \sqrt{x^2 + y^2})^2 + z^2\right]^{\frac{1}{2}}}\left[\frac{a^2-x^2-y^2-z^2}{(a-\sqrt{x^2+y^2})^2+z^2} E(\alpha) + K(\alpha)\right] \qquad (D.29)$$

and

$$\alpha = 2\left[\frac{a\sqrt{x^2 + y^2}}{\left((a + \sqrt{x^2 + y^2})^2+z^2\right)^{\frac{1}{2}}}\right]^{\frac{1}{2}} \qquad (D.30)$$

356.

APPENDIX E

DEMAGNETIZATION FACTOR

E.1 Demagnetization Factor Calculation

Demagnetization factor N_d (where the medium outside the ellipsoid is free space) depend only on the form of ellipsoid and can be written as[105 - 106]

$$N_{d_j} = \frac{abc}{2} A_j; \qquad j = 1, 2, 3 \qquad\qquad (E.1)$$

where a, b, and c are the semi-axis of the ellipsoid as shown in Figure E.1, and

$$A_1 = \int_0^\infty \frac{1}{(s + a^2) R_s} \cdot ds \qquad\qquad (E.2)$$

$$A_2 = \int_0^\infty \frac{1}{(s + b^2) R_s} \cdot ds \qquad\qquad (E.3)$$

$$A_3 = \int_0^\infty \frac{1}{(s + c^2) R_s} \cdot ds \qquad\qquad (E.4)$$
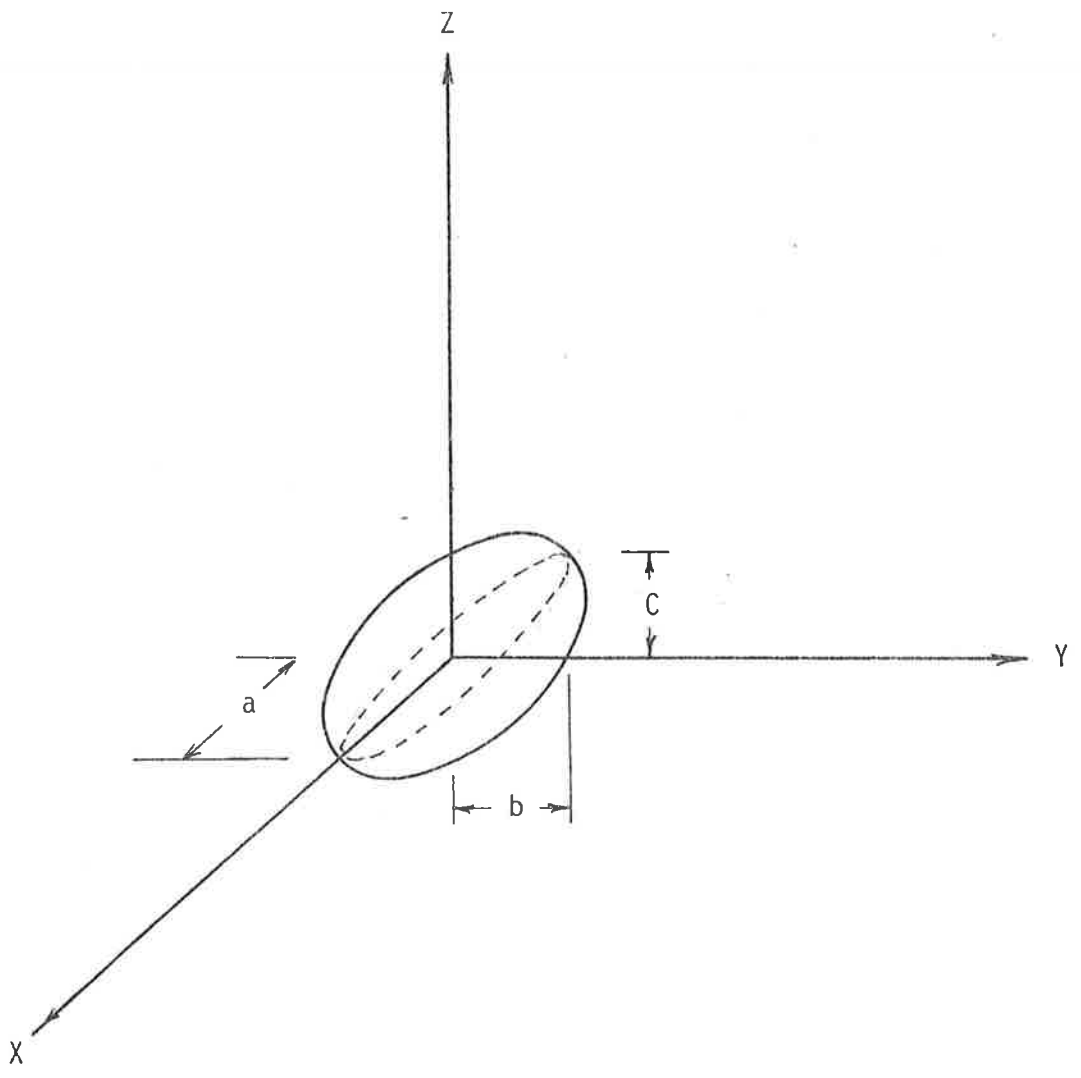
FIGURE E.1.   DIAGRAM SHOWING THE COORDINATES OF AN ELLIPSOID

with

$$R_s = \sqrt{(s + a^2)(s + 6^2)(s + c^2)} \qquad (E.5)$$

Thus by varying the length of the semi-axis of the structures of interest and subsequently approximating the resultant shape to that of an ellipsoid an approximate expression can be obtained for the demagnetization factors.

(i)   Thin Circular Disc

For the condition in which lengths of the semi-axis are such that the ellipsoid degenerates into a thin disc, i.e. $a = b > c$, from Equation (E.1) and Equation (E.2) the demagnetization N_{d_1} becomes[106]

$$N_{d_1} = \frac{1}{\sqrt{(a^2 - c^2)^3}} \left[\frac{\pi}{2} - \text{Arctan} \frac{c}{\sqrt{a^2 - c^2}} \right] - \frac{c}{(a^2 - c^2) a^2} \qquad (E.6)$$

Since $a = b$, then $N_{d_1} = N_{d_2}$, but

$$\sum_{j = 1}^{3} N_{d_j} = 1 \qquad (E.7)$$

therefore

$$N_{d_3} = 1 - 2 N_{d_1} \qquad (E.8)$$

(ii)   <u>Long Thin Rod</u>

If the axis of the ellipsoid are a > b = c, then the ellipsoid degenerates into a long thin rod. The demagnetization factor along the major axis can readily be shown as[106]

$$N_{d_1} = \frac{1 - \omega^2}{\omega^2} \left[\frac{1}{2\omega} \log_e \frac{1 + \omega}{1 - \omega} - 1 \right] \qquad (E.9)$$

where

$$\omega = \sqrt{1 - (b/a)^2} \qquad (E.10)$$

(iii)   <u>Flat Rod</u>

For a flat rod it is considered that a > b > c. The demagnetization factor along the major axis from Equation (E.1) and Equation (E.2) can be expressed by[109]

$$N_{d_1} = \frac{abc}{(a^2 - b^2) \sqrt{a^2 - c^2}} \left[K (v, q) - E (v, q) \right] \qquad (E.11)$$

where

$$v = \text{Arc Sin} \frac{\sqrt{a^2 - c^2}}{a} \qquad (E.12)$$

$$q = \sqrt{\frac{a^2 - b^2}{a^2 - c^2}} \qquad (E.13)$$

and

K (v, q) = Incomplete elliptic integral of the first kind

E (v, q) = Incomplete elliptic integral of the second kind.

The elliptic integrals are subsequently solved by power series expansion[110] .

BIBLIOGRAPHY

1. A. J. Richardson, K. W. Ogden and R. L. Kinnear, "The Evaluation of Bus Priority Traffic Signals", Aust. Road Research, Vol. 8, No. 4, pp 35-46, Dec. 1978.

2. G. Middleton and J. Y. K. Luk, "Area Traffic Control Systems: Some Aspects of Planning and Design", Aust. Road Research, Vol. 9, No. 2, pp 25-34, June 1979.

3. "Electronics: Keeps Traffic on the Move", Siemens Review, Vol. XLVI, No. 4, pp 15-19, July/Aug. 1979.

4. M.A.P. Taylor "Small Area Traffic Analysis Using the LATM Package", Aust. Road Research, Vol. 8, No. 4, pp 48-56, Dec. 1978.

5. F. P. Ziolkowski and K. H. Tsao, "Antennas Buried in a Roadway for Vehicular Traffic Communications", IEEE Trans. Vol. VT-20, No. 4, Nov. 1971, pp 104-114.

6. S. H. Roth, "Automatic Vehicle Monitoring Technology Review", The MITRE Corporation, MTR-6059, Aug. 1971.

7. J. D. Garcia, "Analytic and Experimental Evaluation of Alternative Methods for Automatic Vehicle Monitoring", IPA/Teknekron, N.Y., July 1968.

8. A. L. Anreiev, "Moving Object Identifying Systems", Control Eng., pp 63-70, Oct. 1971.

9. A. S. Palastnick and H. R. Inhelders, "Automatic Identification Systems - Methods of Approach", IEEE Trans., Vol. VT-19, pp 128-136, Feb. 1970.

10. Special Issue on "Automatic Vehicle Monitoring", IEEE Trans., Vol. VT-26, No. 1, Feb. 1977.

11. A. E. Hitsman, "Status Report on Morgantown Personal Rapid Transit (PRT) Systems", Proc. 1972 Southeastern Symp. on Systems Theory, University of Kentucky, Lexington, Tech. Rep. UKY 45-72-EE3, April 1972.

12. "Case Study A - The Network Cab", New Systems Implementation Study, G. M. Res. Labs., Vol. 3, Feb. 1968, pp A1-A83.

13. W. N. Lawrence, "Electronically Controlled Highway Traffic - Survey and Design", presented at the 21st Annual Meeting of the ISA, New York, October 1966.

14. H. J. Payne, "Models of Freeway Traffic and Control", Simulation Council Proceeding, Vol. 1, No. 1, 1971.

15. S. Riter and J. McCoy, "Automatic Vehicle Location - An Overview", IEEE Trans. Vol. VT-26, No. 1, Feb. 1977.

16. R. L. Pera and R. Nenzi, "TANA - An Operating Surveillance System for Highway Traffic Control", Proc. IEEE, Vol. 61, No. 5, pp 542-556, May 1973.

17. R. C. Larson, K. W. Cotton and G. C. Larson, "Evaluating a Police-Implemented AVM System: The St. Louis Experience (Phase I)", IEEE Trans. Vol. VT-26, No. 1, Feb. 1977.

18. P. A. Deslandes and J. D. Last, "A System for Automatic Vehicle Location", IEE Conf. Publication on Automobile Electronics, No. 41, July 1976.

19. R. W. Gibson, "Pinpoint - A Radio System for Locating and Monitoring Vehicles", Philips Technical Review, Vol. 35, No. 1, 1975.

20. K. Eshraghian, "Vehicle Traffic Monitoring", M.Eng.Sc. Dissertation, Department of Electrical Engineering, University of Adelaide, 1977.

21. "Computers Switch Traffic Signals", Electronics, pp 74-76, Feb. 1973.

22. H. Payne, W. Thompson and L. Isaksen, "Design of a Traffic-Responsive Control System for a Los Angeles Freeway", IEEE Trans. Vol. SMC-3, No. 3, pp 213-224, May 1973.

23. J. Hillier, "Area Traffic Control by Computer: Equipment in the Glasgow Experiment", Traffic Eng. and Control, Vol. 9, pp 496-498, 1968.

24. D. C. Gazis and R. B. Potts, "Route Control at Critical Intersections", Proc. ARRB, Vol. 3, part 1, pp 354-363, 1966.

25. A. D. May, "Experimentation with Manual and Automatic Ramp Control", Highway Research Record, No. 59, pp 9-25, 1964.

26. R. Brenner, E. Telford and D. Fisher, "A quantitative Evaluation of Traffic in a Complex Freeway Network", Highway Research Board Bulletin, No. 291, pp 163-206, 1961.

27. J. Smith, "Europe Maps Road-Safety Plan", Electronics, pp 82-83, July 22, 1976.

28. J. S. Drake, J. L. Schafer and A. D. May, "A Statistical Analysis of Speed-Density Hypothesis", Highway Res. Board Rec., No. 154, pp 53-87, 1976.

29. R. Herman and R. W. Rothery, "Microscopic and Macroscopic Aspects of Single Lane Traffic Flow", J. Oper. Rec. Soc., Japan, Vol. 5, pp 74-93, 1959.

30. H. J. Payne, "Models of Freeway Traffic and Control - Mathematical Models of Public Systems", Simulation Council Proc., Vol. 1, No. 1, 1971.

31. M. J. Lighthill and G. A. Whitlam, "On Kinematic Waves II. A Theory of Traffic Flow on Long Crowded Roads", Proc. Roy. Soc. Ser. A., Vol. 229, pp 317-345, 1955.

32. R. T. Underwood, "Some Aspects of the Theory of Traffic Flow", Aust. Road Research, No. 2, pp 35-47, June 1962.

33. D. C. Gazis and C. H. Knapp, "On-Line Estimation of Traffic Densities from Time - Series of Flow and Speed Data", Trans. Sc. Vol. 5, No. 3, pp 283-302, 1971.

34. B. Mikhalkin, "The Estimation of Roadway Behaviour Using Occupancy Detectors", Ph.D. Dissertation, Department of Industrial and Systems Engineering, University of Southern California, 1971.

35. N. E. Nahi and A. N. Trevedi, "Recursive Estimation of Traffic Variables: Section Density and Average Speed", Trans. Sc. Vol. 7, No. 3, Aug. 1973.

36. S. H. Roth, "History of Automatic Vehicle Monitoring (AVM), IEEE Trans. Vol. VT-26, No. 1, Feb. 1977.

37. G. E. Beck, "Hyperbolic Navigation" Van Nostrand-Reinhold, London, England, Chapter 4, 1971.

38. G. J. Sonnenberg, "Radar and Electronic Navigation", Newness-Butterworth, London, England, 4th Edition, Chapter 7, 1970.

39. T. N. Lerzniak, R. Lewis and R. A. McMillen, "A Dead Reckoning/Map Correlation Systems for Automatic Vehicle Tracking", IEEE Trans., Vol. VT-26, No. 1, Feb. 1977.

40. E. N. Skomal, "Results of an AM Broadcast AVL Experiment", IEEE Trans. Vol. VT-26, No. 1, Feb. 1977.

41. L. G. Reynolds, "An Examination of Some Site and Transmission-path Errors of the Decca Navigation System when used over Land", Proc. IEE, No. 63, Jan. 1953.

42. G. S. Kaplan, "An X-Band System Using Semipassive Signpost Reflectors for Automatic Location and Tracking of Vehicles", IEEE Trans. Vol. VT-26, No. 1, Feb. 1977.

43. W. T. Lawrence, "A Magnetic Signpost AVM System with Limited Dead Reckoning", IEEE Transactions, Vol. VT-26, No. 1, pp 23-29, Feb. 1977.

44. G. D. Wilson, "Automatic Vehicle Location System Selection", IEEE 1978 Vehicular Technology Conference 28th Annual Conference, March 1978.

45. P. A. Deslandes and J. D. Last, "A System for Automatic Vehicle Location", IEE Conf. on Automobile Electronics, Publication No. 41, pp 112-115, July 1976.

46. E. N. Skomal, "Comparative Analysis of Six Commercially Available (AVL) Systems", 28th IEEE Vehicular Technology Conference, March 1978.

47. G. D. Wilson, "Automatic Vehicle Location System Selection", 28th IEEE Vehicular Technology Conference, March 1978.

48. V. K. Drebinger and P. Thilo, "Austomatisches Unterscheichen Von Fahrzengasten bei Verkehrszahlung", Siemens-Zeitschrift, 44, 1970.

49. F. P. Ziolkowski and K. H. Tasao, "Antennas Buried in a Roadway for Vehicular Traffic Communications", IEEE Trans. Vol. VT-20, No. 4, pp 104-114, Nov. 1971.

50. J. R. Ullmann, "Pattern Recognition Techniques", Crane, Russak, N.Y. 1973.

51. K. S. Fu, "Sequential Methods in Pattern Recognition and Machine Learning", Academic Press, N.Y. 1968.

52. H. C. Andrews, "Introduction to Mathematical Techniques in Pattern Recognition", Wiley, N.Y., 1972.

53. J. T. Tou and R. C. Gonzalez, "Pattern Recognition Principles", Addison-Wesley, U.S., 1974.

54. N. J. Nilsson, "Learning Machines - Foundation of Trainable Pattern-Classifying Systems", McGraw-Hill, N.Y., 1965.

55. G. S. Sebestyen, "Decision-Making Processes in Pattern Recognition", Macmillan, N.Y., 1962.

56. C. K. Chow, "An Optimum Character Recognition System Using Decision Functions", IRE Trans. EC No. 6, pp 247-254, 1957.

57. J. T. Tou, "Feature Extraction in Pattern Recognition", Pattern Recognition (Pergamon Press), Vol. 1, pp 3-11, 1968.

58. S. Watanabe, "Automatic Feature Extraction in Pattern Recognition", Automatic Interpretation and Classification of Images, Academic Press, N.Y., 1969.

59. S. Watanabe, "Evaluation and Selection of Variables in Pattern Recognition", Computers and Information Sciences - II, Academic Press, N.Y., 1967.

366.

60. E. A. Patrick and F. P. Fischer, "Non Parametric Feature Selection", IEEE Trans. Info. Theory, Vol. IT-15, No. 5, Sept. 1969, pp 577-584.

61. T. L. Henderson and D. G. Lainiotis, "Comments on Linear Feature Extraction", IEEE Trans. PGIT, Vol. IT-15, No. 6, Nov. 1969, pp 728-730.

62. E. L. Lehmann, "The Power of Rank Tests", Ann. Math. Statist. No. 24, pp 23-43, 1953.

63. E. Bunge, "Speaker Recognition by Computer", Philips Tech. Rev. 37, No. 8, pp 207-219, 1977.

64. G. B. Coleman and H. C. Andrews, "Image Segmentation by Clustering", Proc. IEEE Vol. 67, No. 5, May 1979.

65. A. F. Malo, H. S. Mika and V. P. Walbridge, "Traffic Behaviour on an Urban Expressway", Highway Res. Board Bull. No. 235, pp 19-37, 1960.

66. J. N. Constant, "Microwave Automatic Vehicle Identification (MAVI) System", IEEE Transactions Vol. VT-23, No. 2, pp 44-54, May 1974.

67. N. Freedman, "Raytag, An Electronic Remote Data Readout System", Carnahan Conference on Electronic Crime Counter Measures Proc., pp 104-107, April 1973.

68. "Vetag - Vehicle Identification System", Philips Traffic Systems, 1973.

69. R. F. Leaver, "Track-to-Train Communication", System Technology No. 20, pp 30-32, Feb. 1975.

70. A. Koelle, S. Depp and R. W. Freyman, "Short-Range Radio-Telemetry for Electronic Identification Using Modulated RF Backscatter", IEEE Proc. pp 1260-1261, Aug. 1975.

71. K. Garbrecht, "The Microwave System of the Siemens AG for Automatic Car Identification", Siemens AG, ACI Rep. 1972.

72. R. J. Klensch, J. Rosen and H. Staras, "A Microwave Automatic Vehicle Identification System", RCA Review Vol. 34, Dec. 1973.

367.

73. F. Sterzen, "An Electronic License Plate for Motor Vehicles", RCA Review Vol. 35, June 1974.

74. D. M. Holm, "Electronic Identification", Los Alamos Scientifit Lab. Rep. LA-7642-PR, Sept. 1978.

75. C. D. McEwen, "Identity-Transponder System Using C.N. Interrogation", Electronics Letters Vol. II, No. 25/26, pp 642-643, Dec. 1975.

76. J. Sakuagi, S. Kimura, K. Kameda and S. Kamata, "Microwave Automatic Vehicle Identification (AVI) System", IEEE, 29th Veh. Tech. Conference, Illinois, pp 72-76, March 1979.

77. L. B. Milstein and P. K. Das, "Surface Acoustic Wave Devices", IEEE Communications, pp 25-33, Sept. 1979.

78. D. E. N. Davies, M. J. Withers and R. P. Claydon, "Passive Coded Transponder Using an Acoustic Surface Wave Delay Line", Elect. Letters, Vol. II, No. 8, pp 163-164, April, 1975.

79. A. S. Burgess and P. H. Cole, "Passive One-Port Information Storage Using Acoustic Surface Waves", IEEE Trans. pp 24-31, Jan. 1975.

80. A. S. Burgess and P. H. Cole, "Design of Acoustic Surface Wave Devices Using Admittance Formalism", IEEE Trans. pp 611-618, Oct. 1973.

81. P. H. Cole, A. S. Burgess and R. Vaughan, "Article Sorting Using Acoustic Surface Wave Passive One-Port Labels", IREE Conv. Digest, Sydney, pp 277-280, Aug. 1979.

82. Unisearch Ltd., "Passive Labels for Use in Electronic Surveillance Systems", British Patent No. 1298381, 1970.

83. P. H. Cole, "Design Details for 200 MHz Acoustic Surface Wave Labelling System", private communications.

84. P. H. Sabine "Surface Acoustic Scattering at a Periodically Mass-Loaded Surface", Ph.D. Dissertation, Department of Electrical Engineering, University of Adelaide, 1972.

85. A. S. Burgess, "Coded One-Port Acoustic Surface-Wave Delay Lines", Ph.D. Dissertation, Department of Electrical Engineering, University of Adelaide, 1974.

86. Federal Telecommunications Commission, Rules and Regulations: Industrial, Scientific and Medical Services, Part 18, Government Press, Washington, D.C., 1957.

87. S. Silver, "Microwave Antenna Theory and Design", MIT Radiation Lab. Series, Vol. 12, McGraw-Hill, N.Y. 1949.

88. R.W.P. King, "Fundamental Electromagnetic Theory", N.Y., Dover, 1963.

89. R. F. Harrington, "Time Harmonic Electromagnetic Fields", McGraw-Hill, 1961.

90. E. C. Jordan, "Electromagnetic Waves and Radiating Systems", Prentice Hall, 1968.

91. H. S. Oranc, "Ignition Noise Measurements in the VHF/UHF Bands", IEEE Transactions Vol. EMC-17, No. 2, May 1975.

92. E. N. Skomal, "Analysis of Airborne VHF/UHF Incidental Noise Over Metropolitan Areas", IEEE Trans., Vol. EMC-11, No. 2, May 1969.

93. A. K. Roy, "Analysis of Environmental Noise", Private Communications.

94. R. B. Schulz and R. A. Southwick, "APD Measurements V-8 Ignition Emanations:, IEEE Trans., Vol. EMC-16, No. 2, May 1974.

95. T. Hutton and J. W. Kramer, "Transponder for an Automatic Vehicle Identification System", U.S. Patent 3,964,024, 1976.

96. P. H. Cole, K. Eshraghian and A. K. Roy, "Theory and Operation of Passive Subharmonic Transponder", IREE International Conv. Proc. pp 51-54, Aug. 1979.

97. R. F. Harrington, "Introduction to Electromagnetic Engineering", McGraw-Hill, N.Y. 1958.

98. M. Kanda, "Time and Amplitude Statistics for Electromagnetic Noise in Mines", IEEE Trans. Vol. EMC-17, No. 3, pp 122-129, Aug. 1975.

99. P. H. Cole, K. Eshraghian and A. K. Roy, "Efficient Object Identification System", Patent Spec. PD4594, 1979.

100. A. B. Glenn, "Comparison of PSK vs FSK and PSK-AM vs FSK-AM Binary-Coded Transmission System", IRE Trans. on Comm. Systems, pp 87-100, June 1960.

101. S. Pasupathy, "Minimum Shift Keying: A Spectrally Efficient Modulation", IEEE Communications Magazine, July 1979.

102. C. Kittel, "Introduction to Solid State Physics", 2nd Ed. John Wiley & Sons, N.Y. 1957.

103. E. B. Rosa and F. W. Grover, "Formulas and Tables for Calculation of Mutual and Self Inductance", U.S. Bur. Standards, Vol. 8, 1912.

104. A. Van Suchtelen, "Ferroxcube Aerial Rods", Electronic App. Bull. Vol 13, No. 6, Jan. 1952.

105. K. M. Bozorth, "Ferromagnetism", Van Nostrand, Princeton, N.J. 1951.

106. J. A. Osborn, "Demagnetizing Factors of the General Ellipsoid", Physical Review, Vol. 67, No. 11/12, June 1945.

107. J. C. Maxwell, "Electricity and Magnetism", The Clarenden Press, Oxford, 1904, 3rd Ed. Vol. 2, pp 66-70.

108. R. M. Bozorth and D. M. Chapin, J. App. Phys., 12, 320, 1942.

109. "Table of Integrals, Series and Products", I. S. Gradshteyn and I. M. Ryzhik, 4th Edition, 1965, Academic Press, New York and London.

110. "Dutch National Standard", Philips Technical Report on Traffic Control 1977.

111. J. Aitchison, "Statistics II', Oliver and Boyd, Edinburgh, 1971.

112. F. E. Terman, "Electronic and Radio Engineering", McGraw-Hill, N.Y. 1955.

113. R. Plensey and R. E. Collin, "Principles and Applications of Electromagnetic Fields", McGraw-Hill, N.Y. 1961.

114. S. Ramo and J. R. Whinnery, "Fields and Waves in Communication Engineering", J. Wiley & Son, N.Y. 1964.

115. P. H. Cole, K. Eshraghian and A. K. Roy, "Measurement and Characteristics of Environmental Noise Affecting Low Frequency Transponder Operations", IREE International Conv. Proc., pp 457-459, Aug. 1979.

116. K. Eshraghian and F. S. Sin, "Multiprocessor Based Vehicle Sensor", IEA, National Conv. Digest on Microprocessor Systems, Pub. No. 80/15, Sydney, pp 1-5, Nov. 1980

117. M. J. Flynn, "Very High Speed Computing Systems", Proc. IEEE, Vol. 54, 1966.

118. H. S. Stone, "Introduction to Computer Architecture", U. S. Science Research Assn. Inc., 1975.

119. N. A. Clark, "A Multi-microprocessor System", Conference on Microprocessor Systems, 79, National Conference Publication No. 79/12, Nov. 1979.

120. R. H. Frather and D. J. Skellern, "A Microprogrammed Computer Control Unit for Digital Signal Processors", Conference on Microprocessor Systems 78, National Conference Publication No. 73/13, Nov. 1978.

121. A. K. Roy, "Error Characteristics and Prediction", personal communications.

122. R. W. Lucky, J. Salz and E. J. Weldon, "Principles of Data Communications", New York: McGraw-Hill, 1968.

123. W. W. Peterson and E. J. Weldon, "Error-Correcting Codes", 2nd Ed. Cambridge, Mass., M.I.T. Press, 1972.

124. P. J. Mabey, "Mobile Radio Data Transmission - Coding for Error Control", IEEE Trans. Vol. VT-27, No. 3, Aug. 1978.

125. W. W. Merwin, "Introduction to Redundancy Coding", IEEE Trans. Vol. VT-27, No. 3, Aug. 1978.

126. E. R. Berlekamp, "Algebraic Coding Theory", New York, McGraw-Hill, 1968.

127. R. W. Hamming, "Error Detecting and Error Correcting Codes", B.S.T.J., No. 29, pp 147-160, 1950.

128. J. E. Storer, "Passive Network Synthesis", McGraw-Hill, 1957.

129. R. A. Mace- and C. Wilding, "Current Injection Logic", Progress Report No. 742, Mullard Southampton Integrated Circuit Development Department 1973.

130. G. Bergmanns, "A One-Chip I^2L Controller for Appliances", IEEE Jrn. of Solid-State Circuits, Vol. SC-14, No. 3, pp 569-572, June 1979.

131. P. H. Cole, K. Eshraghian and A. K. Roy, "Efficient Object Identification", U.S. Patent Spec. No. 043,634.